THE ENERGETICS, STRUCTURES, AND DYNAMICS OF THE $\delta\delta^*$ EXCITED STATES OF QUADRUPLY BONDED DIMERS

Thesis by

Michael David Hopkins

In Partial Fulfillment of the Requirements

for the Degree of

Doctor of Philosophy

California Institute of Technology

Pasadena, California

1986

(Submitted May 16, 1986)

Acknowledgment

As I prepare to close out my graduate career, I would like to take this opportunity to thank the many people whose advise and encouragement made this thesis possible. First of all, I wish to express my deepest thanks to Harry Gray, to whom I am greatly indebted for all that he has done for me over the last five-plus years. I cannot envision a more stimulating environment in which to learn how to "do chemistry" than that which he has provided, especially with regard to the free reign that he gave me to pursue my own research interests, nor can I think of a person whose knowledge of, and enthusiasm for inorganic chemistry are as inspiring as his. If only a fraction of these attributes have rubbed off on me, I can consider my stay here to have been a worthwhile one.

Of the many Gray group members who have helped me over the years, three deserve special mention: Vince Miskowski, Tom Zietlow, and Steve Rice. I was very fortunate to be able to share nearly all of my Caltech experience with Tommy; not only was his presence instrumental in getting me through the rougher times, but he is also responsible for many of my fonder memories of graduate school. I doubt that there is a topic, chemistry related or otherwise, that we haven't discussed at length at some point. Vinny taught me almost everything I know about spectroscopy and electronic structure, which is to say nearly everything that went into the writing of this thesis. In addition to this spoon-feeding, I am particularly grateful for his help in keeping my spirits up on innumerable all-night helium runs (arrgh), and for 10^9 helpful discussions. I also wish to thank both of them for proofreading this thesis; because of their efforts, any remaining errors are "not entirely my fault." Steve deserves much of the credit for getting me started on my first projects, and for showing me how to be a graduate student.

In addition to these individuals, there are a number of regular and unofficial group members who have helped me by either making the third floor a fit place to work, teaching me new experimental techniques, or through helpful discussions (including driving me home after them): Terry, Janet, Bob, Al, Les, Miriam, Walther, Charlie, Dave, Milo, Dr. Wulf, Mike, Che, Andy Ax, Andy Mav, Alison, Ann, Cindy, Jenny, Lorne, Huey-Jenn, Mary, Catherine, Pat B., and especially that most major of dudes, Tad. I wish them all the best of luck in their future endeavors. I also wish to thank Bill Schaefer and Woody Woodruff for enjoyable collaborations on the crystallography and vibrational spectroscopy, respectively, of the compounds described in this thesis.

I would never have made it to this day in my life had it not been for the tireless support, encouragement, and love provided by my parents. Their values and dedication to excellence have, and always will serve as a source of inspiration for me. I thank them, and my brother Mark, for happy times too numerous to mention. Finally, I wish to thank my wife Rosemary, to whom I dedicate this thesis. She endured my protracted graduate career with far greater patience than could be expected of anyone, and moreover was unwaveringly cheerful and encouraging at times when I was not much more than a zombie. Without her support and the balance she adds to my life, this thesis would not have been possible. Halak boosis.

To Rosemary

Abstract

The results of an experimental investigation of the electronic structures of the $M_2X_4L_4$ (M = Mo, W; X = Cl, Br, I; L = uncharged σ-donor ligand) class of quadruply bonded metal dimers are reported. These results are interpreted within a theoretical framework that is general for all types of weakly interacting orbitals; this is set out in Chapter I. In Chapter II we lay the structural foundation for this investigation by presenting the crystal structures of $Mo_2Br_4(PMe_3)_4$ and $Mo_2I_4(PMe_3)_4$ and comparing their bonding parameters with those previously reported for $Mo_2Cl_4(PMe_3)_4$. Resonance Raman and far-infrared spectral data of these complexes are also reported; comparisons to the available structural data indicate that the metal-metal distance and diatomic force constants, which are fingerprint parameters for the characterization of metal-metal interactions, display different ligand sensitivities. This chapter concludes with a discussion of the energies and intensities of the $^1(\delta \rightarrow \delta^*)$ transitions of these complexes, cast both in terms of their molecular structures as well as within the framework of existing theories of the electronic structural significance of these latter two spectroscopic properties. The data for the $M_2X_4L_4$ complexes lead to a reevaluation of these standard interpretations, and a new postulate, based on charge transfer mixing, is put forth that more adequately accounts for the energies and intensities of the $^1(\delta \rightarrow \delta^*)$ transitions of nearly all quadruply bonded dimers. The $^3(\delta\delta^*)$ state is discussed briefly in Chapter III, wherein it is shown that differing magnetic and spectroscopic properties of the $Mo_2X_4(PMe_3)_4$ and diphosphine-bridged β-$Mo_2X_4(dmpe)_2$ dimers are readily accounted for by the simple theoretical framework set out in Chapter I. The analysis of these data leads to experimental estimates of the energies of the $^3(\delta\delta^*)$ states of these compounds: L = PMe_3, E = 5200 cm^{-1}; L = dmpe, E = 500 cm^{-1}.

In Chapter IV we consider the photophysical properties of the $^1(\delta\delta^*)$ state in light of its energetics relative to the $^3(\delta\delta^*)$ and δ^2 states. Of particular interest is the finding that the photophysical properties of these complexes are perturbed by the nature of the coordination sphere to a different extent than are their $^1(\delta \rightarrow \delta^*)$ energies and intensities. The extensive series of $M_2X_4L_4$ complexes studied allows the estimation of the intrinsic radiative and nonradiative decay properties of this chromophore. Chapter V contains the main body of this thesis, namely the analysis of the high-resolution electronic spectra of the $M_2X_4L_4$ complexes. The unprecedented vibronic detail revealed by these spectra is interpreted using the conceptual base developed over the preceding four chapters, and results in the proposal of a double-well potential energy surface for the $^1(\delta\delta^*)$ state along nontotally symmetric coordinates; this arises from sudden polarization. In the final chapter, the photochemical manifestations of this new excited state description are outlined. Material that supplements the discussion in Chapters I - VI is presented in the appendices.

Table of Contents

List of Figures

Chapter I

Chapter II

Chapter III

Chapter IV

Chapter V

Chapter VI

Appendix II

Appendix III

Appendix IV

List of Tables

CHAPTER I

Introduction

An understanding of the electronic structures of molecules is central to the interpretation of their static and dynamic properties. In the case of compounds containing transition metal ions, such an understanding is usually derived from many different sources. These sources include electronic structural calculations, electronic and ionization spectroscopy and magnetic measurements, all of which provide direct information about the energetics of orbitals and states, as well as x-ray crystallography and vibrational and magnetic resonance spectroscopy, which provide insight into electronic structure to the extent that it is manifested in molecular structure and bonding force constants. A main theme in most such investigations is the identification of those complexes that possess some feature, such as high symmetry or a simple coordination sphere, that makes their electronic structural properties both amenable to study and extendable to other, more complicated systems.

The topic of this thesis is the electronic structure of molecules containing quadruple metal-metal bonds. Because these complexes are one of the structural archetypes of inorganic chemistry, much as ethylene and benzene are to organic chemistry, and inasmuch as they possess one of the simplest geometries for the study of metal-metal interactions, their physical properties have been closely scrutinized, using the techniques described above, in the two decades since this mode of bonding was proposed by F. A. Cotton to account for the diamagnetism, eclipsed geometry, and short metal-metal separation of the $Re_2Cl_8^{2-}$ ion.[1,2] The basic tenet of this large body of work is set out in Figure 1, which displays the qualitative molecular orbital diagram for this class of complexes; the eight d electrons contributed by the two square planar d^4 subunits that make up the dimer are distributed in the metal-metal bonding levels to give a closed-shell $[\sigma^2\pi^4\delta^2]$ configuration. A more quantitative molecular orbital scheme is shown in Figure 2 for $Mo_2Cl_4(PH_3)_4$,[3] a compound that is representative of the class of molecules that are investigated in

Figure 1. Molecular orbital scheme for M_2 ($D_{\infty h}$) and M_2L_8 (D_{4h}) dimers.

Figure 2. LCAO-HFS transition-state energy level diagram for $Mo_2Cl_4(PH_3)_4$ (D_{2d}), reproduced from reference 3.

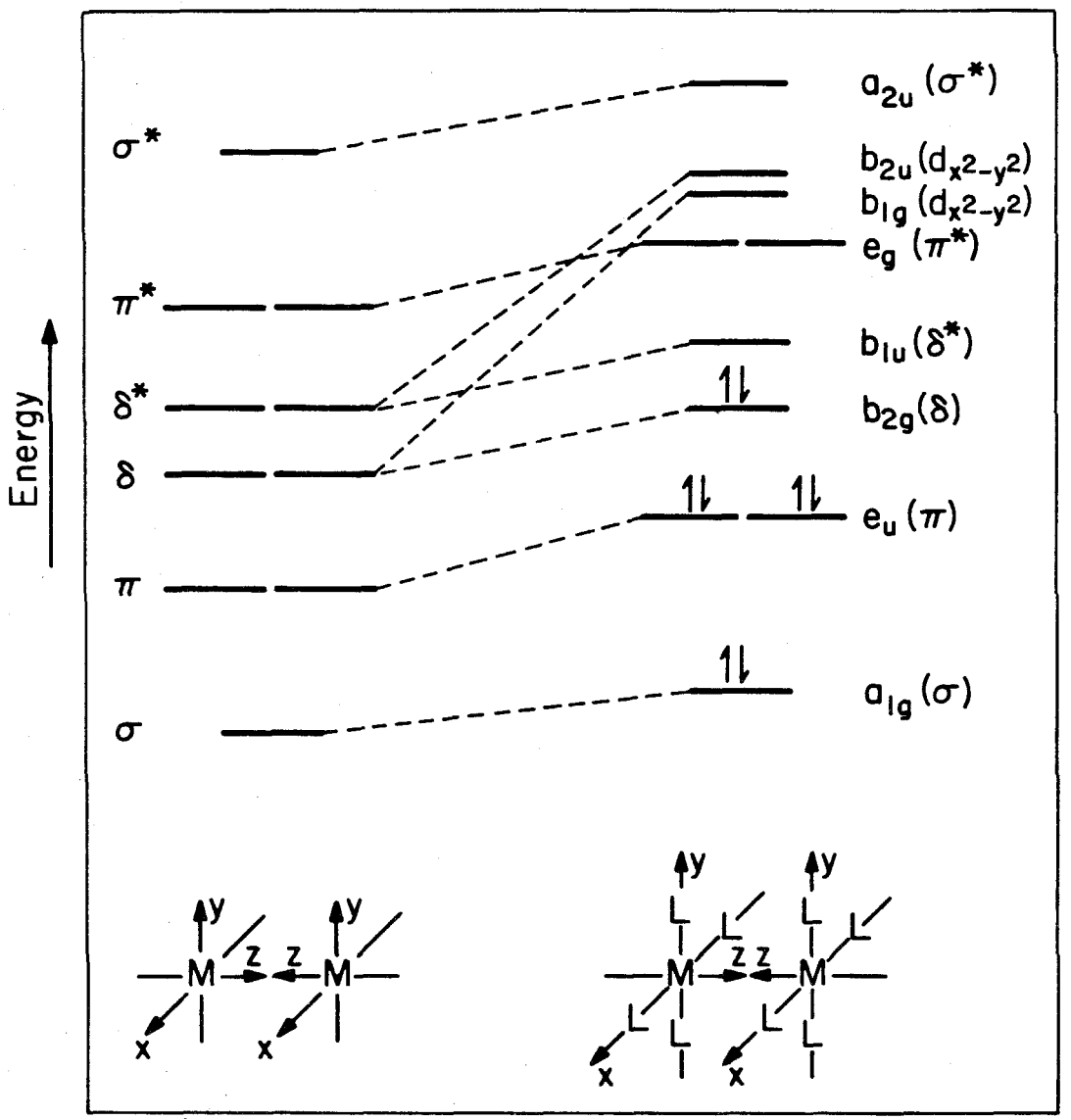
Energy
σ*
π*
δ*
δ
π
σ
a2u (σ*)
b2u (dx2-y2)
b1g (dx2-y2)
eg (π*)
b1u (δ*)
b2g (δ)
eu (π)
a1g (σ)
M
M
z z
y
x
L

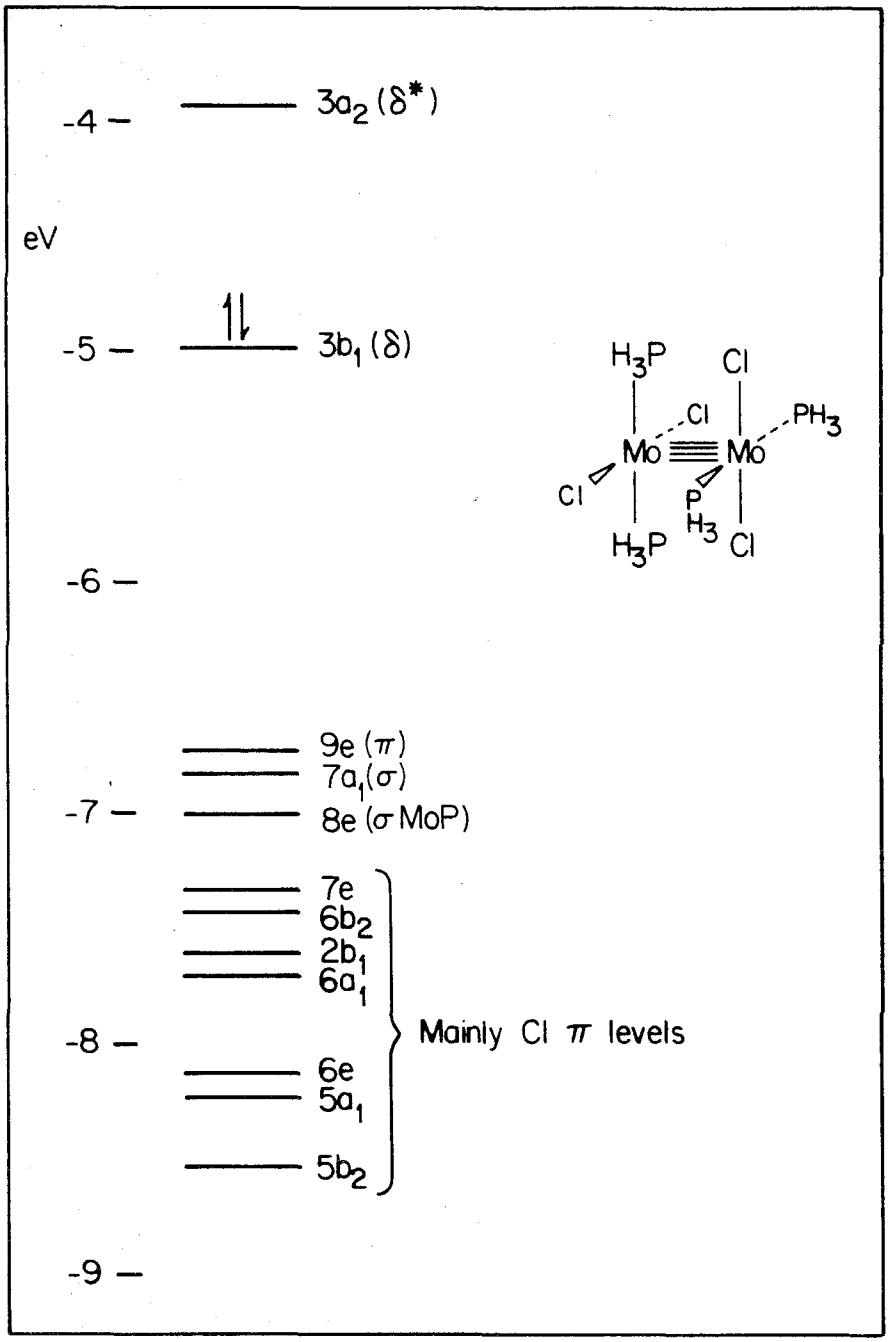
-4
3a2 (δ*)
eV
-5
3b1 (δ)
H3P
Cl
Cl
PH3
Mo
Mo
Cl
P
H3
H3P
Cl
-6
9e (π)
7a1 (σ)
-7
8e (σ MoP)
7e
6b2
2b1
6a1
-8
Mainly Cl π levels
6e
5a1
5b2
-9

this thesis. This diagram shows that while the relative spacings among levels differ from those of the qualitative scheme, the same order is observed. Moreover, there is a clean dichotomy, from an energetic standpoint, of metal-metal- and metal-ligand-localized orbitals. A number of high-quality calculations on other types of quadruply bonded complexes support the generality of this orbital pattern,[4] and many of these schemes, including the one shown in Figure 2,[5] have been borne out by photoelectron spectroscopic experiments.[4]

Considering only the δ and δ^* frontier orbitals of these complexes, a manifold of four electronic states can be generated:[6]

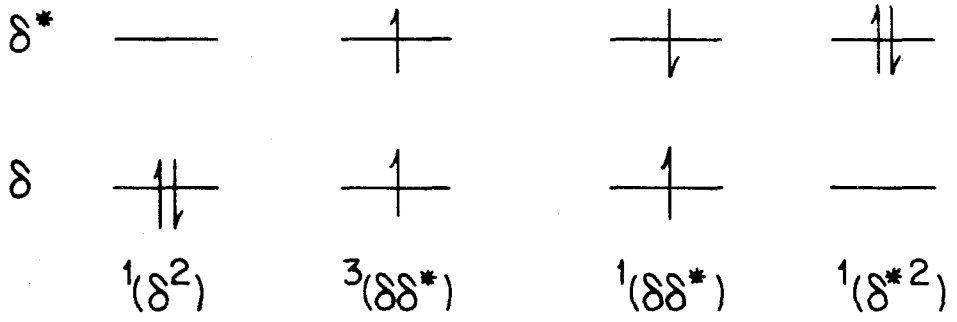

The principle concern of this work will be the elucidation of the properties of the three lowest energy members of this quartet, namely $^1(\delta^2)$, $^3(\delta\delta^*)$, and $^1(\delta\delta^*)$. Before enunciating the specific questions to be addressed herein, however, we digress to present a brief summary of the theoretical framework that will guide all subsequent discussions.

Theoretical Considerations

The concept of metal-metal δ-bonding did not originate with the proposal of the quadruple bond, but rather was first invoked nearly a decade earlier to account for the antiferromagnetism of the copper acetate dimer.[7] This was the same period that

witnessed the widespread application of molecular orbital theory to the π-bonding in simple planar unsaturated organic molecules such as ethylene. What connects these seemingly disparate events, aside from their simultaneous development, is that the thirty year old treatment of the bonding in these systems provides the simplest and most insightful framework through which to examine the energetics of the δ-manifold of states of quadruply bonded dimers. The following outline of the electronic structure of these systems is straightforwardly derived from this early work, and can be found in more detail elsewhere.[8]

The δ-HOMO and δ^*-LUMO of metal dimers possessing an eclipsed geometry are derived from face-to-face d_{xy} orbitals on metal atoms a and b, as indicated in Figure 1. The appropriate linear combinations of these orbitals, assuming that they are pure metal-metal in character, are

$$\delta = d^a_{xy} + d^b_{xy} = \phi_1 \tag{1}$$

$$\delta^* = d^a_{xy} - d^b_{xy} = \phi_2 \tag{2}$$

where the normalization factors have been neglected. Four states can be constructed from these two levels and from the two electrons contributed by a and b. The configurations of these states are

$$^1(\delta^2) = |\phi_1\phi_1|(\alpha\beta) = \Phi_1 \tag{3}$$

$$^3(\delta\delta^*) = |\phi_1\phi_2|(\alpha\beta - \beta\alpha) = \Phi_T \tag{4}$$

$$^1(\delta\delta^*) = |\phi_1\phi_2|(\alpha\beta + \beta\alpha) = \Phi_V \tag{5}$$

$$^1(\delta^{*2}) = |\phi_2\phi_2|(\alpha\beta) = \Phi_2 \tag{6}$$

Factoring the secular equation into diagonalized matrix expressions for the energies of these states gives

$$E_V = W_1 + W_2 + J_{12} + K_{12} \tag{7}$$

$$E_T = W_1 + W_2 + J_{12} - K_{12} \tag{8}$$

$$E(\Phi_1, \Phi_2) = \begin{vmatrix} 2W_1 + J_{11} - \lambda & K_{12} \\ K_{12} & 2W_2 + J_{22} - \lambda \end{vmatrix} = 0 \tag{9}$$

where the W_i are core integrals consisting of one-electron terms, J_{ii} and J_{ij} are one- and two-center coulomb repulsion integrals, and K_{12} is the exchange integral.

The expressions in equations 7-9 are too complex to yield much insight into the energies of the δ-manifold of states, at least from the standpoint of breaking down the energies into experimentally obtainable parameters. A simplifying assumption that can be employed, however, again with substantial precedent for organic systems, is the zero-differential-overlap approximation, which results in $J_{11} = J_{22} = J_{12}$. By additionally referencing all energies to the center of gravity of the one-electron δ and δ^* levels, namely $1/2(W_1 + W_2)$, the repulsion and core integrals drop out and we arrive at

$$E_V = K \tag{10}$$

$$E_T = -K \tag{11}$$

$$E(\Phi_1, \Phi_2) = \begin{vmatrix} -\Delta W - \lambda & K \\ K & \Delta W - \lambda \end{vmatrix} = 0 \tag{12}$$

These equations give, upon rearranging,

$$E(\Phi_2) - E(\Phi_1) = 2\sqrt{\Delta W^2 + K^2} \tag{13}$$

$$E_V - E_T = 2K \tag{14}$$

where ΔW is the energy difference between the one-electron δ and δ^* levels and K is given by

$$K = K_{12} = 1/2[(aa|aa) - (aa|bb)] \tag{15}$$

In equation 15, $(aa|aa)$ is the energy required to transfer a δ electron from metal center a to center b at infinite a-b distance R, and $(aa|bb)$ is an electrostatic correction for finite R. The value of this latter integral is roughly e^2/R in the point-charge limit.

The dependences of the state energies of the δ-manifold on metal-metal distance R are qualitatively indicated in Figure 3. At short distances, the atomic orbitals on adjacent metals interact strongly to generate a large bonding-antibonding orbital splitting (ΔW), while the value of K is simultaneously relatively small due to the size of the $(aa|bb)$ term. This results in the singlet and triplet $\delta\delta^*$ states lying in close energetic proximity to each other, and well above the highly stabilized ground state. As the internuclear separation increases, both ΔW and $(aa|bb)$ decrease, the former much more rapidly than the latter. At the point at which ΔW and K are of equal magnitude, there is now a large splitting between the singlet and triplet $\delta\delta^*$ states, with the latter lying relatively close to the ground state. Proceeding to the separated atom limit ($R \rightarrow \infty$, $\Delta W \rightarrow 0$), the ground state and triplet excited state are degenerate, as are the two singlet excited states some $2K$ higher in energy. The covalent and ionic limits formed by the respective collapse of these two sets of states can be viewed simply as the homolysis and heterolysis of the δ-bond:

$$M - M \rightarrow 2M\cdot \qquad (covalent)$$

$$M - M \rightarrow M^+ \, M:^- \qquad (ionic)$$

The "bonding-antibonding" electronic transition at this limit is thus pure metal-to-metal charge transfer.

The state diagram in Figure 3 is drawn over a much wider range of distances than are found in quadruply bonded dimers. The question that arises at this point is thus what the relative magnitudes of ΔW and K are for typical complexes of

Figure 3. Metal-metal-distance dependence of the energies of the δ-manifold of states.

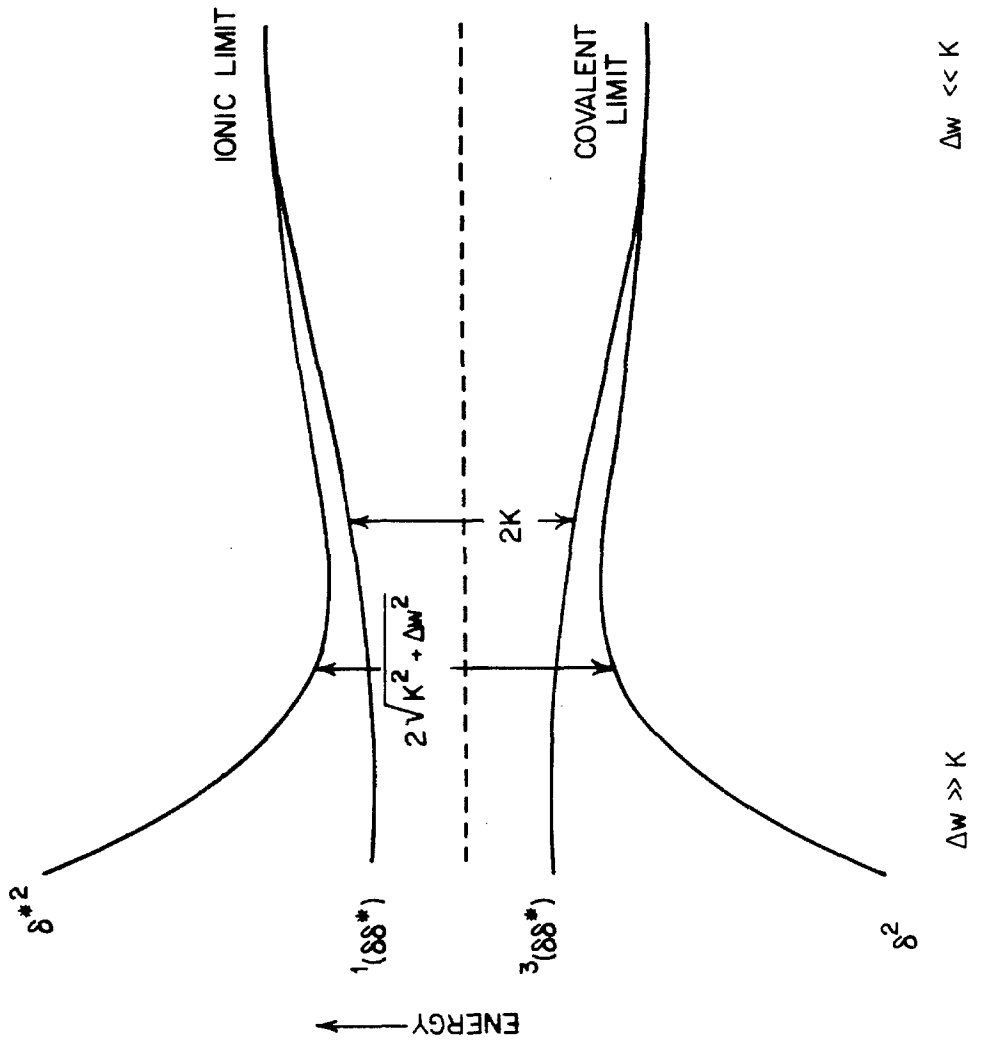
IONIC LIMIT
COVALENT LIMIT
2K
$2\sqrt{K^2+\Delta w^2}$
δ^{*2}
$^1(\delta\delta^*)$
$^3(\delta\delta^*)$
δ^2
ENERGY
R(M$_2$)
$\Delta w \gg K$
$\Delta w \ll K$

this type. Experimental observations are of little help in terms of resolving this question, since the energies of the $^3(\delta\delta^*)$ and $^1(\delta^{*2})$ states relative to the ground state have yet to be reported for any quadruply bonded complex. With respect to the size of ΔW, the spatial orientation of the parent d_{xy} orbitals is unfavorable for strong δ-overlap relative to those from which the σ- and π-interactions are derived, and Figures 1 and 2 suggest that it is this $[\sigma^2\pi^4]$ triple-bond core that determines the internuclear separation (presumably at distances longer than those required for optimal δ-overlap). Combining the calculated splitting of the one-electron δ and δ^* orbitals of $Mo_2Cl_4(PH_3)_4$ ($\Delta W = 8390$ cm^{-1}) taken from Figure 2 with the 17090-cm^{-1} energy of the $^1(\delta \rightarrow \delta^*)$ transition of the closely related $Mo_2Cl_4(PMe_3)_4$ complex, which will be discussed in detail in subsequent chapters, yields $K = 6490$ cm^{-1}; these complexes are thus in the $\Delta W \cong K$ regime described above.

Scope of this Thesis

There are two interesting phenomena predicted by the foregoing theoretical analysis that have been nearly completely ignored in previous studies of these complexes, and which will be investigated in this thesis.[9] Both of these have potentially wide ranging effects on the properties of the δ-manifold of states. Considering first the $^1(\delta\delta^*)$ state, the large size of K relative to the $^1(\delta \rightarrow \delta^*)$ transition energy of the $Mo_2Cl_4(PMe_3)_4$ dimer suggests that this excited state possesses substantial ionic character, in contrast to the covalent $^3(\delta\delta^*)$ and $^1(\delta^2)$ states:

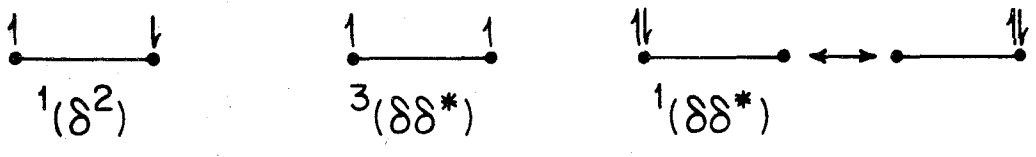

One consequence of this ionic description of $^1(\delta\delta^*)$ is that this state is, in principle, subject to sudden polarization,[10] whereby an instantaneous dipole is generated by some type of molecular distortion from the resonance form pictured above.[11] The molecular structure, photophysics, and reactivity of such a polarized excited state would undoubtedly differ significantly from those of the nonpolar state from which it is derived. With regard to the $^3(\delta\delta^*)$ state, the above estimates of ΔW and K, in conjunction with the energy of the $^1(\delta \rightarrow \delta^*)$ transition of $Mo_2Cl_4(PMe_3)_4$, indicate it should lie 13000 cm^{-1} below its singlet counterpart and only 4100 cm^{-1} above the ground state in this complex. Aside from presenting an interesting experimental challenge to the identification of this state (as already noted, it has yet to be directly observed), this prediction is also of unambiguous photophysical significance, since in most transition metal complexes such singlet-triplet excited state splittings are relatively small and their decay properties are thus dominated by intersystem crossing.

There is a third question that will be addressed in this thesis that, in contrast to the above predictions, is not derived from the preceding theoretical discussion, but rather is notable by its absence from it: How are the energies and physical properties of these states influenced by the nature of the ligands? Our energy expressions were derived from wavefunctions that were, for simplicity, taken to be pure metal-metal in character, yet examination of Figure 2 shows that there are a number of levels of largely ligand parentage that are of the appropriate symmetry to mix with these. The extent to which this ligand character is manifested in the properties of the δ-manifold of states remains largely unexplored to date.

The approach adopted herein for the study of the δ-manifold of states of quadruply bonded dimers has been to examine the structural, spectroscopic, magnetic, and photophysical properties of an extensive series of complexes of the

$M_2X_4L_4$ (M = Mo, W; X = Cl, Br, I; L = uncharged σ-donor ligand) type. This class of compounds is particularly attractive for such a systematic study due to the wide range of ligand perturbations that are available. In Chapter II we lay the structural foundation for this investigation by presenting the crystal structures of $Mo_2Br_4(PMe_3)_4$ and $Mo_2I_4(PMe_3)_4$ and comparing their bonding parameters with those previously reported for $Mo_2Cl_4(PMe_3)_4$. Resonance Raman and far-infrared spectral data of these complexes are also reported; comparisons to the available structural data indicate that the metal-metal distance and diatomic force constants, which are fingerprint parameters for the characterization of metal-metal interactions, display different ligand sensitivities. This chapter concludes with a discussion of the energies and intensities of the $^1(\delta \rightarrow \delta^*)$ transitions of these complexes, cast both in terms of their molecular structures as well as within the framework of existing theories of the electronic structural significance of these latter two spectroscopic properties. The data for the $M_2X_4L_4$ complexes lead to a reevaluation of these standard interpretations, and a new postulate is put forth that more adequately accounts for the energies and intensities of the $^1(\delta \rightarrow \delta^*)$ transitions of nearly all quadruply bonded dimers. Having obtained a conceptual feeling for the ligand sensitivity of the δ^2 and $^1(\delta\delta^*)$ states, we turn briefly to the $^3(\delta\delta^*)$ state in Chapter III, wherein it is shown that the differences between the magnetic and spectroscopic properties of the $Mo_2X_4(PMe_3)_4$ and diphosphine-bridged β-$Mo_2X_4(dmpe)_2$ dimers are readily accounted for by the simple theoretical framework set out in Chapter I. The analysis of these data leads to the first experimental estimate of the energy of a $^3(\delta\delta^*)$ state. We next consider the photophysical properties of the $^1(\delta\delta^*)$ state in light of its energetics relative to the $^3(\delta\delta^*)$ and δ^2 states. Of particular interest is the finding that the photophysical properties of these complexes are perturbed by the nature of the coordination sphere to a differ-

ent extent than are their $^1(\delta \rightarrow \delta^*)$ energies and intensities. The extensive series of $M_2X_4L_4$ complexes studied allows the estimation of the intrinsic radiative and non-radiative decay properties of this chromophore. Chapter V contains the main body of this thesis, namely the analysis of the high-resolution electronic spectra of the $M_2X_4L_4$ complexes. The unprecidented vibronic detail revealed by these spectra is interpreted using the conceptual base developed over the preceding four chapters, and results in the proposal of a potential energy surface for the $^1(\delta\delta^*)$ state that is quite different from that offered by the traditional view of this state. In the final chapter, the photochemical manifestations of this new excited state description are outlined. Material that supplements the discussion in Chapters I - VI is presented in the appendices, two of which (II and IV) depart from the main theme of the text and deal with issues related to the ordering of the levels in molecular orbital diagrams shown in Figures 1 and 2.

References and Notes

1. Cotton, F. A.; Curtis, N. F.; Harris, C. B.; Johnson, B. F. G.; Lippard, S. J.; Mague, J. T.; Robinson, W. R. *Science* **1964**, *145*, 1305-1307.
2. Detailed recountings of "how it all began" are available elsewhere: (a) Cotton, F. A.; Walton, R. A. "Multiple Bonds Between Metal Atoms"; Wiley: New York, 1982; chapter 1. (b) Cotton, F. A. *J. Chem. Ed.* **1983**, *60*, 713-720.
3. Ziegler, T., personal communication. For further details on this calculation, see: Ziegler, T *J. Am. Chem. Soc.* **1984**, *106*, 5901-5908.
4. Reference 2a, chapter 8.
5. Cotton, F. A.; Hubbard, J. L.; Lichtenberger, D. L.; Shim, I. *J. Am. Chem. Soc.* **1982**, *104*, 679-686. Root, D. R.; Blevins, C. H.; Lichtenberger, D. L.; Sattelberger, A. P.; Walton, R. A. *J. Am. Chem. Soc.* **1986**, *108*, 953-959.
6. The shorthand notation used here and throughout the remainder of this work is to represent the electronic configuration of a state solely by the occupancy of the δ and δ^* orbitals; a closed-shell $[\sigma^2\pi^4]$ core is implied in each case. Similarly, electronic transitions are defined by the multiplicity of the final state and the initial and final one-electron orbitals, *e.g.*, the $^1(\delta^2) \rightarrow {}^1(\delta\delta^*)$ transition is indicated by $^1(\delta \rightarrow \delta^*)$.
7. Figgis, B. N.; Martin, R. L. *J. Chem. Soc.* **1956**, 3837-3846. An interesting proposal put forth in this paper is that the diamagnetism of the chromous acetate dimer is consistent with the presence of weak σ, π, and δ metal-metal bonds.
8. (a) Parr, R. G. "The Quantum Theory of Molecular Electronic Structure"; W. A. Benjamin: New York, 1964; chapter 3. (b) Hansen, A. E.; Ballhausen, C. J. *Trans. Faraday Soc.* **1965**, *61*, 631-639. (c) Hay, P. J.; Thibeault, J. C.;

Hoffmann, R. *J. Am. Chem. Soc.* **1975**, *97*, 4884-4899.

9. Historical background on each of the following topics will be presented in more detail in the introductory sections of subsequent chapters.
10. Benard, M.; Veillard, A. *Chem. Phys. Lett.* **1982**, *90*, 160-165.
11. This is yet another concept that has been borrowed from work on the electronic structure of ethylene.

CHAPTER II

Ligand Perturbation of the Molecular and Electronic Structures of Quadruply Bonded Dimers

Introduction

The results from electronic, vibrational, and photoelectron spectroscopy, in conjunction with x-ray crystallography, form the experimental foundation of our present understanding of the molecular and electronic structures of quadruply metal-metal bonded complexes.[1] Investigations employing these techniques have been directed at many members of this diverse set of compounds and their findings have been of central importance in allowing the original qualitative bonding scheme proposed[2] for these systems to be significantly elaborated upon. Examination of the trends observed in these studies has, in addition, led to the delineation of several major electronic and structural subgroups of quadruply bonded complexes.[1] Metal dimers bridged by carboxylates, for example, are set apart from those ligated by halides in that they generally possess, for a given metal, shorter metal-metal bonds, higher frequency metal-metal stretching vibrations, and higher energy $^1(\delta \rightarrow \delta^*)$ electronic transitions. Electronic structural calculations, along with photoelectron spectroscopic experiments, have frequently been employed to elucidate the origin of such electronic differences; in the case of the carboxylate-bridged dimers they are proposed to arise from the mixing of orbitals associated with the M_2 unit with π-levels localized on the carboxylate moiety.[3]

Although the broad variations in the structural and electronic properties of homologous d^4-d^4 complexes of different metals, or of different ligand sets of the same dimetal unit, are well documented in many cases,[1] subtler perturbations resulting from ligand variation within a given subclass of dimers are less well understood. In the following chapters, the results of an investigation of the spectroscopic, magnetic, photophysical, and photochemical properties of a large number of derivatives of the $M_2X_4L_4$ type (M = Mo, W; X = Cl, Br, I; L = uncharged σ-donor ligand), which

form one of the largest subclasses of quadruply bonded dimers. One of the more striking findings of these studies is that parameters such as $^1(\delta \rightarrow \delta^*)$ transition energies,[4] electronic absorption and emission band shapes and intensities,[4-6] and the rates of radiative and nonradiative excited state decay,[6] which are properties associated with the formally metal-metal-localized manifold of electronic states, display a marked sensitivity to the nature of ligands X and L. In order to determine whether this ligand dependence is also reflected in the ground-state properties of these complexes, as well as to provide a structural benchmark for analyzing ligand perturbations of their excited states, we determined the crystal structures of two such derivatives, $Mo_2Br_4(PMe_3)_4$ and $Mo_2I_4(PMe_3)_4$, and the vibrational and electronic spectra of a series of $M_2X_4L_4$ complexes. These results are reported herein, along with a general interpretation of the ligand sensitivity of the energies and intensities of the $^1(\delta \rightarrow \delta^*)$ transitions of quadruply bonded dimers.

Experimental Section

General Procedures.

The preparations of the complexes described in this study were carried out on a high-vacuum manifold (limiting pressure $< 10^{-3}$ torr) or with Schlenk techniques. Dichloromethane (Burdick and Jackson), d_6-benzene (Aldrich), and 2-methylpentane (Phillips) were dried by standard methods,[7] degassed with five or more freeze-pump-thaw cycles, and stored under vacuum with, respectively, activated 4A molecular sieves, sodium metal/benzophenone, and lithium aluminum hydride. Trimethylphosphine (Strem) was degassed with five freeze-pump-thaw cycles and bulb-to-bulb distilled into an evacuated storage flask. All other chemicals were of reagent grade or comparable quality and were used as received.

$Mo_2(O_2CCH_3)_4$,[8] $K_4Mo_2Cl_8$,[9] $W_2Cl_4(PMe_3)_4$,[10] and $Mo_2Cl_4(PMe_3)_4$[11] were prepared according to standard procedures. Elemental and mass spectral analyses were performed by Mr. Larry Henling at the Caltech Analytical Laboratory.

Electronic absorption spectra were recorded on either a Cary 17 or Hewlett-Packard 8450A spectrometer. Spectra were obtained of solutions prepared on the vacuum line in a vessel consisting of a 10 mL round bottom flask, both 1 mm and 1 cm pathlength quartz spectral cells, and a teflon high-vacuum stopcock. Solvent was first vacuum distilled from the appropriate storage flask to a calibrated volumetric cylinder, and from there to the evacuated cell. The baselines of these spectra were corrected for the UV absorption of the solvent. Extinction coefficients were reproducible to $\pm 2\%$. Oscillator strengths of absorption bands were determined by the cut-and-weigh method. ^{31}P NMR spectra were obtained of C_6D_6 solutions prepared and sealed under vacuum and recorded with a Jeol FX90Q FT-NMR spectrometer at 26°C. Resonances are reported relative to external H_3PO_4 (aq). Magnetic susceptibilities were determined with an SHE Corp. 905 VTS SQUID susceptometer (10 kG field) of crystalline samples contained in an aluminum bucket of known magnetization. Raman spectra were recorded with one of two spectrometers: a Spex Ramalog EU equipped with a cooled RCA 31034A photomultiplier tube, an ORTEC 9300 series photon counter, and a Nicolet 1180E Raman data system; or a Spex 14024 spectrometer equipped with 2400 line/mm holographic gratings, a thermoelectric cooled Hamamatsu R955 photomultiplier tube, and a Spex SCAMP data system. Laser excitation was provided by either a Spectra-Physics 171-01(Kr^+) or 171-18(Ar^+) laser. Spectra were taken of both solutions and solids. The former were obtained in the rotating sample mode of N_2-purged solutions sealed in 5 mm-diameter glass capillaries, while the latter were obtained of either polycrystalline samples mounted in an Air Products Displex cryostat at

20 K, or of dilute KCl pellets at room temperature. FTIR spectra were recorded of nujol mulls on polyethylene supports using Perkin-Elmer Model 1800 and Mattson Sirius Model 100 spectrometers.

$Mo_2I_4(PMe_3)_4$.

A vigorously stirred, 0°C suspension of $Mo_2(O_2CCH_3)_4$ (1.67 g, 3.7 mmol) and trimethylphosphine (3 mL, 31.6 mmol) in 35 mL of dichloromethane was treated dropwise with Me_3SiI (5 g, 25.0 mmol), causing an immediate color change from bright orange to dark blue. The resulting suspension was stirred for 6 h at 0°C and then allowed to warm slowly to room temperature, where it was stirred for an additional 24 h. The solvent was removed under vacuum, and the remaining blue-white inhomogeneous solid was extracted with toluene and filtered through a 3 x 20-cm column of 60 - 100 mesh Fluorisil. Vacuum evaporation of the solvent yielded 3.55 g (95 %) of dark blue, microcrystalline $Mo_2I_4(PMe_3)_4$. Anal. Calcd (found) for $C_{12}H_{36}I_4P_4Mo_2$: C, 14.36 (14.26); H, 3.62 (3.47). ^{31}P NMR: δ -15.81(s). χ_M (300 K) = -333×10^{-6}; χ_M (6 K) = -327×10^{-6} emu/mol. This compound is air stable in the solid state and is soluble in hexane, benzene, dichloromethane, acetone, and to a limited extent, methanol. It can be recrystallized from 4:1 dichloromethane:ethanol by evaporation; crystals suitable for x-ray diffraction studies were grown under nitrogen by slow evaporation of a hexane solution.

$Mo_2Br_4(PMe_3)_4$.

This compound was prepared and purified in high yield by the above procedure using Me_3SiBr as the bromide source. Anal. Calcd (found) for $C_{12}H_{36}Br_4P_4Mo_2$: C, 17.67 (17.80); H, 4.45 (4.32). ^{31}P NMR: δ -12.31(s). Mass spectrum: m/z = 816 (parent ion; relative intensity = 28), 740 (816 - PMe_3; 72), 664 (816 - $2PMe_3$; 100), 588 (816 - $3PMe_3$; 41), 508 (816 - $3PMe_3$ - Br; 13). Slow evaporation of a toluene solution of $Mo_2Br_4(PMe_3)_4$ yielded large (up to 5 mm in diameter), dark

red[12] multifaceted prisms that were satisfactory for x-ray diffraction.

$Mo_2Cl_4(AsMe_3)_4$.

A suspension of $K_4Mo_2Cl_8$ (0.75 g, 1.2 mmol) and trimethylarsine (1.5 mL, 14.1 mmol) in 50 mL of methanol was stirred at room temperature for 5 d. Although the color of the reaction mixture did not appear to change over this time period, irradiation of the flask with a UV lamp showed that the red-pink color of the contents was due to intense luminescence, which is absent in the starting material. The reaction mixture was filtered in air and the solid washed thoroughly with methanol, water (until the filtrate was colorless) and methanol again, and dried *in vacuo*. Yield: 0.80 g (82 %). Anal. Calcd (found) for $C_{12}H_{36}As_4Cl_4Mo_2$: C, 17.71 (17.83); H, 4.46 (4.27). The compound is stable to air in the solid state, although solutions decompose rapidly on exposure to oxygen.

X-ray Diffraction Procedures.

The determination of the crystal structures of $Mo_2Br_4(PMe_3)_4$ and $Mo_2I_4(PMe_3)_4$ was carried out in collaboration with Dr. William P. Schaefer and Mr. Michael Bronikowski. Appendix I contains tables of those bond distances and bond angles that are not listed in the text of this chapter, as well as the final heavy atom parameters; tables of anisotropic thermal parameters, calculated hydrogen atom positions, and observed and calculated structure factors for these two compounds are on file with H. B. G. and W. P. S.

Calculations for both structures were performed on a VAX 11/750 computer using the programs of the CRYRM Crystallographic Computing System. Scattering factors for neutral atoms and dispersion corrections for Mo, Br, and I were taken from the International Tables;[15] the function minimized in the least squares was $\Sigma w(F_o^2 - F_c^2)$, where $w = 1/\sigma^2(F_o^2)$.

Crystals that appeared single from oscillation photographs were centered on a

CAD-4 diffractometer equipped with graphite-monochromated Mo Kα radiation (λ = 0.71073 Å). Collection of the data at room temperature and refinement of the structures proceeded as follows.

$Mo_2Br_4(PMe_3)_4$:[14] A monoclinic cell was found similar to that of $Mo_2Cl_4(PMe_3)_4$[11] and unit cell dimensions (Table I) were calculated from the setting angles of 25 reflections with $30° < 2\theta < 40°$. Data were collected for all $\pm h$, k, l with $2\theta < 50°$. Altogether 2772 reflections were scanned in a θ - 2θ mode, including 3 check reflections monitored every 5000 seconds of x-ray exposure time. The check reflections showed no variations greater than those expected from counting statistics. Lorentz and polarization factors were applied and a few duplicate reflections merged to give 2420 reflections that were used in the refinement. Variances were assigned to the values of F_o^2 based on counting statistics plus an additional term $(0.02I)^2$ to account for errors proportional to intensity. Systematic absences in the data were consistent with space group $C2/c$. Absorption corrections were not made because of the small size of the crystal ($\mu r_{max} = 1.3$).

The positional parameters of the $Mo_2Cl_4(PMe_3)_4$ structure[11] and reasonable isotropic thermal parameters served as the starting point of the refinement. The nonhydrogen atoms were given anisotropic thermal parameters after three cycles, and hydrogen atoms, positioned from difference Fourier maps, were included in the structure factor calculations after six cycles. The hydrogen atoms and their isotropic thermal parameters were not refined but were repositioned once. At convergence, $R = \Sigma||F_o| - |F_c||/\Sigma F_o = 0.048$; the goodness of fit $[\Sigma w(F_o^2 - F_c^2)^2/(n - p)]^{1/2} = 2.37$, with n = 2420 data and p = 106 parameters.

$Mo_2I_4(PMe_3)_4$: A monoclinic cell was found and cell dimensions (Table I) were calculated from the setting angles of 25 reflections with $21° < 2\theta < 27°$. Data were collected in the 2θ range 2° - 50° for all $\pm h, k, \pm l$. Altogether 10810 reflections

Table I. Crystal Data for $Mo_2Br_4(PMe_3)_4$ and $Mo_2I_4(PMe_3)_4$

	$Mo_2Br_4(PMe_3)_4$	$Mo_2I_4(PMe_3)_4$
Formula weight	813.85	1003.81
Space group	C2/c	$P2_1/c$
a(Å)	18.472(2)	17.069(3)
b(Å)	9.384(2)	10.784(3)
c(Å)	17.519(3)	16.788(3)
β(deg.)	114.89(1)	105.39(1)
V(Å^3)	2755(3)	2979(2)
Z	4	4
ρ_{calc}(g cm^{-3})	1.97	2.24
F(000)(e^-)	1548.9	1849.8
μ(cm^{-1})	72.7	23.36
crystal dimensions (mm)	0.15 x 0.20 x 0.24	0.16 x 0.17 x 0.27

were scanned in a θ - 2θ mode including 3 check reflections monitored every 10000 seconds of x-ray exposure time. The data were corrected for a slight linear decay and merged to give 5219 independent reflections, of which 4689 had $F_o^2 > 0$ and 4035 had $F_o^2 > 3\sigma(F_o^2)$. Variances were assigned the individual values of F_o^2 based on counting statistics plus an additional term, $0.014F_o^2$; variances of the merged reflections were obtained by standard propagation of error plus another additional term, 0.014 $\overline{F_o^2}$. Systematic absences in the data indicated space group $P2_1/c$ (# 14); assuming four molecules in the unit cell led to a reasonable density (2.24 g cm^{-3}). Again, no absorption corrections were made ($\mu r_{max} = 0.4$).

The structure was solved by Multan,[16] which gave the coordinates of the two molybdenum atoms and three of the iodine atoms. One structure factor-Fourier cycle led to the positions of the remaining nonhydrogen atoms. The hydrogen atoms were found in Fourier maps after six cycles of least squares, refining the positional parameters of all nonhydrogen atoms, anisotropic thermal parameters of Mo, I and P atoms, and isotropic thermal parameters of the carbon atoms in a single matrix. The hydrogen atoms were included as constant contributions in a final three cycles of least squares, with idealized C-H geometries and a thermal parameter equal to that of the carbon atom they were bonded to. At convergence, $R = \Sigma||F_o| - |F_c||/\Sigma F_o = 0.048$ for all data with $F_o^2 > 0$ and 0.039 for the strong data. The goodness of fit, $[\Sigma w(F_o^2 - F_c^2)^2/(n - p)]^{1/2}$, is 2.38 for n = 5219 data and p = 140 parameters. A secondary extinction factor[17] was refined, with a final value of $0.34(1) \times 10^{-6}$.

Results and Discussion

Molecular Structures of $Mo_2X_4(PMe_3)_4$ (X = Cl, Br, I).[18]

In view of the vast body of structural data on quadruply bonded complexes,[1] it is surprising that the crystallographic results reported here for $Mo_2Br_4(PMe_3)_4$ and $Mo_2I_4(PMe_3)_4$, along with that reported by Cotton *et al.* for $Mo_2Cl_4(PMe_3)_4$,[11] complete the first series for which the structures of homologous chloride, bromide and iodide-containing dimers are known. The important bond distances and bond angles of the $Mo_2X_4P_4$ cores of $Mo_2Br_4(PMe_3)_4$ and $Mo_2I_4(PMe_3)_4$ are given in Table II. As might be expected, all three compounds possess the idealized D_{2d} molecular symmetry usually found[19] for species of the $M_2X_4L_4$ type (Figure 1). The principal crystallographic difference among these halogen derivatives is that the iodide adduct crystallizes in a lower symmetry space group ($P2_1/c$) than do the isomorphous ($C2/c$) chloride and bromide complexes, although examination of the former's symmetry-unrelated metal-ligand bond distances and bond angles (Table II) shows that its geometry is nonetheless very regular. In fact, even though the crystallographically imposed symmetries of $Mo_2Br_4(PMe_3)_4$ and $Mo_2I_4(PMe_3)_4$ are C_2 and C_s, respectively, the overall deviations of their $Mo_2X_4P_4$ cores from D_{2d} symmetry are quite small.

Comparison of the molecular structures of these halide derivatives of $Mo_2X_4(PMe_3)_4$ affords an interesting opportunity to gauge the effects on the metal-metal bond of systematic steric and inductive perturbations by these ligands. The average bond distances and bond angles of $Mo_2X_4(PMe_3)_4$ are listed in Table IIIa. Most noteworthy is the fact that the metal-metal distances of these species are independent of the nature of X across this series, spanning a range of only 0.005Å. These distances are comparable to those of the related $Mo_2Cl_4(SMe_2)_4$[20]

Figure 1. The molecular structure of the $Mo_2X_4(PMe_3)_4$ complexes, taken from the parameters for X = Br. This view, drawn by ORTEP, represents the projection of the structure onto the (101) face of the crystal.

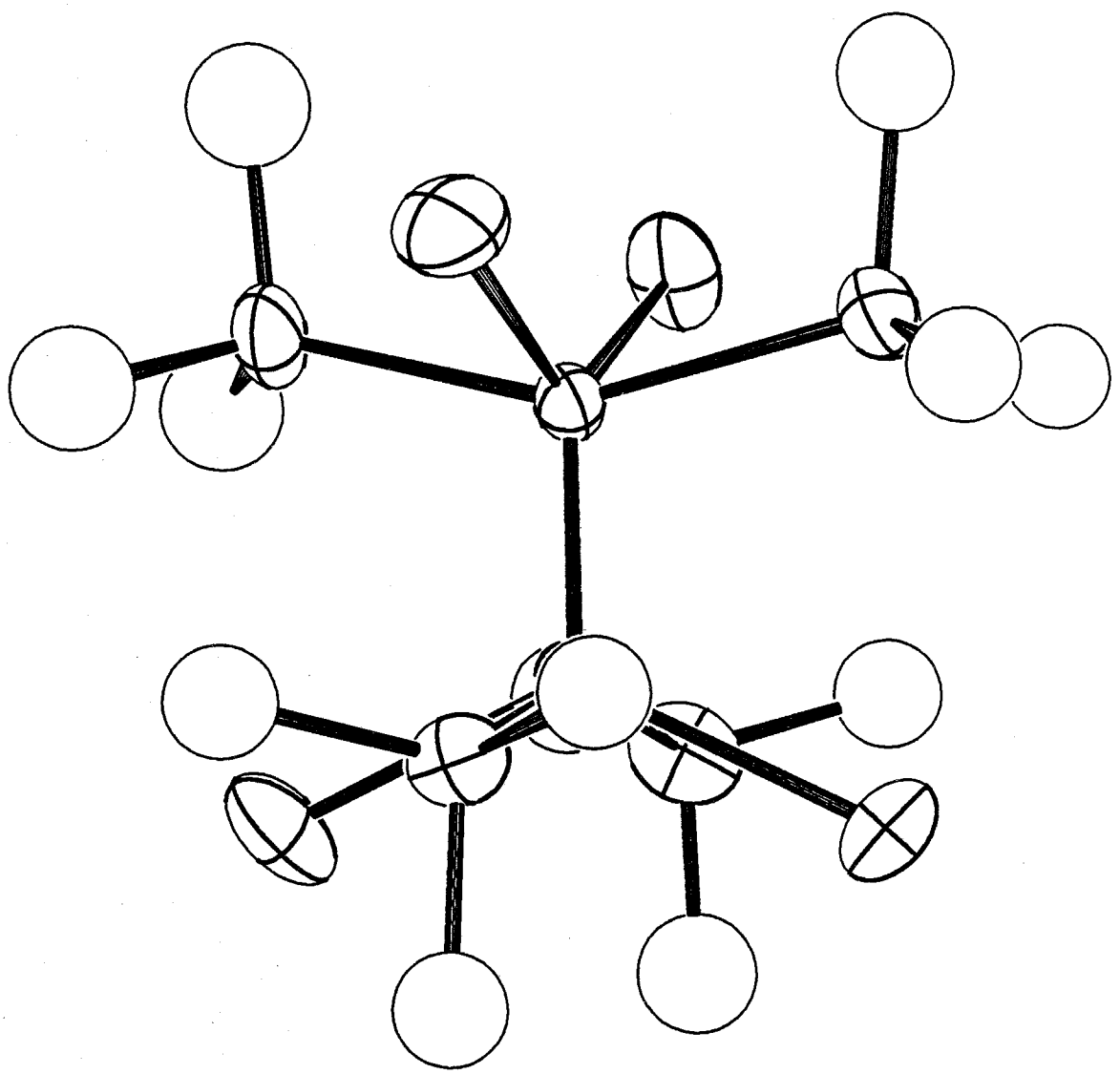

Table II. Bond Distances and Bond Angles of the $Mo_2X_4P_4$ Cores of $Mo_2Br_4(PMe_3)_4$ and $Mo_2I_4(PMe_3)_4$.

Bond Distances

Atom	Atom	Distance (Å) X = Br	X = I
Mo1	Mo2	2.125(1)	2.127(1)
Mo1	X1	2.547(1)	2.755(1)
Mo1	X2	--	2.732(1)
Mo1	P1	2.553(2)	2.568(2)
Mo1	P2	--	2.570(2)
Mo2	X3	2.551(1)	2.762(1)
Mo2	X4	--	2.753(1)
Mo2	P3	2.540(2)	2.559(2)
Mo2	P4	--	2.564(3)

Bond Angles

Atom	Atom	Atom	Angle (deg) X = Br	X = I
Mo2	Mo1	X1	113.65(3)	115.5(1)
		X2	--	114.7(1)
		P1	102.60(5)	103.5(1)
		P2	--	103.6(1)
Mo1	Mo2	X3	113.34(3)	115.5(1)
		X4	--	114.8(1)
		P3	102.91(4)	103.2(1)
		P4	--	103.7(1)

Table III. Average Bond Distances and Bond Angles of Selected $Mo_2X_4L_4$ Complexes

		Distances (Å)			Angles (deg)		Ref.
X	L	M-M	M-X	M-L	MMX	MML	
(a)							
Cl	PMe_3	2.130(0)	2.414(1)	2.545(1)	112.2(1)	102.3(1)	11
Br	PMe_3	2.125(1)	2.549(1)	2.547(2)	113.5(1)	102.8(1)	b
I	PMe_3	2.127(1)	2.751(1)	2.565(2)	115.1(1)	103.5(1)	b
(b)							
CH_3	PMe_3	2.153(1)	2.439(5)	2.513(2)	115.3(1)	102.5(5)	21
Cl	SMe_2	2.144(1)	2.404(2)	2.530(2)	108.7(1)	98.4(1)	20
OCH_2-Bu^t	PMe_3	2.209(1)	2.03(2)	2.54(2)	110	a	28

[a] Not reported.

[b] This work.

and $Mo_2(CH_3)_4(PMe_3)_4$[21] compounds (Table IIIb), and are well within the range considered normal for complexes containing the Mo_2^{4+} unit.[1] It is clear from these results that structural accommodation of the increasing interligand repulsion in the series Cl < Br < I does not occur along the metal-metal bond for complexes of this type, instead being reflected solely in their metal-ligand bond distances and bond angles. Specifically, the differences between the lengths of the metal halide bonds in this series are (d(MoBr) - d(MoCl)) = 0.135Å and (d(MoI) - d(MoBr)) = 0.202Å, in reasonable agreement with the corresponding differences between the ionic radii of these halides, namely $r_{Br} - r_{Cl} = 0.15$Å and $r_I - r_{Br} = 0.24$Å.[22] In addition, there are small increases in both the Mo-Mo-X and Mo-Mo-P bond angles in the order Cl < Br < I, although the former only changes by 3° across this series and the latter by slightly over 1°, as well as a small lengthening (0.02Å) of the Mo-P bond of the iodide adduct relative to the chloride and bromide derivatives.[23]

Although the structural insensitivity of the metal-metal bond to the nature of the halogen ligand seems reasonably accounted for by the small perturbations to the metal-ligand environment of these systems, the electronic interpretation of this finding is less straightforward. The electronic structures of the model systems $Mo_2Cl_4(PH_3)_4$ and $W_2Cl_4(PH_3)_4$ have been previously investigated by SCF-Xα-SW calculations.[25] Of primary importance to this discussion is the fact that the metal-localized δ- and π-bonding levels possess, at least at this level of theory, non-negligible halogen orbital character.[26] Given the increasing ligand polarizability in the series Cl < Br < I, it seems very likely that the metal-metal bonding levels of all three derivatives undergo, to quite different extents, strong metal-halide orbital mixing, with increasing ligand-*d*-orbital participation along this series.[27] That metal-ligand π-interactions can be sufficiently strong to influence the extent of metal-metal bonding is demonstrated by $Mo_2(OCH_2Bu^t)_4(PMe_3)_4$[28] (Table IIIb),

whose internuclear separation is the longest known for a dimolybdenum quadruple bond, being nearly 0.1 Å longer than those of the halide derivatives. In this instance, substantial multiple bond character is attributed to the Mo-O bond, with this repolarization of the *d*-electron density of the metals resulting in a significantly weakened metal-metal bond.[28,29] We see no simple explanation for the total absence of such structural changes in the case of the halogen adducts, except to note that less dramatic perturbations of metal-metal overlap may not manifest themselves in the metal-metal bond length. We are currently pursuing this problem further by examining the photoelectron spectrum of $Mo_2Br_4(PMe_3)_4$, in collaboration with Dr. Jennifer C. Green of Oxford University, for the purpose of comparison with that reported[25] for $Mo_2Cl_4(PMe_3)_4$.

Vibrational Spectroscopy.

Several detailed studies of the Raman spectroscopy of the $Mo_2X_8^{4-}$ (X = Cl, Br) ions have demonstrated that these species exhibit strong resonance enhancement of the totally symmetric $\nu_1(Mo_2)$ vibration upon excitation into the $^1(\delta \rightarrow \delta^*)$ absorption band, as is dramatically manifested in the spectra of these complexes by long overtone progressions (up to $11\nu_1$) in this mode.[30-32] Resonance Raman (RR) spectral data have also been reported for over twenty $Mo_2X_4L_4$ complexes,[33-35] and although they display much shorter progressions ($\leq 3\nu_1$) in the $a_1\nu_1(Mo_2)$ mode, this frequency has been clearly identified in every instance, falling in the range ($330 \leq \nu_1 \leq 358$ cm^{-1}). Since for only one of these latter complexes were both the metal-metal distance and its corresponding stretching frequency known, we obtained RR spectra for the structurally characterized $Mo_2X_4(PMe_3)_4$ series in order to facilitate comparisons among these systems. In addition, complementary far-infrared spectra were obtained for $Mo_2Cl_4(PMe_3)_4$ and $Mo_2Cl_4(AsMe_3)_4$ in the range 50 - 500 cm^{-1}.

The RR data for $Mo_2X_4(PMe_3)_4$ and $Mo_2Cl_4(AsMe_3)_4$ obtained upon excitation into their $^1(\delta \rightarrow \delta^*)$ absorption bands (*vide infra*) are given in Table IV.[36] In benzene solution the extremely strong $a_1\nu_1(Mo_2)$ fundamental for the chloride, bromide, and iodide derivatives of $Mo_2X_4(PMe_3)_4$ is observed at 355, 352, and 343 cm^{-1}, respectively, and that for $Mo_2Cl_4(AsMe_3)_4$ is seen at 356 cm^{-1}. In each instance, two or three overtones of this mode are also observed. The bands attributable to ν_1 are polarized, with the depolarization ratios of the fundamental of this mode for $Mo_2Cl_4(PMe_3)_4$ and $Mo_2Br_4(PMe_3)_4$ being $\rho = 0.33$ and 0.34, respectively, upon excitation at 514.5 nm, in perfect agreement with the value of 1/3 expected for a totally symmetric vibration of a linear oscillator in resonance with an electronic transition between nondegenerate states ($\alpha_{zz} >> \alpha_{xz} = \alpha_{yy}$).[37] RR spectra obtained of polycrystalline samples of these four complexes at low temperature are qualitatively similar to their solution counterparts, and although they display more, and sharper bands, corresponding features between the two sets of spectra seldom differ in frequency by greater than 1 cm^{-1}. The most noticeable improvement in the quality of these spectra arises from a red shift of the fluorescence background, allowing longer overtone progressions in ν_1 to be observed. The low temperature RR spectrum of polycrystalline $Mo_2Br_4(PMe_3)_4$ (Figure 2) is typical in this regard, showing the sharp fundamental at 352.9 cm^{-1}, along with five overtones before the onset of fluorescence. Calculation of the harmonic frequency and anharmonicity constant for this compound from the frequencies of $1\nu_1$-$5\nu_1$ indicates that this vibration is highly harmonic, these values being $\omega_{11} = 352.6$ cm^{-1} and $\chi_{11} = -0.2$ cm^{-1}, respectively. While comparable data for other $Mo_2X_4L_4$ systems have not yet been reported, the magnitude of this anharmonicity is in good agreement with those of the $Mo_2X_8^{4-}$ ions,[31,32] and is probably typical for the metal-metal vibrations of the $Mo_2X_4L_4$ class as a whole.

Table IV. Solid State Resonance Raman and Far-Infrared Data for $Mo_2X_4L_4$ Complexes.[a]

Fundamentals							
$Mo_2Cl_4(AsMe_3)_4$		$Mo_2Cl_4(PMe_3)_4$		$Mo_2Br_4(PMe_3)_4$		$Mo_2I_4(PMe_3)_4$	
Raman[c,d]	Infrared	Raman[b,e,f]	Infrared	Raman[b,e]		Raman[b,f,g]	
A1. 107m	81m	A2. 108w	87m	A3. 106w		A4. 105w	(νMoI)
B1. 123m	89w	B2. 134m	122m	B3. 159m	(νMoBr)	B4. 148w	
C1. 152w	111m	C2. 153w	131m	C3. 209w		C4. 183w	
D1. 217w	(νMoAs)	D2. 185w	182m	D3. 228w		D4. 207m	
E1. 278m[h]	(νMoCl)	E2. 215w	230m (νMoP)	E3. 235w	(νMoP)	E4. 219w	
F1. 337w	208m (νMoAs)	F2. 235w	(νMoP)	267w (δCPC)	F3. 270w	F4. 248m	(νMoP)
G1. 358vs[h]	(νMo$_2$)	223m (δCAsC)	G2. 260w	285s (νMoCl)	G3. 278w	G4. 275w	
H1. 591m	(νAsC)	239m (δCAsC)	H2. 282w	328s (δCPC)	H3. 298w	H4. 286w	
I1. 610m	(νAsC)	288s (νMoCl)	I2. 274w[h]	(νMoCl)	I3. 337w	I4. 343w[h]	(νMo$_2$)
J1. 818w	(νAsC)	338s (νMoCl)	J2. 338m[h]		J3. 352w[h]	(νMo$_2$)	J4. 728w (νPC)
K1. 1448w	(δCH$_3$)		K2. 355vs[h]	(νMo$_2$)	K3. 740w	(νPC)	K4. 737w (νPC)
			L2. 748w	(νPC)			

Resonance Raman Overtones and Combinations

466 (G1+A1)	450	483	441 (I4+A4)
478[h](G1+B1)	478	510 (J3+B3)	487 (I4+B4)
510 (G1+C1)	507 (K2+C2)	802	500 (I4+C4)
535[h](G1+E1)	550	820 (J3+F3)	553 (I4+D4)
710[h](2G1)	618	875 (J3+I3)	597
815 (2G1+A1)	635	708[h](2J3)	683[h](2I4)
832 (2G1+B1)	710[h](2K2)	785	782 (2I4+A4)
855 (2G1+C1)	1060[h](3K2)	808	845 (2I4+C4)
990 (2G1+E1)		950	892 (2I4+D4)
1063[h](3G1)		967 (2J3+F3)	1045[h](3I4)
1153		1023	
1173 (3G1+A1)		1056[h](3J3)	
1187		1293	
1205		1405 (4J3)	
1218		1515	
1263		1532	
1310		1580	
1328		1800	
1368		1652	
∿1410[h](4G1)		1755 (5J3)	
		∿2105 (6J3)	

[a] Frequencies are in cm^{-1}. [b] Polycrystalline solid, 20 K. [c] KCl pellet, 300 K. [d] λ_{ex} = 514.5 nm. [e] λ_{ex} = 520.8 nm. [f] λ_{ex} = 530.9 nm. [g] λ_{ex} = 568.2 nm. [h] Also observed in benzene solution at room temperature.

Figure 2. Raman spectrum of polycrystalline $Mo_2Br_4(PMe_3)_4$ at ca. 20K (λ_{ex} = 530.9 nm). The peak marked with an asterisk is a laser plasma line.

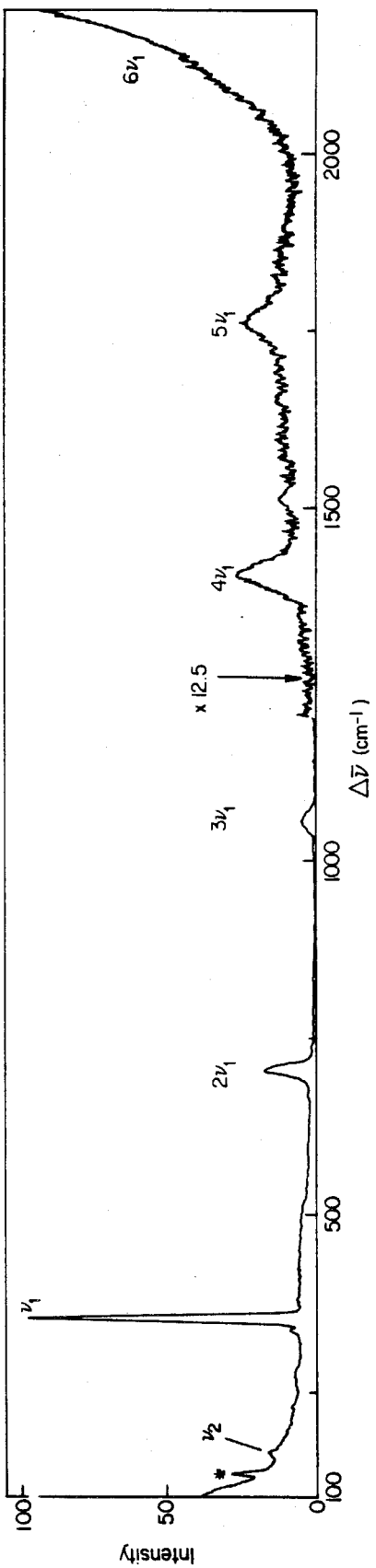
Intensity
100
50
0
100
500
1000
1500
2000
$\Delta\bar{\nu}$ (cm^{-1})
ν_1
ν_2
*
$2\nu_1$
$3\nu_1$
x 12.5
$4\nu_1$
$5\nu_1$
$6\nu_1$

In addition to displaying bands attributable to the $a_1\nu_1(Mo_2)$ mode, the RR spectra of these complexes contain a number of lines arising from both metal-ligand and ligand-localized vibrations (Table IV). Few of these bands are very intense, however, and most are observed only in the solid state spectra; in the absence of depolarization ratios and isotopic shift data, definitive assignments for these modes cannot, for the most part, be offered here, nor have they been assigned in previous studies of these complexes.[33-35] The solid state RR spectrum of $Mo_2Cl_4(AsMe_3)_4$, reproduced in Figure 3, illustrates the low intensity of these bands relative to ν_1. The band at 278 cm^{-1} in this spectrum, which is the most intense of the low frequency lines, and one of comparable intensity observed for $Mo_2Cl_4(PMe_3)_4$ at ~274 cm^{-1}, are assigned to the totally symmetric metal-halide stretch ($a_1\nu_2(MoX)$) by analogy to the assignment for $Mo_2Cl_8^{4-}$, whose various salts display this band between 270-280 cm^{-1}.[31] Previously unassigned lines reported for $Mo_2Cl_4L_4$ (L = PBu^n_3,[33] SMe_2,[34] SEt_2,[34] $AsEt_3$[35]) in the 277-285 cm^{-1}range are probably also attributable to this vibration. The band at 159 cm^{-1} in the spectrum of $Mo_2Br_4(PMe_3)_4$ (Figure 2), while slightly weaker than its counterparts in the chloride spectra, is similarly assigned to ν_2; the corresponding frequency for $Mo_2Br_8^{4-}$ is 169 cm^{-1},[32] and $Mo_2Br_4(AsEt_3)_4$ shows a weak line at 170 cm^{-1}.[35] As has been observed for the $Mo_2X_8^{4-}$ ions,[31,32] the spectra of both $Mo_2Br_4(PMe_3)_4$ and $Mo_2Cl_4(AsMe_3)_4$ display the combination band of this mode with ν_1, with the latter complex additionally showing a combination tone progressing in ν_1 ($2\nu_1 + \nu_2$; Figure 3).

In contrast to those of the chloride and bromide complexes, the RR spectrum of $Mo_2I_4(PMe_3)_4$ displays only weak lines of nearly equal intensity in the low frequency region.[38] Comparing the M-X frequencies of $Re_2X_8^{2-}$ [39] to those of $Mo_2Cl_4L_4$ and $Mo_2Br_4(PMe_3)_4$ and extrapolating to $Mo_2I_4(PMe_3)_4$ yields a value of ca. 110 cm^{-1} for $a_1\nu_1(MoI)$. The only RR mode near this frequency for $Mo_2I_4(PMe_3)_4$

Figure 3. Raman spectrum of a KCl pellet of $Mo_2Cl_4(AsMe_3)_4$ at room temperature (λ_{ex} = 514.5 nm).

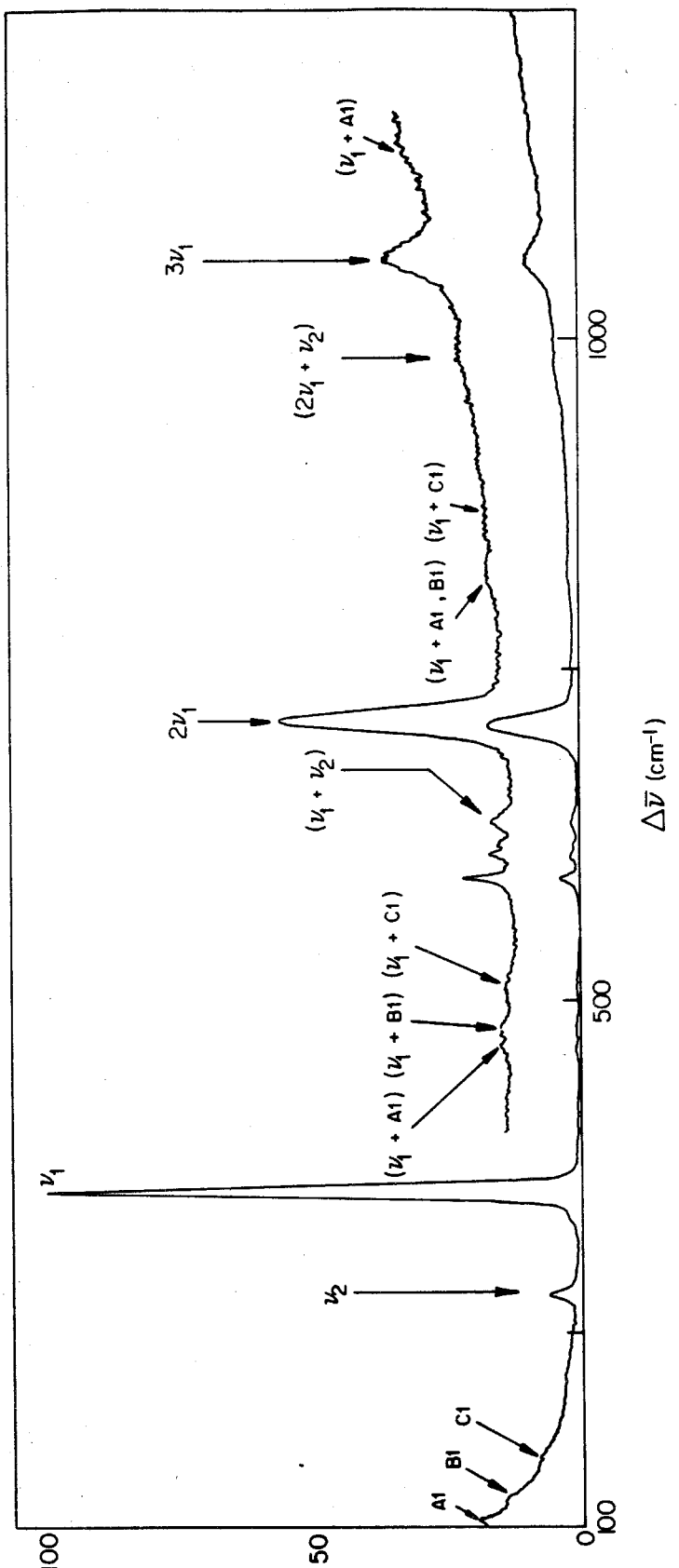
Intensity
100
50
0
100
500
1000
$\Delta\bar{\nu}$ (cm^{-1})
A1
B1
C1
ν_2
ν_1
$(\nu_1 + A1)$ $(\nu_1 + B1)$ $(\nu_1 + C1)$
$(\nu_1 + \nu_2)$
$2\nu_1$
$(\nu_1 + A1, B1)$ $(\nu_1 + C1)$
$(2\nu_1 + \nu_2)$
$3\nu_1$
$(\nu_1 + A1)$

is at 105 cm^{-1} (Table IV). While peaks at similar frequencies also occur in the chloride and bromide derivatives, the 105-cm^{-1} mode of $Mo_2I_4(PMe_3)_4$ is unique among the $Mo_2X_4(PMe_3)_4$ complexes in that it forms combination tones with the ν_1 progression ($\nu_1 + 105$ and $2\nu_1 + 105$), as observed for the Mo-X stretches in other $Mo_2X_4L_4$ complexes, and in the spectra of quadruply bonded halide complexes in general.[30–35] Therefore, we assign the 105-cm^{-1} peak as $a_1\nu_2$(MoI).[40]

Considering only the $Mo_2X_4L_4$ core and ignoring modes associated with the CLC and CH_3 structures, 18 normal modes are predicted for these complexes in D_{2d} symmetry ($5a_1 + a_2 + 2b_1 + 4b_2 + 6e$), one of which ($a_2$) is Raman and infrared silent. The remaining 17 are all, in principle, Raman active, while only ten ($4b_2 + 6e$) are infrared active. The far-IR spectra of $Mo_2Cl_4(AsMe_3)_4$ and $Mo_2Cl_4(PMe_3)_4$ display ten and nine modes, respectively (Table IV, Figure 4). Tentative assignments for these modes, derived from comparisons within the $M_2X_4L_4$ series as well as to other systems,[41] are summarized in Table V. Modes that cannot be assigned specifically include angle bends (δMoMoCl, δMoMoL, and δClMoL) between 100 and 200 cm^{-1} and torsional modes below 100 cm^{-1}. Interestingly, although all of the IR-active modes are, in principle, Raman allowed, with few exceptions an effective exclusion relationship appears to be operating for the IR and Raman fundamentals in these complexes.

With respect to drawing structural conclusions from comparisons of the vibrational frequencies of these complexes, it should be noted that the fact that the $Mo_2X_4(PMe_3)_4$ complexes display different frequencies for ν_1, even though they possess a single metal-metal distance, indicates that this vibration is not purely metal-metal stretching in nature, in contrast to the situation found for $Mo_2(O_2CCH_3)_4$ (which is nearly pure ν(MM)).[42] The primary reason for the difference in mode localization among the $Mo_2X_4L_4$ and $Mo_2(O_2CR)_4$ complexes is

Figure 4. FT-far-infrared spectra of a nujol mull of $Mo_2Cl_4(EMe_3)_4$ at room temperature: (a) E = As; (b) E = P. Peaks marked with an asterisk are due to polyethylene.

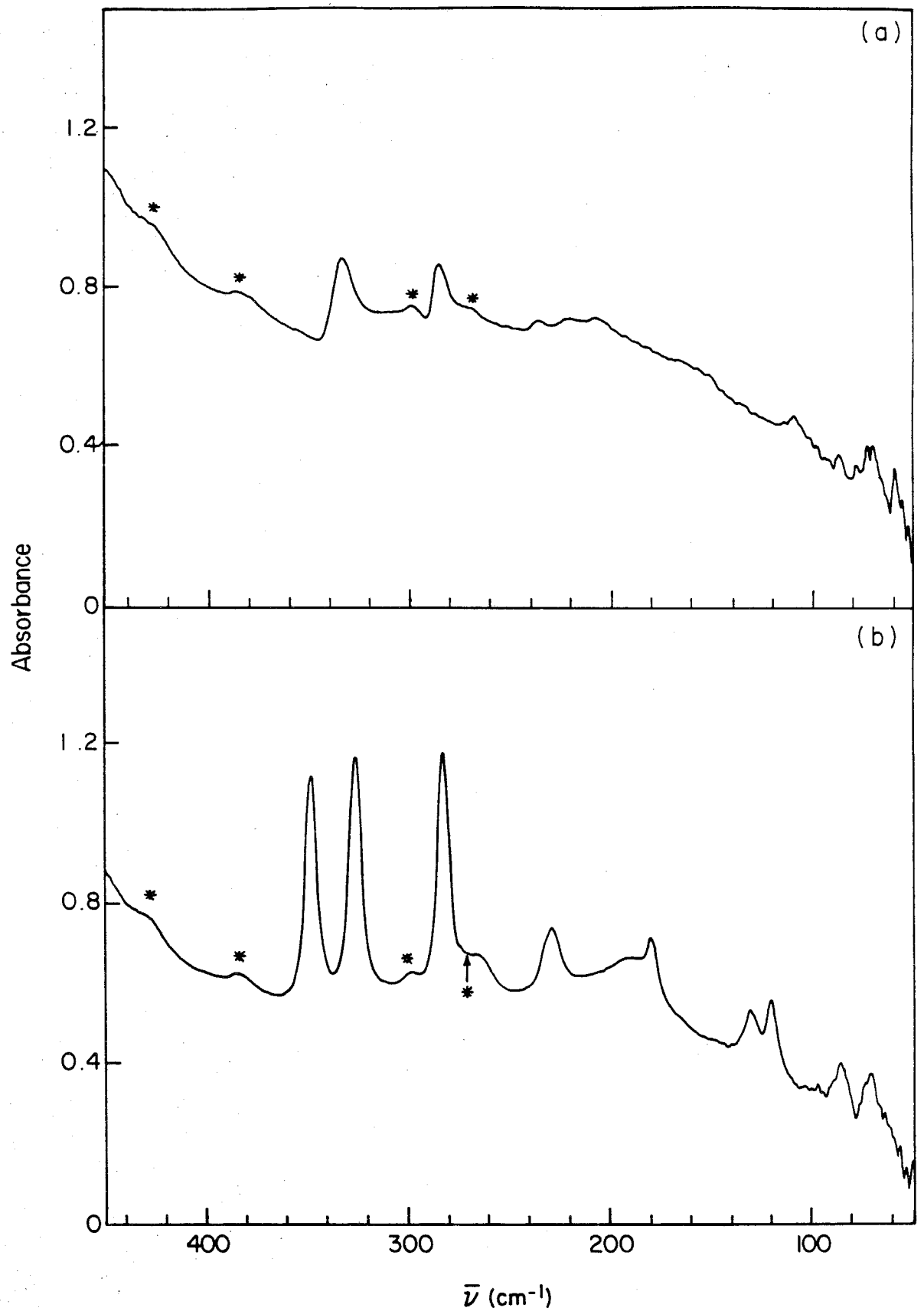
(a)
(b)
1.2
0.8
0.4
0
Absorbance
400
300
200
100
$\bar{\nu}$ (cm^{-1})

Table V Proposed Assignment of Selected Fundamental Vibrations of $Mo_2X_4L_4$ Complexes.

Mode	Frequency/cm^{-1}			
	$Mo_2Cl_4(AsMe_3)_4$	$Mo_2Cl_4(PMe_3)_4$	$Mo_2Br_4(PMe_3)_4$	$Mo_2I_4(PMe_3)_4$
$b_2\nu$(MoL) (IR)	209	230		
$a_1\nu$(MoL) (R, ν_3)	217	235	235	248
$a_1\nu$(MoX) (R, ν_2)	278	274	159	105
$b_2\nu$(MoX) (IR)	288	285		
$e\nu$(MoX) (IR)	336	350		
δ(CLC) (IR)	223	267		
δ(CLC) (IR)	239	328		
$a_1\nu(Mo_2)$ (R, ν_1).	356	355	352	343
ν(CL) (R)	591			
ν(CL) (R)	610			720
ν(CL) (R)	618	746	740	737
$\delta(CH_3)$ (R)	1448			

undoubtedly structural in origin; as suggested by normal coordinate analyses,[43] **G** matrix mixing of metal-metal and metal-ligand modes will be very small for metal-metal-ligand bond angles near 90°, such as those found in the carboxylate systems,[1] while coupling between ν_1 and the totally symmetric ν(MoX, MoL) and $\delta(MoX_2, MoL_2)$ modes should be substantially larger for bond angles on the order of those found for the $Mo_2X_4(PMe_3)_4$ species.[43] Viewed in this light, the range of ν_1 frequencies (12 cm^{-1}) and diatomic metal-metal force constants (k = 5.9 x 10^{-7} $\mu\nu^2$ mdyne/Å; X = Cl, k = 3.54; X = I, k = 3.31 mdyne/Å) spanned by the $Mo_2X_4L_4$ series is not surprising given the large dependence on the mass of X of the frequencies of the metal-ligand modes of these species. Comparisons of ν_1 and k for $M_2X_4L_4$ complexes are thus probably meritorious only for restricted subsets of these complexes; while it is undoubtedly safe to infer that $Mo_2Cl_4(PMe_3)_4$ (ν_1 = 355 cm^{-1}), $Mo_2Cl_4(AsMe_3)_4$ (356 cm^{-1}), and $Mo_2Cl_4(SMe_2)_4$ (358 cm^{-1})[34] have very similar metal-metal distances based on the closeness of their values of ν_1, it is unlikely that such comparisons between complexes containing different ligand sets, or for homologous complexes of different metals,[44] yield meaningful information regarding the relative metal-metal bonding in these systems.

Electronic Spectroscopy.

The room temperature solution spectra of $Mo_2X_4(PMe_3)_4$ and $Mo_2Cl_4(AsMe_3)_4$ are reproduced in Figure 5, and that of $W_2Cl_4(PMe_3)_4$ is shown in Figure 6. The visible absorption region of each spectrum displays three distinct band systems: two strong absorptions, which will be discussed shortly and are labeled I and II, and a weak cluster of bands located between I and II (Figure 7).[45] To higher energy of band II, these spectra display a pattern of absorptions too complex to allow simple correlations between individual bands in the absence of a more detailed spectroscopic study. These transitions remain unassigned at this

Figure 5. Electronic absorption spectra of $Mo_2X_4L_4$ in 2-methylpentane solution at room temperature: (a) X = Cl, L = PMe_3 (—); X = Cl, L = $AsMe_3$ (- - -); (b) X = Br, L = PMe_3; (c) X = I, L = PMe_3.

Figure 6. Electronic absorption spectra of $M_2Cl_4(PMe_3)_4$ in 2-methylpentane solution at room temperature: M = Mo (- - -); M = W (—).

Figure 7. Electronic absorption spectra of $Mo_2X_4(PMe_3)_4$ in 2-methylpentane solution at room temperature in the region of the weak visible absorption bands: X = Cl (- · -); X = Br (- - -); X = I (—).

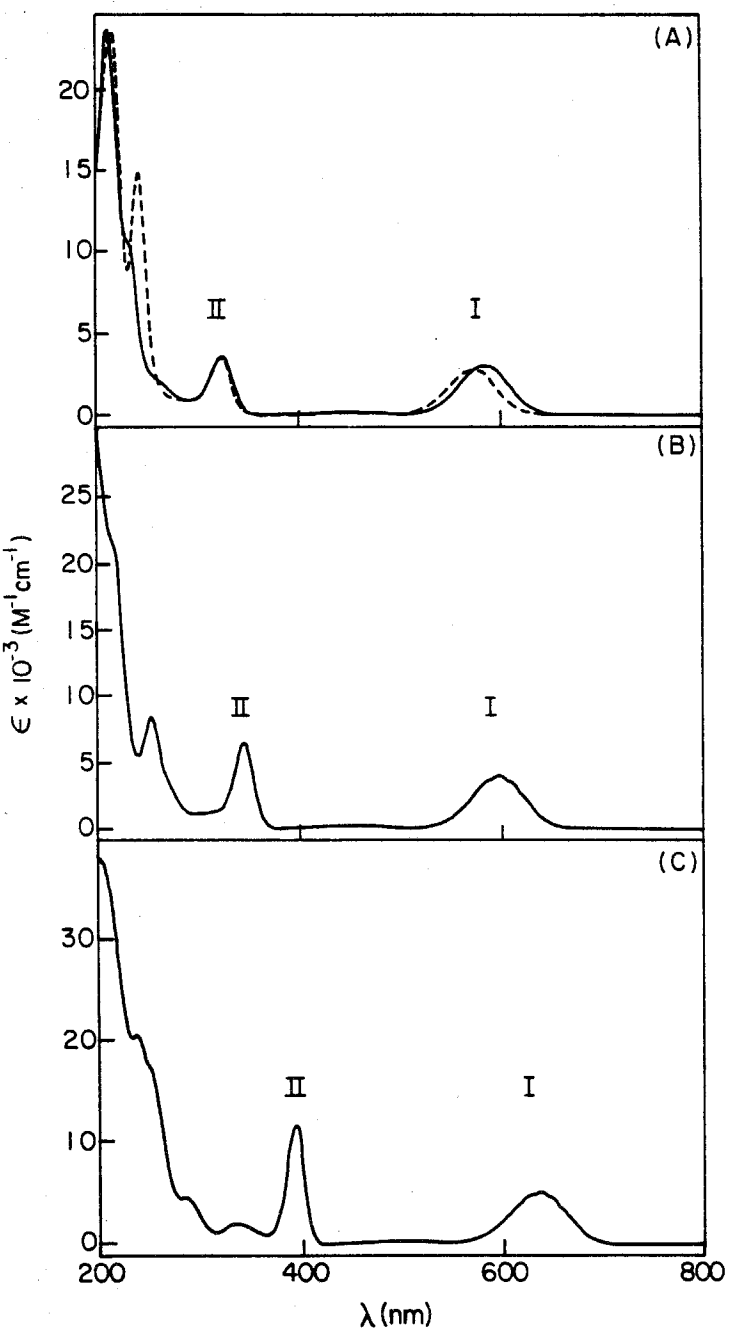
(A)
(B)
(C)
II
I
20
15
10
5
0
25
30
200
400
600
800
λ (nm)
ε x 10⁻³ (M⁻¹cm⁻¹)

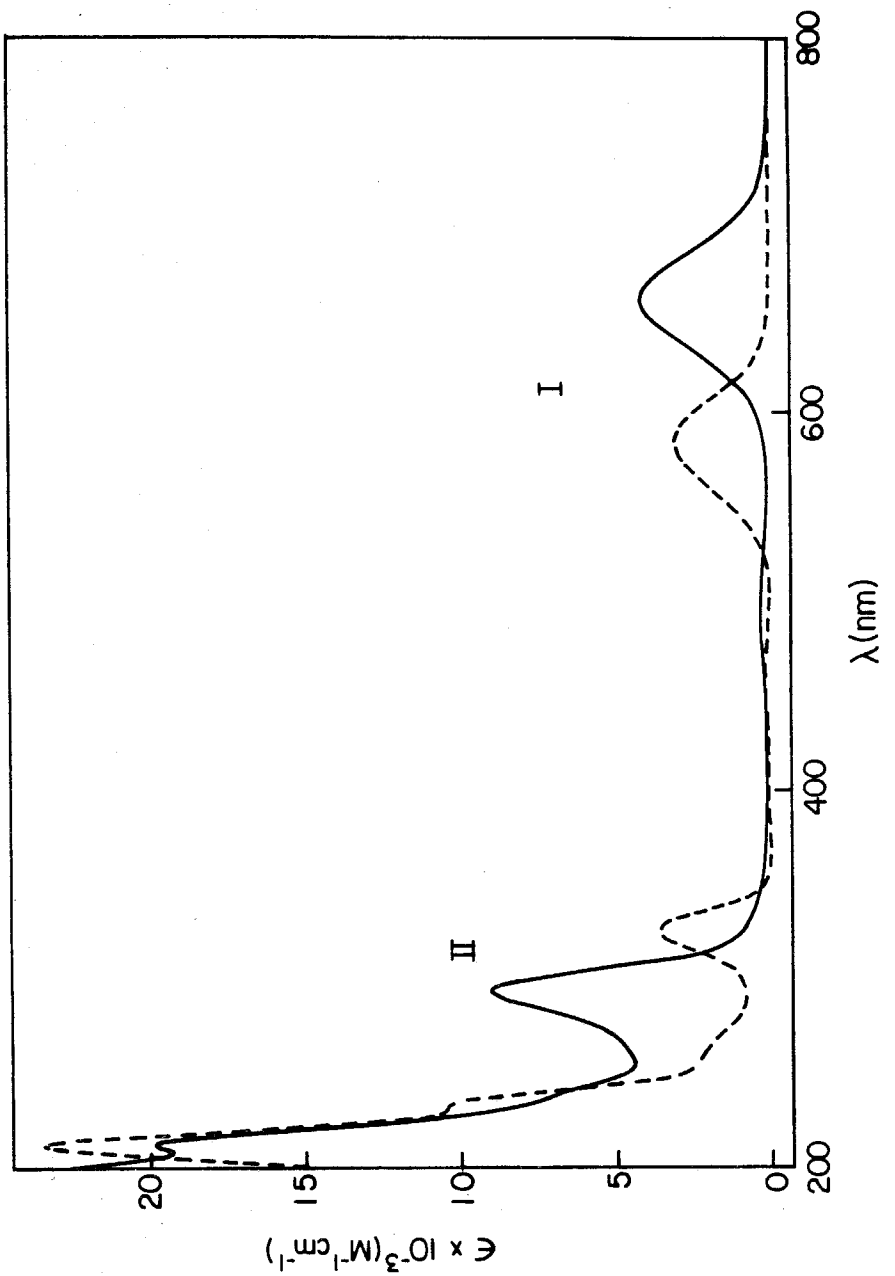
ε x 10⁻³(M⁻¹cm⁻¹)
20
15
10
5
0
200
400
600
800
λ(nm)
I
II

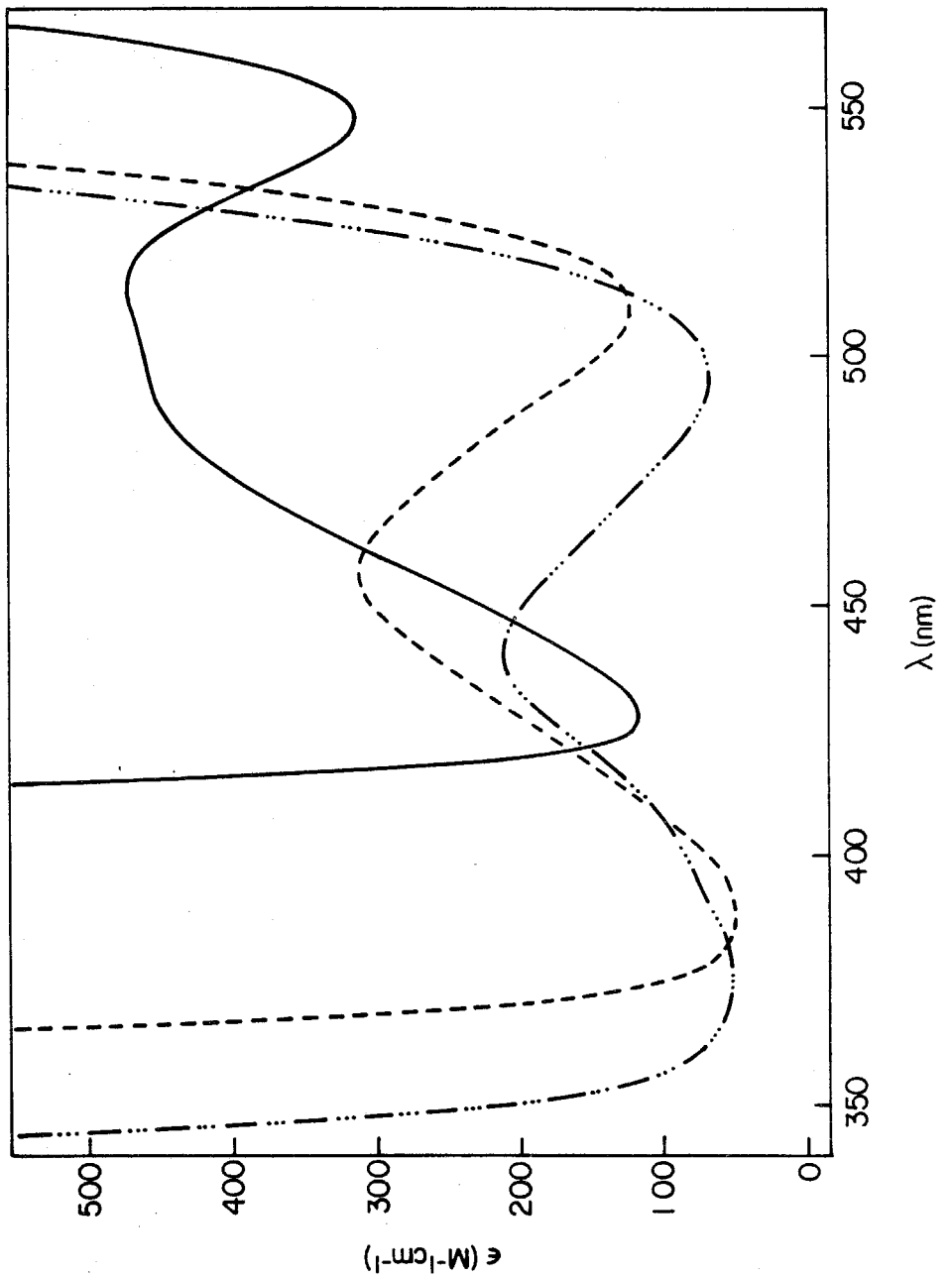
500
400
300
200
100
0
ε (M⁻¹cm⁻¹)
350
400
450
500
550
λ (nm)

time, although we note that the similarity of the UV spectra of $Mo_2Cl_4(PMe_3)_4$ and $Mo_2Cl_4(AsMe_3)_4$, as well as the increasing complexity in this region according to Cl < Br < I, is undoubtedly a reflection of the lowering in energy of the numerous X → M charge transfer transitions that these species should possess. The intense, metal-metal-localized $^1(\pi \rightarrow \pi^*)$ transition presumably also lies in this energy region.[46]

The energies and extinction coefficients of bands I and II for $Mo_2X_4(PMe_3)_4$ and $Mo_2Cl_4(AsMe_3)_4$ are summarized in Table VIa. Band I of $Mo_2X_4L_4$ has been conclusively assigned to the $^1(\delta \rightarrow \delta^*)$ transition on the basis of a detailed spectroscopic study.[4] What is noteworthy in the context of the current discussion is that this band displays a marked sensitivity to the nature of ligand X, systematically both red-shifting and increasing in intensity for $Mo_2X_4(PMe_3)_4$ according to Cl < Br < I. The extinction coefficient of this band for $Mo_2I_4(PMe_3)_4$ is substantially larger than any previously reported for a quadruply bonded complex.[47] Band I is relatively insensitive to ligand L, in contrast, displaying similar intensities for the PMe_3, $AsMe_3$ (Table VIa), and PBu^n_3 (Table VIb) adducts of $Mo_2Cl_4L_4$; the spectra of the two phosphine derivatives are virtually superimposable, in fact, while the arsine complex displays a slight blue shift. Finally, the $^1(\delta \rightarrow \delta^*)$ absorption both red-shifts (1940 cm^{-1}) and increases in intensity upon going from $Mo_2Cl_4(PMe_3)_4$ to $W_2Cl_4(PMe_3)_4$ (Figure 6, Table VIb). Band II displays relative sensitivities toward X and L for $Mo_2X_4L_4$ similar to those observed for band I, although its dependence on X is much greater than that of $^1(\delta \rightarrow \delta^*)$. Specifically, the red shift of band II across the Cl, Br, I series is 5540 cm^{-1}, which is four times greater than that for band I. In addition, the extinction coefficient of this band triples as a result of this perturbation, while that of band I increases, in comparison, by ~60% . The full-width-at-half-maximum (fwhm), which is independent of halide for the

Table VI. Electronic Absorption Data for $M_2X_4L_4$ Complexes.[a]

Compound	Band I [$^1(\delta\rightarrow\delta^*)$]			Band II [LMCT]		ref
	$\bar{\nu}$/cm^{-1}	ϵ/M^{-1} cm^{-1}	f	$\bar{\nu}$	ϵ	
(a)						
$Mo_2Cl_4(AsMe_3)_4$	17420	2970	.023	30960	3630	b
$Mo_2Cl_4(PMe_3)_4$	17090	3110	.024	30860	3720	b
	370			1870		
$Mo_2Br_4(PMe_3)_4$	16720	4060	.030	28990	6650	b
	1000			3670		
$Mo_2I_4(PMe_3)_4$	15720	5250	.040	25320	11850	b
(b)						
$Mo_2Cl_4(PBu^n_3)_4$	17040	3150	.026	30490	3830	5
$W_2Cl_4(PMe_3)_4$	15150	4170	.028	34130	9090	b
$W_2Cl_4(PBu^n_3)_4$	15020	4240	.028	33730	9850	b
β-$Mo_2Cl_4(dmpe)_2$	12450	210	.0018	29150	3660	56

[a]Bands I and II are shown in Figure 5. [b]This work.

$^1(\delta \rightarrow \delta^*)$ transition, decreases significantly across this series: X = Cl, fwhm = 2600; X = Br, 2030; X = I, 1420 cm^{-1}. As is observed for band I, though, band II is little affected by the nature of L, again as illustrated by the close similarity of the $Mo_2Cl_4L_4$ (L = PMe_3, PBu^n_3, $AsMe_3$) spectra. On substitution of tungsten for molybdenum in $M_2Cl_4(PMe_3)_4$, band II increases in intensity by 2.5 times and, in contrast to band I, blue-shifts 3270 cm^{-1} (Figure 6).

The large difference in the sensitivity of the position, intensity, and width of band II toward X relative to that of the $^1(\delta \rightarrow \delta^*)$ transition suggests that this band, in contrast, is not attributable to a transition between orbitals associated with the metal-metal bond framework. Instead, the red shift of this band across the Cl, Br, I series, and its blue shift for the Mo→W perturbation, is entirely consistent with its assignment to an LMCT transition. The lowest energy transition of this type predicted by SCF-Xα-SW and LCAO-HFS transition-state calculations on $Mo_2Cl_4(PH_3)_4$[25,49] and $W_2Cl_4(PH_3)_4$[25] is σ(M-P)→ $\delta^*(M_2)$ in both instances. This is not an unreasonable assignment for these complexes given the close similarity of this band for $Mo_2Cl_4(PMe_3)_4$ and $Mo_2Cl_4(AsMe_3)_4$ [50] and the relative weakness of the Mo-P bond,[23] as well as the fact that the red shift of the lowest-lying $\pi(X)\rightarrow \delta^*(M_2)$ absorption of $Re_2X_8^{2-}$ along this series (Cl→Br: 7000; Br→I: 9000 cm^{-1})[39,46] is substantially larger than that seen for $Mo_2X_4(PMe_3)_4$ (Table VIa). The strong perturbation of the energy and intensity of this absorption upon exchanging bromide or iodide for chloride suggests, however, that this excited state increasingly mixes with X→M states along this series,[26] with $\pi(X)\rightarrow \delta^*(Mo_2)$ perhaps becoming the dominant contributor to the lowest energy charge transfer state of the iodide complex.

The Energies and Intensities of $^1(\delta \rightarrow \delta^*)$ Transitions.

The most obvious question to arise from consideration of the spectral data of

the $Mo_2X_4(PMe_3)_4$ series is why the close similarity of the metal-metal bonding in these complexes that is suggested by their crystal structures is not reflected in the energies and intensities of their $^1(\delta \rightarrow \delta^*)$ transitions. The energy and intensity of this band must reflect, for a given complex, the extent of δ-bonding in that system inasmuch as the magnitudes of these parameters are determined in part by the energetic splitting of the one-electron δ and δ^* levels and the square of the δ-overlap, respectively:[46] Can comparisons of these parameters for different complexes, such as the $Mo_2X_4(PMe_3)_4$ series, provide a more sensitive measure of small differences in δ-bond strength than does the metal-metal distance, or is this electronic transition influenced by effects not associated with metal-metal bonding?

There have been two previous attempts at correlating one or both of these spectral parameters with the extent of δ-bonding in quadruply bonded complexes. Sattelberger and Fackler (SF),[51] and subsequently other workers,[11,32,52,53] pointed out a nearly linear relationship between the metal-metal bond distance and the energy of the $^1(\delta \rightarrow \delta^*)$ band in several limited series of complexes. Specifically, those complexes with shorter metal-metal bonds, and thus presumably larger δ-overlaps, were observed to have higher energy $^1(\delta \rightarrow \delta^*)$ absorptions than did species with longer metal-metal bonds. A second, more comprehensive interpretation of the overall spectral behavior of these systems was offered by Manning and Trogler (MT).[48] Based on a valence-bond approach, these workers proposed that an increase in δ-overlap should result in a red shift of the $^1(\delta \rightarrow \delta^*)$ transition and a concomitant increase in its intensity. MT noted that overall, the spectral parameters of all quadruply bonded dimers formed such a trend: $^1(\delta \rightarrow \delta^*)$ bands at energies of greater than ~18000 cm^{-1} were relatively weak ($\epsilon < 500$), and those at lower energies (~15-17000 cm^{-1}) were relatively intense ($1000 \leq \epsilon \leq 3500$).[47] That this general trend in spectroscopic behavior was, in fact, a manifestation of the magni-

tude of δ-overlap in these complexes was argued by pointing out that those species with the lowest energy and highest intensity absorptions were dimers of third-row transition metals or were complexes containing relatively strongly electron-donating ligands, (e. g., I^-, PR_3, CH_3^-), while high energy, low intensity $^1(\delta \rightarrow \delta^*)$ bands were found for complexes with "hard" ligands (^-O_2CR, SO_4^{2-}, H_2O) as well as for chromium dimers; from the standpoint of the effective charge on the dimetal unit, the former complexes would be expected to possess more diffuse atomic orbitals, and hence larger δ-overlaps, than would the latter species. The absence of an overall correlation of spectroscopic energy with metal-metal distance was rationalized by noting that since it is the σ- and π-interactions that largely determine the metal-metal distances found in quadruply bonded dimers, small differences in δ-bonding would not necessarily affect this bond distance.

While both of these proposals seem intuitively plausible, neither approach provides a totally satisfactory interpretation of the spectroscopic behavior of the $Mo_2X_4L_4$ compounds, nor do they appear to allow self-consistent correlations among the spectra of different subgroups of quadruply bonded complexes. Analysis of the electronic spectra of $Mo_2X_4(PMe_3)_4$, first within the MT framework,[48] leads to the conclusion that the 1400-cm^{-1} red shift and 60 % increase in oscillator strength for the Cl, Br, I series is a manifestation of an increase in δ-overlap resulting from this perturbation. A semiquantitative estimate of the change in overlap (S) in this series, calculated[46] from these spectral parameters, yields $S(Mo_2Cl_4(PMe_3)_4) = 0.17$ and $S(Mo_2I_4(PMe_3)_4) = 0.23$; as was noted in the discussion of their molecular structures, some halogen dependence of the δ-bonding in these systems would not be unanticipated in view of the large difference in polarizability between chloride and iodide, and it is reasonable that a change in overlap of the magnitude inferred here would not affect the metal-metal distance. While the electronic structures of

the $Mo_2X_4(PMe_3)_4$ complexes may indeed differ in exactly this manner, there are several pieces of evidence that suggest that such a conclusion cannot be drawn from this analysis of $^1(\delta \rightarrow \delta^*)$ energy and intensity. With respect to the δ-overlap-dependence of the transition energy, it has been previously demonstrated that complexes of the β-$Mo_2X_4(L\text{-}L)_2$ type that possess a bridging-phosphine-induced twisting about the metal-metal-bond axis, and hence reduced δ-overlap relative to eclipsed (0° twist angle) dimers,[54] show a $^1(\delta \rightarrow \delta^*)$ transition that systematically red-shifts, in contrast to the MT prediction, and loses intensity as the extent of δ-interaction decreases.[55,56] For example, the δ-overlap of β-$Mo_2Cl_4(dmpe)_2$ (dmpe = 1,2-bis(dimethylphosphino)ethane; twist angle = 40°) can be inferred to be no greater than 0.2 times that found in its eclipsed "rotamer", $Mo_2Cl_4(PMe_3)_4$;[54,56] the $^1(\delta \rightarrow \delta^*)$ band of the former complex is red shifted 4640 cm^{-1} relative to that of the latter, and is an order of magnitude less intense (Table VI). The fact that the behavior of the spectroscopic parameters for the β-$Mo_2X_4(L\text{-}L)_2$ compounds (intensity decreases as the energy and δ-overlap decrease) runs opposite that observed overall for quadruply bonded dimers[47] (intensity increases as the energy decreases) suggests that the latter trend is probably not a direct manifestation of a variation in δ-interaction among these systems.

Examination of the spectra of the $Mo_2(O_2CR)_4$ systems,[47] which in the MT model should have among the smallest δ-overlaps, further emphasizes the discrepancies in this correlation. Even though the intensity of the $^1(\delta \rightarrow \delta^*)$ band of $Mo_2(O_2CPr^n)_4$ ($\bar{\nu}_{max}$ = 22700 cm^{-1}, $\epsilon \sim 150$ M^{-1} cm^{-1})[57] is lower than that observed for β-$Mo_2Cl_4(dmpe)_2$, the $^2(\delta \rightarrow \delta^*)$ band of the one-electron-oxidized, $(\sigma^2\pi^4\delta^1)$-configured $Mo_2(O_2CPr^n)_4^+$ ion (the energy of which is a direct measure of the splitting of the one-electron δ and δ^* levels in this system) is centered at 13300 cm^{-1},[57] indicating that the energy of the δ/δ^* orbital splitting ($E(\delta/\delta^*)$)

is significantly larger for these species than those calculated for complexes with relatively intense ($\epsilon > 1000$) $^1(\delta \rightarrow \delta^*)$ absorptions ($Mo_2Cl_4(PH_3)_4$, $E(\delta/\delta^*)$ = 8070;[25] $Mo_2Cl_8^{4-}$, 7900 cm^{-1} [58]), as well as those estimated for compounds with "hard" ligands and weak ($\epsilon \sim 150$) absorptions[47] ($Mo_2(SO_4)_4^{4-}$: $E(\delta/\delta^*)$ = 8500; $Mo_2(SO_4)_4^{3-}$: 7150 cm^{-1});[59] it is also in good agreement with theory ($Mo_2(O_2CH)_4$: $E(\delta/\delta^*)$ = 12180 cm^{-1}).[3] Thus, the intensity of the $^1(\delta \rightarrow \delta^*)$ transition is clearly not directly proportional to $E(\delta/\delta^*)$.

Although the foregoing discussion indicates that the $^1(\delta \rightarrow \delta^*)$ energy tends to increase in tandem with δ-overlap, the above examples also show that this relationship is not as straightforward as the spectroscopic correlations pointed out by SF and others might suggest. These workers noted, for instance, that the red shift of this band (5200 cm^{-1}) for the $M_2(CH_3)_8^{n-}$ (M = Cr, Mo, Re, W)[51,52] complexes was monotonic with increasing bond distance ($\Delta d(W_2 - Cr_2)$ = 0.28 Å), in keeping with the notion that longer metal-metal distances imply relatively weaker δ-interactions. This $^1(\delta \rightarrow \delta^*)$ energy range is larger, however, than that found for $Mo_2Cl_4(PMe_3)_4$ and β-$Mo_2Cl_4(dmpe)_2$ (4640 cm^{-1}, Table VI), for which the corresponding difference in δ-overlap is known to be formally a factor of five,[54-56] as well as for $Mo_2(O_2CPr^n)_4$ and $Mo_2(SO_4)_4^{4-}$ (3300 cm^{-1}),[47] whose one-electron-oxidized counterparts ($Mo_2(O_2CPr^n)_4^+$ and $Mo_2(SO_4)_4^{3-}$: *vide supra*) differ by nearly a factor of two in $E(\delta/\delta^*)$. From these data, the difference in δ-overlap between $W_2(CH_3)_8^{4-}$ and $Cr_2(CH_3)_8^{4-}$ that is inferred by the SF correlation appears to be unrealistically large for such closely related species. Furthermore, the fact that sizeable spectroscopic shifts are observed between complexes that have very similar values of $E(\delta/\delta^*)$ (e.g., $Mo_2Cl_8^{4-}$, $Mo_2Cl_4(PMe_3)_4$)[60] , as well as for those that have nearly identical metal-metal distances (e.g., $Mo_2X_4(PMe_3)_4$), suggests that this relationship of $^1(\delta \rightarrow \delta^*)$ energy to metal-metal distance is not likely

to yield direct information about differences in δ-bonding among these systems.[61]

In formulating an answer to the question posed at the outset of this discussion, it is now clear that while the energy and intensity of the $^1(\delta \rightarrow \delta^*)$ band correlate well with δ-overlap in a few limited series of complexes, such as the torsionally distorted β-$Mo_2X_4(L\text{-}L)_2$ species, there are also numerous inconsistencies, the most notable of which appear to occur when comparisons, particularly of intensities, are attempted among complexes with different ligand sets. We initially noted that these spectral parameters reflect, to some extent, the magnitude of this metal-metal interaction for a given compound; the question raised by the preceding arguments thus concerns the origin of those contributions to the energy, and especially the intensity, of this transition that distort such spectroscopic correlations among complexes. While the data discussed herein do not, in general, corroborate the MT hypothesis, they strongly support the notion[48] that the nature of the ligands plays a central role in determining spectral intensity and energy. The fact that the distinct overall trend of increasing $^1(\delta \rightarrow \delta^*)$ intensity with decreasing transition energy that was noted by MT is not entirely attributable to systematic changes in metal-metal bonding suggests that these parameters may instead reflect strong *excited state* perturbations. Specifically, the mixing of $^1(\delta \rightarrow \delta^*)$ with high-oscillator-strength transitions of similar orbital character and symmetry would provide a mechanism through which intensity could be stolen; band positions would also reflect the coupling between these "zero-order" transitions.

We suggest that what the overall $^1(\delta \rightarrow \delta^*)$ spectral trend represents, as one proceeds from weak, high energy $^1(\delta \rightarrow \delta^*)$ bands to intense, low energy ones, is the gradual lowering in energy, for a given dimetal unit, of $\pi(\text{ligand}) \rightarrow \delta^*(M_2)$ transitions, and hence a concomitant increase in the extent of mixing between the $^1(\delta \rightarrow \delta^*)$ and $\pi(\text{ligand}) \rightarrow \delta^*(M_2)$ transitions.[62] Consequently, those compounds

containing oxygen donors, which have relatively high energy LMCT bands, possess, regardless of δ-overlap, much weaker $^1(\delta \rightarrow \delta^*)$ bands ($\epsilon \leq 500$) than do halide-ligated dimers ($\epsilon \geq 1000$), for which LMCT transitions will be much lower in energy. The spectra of $Mo_2X_4(PMe_3)_4$ (Figure 5) provide an excellent example of this effect within a more restricted series of complexes. These species possess a $\pi(X) \rightarrow \delta^*(Mo_2)$ transition of the same symmetry ($b_1 \rightarrow a_2$; $^1B_2 \leftarrow {}^1A_1$) as $^1(\delta \rightarrow \delta^*)$; the calculated splitting of the $b_1(\pi(Cl))$ and $a_2(\delta^*(Mo_2))$ levels for $Mo_2Cl_4(PH_3)_4$ is between 30000 and 36000 cm^{-1},[25,49] placing this transition in the near-UV region. The dramatic increase in the intensity of the $^1(\delta \rightarrow \delta^*)$ band of these complexes according to Cl < Br < I is indicative of this transition progressively borrowing LMCT intensity, in agreement with the pronounced X $\rightarrow$ M red shift across this series (*cf.* band II). In contrast, the splitting of these orbitals for $Mo_2(O_2CH)_4$, a compound that is representative of the lower limit of $^1(\delta \rightarrow \delta^*)$ intensity, is ~63000 cm^{-1};[3] the fact that $Mo_2(O_2CPr^n)_4$ and β-$Mo_2Cl_4(dmpe)_2$ have very similar $^1(\delta \rightarrow \delta^*)$ intensities, even though they nearly define the respective high- and low-δ-overlap limits for d^4-d^4 complexes, is quite reasonable from the standpoint of this charge-transfer-mixing interpretation.

References and Notes

1. Cotton, F. A.; Walton, R. A. "Multiple Bonds Between Metal Atoms"; Wiley: New York, 1982.
2. Cotton, F. A.; Curtis, N. F.; Harris, C. B.; Johnson, B. F. G.; Lippard, S. J.; Mague, J. T.; Robinson, W. R.; Wood, J. S. *Science* **1964**, *145*, 1305-1307.
3. Norman, J. G., Jr.; Kolari, H. J. *J. Chem. Soc., Chem. Commun.* **1975**, 649-651. Norman, J. G.; Kolari, H. J.; Gray, H. B.; Trogler, W. C. *Inorg. Chem.* **1977**, *16*, 987-993.
4. Chapter V. Hopkins, M. D.; Gray, H. B. *J. Am. Chem. Soc.* **1984**, *106*, 2468-2469.
5. Miskowski, V. M.; Goldbeck, R. A.; Kliger, D. S.; Gray, H. B. *Inorg. Chem.* **1979**, *18*, 86-89.
6. Chapter IV. Zietlow, T. C.; Hopkins, M. D.; Gray, H. B. *J. Solid State Chem.* **1985**, *57*, 112-119.
7. Perrin, D. D.; Armarego, W. L. F.; Perrin, D. R. "Purification of Laboratory Chemicals"; Pergamon: Oxford, 1966.
8. Holste, G.; Schafer, H. *Z. Anorg. Allg. Chem.* **1972**, *391*, 263-270.
9. Brencic, J. V.; Cotton, F. A. *Inorg. Chem.* **1970**, *9*, 351-353.
10. Schrock, R. R.; Sturgeoff, L. G.; Sharp, P. R. *Inorg. Chem.* **1983**, *22*, 2801-2806. Sharp, P. R.; Schrock, R. R. *J. Am. Chem. Soc.* **1980**, *102*, 1430-1431.
11. Cotton, F. A.; Extine, M. W.; Felthouse, T. R.; Kolthammer, B. W. S.; Lay, D. G. *J. Am. Chem. Soc.* **1981**, *103*, 4040-4045.
12. Contrary to several reports of $Mo_2Cl_4(PMe_3)_4$[11,13] and $Mo_2Br_4(PMe_3)_4$[14b] existing as *dark blue* crystals, both materials are actually red as solids due to intense luminescence in room light.[4]

13. Carmona, E.; Galindo, A.; Sanchez, L.; Nielson, A. J.; Wilkinson, G. *Polyhedron* **1984**, *3*, 347-352. Andersen, R. A.; Jones, R. A.; Wilkinson, G. *J. Chem. Soc., Dalton Trans.* **1978**, 446-453.

14. *a.* Following completion of this work a report of the synthesis and crystal structure of $Mo_2Br_4(PMe_3)_4$ appeared.[14b] Since the preparative route described by these workers is not as straightforward as that given here, and inasmuch as the crystallographic results are mentioned solely in the abstract of their paper, we present here the full details of our x-ray structure determination. Both crystal structures are in good agreement with respect to unit cell dimensions and bond distances and angles. *b.* Ahmed, K. J.; Chisholm, M. H.; Huffman, J. C. *Organometallics* **1985**, *4*, 1168-1174.

15. "International Tables for Crystallography"; Kynoch Press: Birmingham, England, 1974; vol IV, pp 72 and 149.

16. Main, P.; Hull, S. E.; Lessinger, L.; Germain, G.; De Clerq, J.-P.; Woolfson, M. M. "Multan 78"; University of York: York, England.

17. Larson, A. C. *Acta Cryst.* **1967**, *23*, 664-665, eqn. 3.

18. Future references to the $Mo_2X_4(PMe_3)_4$ (X = Cl, Br, I) series as a whole will be given as $Mo_2X_4(PMe_3)_4$. The notation $M_2X_4L_4$ does not, however, restrict X to these three halides.

19. Two centrosymmetric (D_{2h}) species, Mo_2X_4(4-picoline)$_4$ (X = Cl, Br), have been structurally characterized (Brencic, J. V.; Golic, L.; Leban, I.; Segedin, P. *Monatsh. Chem.* **1979**, *110*, 1221-1228).

20. Cotton, F. A.; Fanwick, P. E. *Acta Cryst.* **1980**, *B36*, 457-459. Marsh, R. E. *Acta Cryst.* **1981**, *B37*, 1985-1988.

21. Girolami, G. S.; Mainz, V. V.; Andersen, R. A.; Vollmer, S. H.; Day, V. W. *J. Am. Chem. Soc.* **1981**, *103*, 3953-3955.

22. Weast, R. C. (ed.) "CRC Handbook of Chemistry and Physics"; CRC Press: Cleveland, 1977 (58th ed.); p F-213.

23. We note here, as others have previously on related systems,[11,24,25] that the Mo-P bonds of $Mo_2X_4(PMe_3)_4$ appear to be anomalously long relative to the Mo-X bonds. Comparison of these distances in $Mo_2Cl_4(PMe_3)_4$ (d(Mo-Cl) = 2.414(1)Å, d(Mo-P) = 2.545(1))[11] to those reported for its most closely related monomeric analogue, *trans*-$MoCl_2(PMe_3)_4$ (2.420(6) and 2.496(3), respectively) (Carmona, E.; Marin, J. M.; Poveda, M. L.; Atwood, J. L.; Rogers, R. D. *Polyhedron* **1983**, *2*, 185-193) serves to illustrate this point clearly. Some discussion of this result in the context of an SCF-Xα-SW calculation has been offered elsewhere.[25]

24. Cotton, F. A.; Felthouse, T. R. *Inorg. Chem.* **1981**, *20*, 3880-3886.

25. Cotton., F. A.; Hubbard, J. L.; Lichtenberger, D. L.; Shim, I. *J. Am. Chem. Soc.* **1982**, *104*, 679-686.

26. Atomic contributions (percent):[25] $\delta(Mo_2)$ (72 Mo, 14 Cl, 1 P); $\pi(Mo_2)$ (52 Mo, 32 Cl, 8 P); σ(MoP) (18 Mo, 11 Cl, 48 P).

27. Mixing of halide *d*-orbitals with the δ and δ^* levels of $Mo_2X_4(PMe_3)_4$ has been invoked to explain trends in the oxidation and reduction potentials of these complexes, that are "inverted" relative to those predicted from electronegativity arguments (Zietlow, T. C. *Ph. D. Thesis*, California Institute of Technology, Pasadena, CA, 1985).

28. Chisholm, M. H.; Folting, K.; Huffman, J. C.; Tatz, R. J. *J. Am. Chem. Soc.* **1984**, *106*, 1153-1154.

29. Coffindaffer, T. W.; Niccola, G. P.; Powell, D.; Rothwell, I. P.; Huffman, J. C. *J. Am. Chem. Soc.* **1985**, *107*, 3572-3583.

30. Angell, C. L.; Cotton, F. A.; Frenz, B. A.; Webb, T. R. *J. Chem. Soc., Chem.*

Commun. **1973**, 399-400. Clark, R. J. H.; Franks, M. L. *ibid.* **1974**, 316-317.

31. Clark, R. J. H.; Franks, M. L. *J. Am. Chem. Soc.* **1975**, *97*, 2691-2697.
32. Clark, R. J. H.; D'Urso, N. R. *J. Am. Chem. Soc.* **1978**, *100*, 3088-3091.
33. San Filippo, J., Jr.; Sniadoch, H. J. *Inorg. Chem.* **1973**, *12*, 2326-2333.
34. San Filippo, J., Jr.; Sniadoch, H. J.; Grayson, R. L. *Inorg. Chem.* **1974**, *13*, 2121-2130.
35. Ribas, J.; Jugie, G.; Poilblanc, R. *Trans. Met. Chem.* **1983**, *8*, 93-98.
36. Although the intense fluorescence of these complexes[4] required excitation wavelengths to be significantly blue-shifted from the $^1(\delta \rightarrow \delta^*)$ λ_{max} in order for usable baselines to be obtained, resonance enhancement is nonetheless observed.
37. Clark, R. J. H.; Stewart, B. *Struct. Bonding* **1979**, *36*, 1-80.
38. A similar observation has been reported for $Re_2I_8^{2-}$,[39] for which the intensity of ν_2 is much weaker than the corresponding modes of $Re_2X_8^{2-}$ (X = F, Cl, Br) upon $^1(\delta \rightarrow \delta^*)$ excitation.
39. Clark, R. J. H.; Stead, M. J. *Inorg. Chem.* **1983**, *22*, 1214-1220.
40. Strong resonance enhancement of metal-ligand vibrational modes has been observed for the $Re_2X_8^{2-}$ ions upon excitation into the LMCT transitions of these complexes.[39] In an attempt to obtain depolarization ratios of these modes for the $Mo_2X_4L_4$ complexes, we acquired Raman spectra of benzene solutions of $Mo_2Cl_4(PMe_3)_4$ and $Mo_2Br_4(PMe_3)_4$ using excitation lines of 351.1 and 363.8 nm, respectively, which are in close proximity to LMCT bands of these species (*vide infra*). The spectrum of the chloride derivative displayed only ν_1 and ν_2, with roughly equal intensity, while the bromide showed only ν_1; these lines were very weak, and no overtones were observed.
41. Nakamoto, K. "Infrared and Raman Spectra of Inorganic and Coordination Compounds"; Wiley: New York, 1978 (3rd ed.).

42. Hutchinson, B.; Morgan, J.; Cooper, C. B., III: Mathey, Y.; Shriver, D. F. *Inorg. Chem.* **1979**, *18*, 2048-2049.

43. Bratton, W. K.; Cotton, F. A.; Debeau, M.; Walton, R. A. *J. Coord. Chem.* **1971**, *1*, 121-131.

44. Ref. 1, p.428.

45. Low temperature polarized single-crystal spectra of this spectral region, and tentative assignments of these weak bands, are presented in Appendix II.

46. Trogler, W. C.; Gray, H. B. *Acc. Chem. Res.* **1978**, *11*, 232-239.

47. Ref. 48, Table XIII.

48. Manning, M. C.; Trogler, W. C. *J. Am. Chem. Soc.* **1983**, *105*, 5311-5320.

49. Ziegler, T., personal communication. For further details on this calculation, see: Ziegler, T. *J. Am. Chem. Soc.* **1984**, *106*, 5901-5908, and Figure 2 of Chapter I.

50. Lone pair ionization energies of homologous arsines and phosphines are generally similar (Elbel, S.; Tom Dieck, H. *Z. Naturforsch., B: Anorg. Chem., Org. Chem.* **1976**, *31B*, 178-189).

51. Sattelberger, A. P.; Fackler, J. P. *J. Am. Chem. Soc.* **1977**, *99*, 1258-1259.

52. Collins, D. M.; Cotton, F. A.; Koch, S.; Millar, M.; Murillo, C. A. *J. Am. Chem. Soc.* **1977**, *99*, 1259-1261. Cotton, F. A.; Koch, S.; Mertis, K.; Millar, M.; Wilkinson, G. *J. Am. Chem. Soc.* **1977**, *99*, 4989-4992.

53. Bohmer, W. H.; Madeja, K.; Kurras, E.; Rosenthal, U. *Z. Chem.* **1978**, *18*, 453-454. Cotton, F. A.; Fanwick, P. E. *J. Am. Chem. Soc.* **1979**, *101*, 5252-5255. Cotton, F. A.; Mott, G. N.: Schrock, R. R.; Sturgeoff, L. G. *J. Am. Chem. Soc.* **1982**, *104*, 6781-6782. Fanwick, P. E.; Bursten, B. E.; Kaufmann, G. B. *Inorg. Chem.* **1985**, *24*, 1165-1169.

54. Campbell, F. L., III; Cotton, F. A.; Powell, G. L. *Inorg. Chem.* **1984**, *23*,

4222-4226.

55. Campbell, F. L., III: Cotton, F. A.; Powell, G. L. *Inorg. Chem.* **1985**, *24*, 177-181.

56. Chapter III. Hopkins, M. D.; Zietlow, T. C.; Miskowski, V. M.; Gray, H. B. *J. Am. Chem. Soc.* **1985**, *107*, 510-512.

57. Appendix III.

58. Norman, J. G., Jr.; Ryan, P. B. *J. Comput. Chem.* **1980**, *1*, 59-63.

59. Appendix IV.

60. $\Delta E(^1(\delta \rightarrow \delta^*)) = 1900\ cm^{-1}$. $E(\delta/\delta^*)$ differs by less than 200 cm^{-1} between $Mo_2Cl_8^{4-}$ and $Mo_2Cl_4(PH_3)_4$.[25]

61. Comparisons of the transition energies of the original SF series present a separate problem that has been discussed elsewhere,[55,56] namely that (in contrast to the β-$Mo_2X_4(L\text{-}L)_2$ complexes) contributions to the $^1(\delta \rightarrow \delta^*)$ energy arising from two-electron terms are not likely to remain constant over the range of metal-metal distances and transition series spanned by the $M_2(CH_3)_8^{n-}$ compounds.

62. Charge transfer transitions of the $\delta(M_2) \rightarrow \pi^*$(ligand) type will also be effective at intensity lending, provided they possess the correct symmetry for mixing with $^1(\delta \rightarrow \delta^*)$. It is because of this latter point that the $^1(\delta \rightarrow \delta^*)$ transitions of the $M_2(O_2CR)_4$ complexes are weak even though they are in close energetic proximity to intense MLCT bands (Santure, D. J.; Huffman, J. C.; Sattelberger, A. P. *Inorg. Chem.* **1985**, *24*, 371-378); theory indicates[3] that none of the low-lying MLCT states of these species have the correct symmetry.

CHAPTER III

The $^3(\delta\delta^*)$ State

Introduction

The lowest lying electronic excited state of complexes containing quadruple metal-metal bonds is a spin triplet of configuration $[\sigma^2\pi^4\delta\delta^*]$. Although the energy of this state has yet to be directly determined by magnetic or spectroscopic measurements,[1] theoretical considerations of weakly interacting orbitals,[2-5] as well as indirect experimental evidence,[3,6,7] suggest that it lies much closer to the δ^2 ground state than to its singlet counterpart. Specifically, a 4100-cm^{-1} splitting of the $^1(\delta^2)$ and $^3(\delta\delta^*)$ states is predicted for $Mo_2Cl_4(PMe_3)_4$ using the simple theory outlined in Chapter I, and a value of 3200 cm^{-1} is obtained for this splitting in $Re_2Cl_8^{2-}$ from an *ab initio* generalized valence bond calculation;[4] the respective singlet-triplet $\delta\delta^*$ energy gaps of these two compounds, in contrast, are estimated to be 13000 and 11200 cm^{-1}. Possible manifestations of a small $^1(\delta^2)/^3(\delta\delta^*)$ splitting in the physical properties of complexes of these types include the observation of fluorescence, but not phosphorescence, for $Mo_2Cl_4(PBu^n_3)_4$[3] and related compounds,[6] and a barrier to rotation about the metal-metal bond of only 10 kcal/mol for quadruply bonded $Mo_2(porphyrin)_2$ dimers.[7]

Over the past several years, a number of d^4-d^4 dimers have been reported in which the two ML_4 subunits that make up these complexes are partially or completely staggered with respect to each other due to a bridging-ligand-induced rotation about the metal-metal bond.[8-12]

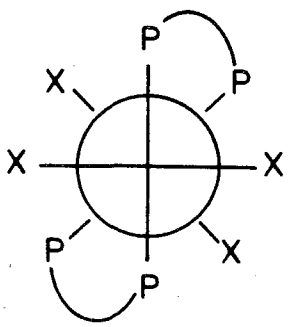

While the rotationally symmetric $[\sigma^2\pi^4]$ triple-bond core remains intact in these twisted systems, the extent of δ-interaction between adjacent d_{xy} functions is progressively reduced, relative to that found in eclipsed dimers, as the torsion angle increases, with no overlap remaining at 45°.[9] Reported herein are the magnetic and spectroscopic properties of two sets of d^4-d^4 complexes that nearly span the range of δ-interactions: β-$Mo_2X_4(dmpe)_2$ (dmpe = 1,2-bis(dimethylphosphino)ethane; X = Cl, Br; D_2 symmetry), which possess twist angles of 35 - 40°, and their eclipsed (D_{2d}) $Mo_2X_4(PMe_3)_4$ rotamers.[13]

Experimental Section

Tetrahydrofuran, obtained from Burdick and Jackson, was dried and stored *in vacuo* over sodium metal/benzophenone. All other chemicals were of reagent grade or comparable quality and were used as received. $Mo_2Cl_4(PMe_3)_4$,[16] $Mo_2Br_4(PMe_3)_4$,[16] β-$Mo_2Cl_4(dmpe)_2$[9] (dmpe = 1,2-bis(dimethylphosphino)ethane), β-$Mo_2Br_4(dmpe)_2$,[10] β-$Mo_2Cl_4(dppe)_2$ [11] (dppe = 1,2-bis(diphenylphosphino)ethane), and β-$Mo_2Cl_4(S,S\text{-dppb})_2$[12] (S,S-dppb = (S,S)-2,3-(diphenylphosphino)butane) were prepared according to standard methods; satisfactory carbon and hydrogen analyses were obtained for each. The procedures and instrumentation used for spectroscopic and variable-temperature magnetic measurements have been described elsewhere.[16]

Results and Discussion

While $Mo_2Cl_4(PMe_3)_4$ and $Mo_2Br_4(PMe_3)_4$ display the rigorous diamagnetism typical of eclipsed d^4-d^4 dimers of this type, their torsionally distorted counterparts

are paramagnetic under the same conditions. The temperature dependence of the magnetic susceptibility of these complexes, shown for β-$Mo_2Cl_4(dmpe)_2$ in Figure 1, is consistent with an antiferromagnetically coupled two-spin system. Although the Ne'el point is not observed within the temperature limits of this experiment,[17] a crude fit of the data (employing standard approximations of the limiting magnetic moment,[18] and correcting for the paramagnetic impurity) places the energy $(-2J)$[19] of the thermally populated triplet state in the 400 - 500 cm^{-1} range for both twisted species, which is roughly an order of magnitude less than that anticipated for their eclipsed rotamers. This marked deviation in the electronic properties of the two types of complexes is also manifested in their electronic spectra, as reproduced for the chloro compounds in Figure 2. The metal-metal-localized $^1(\delta \rightarrow \delta^*)$ transition of β-$Mo_2Cl_4(dmpe)_2$ is, like its triplet counterpart, lower in energy than its analogue in $Mo_2Cl_4(PMe_3)_4$ (Table I), as well as being lower in intensity ($Mo_2Cl_4(PMe_3)_4$: $\epsilon_{max} = 3110$; β-$Mo_2Cl_4(dmpe)_2$: $\epsilon_{max} = 210$ M^{-1} cm^{-1}).[20,21]

Table I. Electronic Absorption Data for $Mo_2X_4(PMe_3)_4$ and β-$Mo_2X_4(dmpe)_2$ Complexes.

Compound	Band I [$^1(\delta \rightarrow \delta^*)$]		Band II [$\sigma(MoP) \rightarrow \delta^*(Mo_2)$]	
	ν (cm^{-1})	Shift (cm^{-1})	ν (cm^{-1})	Shift (cm^{-1})
$Mo_2Cl_4(PMe_3)_4$	17090	4640	30860	1710
β-$Mo_2Cl_4(dmpe)_2$	12450		29150	
$Mo_2Br_4(PMe_3)_4$	16720	4720	28990	1890
β-$Mo_2Br_4(dmpe)_2$	12000		27100	

The energetic differences between the $\delta\delta^*$ states of $Mo_2X_4(PMe_3)_4$ and β-$Mo_2X_4(dmpe)_2$ can readily be attributed to the orbital overlap dependence of the

Figure 1. Temperature dependence of the corrected magnetic susceptibility (○) and magnetic moment (□) of a powdered sample of β-$Mo_2Cl_4(dmpe)_2$. The room temperature magnetic susceptibility of $Mo_2Cl_4(PMe_3)_4$ (-280 x 10^{-6} emu/mol; crystalline sample, Faraday balance, 300 K) was used as the diamagnetic correction.

Figure 2. Electronic absorption spectra of β-$Mo_2Cl_4(dmpe)_2$ (—) and $Mo_2Cl_4(PMe_3)_4$ (- - -) in tetrahydrofuran solution at room temperature.

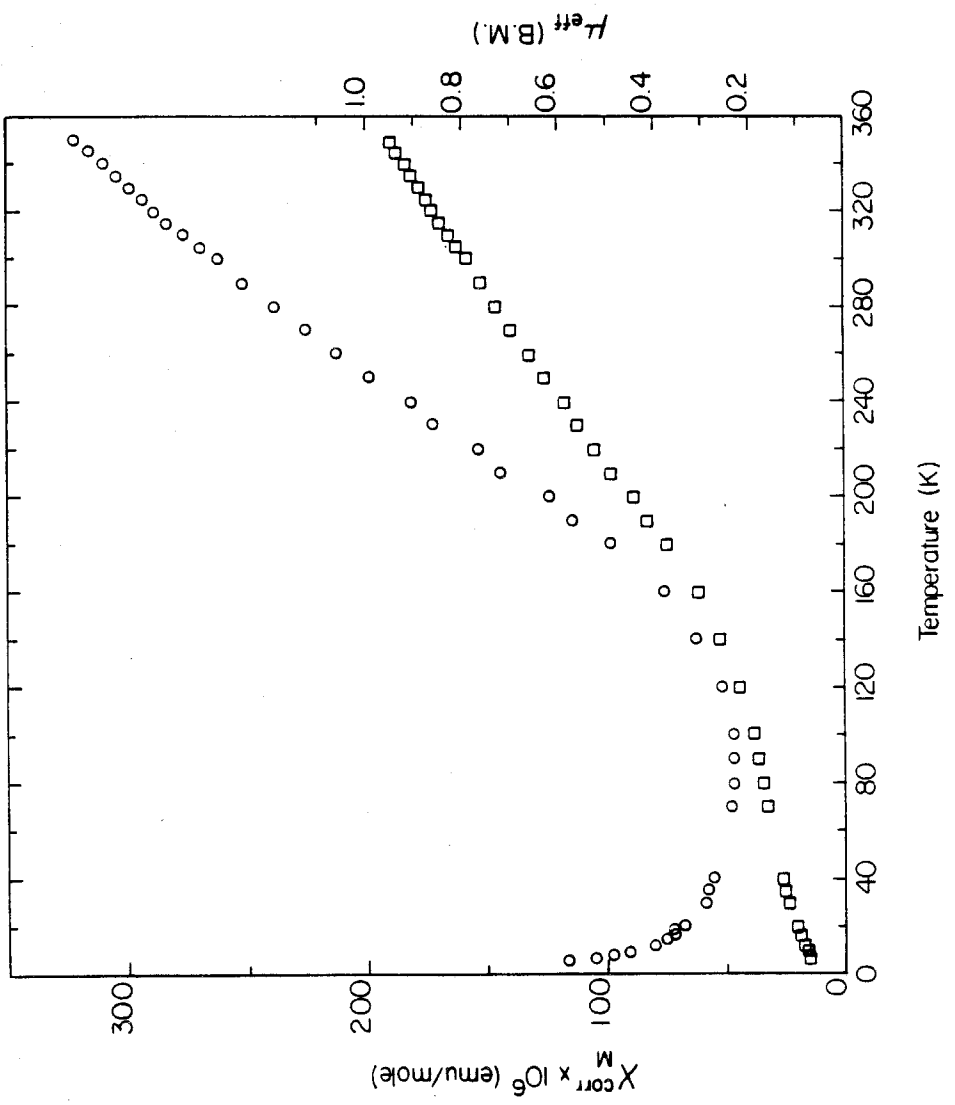
$\chi_M^{corr} \times 10^6$ (emu/mole)
μ_{eff} (B.M.)
Temperature (K)
0
100
200
300
0.2
0.4
0.6
0.8
1.0
0
40
80
120
160
200
240
280
320
360

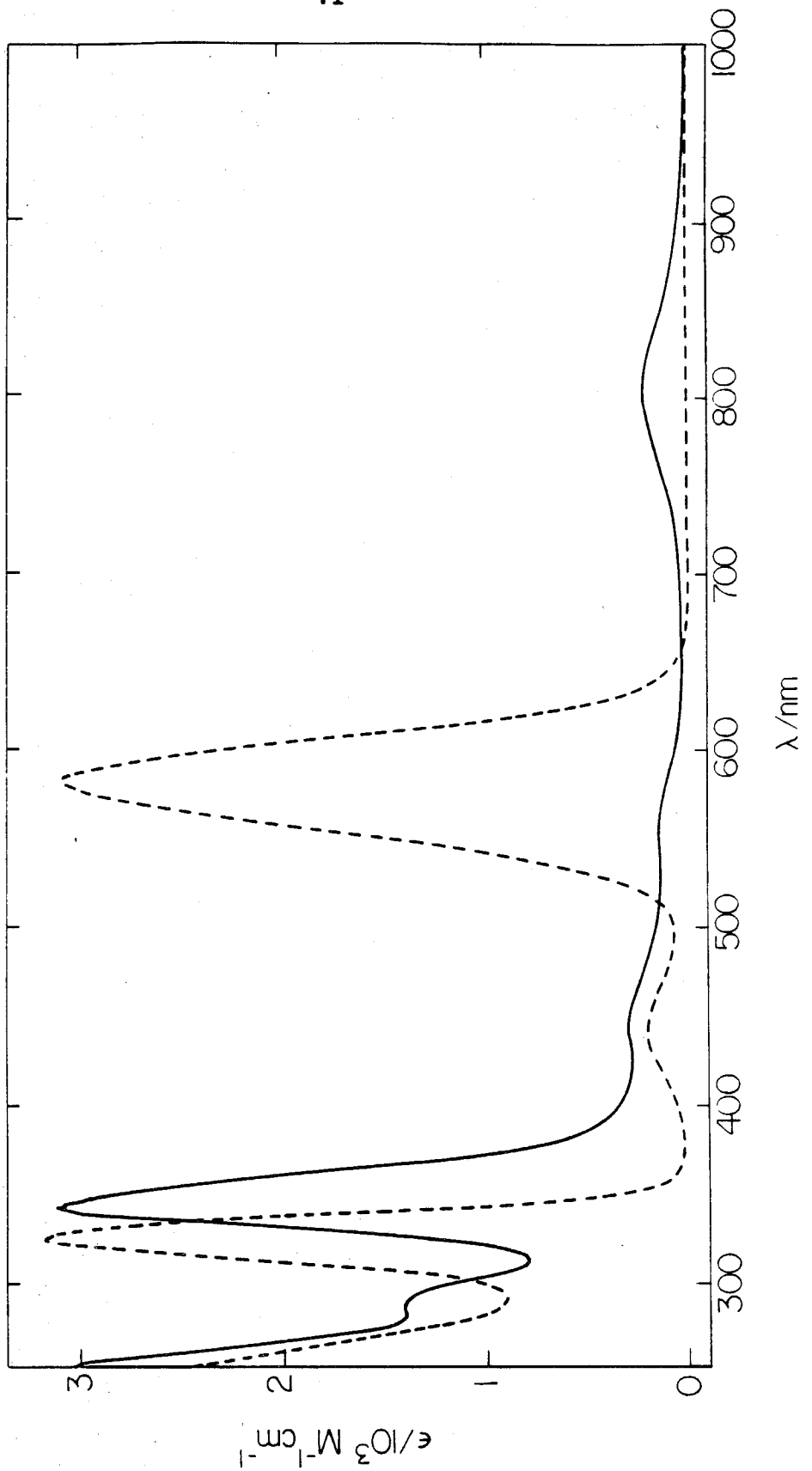
ε/10³ M⁻¹cm⁻¹
0
1
2
3
300
400
500
600
700
800
900
1000
λ/nm

one- and two-electron interactions defined in Chapter I. It has been proposed by Cotton *et al.* that the torsion angle dependence of the δ-overlap is $S = \cos(2\theta)$;[9] torsion angles of 35 - 40°, such as those found for β-$Mo_2X_4(dmpe)_2$, reduce the δ-interaction to 0.17(X = Cl) and 0.34(X = Br) times that found at 0°. Inasmuch as the δ-overlaps of the eclipsed $Mo_2X_4(PMe_3)_4$ complexes are only on the order of ~0.1, as noted in the preceding chapter, the energetic splittings of the one-electron δ and δ^* levels of β-$Mo_2Cl_4(dmpe)_2$ and β-$Mo_2Br_4(dmpe)_2$ are clearly quite small. This is borne out by the fact that the $\sigma(MoP) \rightarrow \delta^*(Mo_2)$ bands (*cf.* band II)[16] of the twisted complexes are red-shifted nearly 2000 cm^{-1} from their analogues in the eclipsed dimers, as well as by the concomitant reduction in the intensity of the $^1(\delta \rightarrow \delta^*)$ transition; the δ-overlap of β-$Mo_2Cl_4(dmpe)_2$ is estimated, using a standard relationship for the oscillator strengths of N → V transitions,[22] to be ~0.3 times that of $Mo_2Cl_4(PMe_3)_4$. As a result of this reduction in overlap, the covalent δ^2 and $^3(\delta\delta^*)$ states of the eclipsed species should collapse to a nearly degenerate pair of spin states derived from the weakly coupled d_{xy} functions of each metal of the twisted complexes, as shown schematically in Figure 3. This is reflected in the substantial population of both spin states of β-$Mo_2X_4(dmpe)_2$ at room temperature. In contrast, the energy of the ionic $^1(\delta\delta^*)$ state is dominated by an electronic repulsion term ($2K$) that remains roughly invariant over the range of overlaps ($0.01 \leq S \leq 0.1$) and distances spanned by these species since the $(aa|aa)$ and $(aa|bb)$ integrals that this term is composed of are not dependent on torsion angle; this latter fact is responsible for the differences between Figure 3 of Chapter I and the scheme shown here. Thus, even near the zero-δ-overlap limit, β-$Mo_2Cl_4(dmpe)_2$ and β-$Mo_2Br_4(dmpe)_2$ display $^1(\delta \rightarrow \delta^*)$ transitions that are only ~4500 cm^{-1} red-shifted from those of their eclipsed counterparts. The sum of this red shift and the value of $-2J$ obtained for β-$Mo_2X_4(dmpe)_2$ places the position of

Figure 3. Energies of the lowest electronic states of $Mo_2Cl_4(PMe_3)_4$ and β-$Mo_2Cl_4(dmpe)_2$.

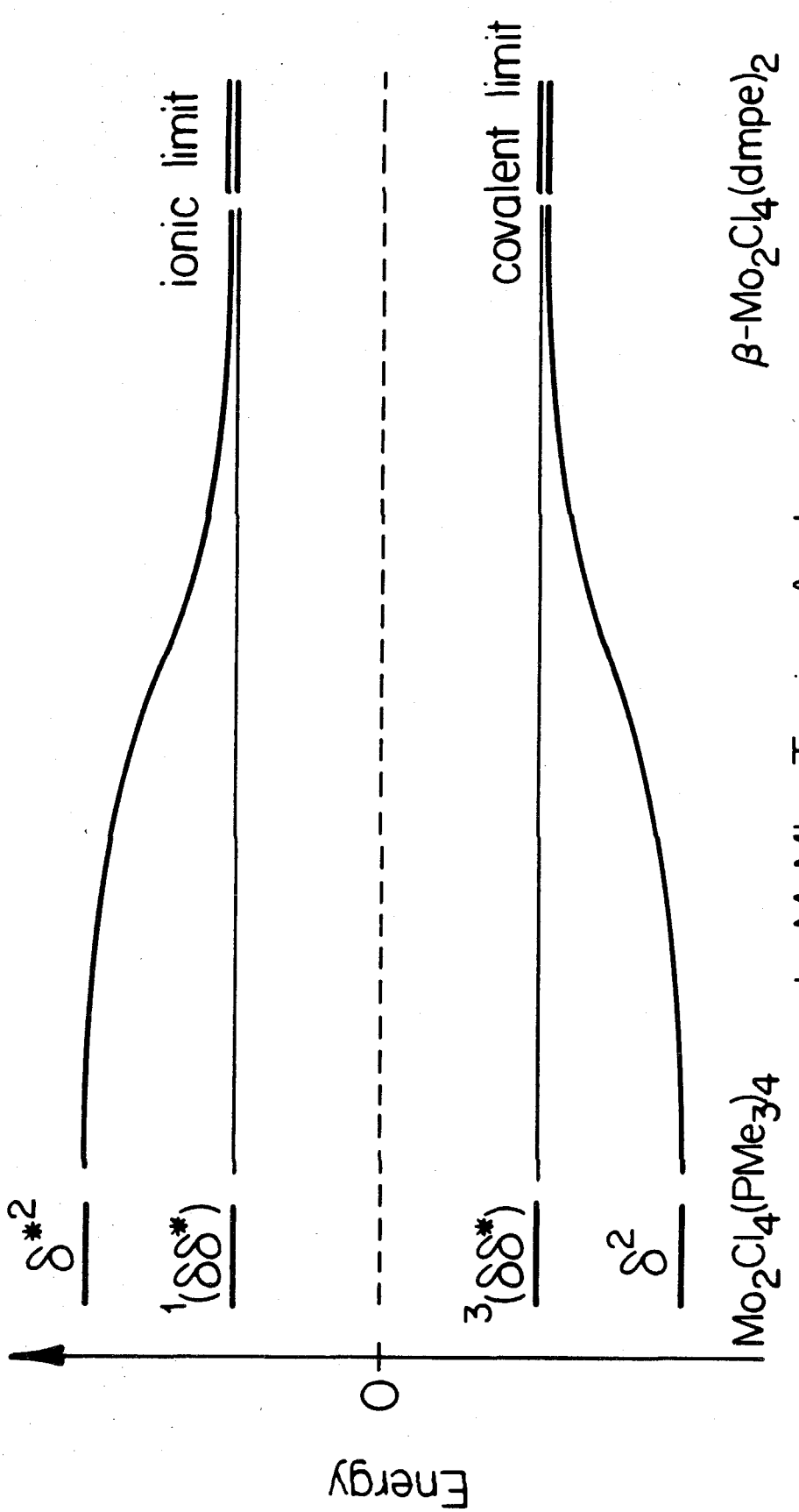
Energy
O
δ*2
1(δδ*)
3(δδ*)
δ2
ionic limit
covalent limit
Mo2Cl4(PMe3)4
L4M-ML4 Torsion Angle
β-Mo2Cl4(dmpe)2

the $^3(\delta\delta^*)$ states of $Mo_2Cl_4(PMe_3)_4$ and $Mo_2Br_4(PMe_3)_4$ ~5200 cm^{-1} above their ground states and over 10000 cm^{-1} below $^1(\delta\delta^*)$.

In addition to providing the first experimental estimate of the energy of the $^3(\delta\delta^*)$ state of quadruply bonded dimers, the data and analysis presented above yield insight into two aspects of the discussions in the preceding chapters. First, we note that the 6480-cm^{-1} value of K estimated for $Mo_2Cl_4(PMe_3)_4$ in Chapter I is in very good agreement with one-half the $^1(\delta \rightarrow \delta^*)$ transition energy ($2K$) of β-$Mo_2Cl_4(dmpe)_2$ (6230 cm^{-1}). This seems to support the validity of the approximations employed in the derivation of the energies of the δ-manifold of states.[22] Finally, the red shift of the $^1(\delta \rightarrow \delta^*)$ band observed upon exchanging bromide for chloride in $Mo_2X_4(PMe_3)_4$ is mirrored by the spectra of their torsionally distorted counterparts. Thus, in contrast to the prediction of Manning and Trogler,[23] who have suggested that such red shifts with larger halides are due to an increase in δ-overlap (ΔW), the theoretical framework presented here indicates that these shifts are actually more the result of a reduction of K: $Mo_2Cl_4(PMe_3)_4$, ΔW = 8950, K = 6200 cm^{-1}; $Mo_2Br_4(PMe_3)_4$, ΔW = 9070, K = 5900 cm^{-1}. This trend is well established for mononuclear transition metal complexes, and is a manifestation of the nephalauxetic effect.[24]

References and Notes

1. Two early proposals along this line, namely that the 14950-cm^{-1} emission band of $Mo_2Cl_8^{4-}$ was attributable to $^3(\delta^* \rightarrow \delta)$ phosphorescence (Trogler, W. C.; Solomon, E. I.; Gray, H. B. *Inorg. Chem.* **1977**, *16*, 3031-3033) and that the 6250-cm^{-1} absorption band of this species arose from the $^3(\delta \rightarrow \delta^*)$ excitation (Clark, R. J. H.; Franks, M. L. *J. Am. Chem. Soc.* **1975** *97*, 2691-2697), have been questioned in subsequent studies (Fraser, I. F.; Peacock, R. D. *Chem. Phys. Lett.* **1983**, *98*, 620-623; Clark, R. J. H.; D'Urso, N. R. *J. Am. Chem. Soc.* **1978**, *100*, 3088-3091). The only as yet unrefuted claim of a $^3(\delta\delta^*)$ energy was put forth in a recent single-crystal electronic spectroscopic study of $Re_2(O_2CCMe_3)_4Cl_2$ (Martin, D. S.; Huang, H. -W.; Newman, R. A. *Inorg. Chem.* **1984**, *23*, 699-701), where it was reported that the $^3(\delta \rightarrow \delta^*)$ transition is located at 16500 cm^{-1}, which is only 4100 cm^{-1} below $^1(\delta \rightarrow \delta^*)$. We shall comment on this assignment at the conclusion of this chapter.
2. Chapter I.
3. Miskowski, V. M.; Goldbeck, R. A.; Kliger, D. S.; Gray, H. B. *Inorg. Chem.* **1979**, *18*, 86-89.
4. Hay, P. J. *J. Am. Chem. Soc.* **1982**, *104*, 7007-7017.
5. Noodleman, L; Norman, J. G., Jr. *J. Chem. Phys.* **1979**, *70*, 4903-4906.
6. Chapter IV.
7. Collman, J. P.; Woo, L. K. *Proc. Natl. Acad. Sci.* **1984**, *81*, 2592-2596.
8. Best, S. A.; Smith, T. J.; Walton, R. A. *Inorg. Chem.* **1978**, *17*, 99-104. Abbott, E. H.; Bose, K. S.; Cotton, F. A.; Hall, W. T.; Sekutowski, J. C. *Inorg. Chem.* **1978**, *17*, 3240-3245. Cotton, F. A.; Fanwick, P. E.; Fitch, J. W.; Glicksman, H. D.; Walton, R. A. *J. Am. Chem. Soc.* **1979**, *101*, 1752-

1757. Schrock, R. R.; Sturgoff, L. G.; Sharp, P. R. *Inorg. Chem.* **1983**, *22*, 2801-2806. Campbell, F. L., III; Cotton, F. A.; Powell, G. L. *Inorg. Chem.* **1984**, *23*, 4222-4226. Agaskar, P. A.; Cotton, F. A.; Derringer, D. R.; Powell, G. L.; Root, D. R.; Smith, T. J. *Inorg. Chem.* **1985**, *25*, 2786-2791.

9. Cotton, F. A.; Powell, G. L. *Inorg. Chem.* **1983**, *22*, 1507-1510.
10. Campbell, F. L., III; Cotton, F. A.; Powell, G. L. *Inorg. Chem.* **1985**, *24*, 177-181.
11. Agaskar, P. A.; Cotton, F. A. *Inorg. Chem.* **1984**, *23*, 3383-3387.
12. Agaskar, P. A.; Cotton, F. A.; Fraser, I. F.; Peacock, R. D. *J. Am. Chem. Soc.* **1984**, *106*, 1851-1853.
13. While the small stoichiometric difference between dmpe and $2(PMe_3)$ prevents β-$Mo_2X_4(dmpe)_2$ and $Mo_2X_4(PMe_3)_4$ from being considered rotamers in the strictest sense, the electronic similarity of the two phosphines, in addition to the close structural correlation of the ML_4 subunits of the two sets of complexes,[14] suggests that the metals of both the PMe_3 and dmpe species lie, for a given halide, in nearly identical ligand fields, with the fundamental difference between them being the torsion angle.
14. Structural comparison of $Mo_2Cl_4(PMe_3)_4$[15] and (β-$Mo_2Cl_4(dmpe)_2$)[9]: d(MoMo) = 2.13 Å(2.18); d(MoCl) = 2.41(2.40); d(MoP) = 2.55(2.53); ∠(MoMoCl) = 112°(111); ∠(MoMoP) = 102(98); ∠(MoMo torsion) = 0(40.0). Structural comparison of $Mo_2Br_4(PMe_3)_4$[16] and (β-$Mo_2Br_4(dmpe)_2$)[10]: d(MoMo) = 2.13(2.17); d(MoBr) = 2.55(2.55); d(MoP) = 2.55(2.54); ∠(MoMoBr) = 114(109); ∠(MoMoP) = 103(102); ∠(MoMo torsion) = 0(36.5).
15. Cotton, F. A.; Extine, M. W.; Felthouse, T. R.; Kolthammer, B. W. S.; Lay, D. G.; *J. Am. Chem. Soc.* **1981**, *103*, 4040-4045.
16. Chapter II.

17. Sample decomposition occurs above ~375 K, as evidenced by an increase in the signal attributable to the paramagnetic impurity.
18. Earnshaw, A. "Introduction to Magnetochemistry"; Academic Press: New York, 1968.
19. In this instance J is defined as the coupling constant. Subscripted J's refer to coulomb integrals, as noted in Chapter I.
20. No other bands were observed in the electronic spectrum of β-$Mo_2Cl_4(dmpe)_2$ between 1000 and 1600 nm.
21. In contrast to β-$Mo_2Cl_4(dmpe)_2$ and β-$Mo_2Br_4(dmpe)_2$, β-$Mo_2Cl_4(dppe)_2$ ($\angle$MoMo torsion = 30.5°)[11] and β-Mo_2Cl_4(S,S-dppb)$_2$ (24.6°)[12] display higher energy $^1(\delta \rightarrow \delta^*)$ transitions (785 and 741 nm, respectively), and are diamagnetic at room temperature.
22. In light of this agreement between the experimental results and simple theory, we now reconsider the $^3(\delta \rightarrow \delta^*)$ assignment in the spectrum of $Re_2(O_2CCMe_3)_4Cl_2$.[1] Using the 14490-cm^{-1} $^2(\delta \rightarrow \delta^*)$ band of $Re_2(O_2CCMe_3)_4Cl_2^-$ (Dunbar, K. R.; Walton, R. A. *Inorg. Chem.* **1985**, *24*, 5-10) as the value of ΔW yields a $^3(\delta \rightarrow \delta^*)$ excitation energy of 10390 cm^{-1} for the neutral complex, in very poor agreement with the proposed 16500-cm^{-1} spectroscopic assignment.
23. Manning, M. C.; Trogler, W. C. *J. Am. Chem. Soc.* **1983**, *105*, 5311-5320.
24. Parts of this chapter have previously been published: Hopkins, M. D.; Zietlow, T. C.; Miskowski, V. M.; Gray, H. B. *J. Am. Chem. Soc.* **1985**, *107*, 510-512.

CHAPTER IV

Photophysics of the $^1(\delta\delta^*)$ State

Introduction

The most visually striking property of quadruply metal-metal bonded dimers is the intense luminescence displayed by a variety of derivatives of this class of compounds.[1-9] Although the emissive states of these complexes have been fairly well characterized from a spectroscopic standpoint,[2-4,6-9] their photophysical properties have been virtually neglected.[1,2,10] In one of the more comprehensive studies along these lines,[2] it was shown that the emission observed for $Mo_2Cl_4(PBu^n_3)_4$ was unambiguously attributable to fluorescence of the $^1(\delta\delta^*)$ state. In contrast, the $^3(\delta\delta^*)$ excited state did not appear to manifest itself in the photophysical properties of this species either through phosphorescence or as a long-lived transient.[2] It is clear from the results in the preceding chapter that this is entirely consistent with the $^3(\delta\delta^*)$ state lying only a few thousand wavenumbers above the $^1(\delta^2)$ ground state in complexes of this type.

Our interest in the photophysics of the $M_2X_4L_4$ class as a whole was originally motivated by the observation that the emission of the $Mo_2Cl_4(PMe_3)_4$ dimer appeared to be much more intense than that of the electronically similar $Mo_2Cl_4(PBu^n_3)_4$ compound: the PBu^n_3 derivative is a blue solid, while crystals of the PMe_3 species are bright red. In addition to attempting to determine the generality of the original conclusions on the photophysics of such species,[2] especially in light of the discussion of the ligand sensitivity of the energies and intensities of their $^1(\delta \rightarrow \delta^*)$ transitions,[12] it was hoped that an understanding of the radiative and nonradiative processes of the $M_2X_4L_4$ class would yield some insight into the nature of the potential energy surfaces of the $^1(\delta^2)$ and $^1(\delta\delta^*)$ states, and thus into the high-resolution absorption and emission spectra that will be presented in Chapter V. Reported herein are the ligand, temperature, and medium dependencies of the

photophysical properties of the $Mo_2X_4L_4$ chromophore.[13]

Experimental Section

Materials.

The solvents used in this study were dried by standard methods,[14] degassed with a minimum of five freeze-pump-thaw cycles on a high-vacuum manifold (limiting pressure $< 10^{-3}$ torr), and stored under vacuum with a drying agent: 2-methylpentane (Phillips) and cyclohexane (Aldrich) with lithium aluminum hydride; benzene (Burdick & Jackson), d_6-benzene (MSD Isotopes; 99.6+ atom-% D), tetrahydrofuran (Burdick & Jackson), and 2-methyltetrahydrofuran (Aldrich) with sodium metal/benzophenone; d_{12}-cyclohexane with titanocene; and dichloromethane (Burdick & Jackson) and 2-propanol (Aldrich) with activated 4A molecular sieves. *N*,*N*-dimethylformamide (Mallinckrodt) was distilled under reduced pressure and degassed with five freeze-pump-thaw cycles immediately prior to use. All other chemicals were of reagent grade or comparable quality and were used as received. The complexes $Mo_2X_4(PR_3)_4$ (X = Cl, R = Me,[12] Et, n-Pr, n-Bu;[15] X = Br, R = Me,[12] Et;[16] X = I, R = Me[12]), $Mo_2Cl_4(AsMe_3)_4$,[12] and $W_2Cl_4(PMe_3)_4$[17] were prepared according to standard procedures; satisfactory carbon and hydrogen elemental analyses were obtained for each.

Spectroscopic Measurements.

Electronic absorption spectra were recorded on either a Cary 17 or Hewlett-Packard 8450A spectrometer; emission spectra were recorded and corrected for spectrometer response with instrumentation that will be described elsewhere.[8] Spectra were obtained of solutions prepared on a vacuum line in a vessel consisting of a 10 mL round bottom flask, a 1 cm pathlength quartz spectral cell, and a teflon high-

vacuum stopcock. Solvent was bulb-to-bulb distilled into the evacuated cell from the appropriate storage flask and degassed with two additional freeze-pump-thaw cycles. Highly dilute solutions were used for emission spectra and quantum yield determinations[18] (optical density < 0.1 at the $^1(\delta \rightarrow \delta^*)$ absorption maximum) because of the strong self-absorption of the emission. The luminescence quantum yield standard employed in this study was $Mo_2Cl_4(PBu^n_3)_4$ in 2-methylpentane, which has a wavelength-independent quantum yield of 0.013 at room temperature.[2]

Emission Lifetime Measurements.

Emission lifetimes were measured with a computer-controlled Nd:YAG laser system that has been described elsewhere.[19] All samples were excited at a right angle to the detection monochrometer with the second harmonic output (532 nm) of the laser. Precautions were taken to minimize the photoinduced local heating of both solution and solid-state samples upon excitation: the absorbance at the 532-nm excitation wavelength was held to 0.1 or less in the former case, and the laser was operated at the lowest possible output power for the latter. Lifetimes were determined from the average of a minimum of 500 emission intensity decays; these decays exhibited first-order kinetics over at least three halflives.

Temperature control for variable-temperature experiments was achieved with several different apparatus. Emission lifetimes at low temperature (4.2 - 70 K) were acquired with an Oxford Instruments Ltd. cryostat that will be described in detail in the following chapter. Samples at these temperatures consisted of crystalline solids mounted on thin copper flats with petroleum jelly or silicon grease. For 77 K measurements, solutions or crystalline solids sealed in evacuated NMR tubes were held in a liquid-nitrogen-filled quartz finger dewar. A continuous-flow nitrogen gas dewar was employed for higher temperature experiments (100 - 350 K). Solution samples were contained in an evacuable, 1 mm pathlength quartz cell to which a

calibrated copper/constantan thermocouple had been attached. With the exception of the 77 K measurements, samples were allowed to thermally equilibrate for 20 - 30 minutes before lifetimes were acquired.

Data Analysis.

Nonlinear least-squares analyses of the photophysical data were obtained with a computer program employing a standard Taylor-series/gradient algorithm.[20] The criterion for convergence was

$$\sum_i (x_{calc} - x_{obs})^2 < 10^{-11}$$

for i data points.

Results

Ligand and Temperature Dependence of the $Mo_2X_4L_4$ Emission Lifetime.

A variety of complexes of the $Mo_2X_4L_4$ type were examined in this study with the aim of differentiating the intrinsic photophysical properties of this chromophore from ligand-dependent excited-state-decay phenomena. These series of compounds, which consist of dimers differing by systematic ligand perturbations both within and outside the metal coordination sphere, are composed as follows: $Mo_2Cl_4(PR_3)_4$ (R = Me, Et, n-Pr, n-Bu) and $Mo_2Br_4(PR_3)_4$ (R = Me, Et); $Mo_2Cl_4(EMe_3)_4$ (E = P, As); and $Mo_2X_4(PMe_3)_4$ (X = Cl, Br, I).

The room temperature absorption and emission spectra of the $Mo_2X_4(PMe_3)_4$ complexes in saturated hydrocarbon solution, the fluid medium in which the longest emission lifetimes and highest quantum yields are observed (*vide infra*),[21] are reproduced in Figure 1. In each instance there is sizeable overlap of the emission band with the low energy flank of the $^1(\delta \rightarrow \delta^*)$ band, consistent with the assignment

Figure 1. Absorption (—) and corrected emission (- - -) spectra of $Mo_2X_4(PMe_3)_4$ (X = Cl, Br, I) in 2-methylpentane at room temperature.

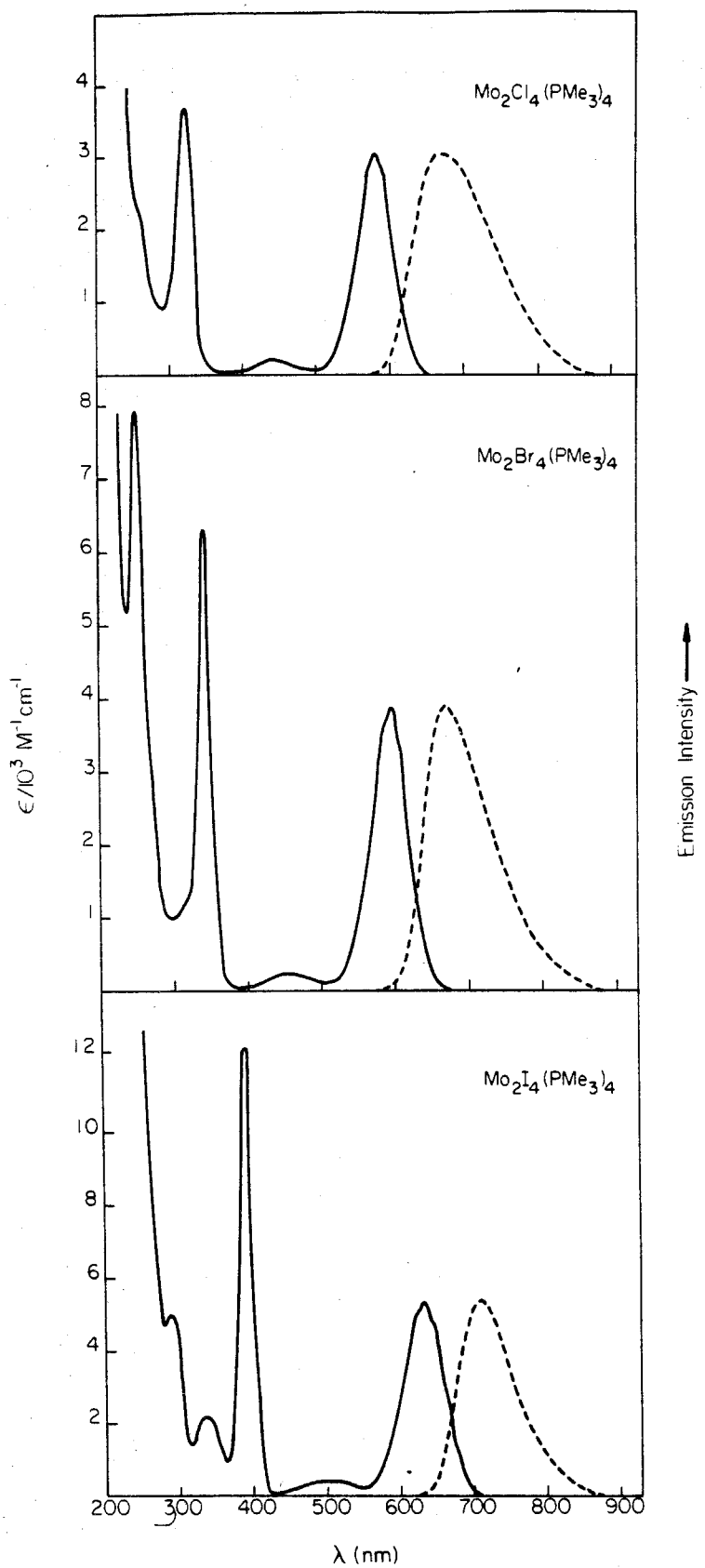
$Mo_2Cl_4(PMe_3)_4$
$Mo_2Br_4(PMe_3)_4$
$Mo_2I_4(PMe_3)_4$
$\epsilon/10^3\ M^{-1}cm^{-1}$
Emission Intensity
λ (nm)
200
300
400
500
600
700
800
900

of the luminescence to $^1(\delta\delta^*)$ fluorescence. The pertinent spectroscopic and photophysical parameters for these and the other $Mo_2X_4L_4$ complexes in this solvent are set out in Table I. We initially note three observations common to this class of compounds. First, the radiative rate constant k_r

$$k_r = \frac{\phi_{em}}{\tau} = \phi_{em} k_{obs} \tag{1}$$

of each complex at room temperature is in reasonable agreement with that estimated[22] (k_r^{calc}) from the oscillator strength (f) of its $^1(\delta \rightarrow \delta^*)$ transition, again in accordance with the assignment of the emission as $^1(\delta^* \rightarrow \delta)$. Second, all lifetimes and quantum yields are independent of excitation energy throughout the visible region, with the former additionally being a constant function of the wavelength at which the emission is monitored.[23] Third, the luminescence lifetime of every $Mo_2X_4L_4$ compound is longer, often substantially so, at 77 K than at room temperature. With regard to this latter point, it has been previously demonstrated[2] for $Mo_2Cl_4(PBu_3^n)_4$ that this increase in lifetime with decreasing temperature is mirrored by an increase in the emission quantum yield, thus indicating that the nonradiative decay rate k_{nr}[24]

$$k_{nr} = k_{obs} - k_r \tag{2}$$

is temperature dependent, and that the radiative rate is not. That this aspect of the temperature dependence of the lifetime is a general one for the $Mo_2X_4L_4$ class of complexes may be inferred from the fact that the oscillator strength of the $^1(\delta \rightarrow \delta^*)$ transition, which is roughly proportional to k_r at room temperature, is also independent of temperature (Table I).

Aside from these general observations, it is clear from the data in Table I that the room temperature emission lifetime and quantum yield of the $Mo_2X_4L_4$

Table I. Spectroscopic and Photophysical Parameters of $M_2X_4L_4$ Complexes in 2-methylpentane.

Compound	Absorption $^1(\delta\rightarrow\delta^*)$			Emission $^1(\delta^*\rightarrow\delta)$					
	λ_{max}/nm	f(300K)	f(77K)	λ_{max}/nm	ϕ(300K)	τ/ns (300K)	τ/ns (77K)	k_r /10^6 s^{-1}	k_r^{calc}/10^6 s^{-1}
$Mo_2Cl_4(PMe_3)_4$	585	0.024	0.025	673	0.259	125	170	2.1	5.3
$Mo_2Cl_4(PEt_3)_4$	589	0.025	----	674	0.013	∿15	185	∿1	5.4
$Mo_2Cl_4(PPr^n_3)_4$	587	0.026	----	672	0.016	∿20	185	∿0.8	5.8
$Mo_2Cl_4(PBu^n_3)_4$	587	0.026	0.027	675	0.013	∿15	185	∿1	5.9
$Mo_2Cl_4(AsMe_3)_4$	574	0.023	----	639	0.035	∿20	180	∿1.8	5.6
$Mo_2Br_4(PMe_3)_4$	598	0.030	0.034	671	0.162	90	145	1.8	6.7
$Mo_2Br_4(PEt_3)_4$	599	----	----	669	----	<10	145	---	---
$Mo_2I_4(PMe_3)_4$	636	0.040	0.039	713	0.123	30	105	4.1	7.9
$W_2Cl_4(PMe_3)_4$	660	0.028	----	756	0.025	55	60	0.6	4.9

chromophore is a sensitive function of the nature of X and L. The most striking of these differences, especially in connection with the discussion in Chapter II of the energies and intensities of the $^1(\delta \rightarrow \delta^*)$ transitions of these compounds, is the observation that the variations in these parameters upon nonchromophoric substitutions (*e.g.*, $Mo_2Cl_4(PR_3)_4$, $Mo_2Br_4(PR_3)_4$) are larger than those for substitutions that significantly perturb the $^1(\delta \rightarrow \delta^*)$ transition (*e.g.*, $Mo_2X_4(PMe_3)_4$). Inasmuch as the difference in lifetime between room temperature and 77 K for a given compound ranges from less than a factor of 1.5 to an order of magnitude or greater, however, comparisons among the lifetimes of these compounds must be made over an extensive temperature range rather than at a single temperature. Arrhenius-plot representations of the variable-temperature lifetime behavior of the $Mo_2Cl_4(PR_3)_4$, $Mo_2Cl_4(EMe_3)_4$, and $Mo_2X_4(PMe_3)_4$ series of complexes are displayed in Figures 2a - c, respectively. Note, for purposes of comparison, that the data for $Mo_2Cl_4(PMe_3)_4$ are shown in each figure. As is usually found for data of this type, all plots display a marked deviation from linearity. Specifically, the emission lifetime decreases nearly linearly with increasing temperature in the vicinity of room temperature, while in the low temperature region it is temperature independent; this latter behavior extends down to 5 K.[25] The overall photophysical behavior of each $Mo_2X_4L_4$ complex can be reasonably accounted for with a modified Arrhenius expression of the form

$$k_{nr} = k_{nr}^0 + k_{nr}^1 exp\left(\frac{-E_a}{k_b T}\right) \qquad (3)$$

where k_{nr}^0 and $k_{nr}^1 \exp(-E_a/k_bT)$ represent the nonradiative rate in the low and high-temperature regimes, respectively. Shown in Figure 3 is a comparison of the observed data of $Mo_2Cl_4(PMe_3)_4$ with that calculated by both a nonlinear least-

Figure 2. (a) Temperature dependence of k_{obs} of $Mo_2Cl_4(PR_3)_4$ in 2-methylpentane: (⬡), R = Me; (▶), R = Et; (□), R = n-Pr; (◇), R = n-Bu. (b) Temperature dependence of k_{obs} of $Mo_2Cl_4(EMe_3)_4$ in 2-methylpentane solution: (⬡), E = P; (▷), E = As. (c) Temperature dependence of k_{nr} of $Mo_2X_4(PMe_3)_4$ in 2-methylpentane solution: (⬡), X = Cl; (▷), X = Br; (□), X = I.

Figure 3. Comparison of the experimental emission lifetime of $Mo_2Cl_4(PMe_3)_4$ with that calculated by a nonlinear least-squares fit of the entire data curve to equation 3 (solid line; parameters listed in Table II) and by a linear regression analysis (xxx) of the high temperature (T > 300 K) and low temperature (T < 200 K) regions of the data. The upper plot shows the calculated residuals of the nonlinear least-squares fit.

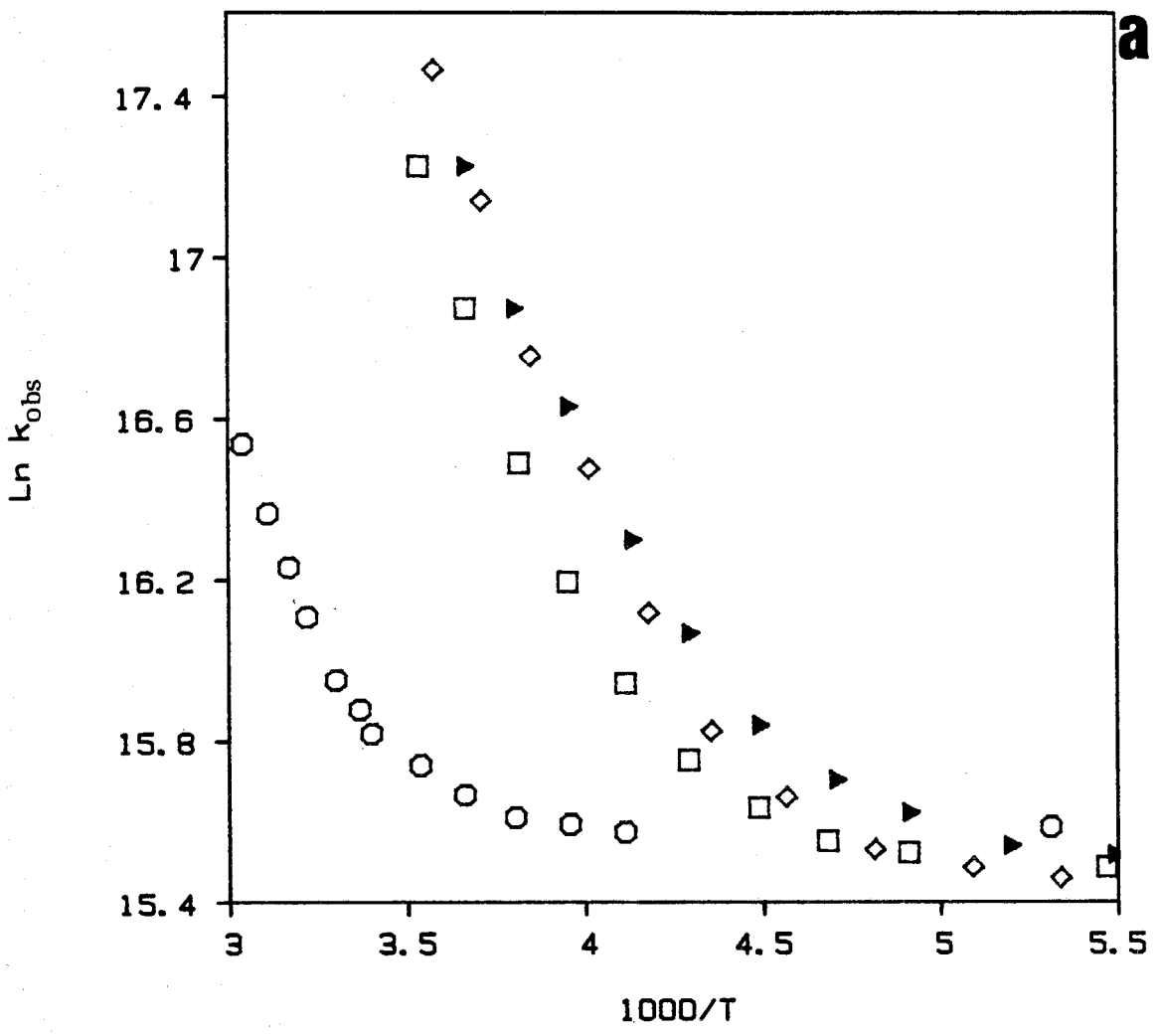
a
17.4
17
16.6
16.2
15.8
15.4
Ln k_{obs}
3
3.5
4
4.5
5
5.5
1000/T

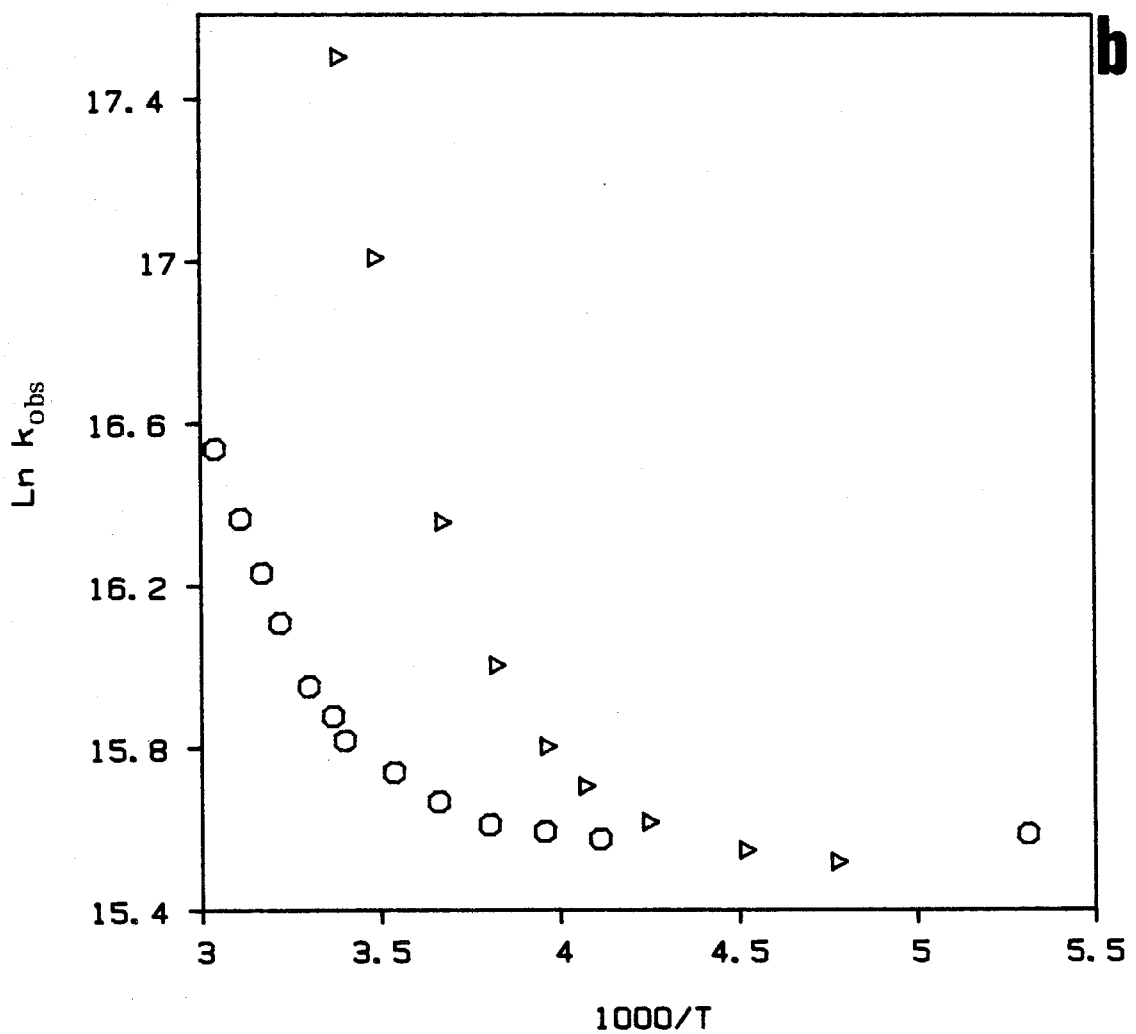
b
17.4
17
16.6
16.2
15.8
15.4
Ln k_{obs}
3
3.5
4
4.5
5
5.5
1000/T

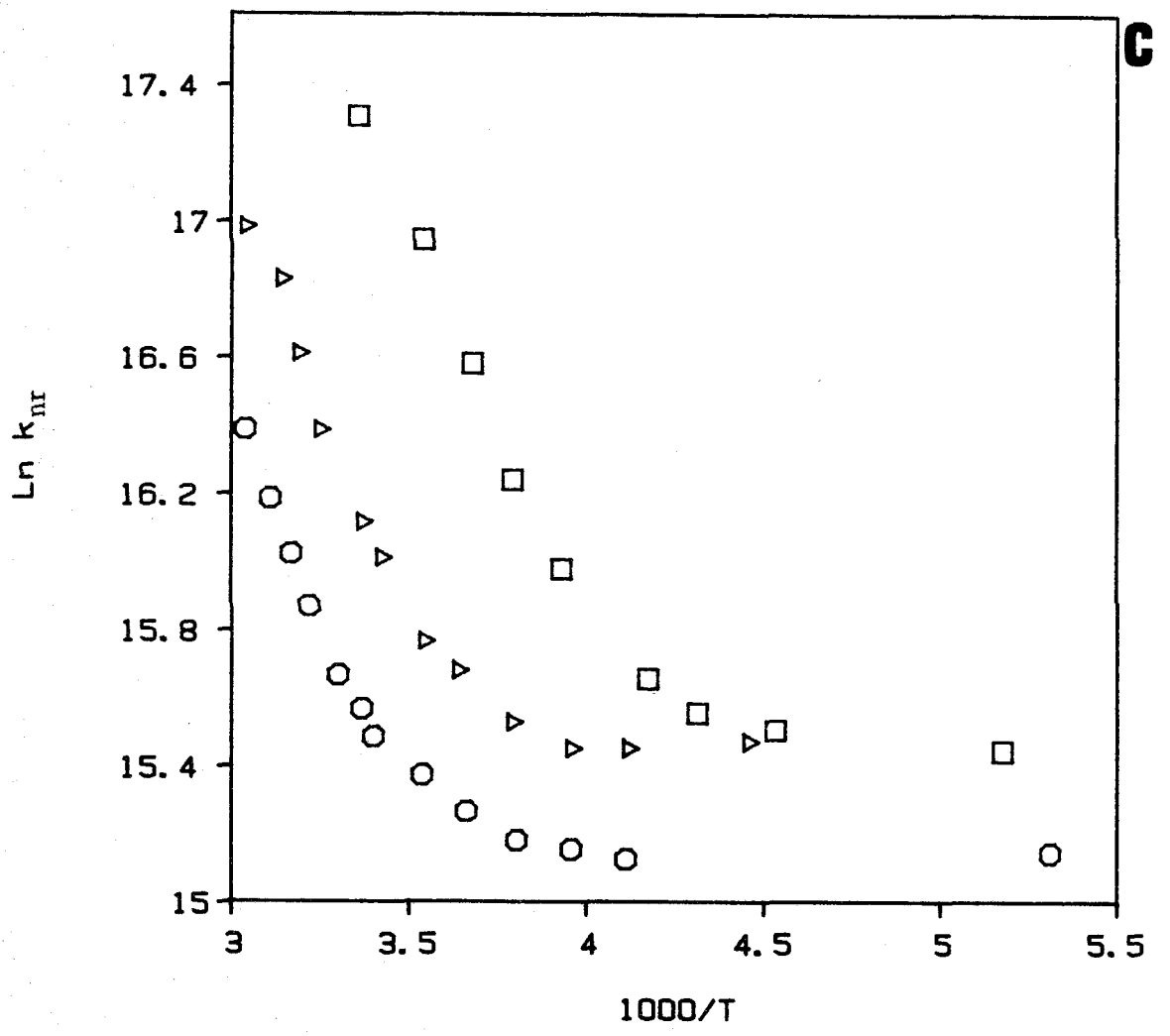
C
17.4
17
16.6
16.2
15.8
15.4
15
Ln k_{nr}
3
3.5
4
4.5
5
5.5
1000/T

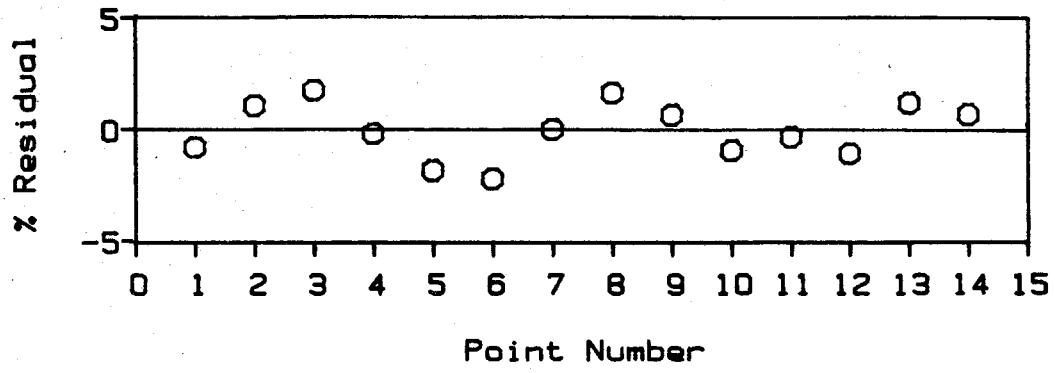
% Residual
5
0
-5
0 1 2 3 4 5 6 7 8 9 10 11 12 13 14 15
Point Number

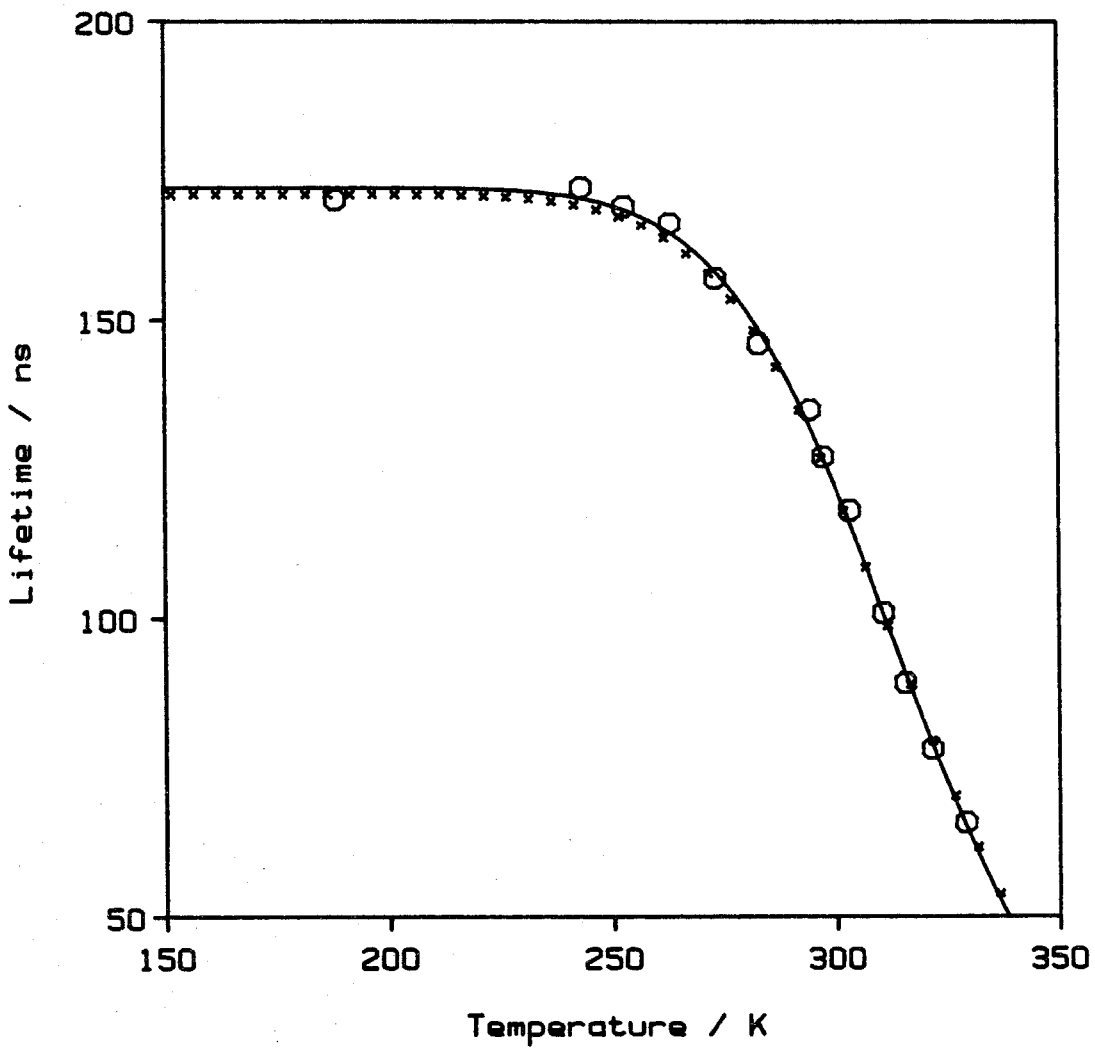
Lifetime / ns
200
150
100
50
150 200 250 300 350
Temperature / K

squares fit of the data to equation (3), as well as that calculated from linear regression analyses of the data near the two temperature limits. The close agreement of the calculations with each other and with the observed data suggests that the nonlinear region of the data that connects the two temperature regimes is simply a convolution of these two linear limits, and thus does not require an additional term in the overall rate expression.

The parameters calculated by fitting the variable-temperature lifetime of the $Mo_2Cl_4(PR_3)_4$, $Mo_2Cl_4(EMe_3)_4$, and $Mo_2X_4(PMe_3)_4$ complexes to equation (3) are set out in Table II. Note that these parameters for the $Mo_2Cl_4(PR_3)_4$ and $Mo_2Cl_4(EMe_3)_4$ series are derived from analyses of k_{obs} rather than k_{nr} since the emission lifetimes of most of these compounds at room temperature are too short to allow accurate estimates of k_r (Table I). Comparisons among these parameters for the $Mo_2Cl_4(PR_3)_4$ and $Mo_2Cl_4(EMe_3)_4$ systems are thus valid if k_r is roughly constant; the near equivalence of the values of k_r^{calc} (Table I) and k^0 (Table IIa) suggest that this is indeed the case. For the $Mo_2X_4(PMe_3)_4$ series (Table IIb), values of k_{nr} were obtained from the observed data using equation (2) with the assumption that k_r is temperature independent.[26]

The most noteworthy feature of the data presented in Tables I and II is that the dramatically differing photophysical behavior of these derivatives at room temperature seems to be largely attributable to variations the Arrhenius preexponential term k^1. Also quite striking is the fact that the lifetime of $W_2Cl_4(PMe_3)_4$ (Table I), in contrast, is essentially constant over this same range of temperatures.

Medium Dependence of the Photophysical Properties of $Mo_2Cl_4(PMe_3)_4$.

The luminescence lifetimes and quantum yields of the $Mo_2X_4L_4$ complexes are substantially less in polar or unsaturated hydrocarbon solvents than those reported in the previous section for saturated hydrocarbon solution. While for most com-

Table II. Arrhenius Parameters for $Mo_2X_4L_4$ Complexes in 2-methylpentane.[a]

Compound	$E_a/10^3$ cm^{-1}	$k^0/10^6$ sec^{-1}	$k^1/10^{12}$ sec^{-1}
(a)			
$Mo_2Cl_4(PMe_3)_4$	3.3	5.8	14.6
$Mo_2Cl_4(PEt_3)_4$	2.2	5.4	4.1
$Mo_2Cl_4(PPr^n_3)_4$	2.4	5.3	4.6
$Mo_2Cl_4(PBu^n_3)_4$	2.3	5.2	3.8
(b)			
$Mo_2Cl_4(PMe_3)_4$	3.3	3.7	14.6
$Mo_2Br_4(PMe_3)_4$	3.5	5.1	20.0
$Mo_2I_4(PMe_3)_4$	2.5	5.3	4.5

[a]Parameters derived from nonlinear least-squares fit of observed data to $k_{obs} = k^0 + k^1 \exp(-E_a/k_bT)$ (part a) and $k_{nr} = k^0_{nr} + k^1_{nr} \exp(-E_a/k_bT)$ (part b).

pounds these lifetimes are below the detection limit of our apparatus, the emission of the $Mo_2Cl_4(PMe_3)_4$ dimer is sufficiently long-lived in most solvents to probe the origin of this effect. The spectroscopic and photophysical parameters of this complex in a variety of solvents are set out in Table III. The data are arranged to highlight four parallel trends: proceeding down the table, the $^1(\delta \rightarrow \delta^*)$ absorption maximum systematically blue shifts, the fluorescence band red shifts, and both the emission lifetime and quantum yield decrease. A compilation of experimental and empirical parameters that characterize these solvents is given in Table IV; in no instance is there a clear correlation between the solvent trend imposed by any one of these parameters and that obtained from the observed data. Also included in Table III are two significant solvent perturbations that are *not* of photophysical significance for this complex: solvent deuteration (h_{12}- *vs.* d_{12}-cyclohexane and h_6- *vs.* d_6-benzene) and viscosity (nujol *vs.* 2-methylpentane and cyclohexane).

Since the decrease in the room temperature emission lifetime of $Mo_2Cl_4(PMe_3)_4$ (as one proceeds down Table III) is mirrored by the relative quantum yield, the medium dependence of these parameters can be attributed to the solvent sensitivity of the nonradiative decay rate. Specifically, k_{nr} increases by a factor of five from 2-methylpentane and dichloromethane and, based on the ratio of the lifetimes, at least doubles again from dichloromethane to *N*,*N*-dimethylformamide and acetonitrile; k_r, in contrast, is nearly constant. Examining the variable-temperature lifetime behavior of $Mo_2Cl_4(PMe_3)_4$ in the four solvents from Table III that remain fluid over an appreciable temperature range reveals (Figure 4) that there is a marked temperature dependence of the lifetime in each solvent, which, as was argued in the previous section, is due to the temperature dependence of k_{nr}. Interestingly, the lifetime of $Mo_2Cl_4(PMe_3)_4$ in each solvent approaches the same limiting value at low temperature.

Table III. Medium Dependence of the Spectroscopic and Photophysical Parameters of $Mo_2Cl_4(PMe_3)_4$.[a]

Solvent	Absorption $^1(\delta\rightarrow\delta^*)$		Emission $^1(\delta^*\rightarrow\delta)$					
	λ_{max}/nm	$\Delta\bar{\nu}_{max}$/cm^{-1}[b]	λ_{max}	$\Delta\bar{\nu}_{max}$[b]	τ/ns	ϕ_{rel}[c]	$k_r/10^6$ s^{-1}	$k_{nr}/10^6$ s^{-1}
2-methylpentane	585	0	673	0	125	1.0	2.1	5.9
cyclohexane	d	-	d	-	122	d	---	---
d_{12}-cyclohexane	d	-	d	-	125	d	---	---
nujol	d	-	d	-	120	d	---	---
benzene	584	+30	682	-195	80	0.46	1.5	11.0
d_6-benzene	d	-	d	-	77	d	---	---
i-propanol	583	+60	694	-450	65	0.32	1.3	14.1
dichloromethane	582	+90	694	-450	35	0.18	1.3	27.2
N,N-dimethyl-formamide	581	+120	695	-470	<15	0.11	---	---
acetonitrile	580	+150	696	-490	<15	0.09	---	---

[a]All values recorded at room temperature (23°C).

[b]Frequency shift of band maximum relative to 2-methylpentane.

[c]Not corrected for index of refraction.

[d]Not measured; presumably identical to the solvent reported above.

Figure 4. Temperature dependence of k_{obs} of $Mo_2Cl_4(PMe_3)_4$ in various solvents: (◯) = 2-methylpentane; (▶) = nujol; (□)= *i*-propanol; (◇) = dichloromethane.

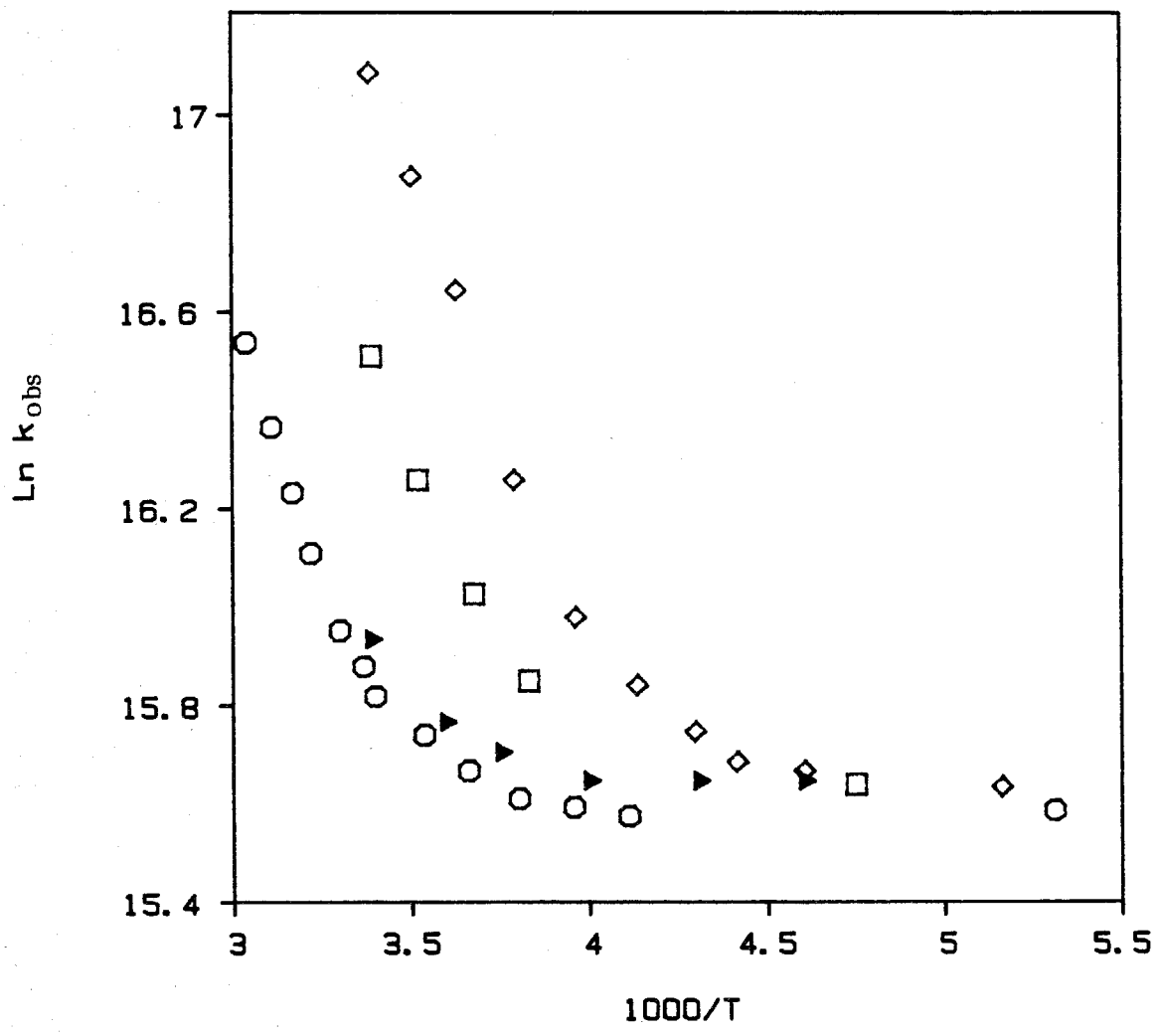
17
16.6
16.2
15.8
15.4
Ln k_{obs}
3
3.5
4
4.5
5
5.5
1000/T

Table IV. Physical and Empirical Constants of Solvents.[a]

Solvent	D_s[b]	D_{op}[b]	μ_g[b]	E_T[c]	Z[d]	AN[e]	DN[e]
hexane	1.9	1.882	0	30.9	---	0.0	0.0
benzene	2.27	2.244	0	34.5	54.0	8.2	0.1
i-propanol	18.3	1.89	1.66	48.6	76.3	33.5	---
dichloromethane	8.9	2.028	1.6	41.1	64.2	20.4	---
N,N'-dimethyl formamide	36.7	2.0458	48.3	43.8	68.5	16.0	26.6
acetonitrile	36.2	1.8066	3.92	46.0	71.3	18.9	14.1

[a] D_s and D_{op} are the static and optical dielectric constants, μ_g is the gas phase dipole moment, E_T and Z are empirical solvent scales related to optical charge charge transfer energies of pyridinium derivatives, and AN and DN are the Gutman acceptor number and donor number, respectively.

[b] Lever, A. P. B. "Inorganic Electronic Spectroscopy"; Elsevier: Amsterdam, 1984, p. 211.

[c] Reichardt, C. Angew. Chem., Int. Ed. Engl. **1965**, 4, 29.

[d] Kosower, E. M. J. Am. Chem. Soc. **1958**, 80, 3253.

[e] Gutman, U. "The Donor-Acceptor Approach to Molecular Interactions"; Plenum: New York, 1980.

Discussion

The interpretation of molecular photophysics usually requires some understanding of the nature of the potential energy surfaces of the states between which the radiative and nonradiative processes occur. Because the details of the surface of the $^1(\delta\delta^*)$ state will not be presented until the following chapter, some of the following discussion will be based on elementary considerations of the theory of nonradiative decay, and will be reconsidered at the conclusion of Chapter V. The rationale for presenting this chapter first is that the interpretation of the vibronic structure resolved in the $^1(\delta \rightarrow \delta^*)$ and $^1(\delta^* \rightarrow \delta)$ transitions at low temperature relies in part on the findings presented herein.

The data in Tables I and III indicate that the sensitivity of the emission lifetimes and quantum yields of the $Mo_2X_4L_4$ complexes to ligand, temperature, and medium can be traced to variations in their rates of nonradiative decay. The radiative rate of this chromophore, in contrast, is only slightly perturbed by these variables, instead being sensitive only to the oscillator strength of the $^1(\delta \rightarrow \delta^*)$ transition. The key conclusion to be drawn from this latter observation is that the molecular distortions that these species undergo upon population of the $^1(\delta\delta^*)$ excited state do not alter the dipole-allowed character of the $^1(\delta^* \rightarrow \delta)$ transition. As noted in a previous investigation of complexes of this type,[2] this behavior is quite different from that encountered for the $Re_2Cl_8^{2-}$ ion, the radiative rate of which is four orders of magnitude below its Strickler-Berg[22] expectation value. This is indicative of an excited state distortion that imparts the $^1(\delta^* \rightarrow \delta)$ transition with substantial forbidden character.

In contrast to the straightforward explanation of the radiative processes of the

$M_2X_4L_4$ complexes, the interpretation of their nonradiative decay rates, and the identification of the specific pathways responsible for the radiationless deactivation of the $^1(\delta\delta^*)$ state, is a considerably more difficult task. It is traditional to commence the discussion of these aspects of the photophysics of transition metal complexes with a summary of the theoretical treatment of Englman and Jortner.[31] Because of the complexity of metal complexes from an electronic and vibrational standpoint, however, it is also traditional to not draw anything resembling an unambiguous conclusion concerning the nature of these processes. Because the nonradiative properties described here are no less complex than those reported for most mononuclear species, we will not deviate from this useful precedent. Quite briefly, and ignoring the numerous approximations employed in the following derivations, the nonradiative transition probability is given by

$$W = \frac{C^2}{\hbar^2} exp(-G) \int_{-\infty}^{\infty} exp\left[\frac{-i\Delta E_t}{\hbar} + G_+(t) + G_-(t)\right] dt \qquad (4)$$

where G, which is a dimensionless parameter that is a measure of the displacement of the two adiabatic potential energy surfaces with respect to each other, is given by

$$G \cong \frac{E_M}{\hbar < \omega >} coth\left(\frac{\hbar < \omega >}{2kT}\right) \qquad (5)$$

In equation 5, E_M is roughly one-half the difference of the energies of the vertical transitions between the two surfaces, and $< \omega >$ is the average vibrational frequency taken over all normal modes. Two analytical limits for the evaluation of the integral in the expression for W are derived from the magnitude of G; the potential energy surfaces corresponding to these two limits are shown in Figure 5. For $G \gg 1$, which is refered to as the strong coupling limit, equation 4 reduces to

$$W_{SC} = \frac{C^2}{\hbar} \sqrt{\frac{2\pi}{E_M k_b T^*}} exp\left(\frac{-E_a}{k_b T^*}\right) \qquad (6)$$

Figure 5. Qualitative representation of the ground and excited state potential energy surfaces in the (a) weak- and (b) strong-coupling regimes of nonradiative decay.

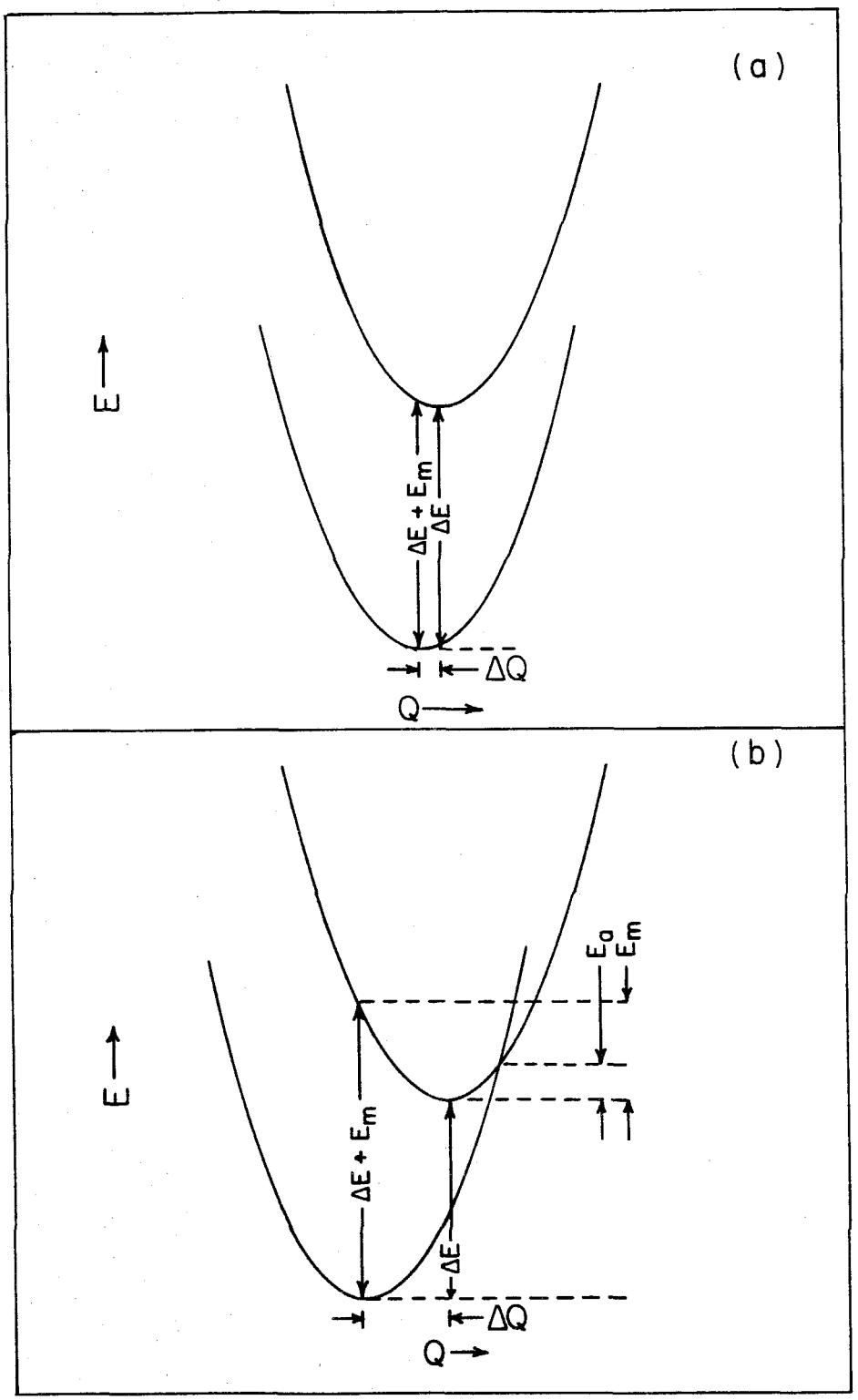
(a)
E
ΔE + Em
ΔE
ΔQ
Q
(b)
E
Eo
Em
ΔE + Em
ΔE
ΔQ
Q

where C is a matrix element connecting the two states, and T^* and E_a are given by

$$T^* = \frac{1}{2}\frac{\hbar < \omega >}{k_b} coth\left(\frac{\hbar < \omega >}{2k_bT}\right) \tag{7}$$

$$E_a = \frac{(\Delta E - E_M)^2}{4E_M} \tag{8}$$

Two additional expressions can be derived from equation 6 by considering its high- (9) and low- (10) temperature limits

$$W_{SC}^{HT} = \frac{k_bT}{\hbar} C^2 \sqrt{\frac{2\pi}{E_M(k_bT)^3}} exp\left(\frac{-E_a}{k_bT}\right) \tag{9}$$

$$W_{SC}^{LT} = C^2 \sqrt{\frac{4\pi}{E_M\hbar < \omega >}} exp\left(\frac{-2E_a}{\hbar < \omega >}\right) \tag{10}$$

In the weak coupling regime ($G \leq 1$), W is given by

$$W_{WC} = \frac{C^2}{\hbar} \sqrt{\frac{2\pi}{\hbar\omega_m \Delta E}} exp\left(\frac{-\gamma\Delta E}{\hbar\omega_m}\right) \tag{11}$$

where ΔE is the difference in the zero-point energies of the two surfaces, γ is a measure of the displacement of the surfaces, and ω_m is the value of the highest frequency normal mode.

Examining first the low temperature region of the variable temperature lifetimes of the $Mo_2X_4L_4$ complexes in light of the above discussion indicates that either the strong or weak coupling limits could account for the observed behavior of these species. While we have not attempted to differentiate between these two regimes, a key experimental test along these lines would be H/D isotope exchange, since, according to equation 11, the nonradiative rate should be sensitive to the highest frequency vibrations in the molecule, which are efficient accepting modes;[32] the emission of $Mo_2Cl_4(P(CH_3)_3)_4$ would presumably be shorter lived than that of $Mo_2Cl_4(P(CD_3)_3)_4$. A second prediction of equation (11) is the presence of an

energy gap dependence of the nonradiative rate, and this has been invoked by others as evidence for the weak coupling limit in some types of metal complexes.[33] Since the low-temperature lifetimes of the $M_2X_4L_4$ species increase with decreasing $^1(\delta \rightarrow \delta^*)$ transition energy (Table I), such an effect could be claimed here. The energy dependence is a fairly small one, however, and its interpretation is further clouded by the fact that $k_{nr} \cong k_r$ at these temperatures; as noted in Chapter II, there is, in essence, an energy gap dependence of the $^1(\delta \rightarrow \delta^*)$ oscillator strength, and hence also of k_r.

There is less ambiguity regarding the interpretation of the high-temperature region of the variable-temperature lifetime data within the Englman and Jortner framework, since only the expressions for the strong coupling nonradiative regime contain temperature as a variable. Moreover, equation 9 strongly resembles an Arrhenius rate expression. The nonradiative decay scenario suggested by this comparison is that at high temperatures the $^1(\delta\delta^*)$ state is depopulated *via* a surface crossing with a different electronic state. While this second state is indicated to be the ground state in Figure 5, this need not be the case; higher energy excited states may also be involved. This latter possibility seems to be the more likely of the two; the large separation of the $^1(\delta\delta^*)$ and $^1(\delta^2)$ states ($\Delta E + E_M$ = 15000 - 20000 cm^{-1}) would require a value of E_M much larger than is experimentally observed, as can be inferred from the discussion in the following chapter. Because the $^3(\delta\delta^*)$ and $^1(\delta^2)$ states lie in close energetic proximity, similar considerations also make it an unlikely candidate for such a crossing. There are, however, several excited states that lie just above $^1(\delta\delta^*)$, as discussed in Appendixes II and IV. Because the energetic differences between $^1(\delta\delta^*)$ and these upper states are dependent on the nature of the inner coordination sphere, the variations among the Arrhenius activation energies of the $Mo_2X_4(PMe_3)_4$ series and $Mo_2Cl_4(AsMe_3)_4$ are not particularly

surprising. In contrast, the electronic spectra of the $Mo_2Cl_4(PR_3)_4$ compounds are superimposible, which suggests that they should possess identical E_a's. While the fact that they do not may simply represent the uncertainty in these values,[34] it is also possible that the barrier to the activated decay process, or even the process itself, differs among these species.

If we assume, for simplicity, that the nonradiative activation energies of the $Mo_2Cl_4(PR_3)_4$ series are identical, then the differences in the rates of nonradiative decay among these compounds are entirely due to the k^1 preexponential term, the value of which is on the order of 10^{13} s^{-1}.[35] While this is in reasonable agreement with expectations for a unimolecular reaction,[36] this should not be taken too seriously as an indication that either the simple rate expression used here (3), or that derived from a more rigorous approach (9), is successful in decomposing the overall nonradiative rate into physically interpretable parameters, especially since values of k^1 as high as 10^{22} s^{-1} have been reported for such processes.[37] In any case, the only variable in the preexponential term of equation (9) that is left to explain these ligand-induced lifetime perturbations is C, which is the matrix element that connects the initial and final states. Needless to say, the exact fashion in which this term depends on the length of the alkyl chain is less than obvious.

Although the conclusions drawn from the analysis of the nonradiative rates within the Englman and Jortner framework are less than satisfying, there is one aspect of the photophysical properties of the $M_2X_4L_4$ compounds that seems to be interpretable from a more intuitive standpoint. Specifically, while there is a large difference in the nonradiative rates of $Mo_2Cl_4(PMe_3)_4$ and $Mo_2Cl_4(PEt_3)_4$, additional lengthening of the alkyl chain of the phosphine does not alter this rate further. Inasmuch as introducing carbon-carbon bonds, or, more specifically, introducing the vibrations associated with this linkage, into the $M_2X_4L_4$ chromophore

greatly enhances nonradiative decay, we conclude that these are efficient *promoting modes*[32] for deactivating the $^1(\delta\delta^*)$ state. The fact that additional lengthening of the alkyl chain does not increase the nonradiative rate further is evidence that the efficiency of these modes is very high indeed.[39]

References and Notes

1. Fleming, R. H.; Geoffroy, G. L.; Gray, H. B.; Gupta, A.; Hammond, G. S.; Kliger, D. S.; Miskowski, V. M. *J. Am. Chem. Soc.* **1976**, *98*, 48-50.
2. Miskowski, V. M.; Goldbeck, R. A.; Kliger, D. S.; Gray, H. B. *Inorg. Chem.* **1979**, *18*, 86-89.
3. Trogler, W. C.; Solomon, E. I.; Trajberg, I.; Ballhausen, C. J.; Gray, H. B. *Inorg. Chem.* **1977**, *16*, 828-836.
4. Trogler, W. C.; Solomon, E. I.; Gray, H. B. *Inorg. Chem.* **1977**, *16*, 3031-3033.
5. Morgante, C. G.; Struve, W. S. *Chem. Phys. Lett.* **1979**, *63*, 344-346.
6. Manning, M. C.; Trogler, W. C. *J. Am. Chem. Soc.* **1983**, *105*, 5311-5320.
7. Fraser, I. F.; Peacock, R. D. *Chem. Phys. Lett.* **1983**, *98*, 620-623.
8. Chapter V. Hopkins, M. D.; Gray, H. B. *J. Am. Chem. Soc.* **1984**, *106*, 2468-2469.
9. Fanwick, P. E. *Inorg. Chem.* **1985**, *24*, 258-263.
10. Miskowski, V. M.; Twarowski, A. J.; Fleming, R. H.; Hammond, G. S.; Kliger, D. S. *Inorg. Chem.* **1978**, *17*, 1056-1059.
11. In fact, reference 2 is one of the most insightful papers yet written on the properties of the excited states of quadruply bonded dimers.
12. Chapter II.
13. A preliminary account of this work has appeared: Zietlow, T. C.; Hopkins, M. D.; Gray, H. B. *J. Solid State Chem.* **1985**, *57*, 112-119.
14. Perrin, D. D.; Armarego, W. L. F.; Perrin, D. R. "Purification of Laboratory Chemicals"; Pergamon: Oxford, 1966.
15. Glicksman, H. D.; Hamer, A. D.; Smith, T. J.; Walton, R. A. *Inorg. Chem.* **1975**, *15*, 2205-2209.

16. San Filippo, J., Jr.; Sniadoch, H. J.; Grayson, R. L. *Inorg. Chem.* **1974**, *13*, 2121-2130.

17. Schrock, R. R.; Sturgeoff, L. G.; Sharp, P. R. *Inorg. Chem.* **1983**, *22*, 2801-2806. Sharp, P. R.; Schrock, R. R. *J. Am. Chem. Soc.* **1980**, *102*, 1430-1431.

18. Demas, J. N.; Crosby, G. A. *J. Phys. Chem.* **1971**, *75*, 991-1024.

19. Nocera, D. G.; Winkler, J. R.; Yocom, K. M.; Bordignon, E.; Gray, H. B. *J. Am. Chem. Soc.* **1984**, *106*, 5145-5150.

20. Marquardt, D. W. *J. Soc. Ind. Appl. Math.* **1963**, *11*, 431-441.

21. The temperature and ligand dependence of the emission of the $Mo_2X_4L_4$ chromophore reported herein for the solution phase is also observed in the solid state. Since quantum yields for the latter are unattainable in our laboratory, however, discussion of the photophysical properties of these systems will largely be restricted to fluid media.

22. Porter, G. B. in "Concepts of Inorganic Photochemistry", Adamson, A. W.; Fleischauer, P. D. eds.; Wiley: New York, 1975, ch. 2.

23. Wavelength-dependent emission quantum yields have been reported previously for one quadruply bonded complex (*cis*-$Mo_2(mhp)_2Cl_2(PEt_3)_2$)[9]; no explanation of this observation has been offered.

24. All emission lifetimes reported in this study were acquired under conditions. Thus, k_{nr} refers strictly to the rate of decay of the $^1(\delta\delta^*)$ state *via* internal conversion, intersystem crossing, etc., and does not contain contributions from excited state reaction rates.

25. $Mo_2Cl_4(PMe_3)_4$ (solid state): τ(70 K) = 115 ns; τ(40 K) = 120 ns; τ(4.2 K) = 120 ns.

26. The approach described here for evaluating k_{nr} has not been employed in previous studies of the variable-temperature photophysics of transition metal com-

plexes since these have nearly exclusively focussed on spin-forbidden luminescent processes (see references 27-30 for examples). For "phosphorescence", $k_r << k_{obs}$ and thus $k_{nr} \sim k_{obs}$, while for the fluorescent quadruply bonded complexes described here k_r and k_{nr} are of nearly equal magnitude.

27. Bergkamp, M. A.; Watts, R. J.; Ford, P. C. *J. Phys. Chem.* **1981**, *85*, 684-686. ($Rh(NH_3)_5X^{2+}$).

28. Durham, B.; Caspar, J. V.; Nagle, J. K.; Meyer, T. J. *J. Am. Chem. Soc.* **1982**, *104*, 4803-4810. ($Ru(bpy)_3^{2+}$).

29. Endicott, J. F.; Tamilarasan, R.; Lessard, R. B. *Chem. Phys. Lett.* **1984**, *112*, 381-386. (Cr(III) complexes).

30. Zietlow, T. C. *Ph. D. Thesis*, California Institute of Technology, Pasadena, CA, 1985, chapters 2 and 3.

31. Englman, R.; Jortner, J. *Mol. Phys.* **1970**, *18*, 145-164.

32. Lin, S. H.; Bersohn, R. *J. Chem. Phys.* **1968**, *48*, 2732-2736.

33. Caspar, J. V.; Kober, E. M.; Sullivan, B. P.; Meyer, T. J. *J. Am. Chem. Soc.* **1982**, *104*, 630-632.

34. Because the transition between the high- and low-temperature regions of the lifetime data occurs fairly close to room temperature, the data points for the activated process, from which E_a is determined, have not yet approached linearity. This is a major source of error in E_a.

35. The main exception to this is $W_2Cl_4(PMe_3)_4$, which must have a fairly small k^1 in order for the activated region of the variable-temperature lifetime data to be shifted well above room temperature.

36. Moore, J. W.; Pearson, R. G. "Kinetics and Mechanism"; Wiley: New York, 1981; pp 116-129.

37. Endicott, J. F., presented at the Biennial Inorganic Chemistry Symposium,

York University, Toronto, Canada, June 1985.

38. Such promoting modes are excluded from the Englman and Jortner treatment, and are replaced $< \omega >$ for simplicity.

39. We shall delay discussion of the medium effects on the photophysical properties of $Mo_2Cl_4(PMe_3)_4$ until the following chapter.

CHAPTER V

The Molecular and Electronic Structure of the $^1(\delta\delta^*)$ State

Introduction

The $^1(\delta \rightarrow \delta^*)$ electronic transition of quadruply metal-metal bonded complexes has been the subject of extensive spectroscopic and theoretical study in the 15 years following the first correct identification of this band in the spectrum of the $Re_2Cl_8^{2-}$ ion.[1,2] The motivation for investigations along these lines is two-fold: First, the energy and intensity of this transition are fingerprint parameters that can be used (albeit with limited success, as noted in Chapter II) to qualitatively estimate the differences in ground state δ-overlap among these complexes,[3-5] and second, analysis of the vibronic structure resolved within this transition at low temperature yields insight into the nature of the bonding in the $^1(\delta\delta^*)$ excited state.[2,6-10] Because these excited states have only a fleeting existence ($\tau \sim 10^{-9}$ - 10^{-7} s), this latter form of analysis is as crucial to the elucidation of their molecular structures as is x-ray crystallography to the study of their ground states.

In evaluating the structural distortions associated with population of the $^1(\delta\delta^*)$ excited state of quadruply bonded dimers, previous spectroscopic studies[6-10] have emphasized elongation along the metal-metal axis as the principle distortion. The observation of long, intense progressions in the metal-metal stretching mode ($\nu_1(M_2)$) in this band at high resolution[2] has led, in fact, to the proposal that the metal-metal-localized character of this transition is extremely high for some types of quadruply bonded complexes,[11] and this seems entirely reasonable inasmuch as $^1(\delta \rightarrow \delta^*)$ is a metal-metal bonding-antibonding transition. As was noted in Chapter II, however, there is a great deal of evidence to support the notion that the nature of the ligand plays a large role in determining the intensity and energy of the $^1(\delta \rightarrow \delta^*)$ transition in many classes of these complexes, including cases, such as the $Mo_2X_4(PMe_3)_4$ (X = Cl, Br, I) series, where these ligand perturbations have

no effect upon the metal-metal distance of the chromophore. Clearly, an adequate description of the potential energy surfaces of the $^1[\sigma^2\pi^4\delta^2]$ and $^1[\sigma^2\pi^4\delta\delta^*]$ states of such compounds cannot be derived from analysis of their spectra solely within this metal-metal-localized vibronic framework. Reported in this chapter are the results of a high-resolution spectroscopic study of the $^1(\delta \rightarrow \delta^*)$ and $^1(\delta^* \rightarrow \delta)$ transitions of the $M_2X_4L_4$ (M = Mo, W; X = Cl, Br, I; L = PR_3, $AsMe_3$) class of complexes. This investigation has led to a reconsideration of the traditional view[2] of the molecular structures of the $^1(\delta\delta^*)$ excited state of quadruply bonded dimers.[12]

Experimental Section

Materials.

2-Methylpentane was dried by refluxing with lithium aluminum hydride, degassed with five freeze-pump-thaw cycles on a high-vacuum manifold (limiting pressure $< 10^{-3}$ torr), and bulb-to-bulb distilled to an evacuated storage flask containing lithium aluminum hydride. The complexes $Mo_2X_4(PMe_3)_4$ (X = Cl, Br, I),[13] $Mo_2Cl_4(PR_3)_4$ (R = Et, n-Pr, n-Bu),[14] $Mo_2Br_4(PEt_3)_4$,[15] $Mo_2Cl_4(AsMe_3)_4$,[13] $Mo_2Cl_4(SMe_2)_4$,[16] $W_2Cl_4(PMe_3)_4$,[17] $(TBA)_2Re_2Cl_8$ [18] (TBA = $(n\text{-}C_4H_9)_4N$), and $K_4Mo_2Cl_8$[19] were prepared according to standard procedures; satisfactory carbon and hydrogen elemental analyses were obtained for each. $MoWCl_4(PMe_3)_4$[20] was supplied by R. L. Luck and R. H. Morris of the University of Toronto, and was recrystallized from hexane. Crystals of $Mo_2Cl_4(PMe_3)_4$ and $Mo_2Br_4(PMe_3)_4$ for single-crystal experiments were grown by slow evaporation of dichloromethane and toluene solutions, respectively.

Spectroscopic Measurements.

High-resolution emission spectra were recorded on an instrument constructed

at Caltech that has been described previously.[21] This spectrometer was calibrated at high resolution against the output of a medium pressure Hg/Xe arc lamp. Correction of emission intensities for spectrometer response[22] was accomplished either by digitally recording the data *via* a computer interface (On Line Instrument Systems Inc. Model 3820 data collection system) and processing with an internal computer program, or by point-by-point multiplication of analog spectra by the appropriate correction factors. Absorption spectra were recorded with a Cary 17 spectrophotometer that was wavelength-calibrated with a deuterium lamp. Polarized light for single-crystal absorption measurements was obtained with dual Glan-Thompson air-spaced calcite polarizers. Low-temperature absorption and emission experiments were performed with three temperature control systems: a quartz optical dewar of local design (77 K measurements); an Oxford Instruments CF-204 continuous-flow cryostat equipped with a Model 3120 temperature controller, Model VC30 flow regulator, Model GFS300 gas-cooled transfer line, and a Rh/Fe thermocouple (5 K measurements); or an Andonian Associates Model 024 liquid helium dewar system that has been described elsewhere[23] (5 K measurements).

Hydrocarbon solutions for 77 K glassy matrix experiments were prepared on the vacuum line in an evacuable 1 cm pathlength quartz cuvette attached to a high-vacuum teflon stopcock. Highly dilute solutions (optical density < 0.1 at the $^1(\delta \rightarrow \delta^*)$ absorption maximum) were used for emission measurements because of the strong self-absorption of the emission by these compounds. Samples for 5 K high-resolution emission spectra consisted of polycrystalline arrays mounted on copper foil with petroleum jelly or silicone grease. Absorption spectra at 5 K were recorded of CsX pellets that were pressed at high pressure, reground, and pressed again to attain good optical quality, or of single crystals mounted on quartz flats. These latter samples were carefully masked with heat conducting grease (fine copper

powder suspended in vacuum grease) in order to provide good thermal contact with the cold station of the dewar. Single crystals for polarized absorption and emission spectra were mounted such that the crystal extinction directions were at 45° angles to the entrance slit of the detection monochromator, thus minimizing band-shape errors introduced by polarization-dependent grating artifacts (*i.e.*, Wood's Anomaly). Crystal thicknesses (for extinction coefficient calculations) were determined with a micrometer. The crystal from which low-temperature absorption data for $Mo_2Cl_4(PMe_3)_4$ were obtained did not survive warm-up, and thus no extinction coefficients could be determined in this case.

The crystal faces of the isomorphous ($C2/c$) $Mo_2Cl_4(PMe_3)_4$[24] and $Mo_2Br_4(PMe_3)_4$[13] dimers were determined by x-ray photographic methods and polarized optical microscopy. Polarized single-crystal spectra were recorded of the prominent (101) face of these crystals; the molecular z axis is colinear with the crystallographic b axis, which is contained by this crystal face (see Chapter II, Figure 1). Under the crystallographically imposed C_2 symmetry of these dimers, polarization parallel to molecular-z ($\parallel b$) is rigorously split from that parallel to x and y ($\perp b$). Consistent with this, examination of the (101) crystal face under a polarizing microscope showed sharp extinctions parallel and perpendicular to b that transmitted dark blue and light greenish-yellow light, respectively. Although the molecular-x and -y directions are not strictly equivalent under C_2 symmetry, the deviations of the molecular structures of $Mo_2Cl_4(PMe_3)_4$ and $Mo_2Br_4(PMe_3)_4$ from D_{2d} symmetry, for which x and y are degenerate, are quite small.

Franck-Condon Calculations.

Franck-Condon calculations of absorption and emission bands were performed with the computer program SPCT, which was written by V. M. Miskowski and D. E. Brinza and modified for the IBM PC/AT by M. S. Albin and the author. Vi-

bronic line intensities are calculated by this program using standard formalisms;[25] the energy of the electronic origin(s), initial and final state vibrational frequencies of up to three modes, and the Huang-Rhys factors ($S \equiv I_{0-1}/I_{0-0}$) serve as adjustable parameters. To obtain the final intensity profile, a convoluted homogeneous (Lorentzian) and inhomogeneous (Gaussian) line shape is computed and summed for all lines, and a correction for the frequency dependence of the transition probability (*cf.* Einstein A and B coefficients)[26] is applied.

Results

The $^1(\delta \rightarrow \delta^*)$ absorption and $^1(\delta^* \rightarrow \delta)$ emission bands of many complexes of the $M_2X_4L_4$ type are highly vibronically resolved at low temperature. Since the extent of this resolution is generally very sensitive to both medium and temperature, and since these dependencies differ, in turn, from derivative to derivative, we have obtained complementary spectral data for these compounds under several conditions. Our results will be presented in the following order: isotropic absorption and emission spectra of glassy hydrocarbon matrices at 77 K; emission spectra of polycrystalline solids at 5 K; and absorption spectra of alkali halide pellets and polarized single crystals at 5 K.

77 K Absorption and Emission Spectra.

The absorption and emission spectra observed for $M_2X_4L_4$ complexes in 2-methylpentane at 77 K show, with one exception, a progression in a single vibrational mode, the spacings of which correspond to the metal-metal stretching frequencies ($\nu_1(M_2)$) of the excited (ν_1^*) and ground states (ν_1), respectively. In all instances, there is a strong overlap of the $^1(\delta \rightarrow \delta^*)$ absorption and $^1(\delta^* \rightarrow \delta)$ emission 0-0 bands, confirming that they represent transitions between the same

states.[27] The vibronic peak maxima and spacings observed for these spectra are set out in Table I; the values of ν_1^* for the $^1(\delta\delta^*)$ excited states of these compounds are no more than 10% lower than those of their δ^2 ground states, which is consistent with the weakly bonding nature of the δ-interaction that is cancelled upon $^1(\delta \rightarrow \delta^*)$ excitation.

Reproduced in Figure 1 are the spectra of the $Mo_2X_4(PMe_3)_4$ (X = Cl, Br, I) series of complexes. Although the extinction coefficients and energies of the transitions depend strongly on the nature of the halide ligand X, as was discussed in detail in the preceding chapter, the absorption band profiles of all three complexes are virtually identical. In each spectrum, the 0-2 vibronic transition is the most intense feature, with the intensities of the other progression members being defined by very similar Huang-Rhys factors. This intensity pattern is also observed for the $^1(\delta \rightarrow \delta^*)$ bands of $Mo_2Cl_4(AsMe_3)_4$,[29] $Mo_2Br_4(PEt_3)_4$,[29] and $Mo_2Cl_4(PBu^n_3)_4$[30] in 2-methylpentane at 77 K, as well as for single crystals of $K_4[Mo_2Cl_8]2H_2O$ at 5 K,[31] and thus appears to be the general band profile for all unbridged d^4-d^4 molybdenum dimers at this level of resolution. The only difference of note among the absorption spectra in Figure 1 is that the individual vibronic transitions broaden slightly across the series I < Br < Cl, resulting in a small change in the ratio of the intensities of the 0-1 and 0-3 lines. The line width is not markedly sensitive to changes in ligand L, however, as demonstrated by the similarity of the $^1(\delta \rightarrow \delta^*)$ bands of $Mo_2Cl_4(PBu^n_3)_4$, $Mo_2Cl_4(PMe_3)_4$, and $Mo_2Cl_4(AsMe_3)_4$.

In contrast to their $^1(\delta \rightarrow \delta^*)$ transitions, the intensity profiles of the $^1(\delta^* \rightarrow \delta)$ emission bands of the $Mo_2X_4L_4$ complexes are a highly sensitive function of ligand. Examining first the $Mo_2X_4(PMe_3)_4$ series (Figure 1) reveals that a large, progressive broadening of the individual vibronic transitions of the bromo and chloro complexes results in the striking deviation of their absorption and emission spectra from the

Table I. Vibronic Peak Maxima and Spacings of the $^1(\delta\rightarrow\delta^*)$ Absorption and $^1(\delta^*\rightarrow\delta)$ Emission Bands of $M_2X_4L_4$ in 2-methylpentane at 77 K.

Compound	$^1(\delta\rightarrow\delta^*)$ $\bar{\nu}/cm^{-1}$		$^1(\delta^*\rightarrow\delta)$ $\bar{\nu}/cm^{-1}$	
$Mo_2Cl_4(PMe_3)_4$	16480		16290	
		350		390
	16830		15900	
		330		380
	17160		15520	
		340		370
	17500		15150	
		330		290
	17830		14860	
	Av. = 335(10)		Av. = 355(30)	
$Mo_2Br_4(PMe_3)_4$	16120		14620	
		350		360
	16470		14820	
		330		160
	16800		14980	
		330		360
	17130		15170	
		340		170
	17470		15340	
	Av. = 340(10)		15540	340
				140
			15680	
				360
			16040	
			Av. = 160(10)	
			Av. = 355(10)	
$Mo_2I_4(PMe_3)_4$	15160		15110	
		320		350
	15480		14760	
		320		350
	15800		14410	
		310		340
	16110		14070	
		330		340
	16440		13730	
	Av. = 320(10)		Av. = 345(10)	
$Mo_2Cl_4(AsMe_3)_4$	16850		16640	
		330		380
	17180		16260	
		350		340
	17530		15920	
		330		
	17860			
		340		
	18200			
	Av. = 340(10)		Av. = 360(30)	
$Mo_2Cl_4(PEt_3)_4$			16180	
				340
			15840	
				350
			15490	
				360
			15130	
			Av. = 350(10)	
$Mo_2Cl_4(PPr^n_3)_4$			16230	
				360
			15870	
				350
			15520	
				350
			15170	
			Av. = 355(10)	

Table I. (continued)

Compound	$^1(\delta \rightarrow \delta^*)$ $\bar{\nu}/cm^{-1}$		$^1(\delta^* \rightarrow \delta)$ $\bar{\nu}/cm^{-1}$	
$Mo_2Cl_4(PBu^n_3)_4$		Av. = 320(10)[a]	16220 15870 15520 15160	350 350 360 Av. = 355(10)
$Mo_2Br_4(PEt_3)_4$	15990 16310 16630 16960 17290	320 320 330 330 Av. = 325(10)	15900 15550 15200 14860 14540	350 350 340 320 Av. = 340(10)
$W_2Cl_4(PMe_3)_4$	14780 15040 15280	260 240 Av. = 250(30)	unstructured emission	

[a]Ref. 30.

Figure 1. Absorption (—) and corrected emission (- - -) spectra of $Mo_2X_4(PMe_3)_4$ in 2-methylpentane at 77 K: (a) X = Cl; (b) X = Br; (c) X = I.

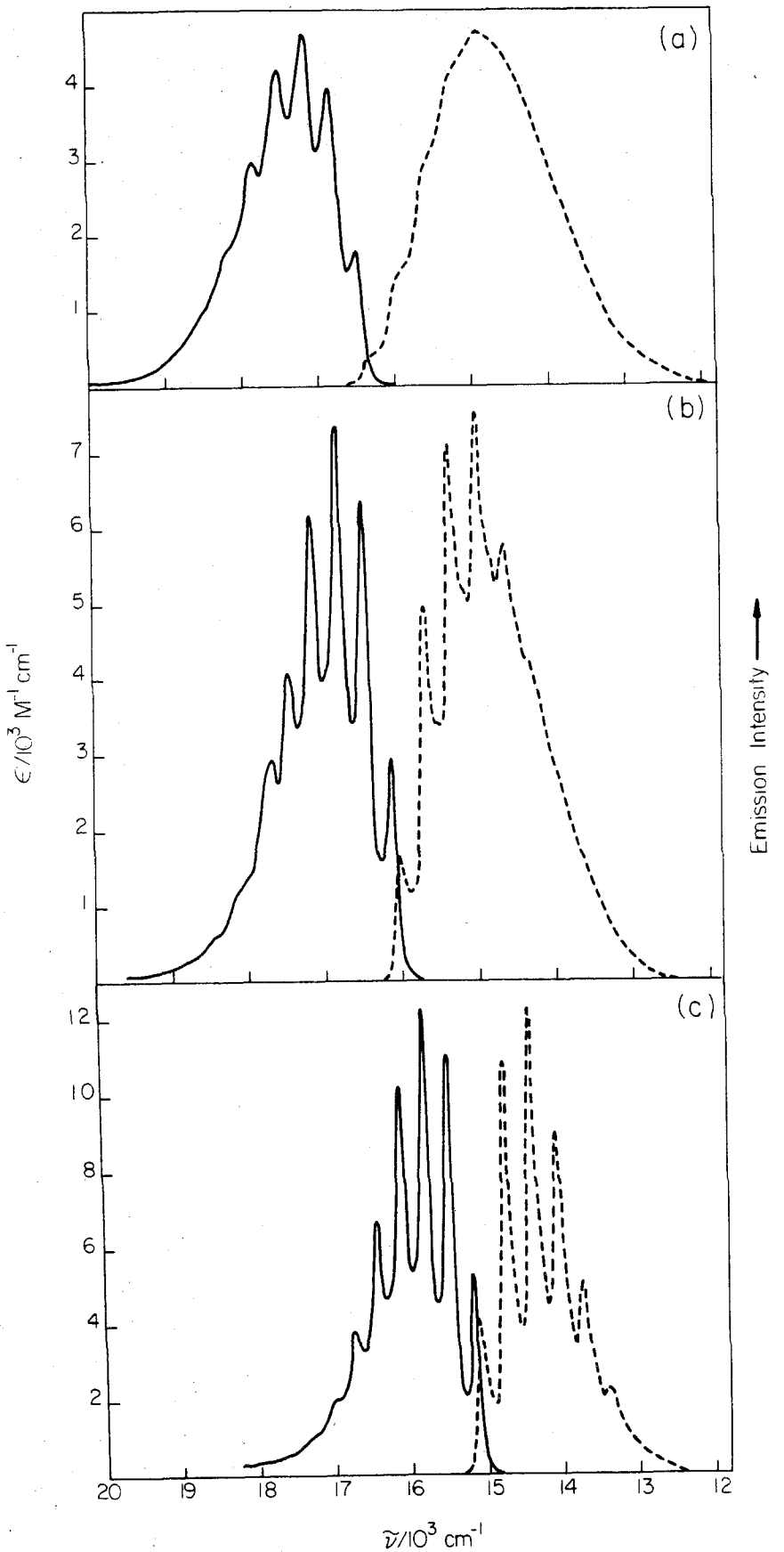
(a)
(b)
(c)
$\epsilon/10^3\ M^{-1}\ cm^{-1}$
Emission Intensity
$\tilde{\nu}/10^3\ cm^{-1}$
20
19
18
17
16
15
14
13
12

mirror-image relationship displayed by the spectra of the iodo complex. While a progression in the metal-metal stretching vibration, the Raman frequency of which (X = Br, ν_1 = 353; X = I, ν_1 = 343 cm^{-1})[13] agrees very closely with the observed vibronic peak spacings (X = Br, ν_1 = 355; X = I, ν_1 = 345 cm^{-1}), clearly dominates the spectra of $Mo_2Br_4(PMe_3)_4$ and $Mo_2I_4(PMe_3)_4$, this broadening results in a short, irregularly spaced progression for $Mo_2Cl_4(PMe_3)_4$ (ν_1(Raman) = 355 cm^{-1}).[13] One clue as to the origin of the variable line width is seen in the spectrum of $Mo_2Br_4(PMe_3)_4$, which shows a weak but regularly spaced (160 cm^{-1}) shoulder adjacent to $\nu_1(Mo_2)$.

In addition to this dependence on ligand X, the emission intensity profile is also highly sensitive to ligand perturbations that are, in an energetic sense, nonchromophoric. Shown in Figure 2 are the $^1(\delta^* \rightarrow \delta)$ bands of the $Mo_2Cl_4(PR_3)_4$ series. Proceeding from R = Me to R = n-Pr, the individual vibronic transitions become sharper and the Franck-Condon maximum moves one quantum of $\nu_1(Mo_2)$ closer to the electronic origin. Although this trend is in the correct direction for producing a band of mirror symmetry with absorption, this relationship is not achieved for the $Mo_2Cl_4(PR_3)_4$ series since no additional change in bandshape is observed on going from $Mo_2Cl_4(PPr^n_3)_4$ to $Mo_2Cl_4(PBu^n_3)_4$.[32] A similar R-group sensitivity is observed for the X = Br series; unlike $Mo_2Br_4(PMe_3)_4$ (Figure 1b), the 0-2 and 0-3 transitions in the emission spectrum of $Mo_2Br_4(PEt_3)_4$ are of equal intensity. It is important to note that under the conditions at which these spectra were acquired (2-methylpentane glass at 77 K), these perturbations of R have no effect, for a given halide, on the emission lifetime of the $^1(\delta\delta^*)$ state,[33] nor do they significantly affect the radiative rate constant of the $Mo_2Cl_4(PR_3)_4$ chromophore in this solvent at room temperature.[12,33] In marked contrast to these R-group effects, the emission bandshape is not sensitive to exchange of the *ligating* atom of ligand L; apart from

Figure 2. Corrected emission spectra of $Mo_2Cl_4(PR_3)_4$ in 2-methylpentane at 77 K: (a) R = Me; (b) R = Et; (c) R = n-Pr; (d) R = n-Bu.

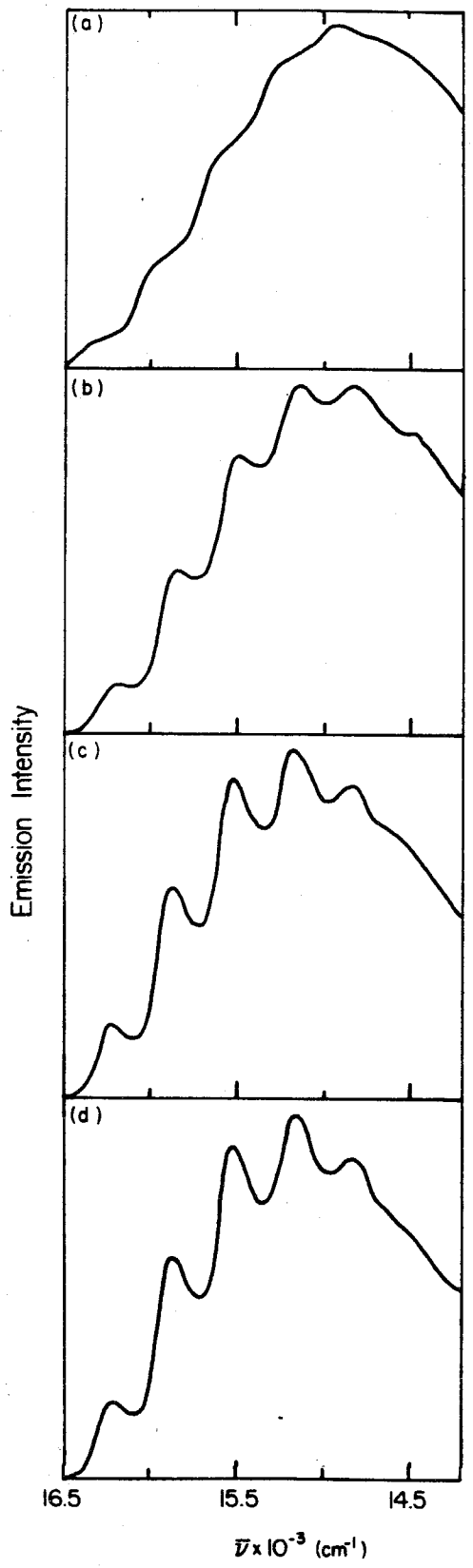
(a)
(b)
(c)
(d)
Emission Intensity
16.5
15.5
14.5
$\bar{\nu} \times 10^{-3}$ (cm^{-1})

their difference in transition energy, the $^1(\delta^* \rightarrow \delta)$ spectra of $Mo_2Cl_4(PMe_3)_4$ and $Mo_2Cl_4(AsMe_3)_4$[29] are virtually superimposable, showing the same broad, irregularly spaced vibronic features (Table I). This is a fairly surprising result since the exchange of arsenic for phosphorous in the inner coordination sphere of the dimer is analogous, from the standpoint of the principle quantum number of the ligating atom, to exchanging bromide for chloride.

The electronic spectra of $W_2Cl_4(PMe_3)_4$, unlike those of the Mo_2 species, are poorly vibronically resolved in 2-methylpentane at 77 K. The $^1(\delta \rightarrow \delta^*)$ absorption band (Figure 3) displays a weak 250-cm^{-1} progression in $\nu_1^*(W_2)$ – this frequency is slightly lower than that of the ground state (261 cm^{-1}),[34] as expected – and the $^1(\delta^* \rightarrow \delta)$ emission band shows no vibronic structure whatsoever.

5 K Emission Spectra.

The 5 K solid state emission spectra of several of the $M_2X_4L_4$ complexes display an amount of vibrational fine structure unprecedented for quadruply bonded dimers. The emission spectra of polycrystalline solids of the $Mo_2X_4(PMe_3)_4$ series of compounds and for $Mo_2Cl_4(AsMe_3)_4$ are reproduced in Figures 4 and 5, respectively, and their vibronic peak maxima and spacings are set out in Table II. In addition, the polarized emission spectrum of $Mo_2Br_4(PMe_3)_4$ (Figure 4b) was obtained for a single crystal; the emission intensity from this sample at both room and low temperature was appreciable only for polarization parallel to molecular-z, as expected for the $^1(\delta^* \rightarrow \delta)$ transition. Crucially, all of the vibronic transitions in this spectrum displayed the same polarization ratio.

As was observed at 77 K, the emission spectra of the $Mo_2X_4L_4$ complexes are dominated by a progression in $\nu_1(Mo_2)$, which is identified in Figures 4 and 5. The observed frequency of this mode, obtained from the spacing of the 0-0 and 0-1 lines, agrees with the Raman values for all compounds except $Mo_2Cl_4(AsMe_3)_4$,

Figure 3. Absorption spectrum of $W_2Cl_4(PMe_3)_4$ in 2-methylpentane at 77 K.

Figure 4. Emission spectra of polycrystalline $Mo_2X_4(PMe_3)_4$ at ca. 5 K (uncorrected for spectrometer response): (a) X = Cl; (b) X = Br; (c) X = I. The $\nu_1(Mo_2)$ progression-forming mode and an (MoX) subprogression are identified. The arrows indicate the positions of the corrected emission intensity maxima. Fluorescence in the region of the electronic origin is strongly quenched by self-absorption.

Figure 5. Emission spectrum of polycrystalline $Mo_2Cl_4(AsMe_3)_4$ at ca. 5 K (uncorrected for spectrometer response). The $\nu_1(Mo_2)$ progression-forming mode is identified. Fluorescence in the region of the electronic origin is strongly quenched by self-absorption.

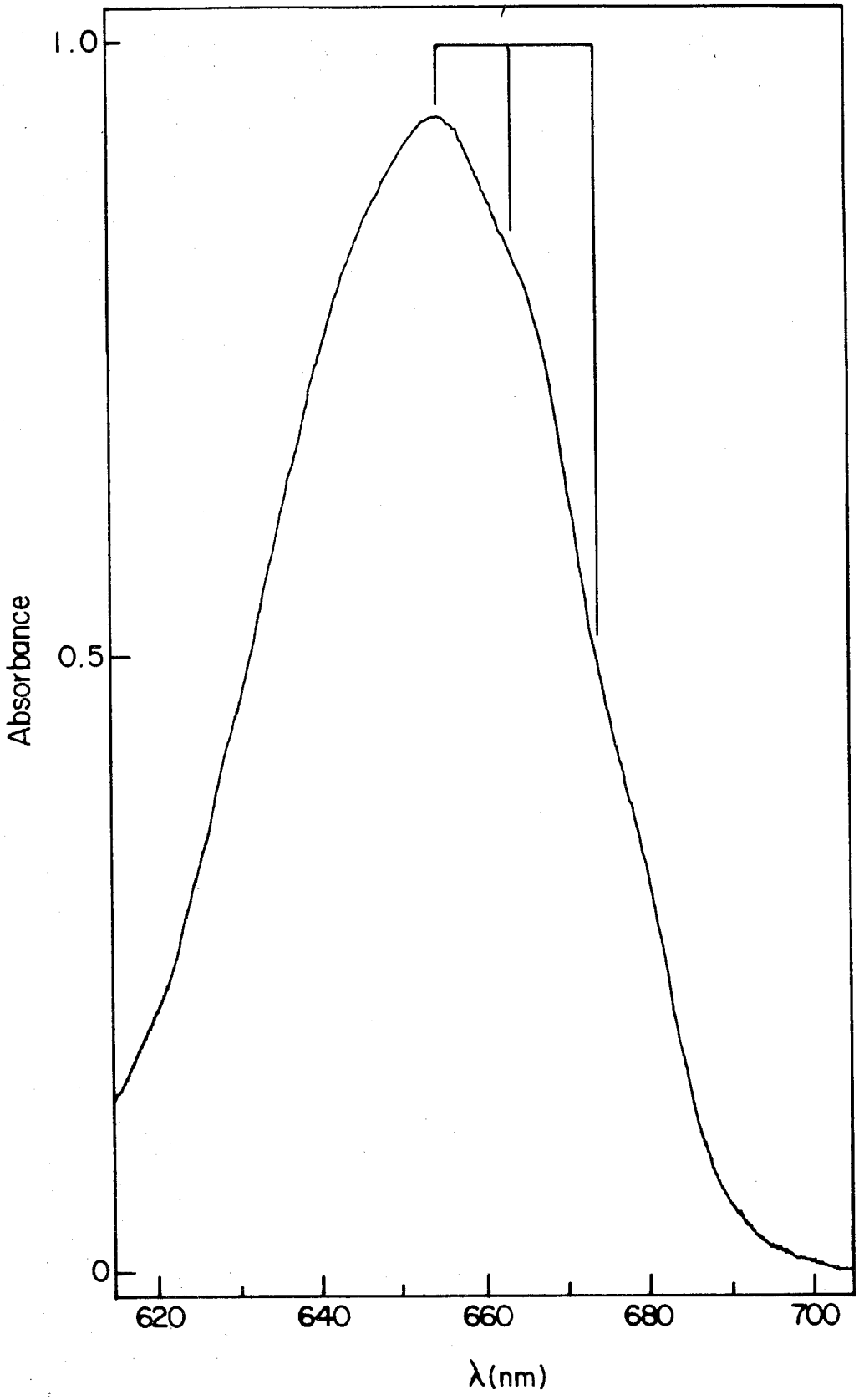
1.0
0.5
0
Absorbance
620
640
660
680
700
λ(nm)

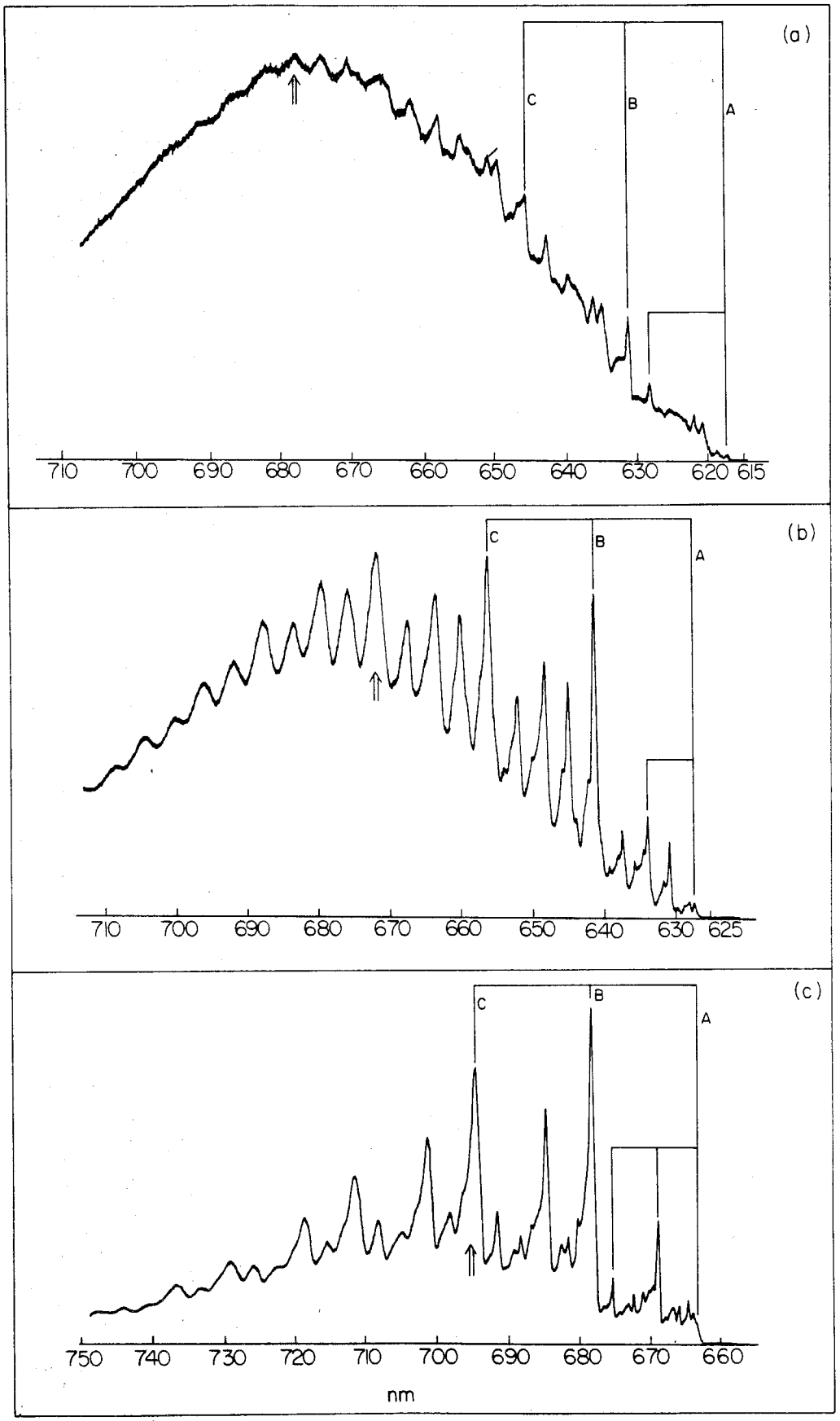
(a)
C
B
A
710 700 690 680 670 660 650 640 630 620 615
(b)
C
B
A
710 700 690 680 670 660 650 640 630 625
(c)
C
B
A
750 740 730 720 710 700 690 680 670 660
nm

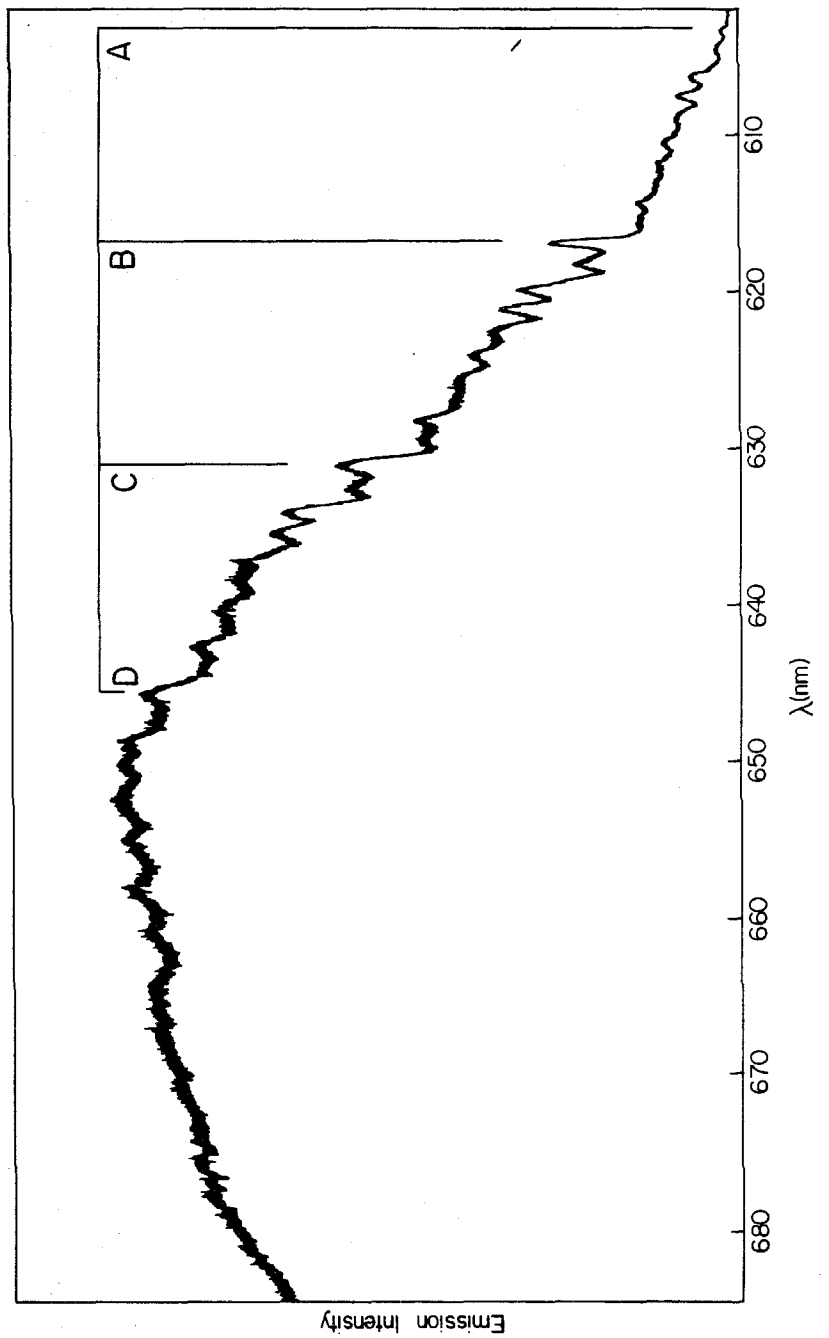
A
B
C
D
610
620
630
640
650
660
670
680
λ(nm)
Emission Intensity

Table II. Vibronic Peak Maxima and Spacings in the 5 K Emission Spectra of Crystalline $M_2X_4L_4$.[a]

Band	$\bar{\nu}_{max}$ (cm^{-1})	Spacings (cm^{-1})
	$Mo_2Cl_4(PMe_3)_4$	
A	16200	38
	a 16162	91
	16129	
	b 16109	124
	c 16076	92
	16044	124
	(2b) 16017	119
	(bc) 15990	
	(2c) 15952	285
	d 15915	
	15873	359
B	15841	93
	b 15748	126
	c 15715	284
	d 15557	359
C	15482	92
	b 15390	126
	c 15356	285
	d 15197	372
D	15110	
	$Mo_2Cl_4(AsMe_3)_4$	
A	16576	34
	a 16542	80
	16513	
	b 16496	113
	c 16463	
	16437	115
	16426	118
	16399	
	(bc) 16381	296
	(2c) 16345	
	16333	367
	d 16280	
	16250	
B	16209	74
	b 16135	105
	c 16104	290
	d 15919	362
C	15847	
D	15486	361

Table II. (continued)

Band	$\bar{\nu}_{max}$ (cm^{-1})	Spacings (cm^{-1})

$Mo_2Br_4(PMe_3)_4$

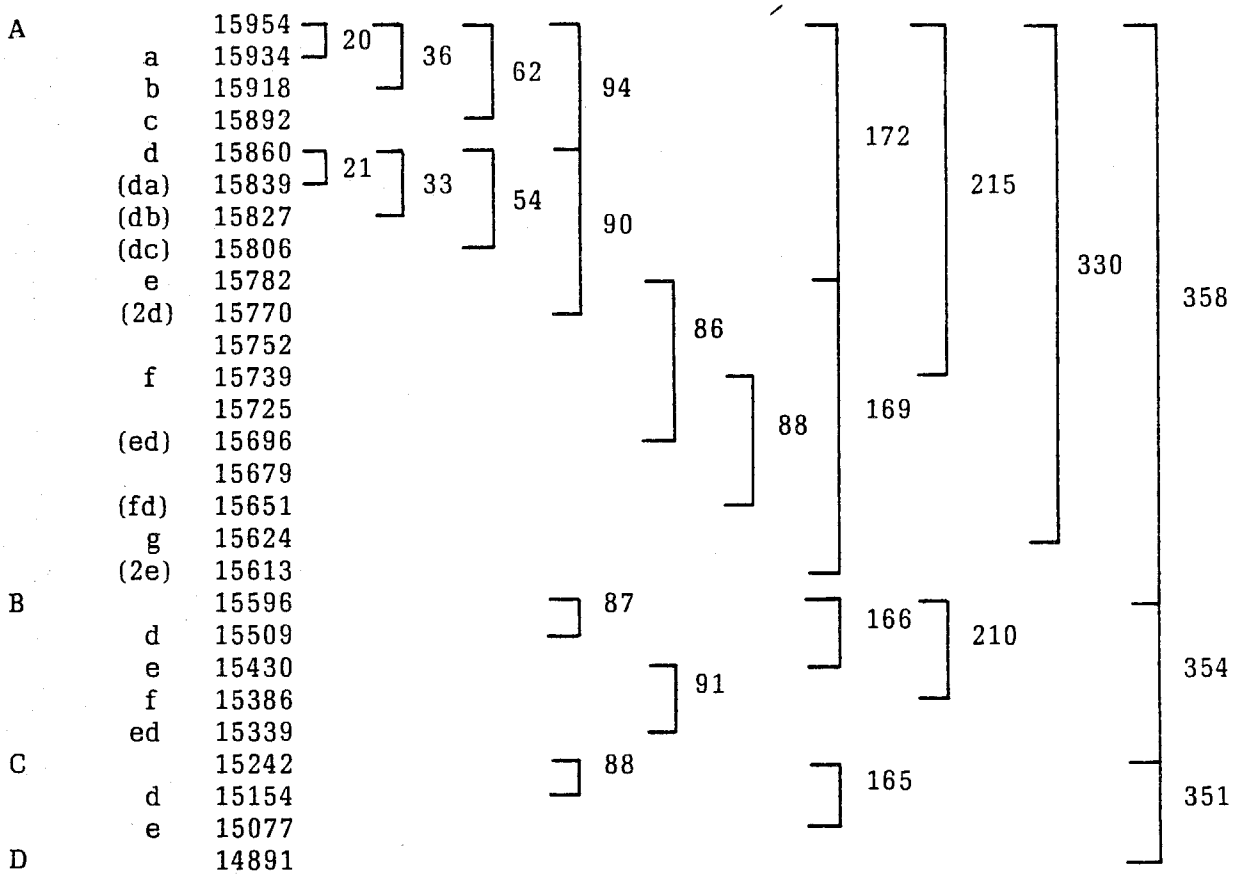

Table II. (continued)

Band	$\bar{\nu}_{max}(cm^{-1})$	Spacings (cm^{-1})

$Mo_2I_4(PMe_3)_4$

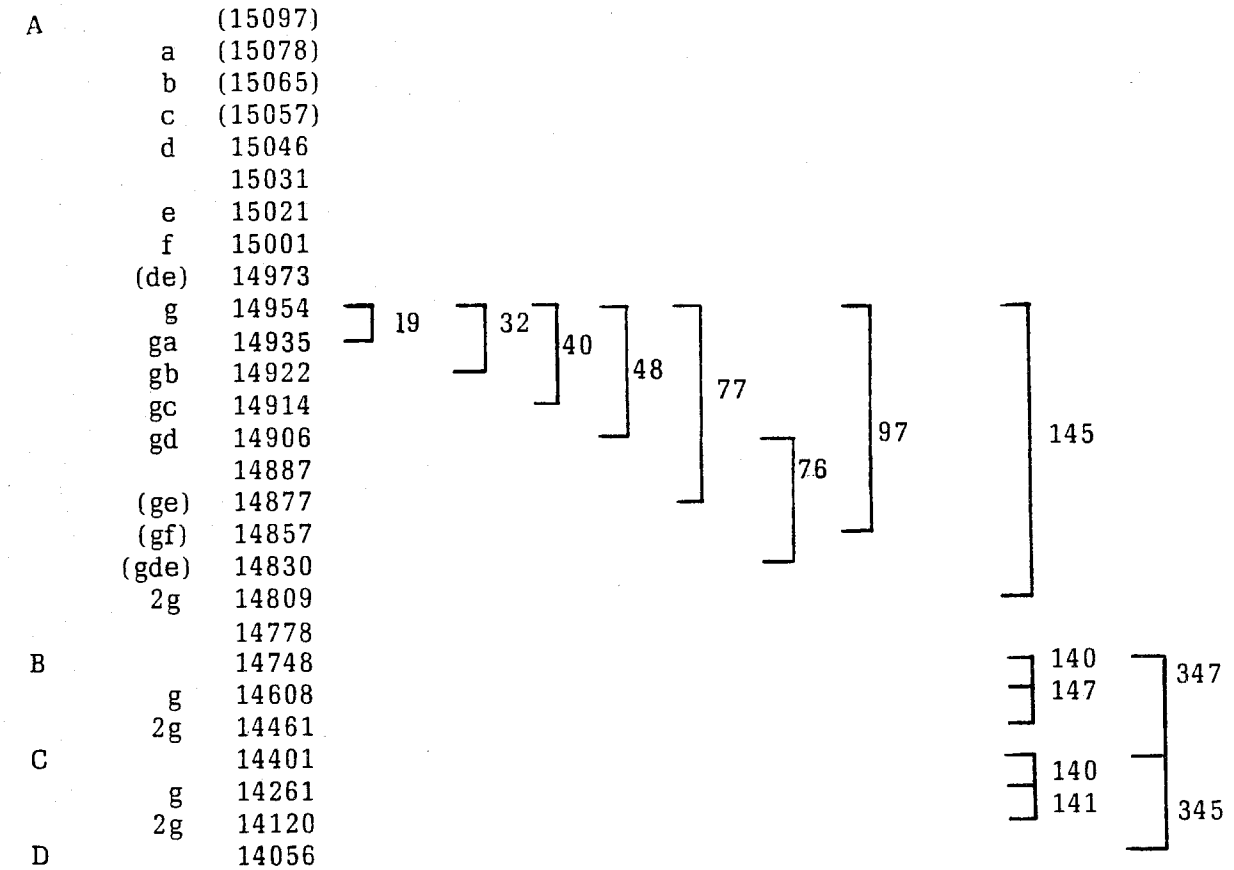

Table II. (continued)

Band		$\bar{\nu}_{max}(cm^{-1})$	Spacings (cm^{-1})
			$W_2Cl_4(PMe_3)_4$
A		14274	34
		14252	
	a	14240	126
		14191	
		14184	165
		14172	
	b	14148	
	c	14109	
		14066	
		14021	
B		14008	166
	d	13995	
	e	13977	126
	f	13964	
	(2c)	13943	161
	b	13882	
	c	13847	

266, 279, 297, 310

[a]Bands with letter designations are shown in Figures 4, 5, and 11 (capital letters) and Figures 6-9 and 11 (small letters); those designated by letters in parentheses are not in the figures but are inferred to be members of the same progression.

which displays a spacing that is ~10 cm^{-1} higher than the known frequency of ν_1 = 356 cm^{-1}.[13] In addition to the ν_1 mode, these spectra show subprogressions in as many as seven distinct vibrational modes; these bands are weaker than those for the ν_1 progression in all cases. Because of severe spectral congestion, the subprogressions built on higher quanta of ν_1 are not as well resolved as those in the vicinity of the electronic origin, as is manifested in the apparent anharmonicity of ν_1 (Table II) that is introduced by the blurring of individual vibronic transitions. This is particularly true for the X = Cl compounds, for which vibronic structure is observed only on the blue flank of the spectra. With regard to comparison of these data with those described in the previous section, this behavior, as well as the increasing redistribution of intensity from the ν_1 mode into the vibronic side bands for the chloro and bromo derivatives relative to the iodo compound, are consistent with the halide-dependent line width observed in the emission spectra of the $Mo_2X_4(PMe_3)_4$ series at 77 K. The strong qualitative resemblance of the $Mo_2Cl_4(PMe_3)_4$ and $Mo_2Cl_4(AsMe_3)_4$ spectra at 77 K is also borne out by the high resolution spectra. Unlike the enhanced resolution seen for these complexes at 5 K, however, the emission spectra of the $Mo_2Cl_4(PR_3)_4$ (R = Et, n-Pr, n-Bu) species contained only the single ν_1 progression seen at 77 K, with slightly sharper lines, while the related compounds $Mo_2Cl_4(SMe_2)_4$ and $MoWCl_4(PMe_3)_4$ were not vibronically structured.

Expanded views of the origin regions of the emission spectra of the $Mo_2X_4(PMe_3)_4$ series and of $Mo_2Cl_4(AsMe_3)_4$ are shown in Figures 6-9. Comparison of this region for $Mo_2Cl_4(PMe_3)_4$ and $Mo_2Cl_4(AsMe_3)_4$ (Figure 6) reveals a nearly one-to-one correlation of vibronic peaks and intensities: the spectra consist of three major subprogressions (*b*, *c*, and *d*) of similar intensity built on ν_1, as well as a number of weaker features that either represent combination bands of

Figure 6. Origin regions of the emission spectra of polycrystalline $Mo_2Cl_4(EMe_3)_4$ at ca. 5 K (uncorrected for spectrometer response): (a) E = P; (b) E = As. Full spectra are shown in Figures 4a and 5, respectively.

Figure 7. Origin region of the emission spectrum of polycrystalline $Mo_2Br_4(PMe_3)_4$ at ca. 5 K (uncorrected for spectrometer response). The full spectrum is shown in Figure 4b.

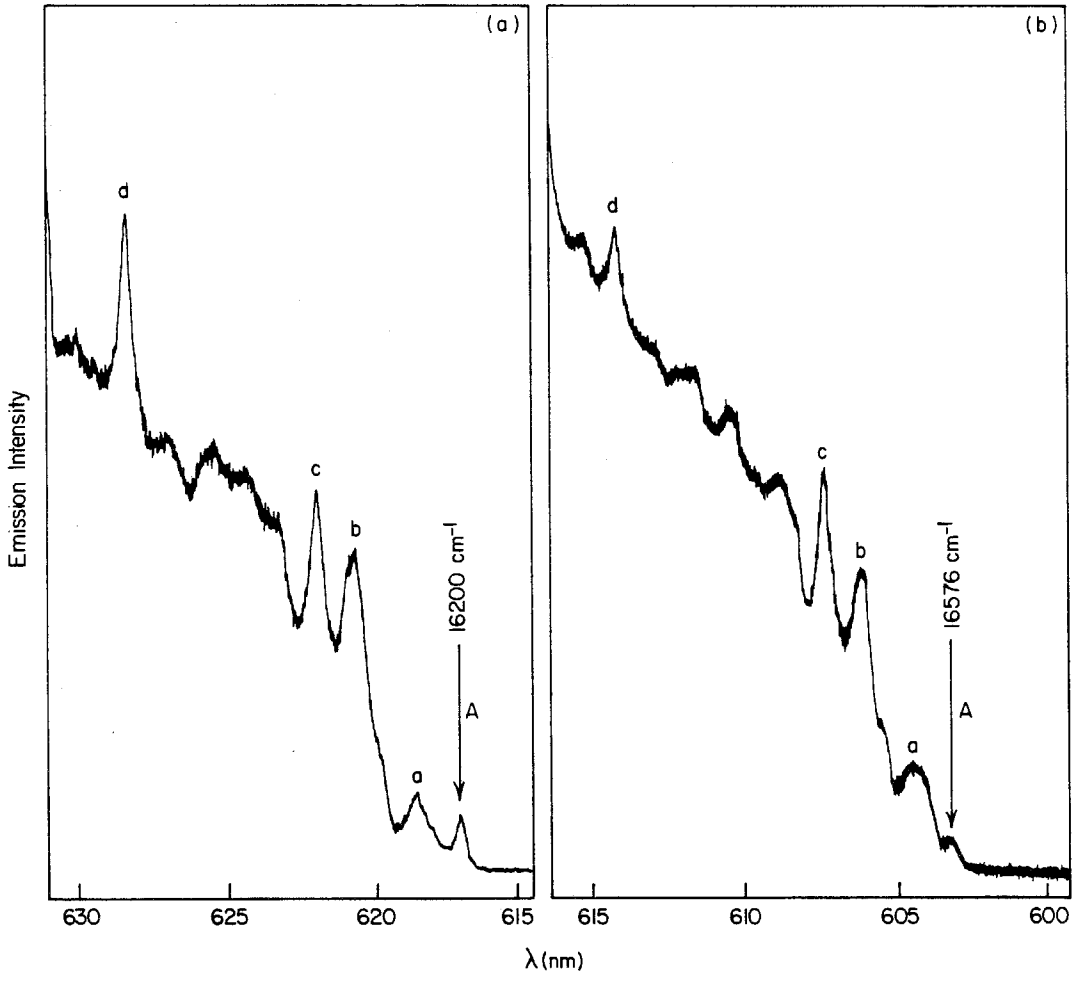
(a)
(b)
d
c
b
a
A
16200 cm⁻¹
16576 cm⁻¹
Emission Intensity
630
625
620
615
610
605
600
λ(nm)

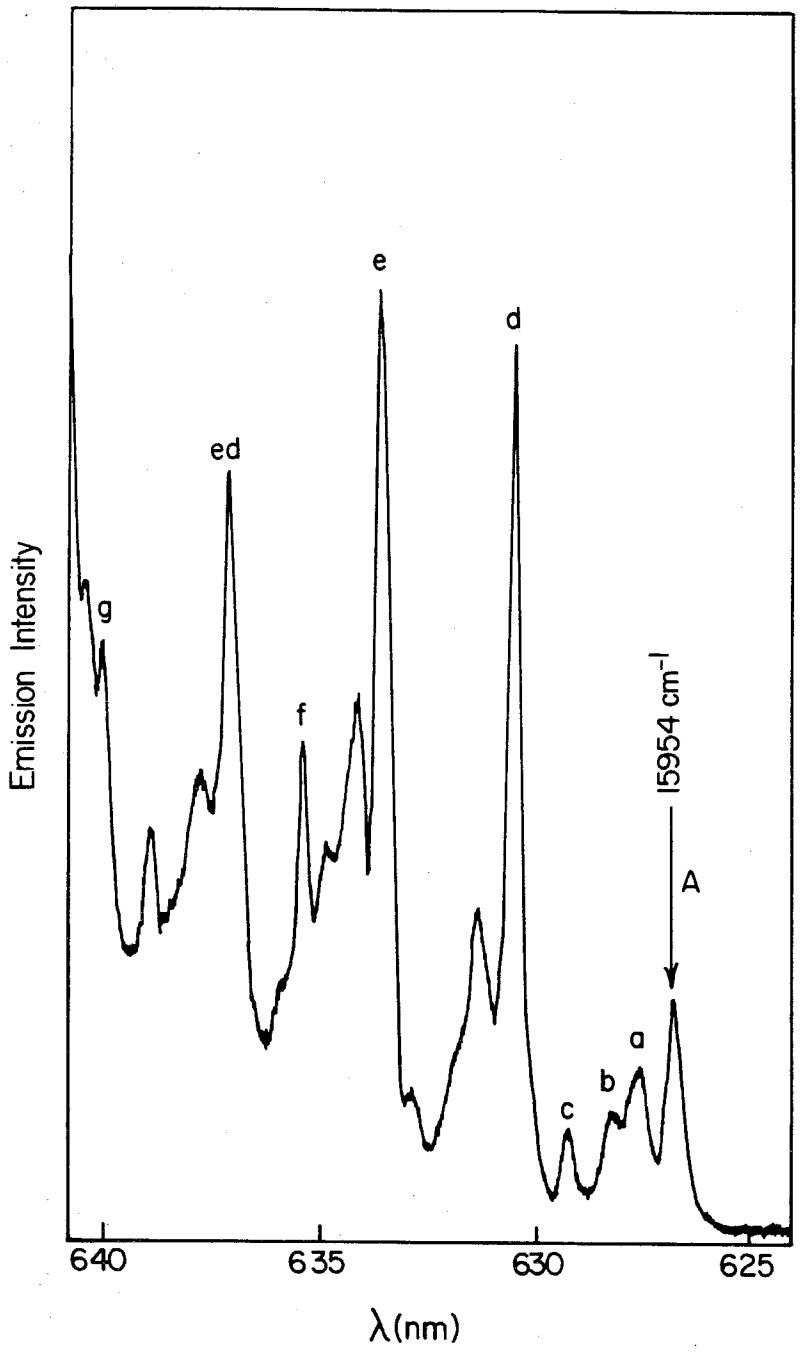
Emission Intensity
g
ed
f
e
d
c
b
a
A
15954 cm⁻¹
640
635
630
625
λ(nm)

these modes or are other fundamental vibrations of lower Franck-Condon activity. Specifically, the second members of the subprogressions of modes *b* and *c* built on the 0-0 line (band *A*) are readily identified, as well as a line attributable to $b + c$. Mode *a*, which has a frequency ($\sim$35 cm^{-1}) and relative intensity appropriate for a crystal lattice (phonon) vibration, appears as a weak combination band with these lines, most noticeably with mode *d*. The line for the first quantum of mode *a* (at 617 and 603 nm for $Mo_2Cl_4(PMe_3)_4$ and $Mo_2Cl_4(AsMe_3)_4$, respectively) is slightly broader than those for modes *b*, *c*, and *d*, and thus may be composed of more than one transition.

The spectrum of $Mo_2Br_4(PMe_3)_4$ (Figure 7), which is less spectrally congested near the origin region than are those of the chloride complexes, consists of seven prominent subprogressions. The frequency of the strongest of these (mode *e*, ca. 170 cm^{-1}) is very close to that of the weak subprogression observed for this compound in 2-methylpentane at 77 K (160 cm^{-1}; Table I). Two quanta of the progression in this mode are observed within the origin region, as well as combinations of *e* with the other intense subprogression, mode *d*. This latter line typifies the remarkable sharpness of the individual vibronic transitions of the $Mo_2X_4L_4$ dimers; the full-width-at-half-maximum (fwhm) of the first member of the *d* subprogression at ca. 630 nm (Figure 7) is slightly less than 8 cm^{-1}. Two other modes, *f* and *g*, are observed at higher frequencies than *d* and *e*, but these have relatively small Huang-Rhys factors. As was observed for the chloride complexes, weak phonon side bands (modes *a*, *b*, and *c*) are associated with each of the intense features of the spectrum. Two of these (*a* and *b*), are seen as discrete bands only near the origin (628 nm), merging into a single band when in combination with other vibronic transitions. This fact may be of relevance regarding the band shape of mode *a* of $Mo_2Cl_4(PMe_3)_4$ and $Mo_2Cl_4(AsMe_3)_4$ (*vide supra*).

The emission spectrum of $Mo_2I_4(PMe_3)_4$ (Figure 8), which displays the best resolved vibronic features of this class of complexes, also contains progressions in seven modes in addition to ν_1. In keeping with the trends observed between the chloride and bromide complexes, the frequency of the most intense mode (*g*: 145 cm^{-1}) is less than that observed for the comparable bands of $Mo_2Br_4(PMe_3)_4$ (*e*: 170 cm^{-1}) and $Mo_2Cl_4(PMe_3)_4$ (*d*: 285 cm^{-1}), and it is the only subprogression of $Mo_2I_4(PMe_3)_4$ possessing appreciable intensity; $Mo_2Br_4(PMe_3)_4$ and $Mo_2Cl_4(PMe_3)_4$ display, respectively, two and three relatively intense subprogressions. The emission spectrum of this compound is set apart from those of the other members of the $Mo_2X_4(PMe_3)_4$ series, however, by the almost total self-absorption of the 0-0 line, as well as a marked diminution of the intensity of phonon modes *a*, *b*, and *c* near the origin. The positions of the latter lines are shown in Figure 8 for their progression built on one quantum of *g*, and their estimated positions, including that of the 0-0 line (band *A*), are displayed in the expanded view of the origin region illustrated in Figure 9. This cluster of phonon side bands strongly resembles, with respect to both intensity and frequency, that seen for $Mo_2Br_4(PMe_3)_4$. The spectrum shown in Figure 9 also reveals that all of the vibronic transitions of $Mo_2I_4(PMe_3)_4$ are split into doublets of unequal intensity that are separated by ca. 4 cm^{-1}; the estimated positions of bands *A*, *a*, *b*, and *c* in Figure 9 are those of the higher energy of their two components. This doublet pattern is attributable to a factor group (Davydov) crystal splitting of the $^1(\delta^* \rightarrow \delta)$ transition.[35]

The 5 K emission spectrum of $W_2Cl_4(PMe_3)_4$ is reproduced in Figure 10, and an expanded view of the origin region is shown in Figure 11. Comparison of the vibronic intensity profile of this species with that of homologous $Mo_2Cl_4(PMe_3)_4$ (Figures 4 and 6) does not reveal any of the obvious similarities that are seen between the spectrum of this latter dimer and that of $Mo_2Cl_4(AsMe_3)_4$. Instead,

Figure 8. Origin region of the emission spectrum of polycrystalline $Mo_2I_4(PMe_3)_4$ at ca. 5 K (uncorrected for spectrometer response). The full spectrum is shown in Figure 4c.

Figure 9. Expanded view of the origin region of the emission spectrum of polycrystalline $Mo_2I_4(PMe_3)_4$ at ca. 5 K (uncorrected for spectrometer response). Estimated positions of the 0-0 line and of subprogressions *a* and *b*, which are quenched by self-absorption, are displayed for the higher energy of the two factor group (Davydov) components of the spectrum.

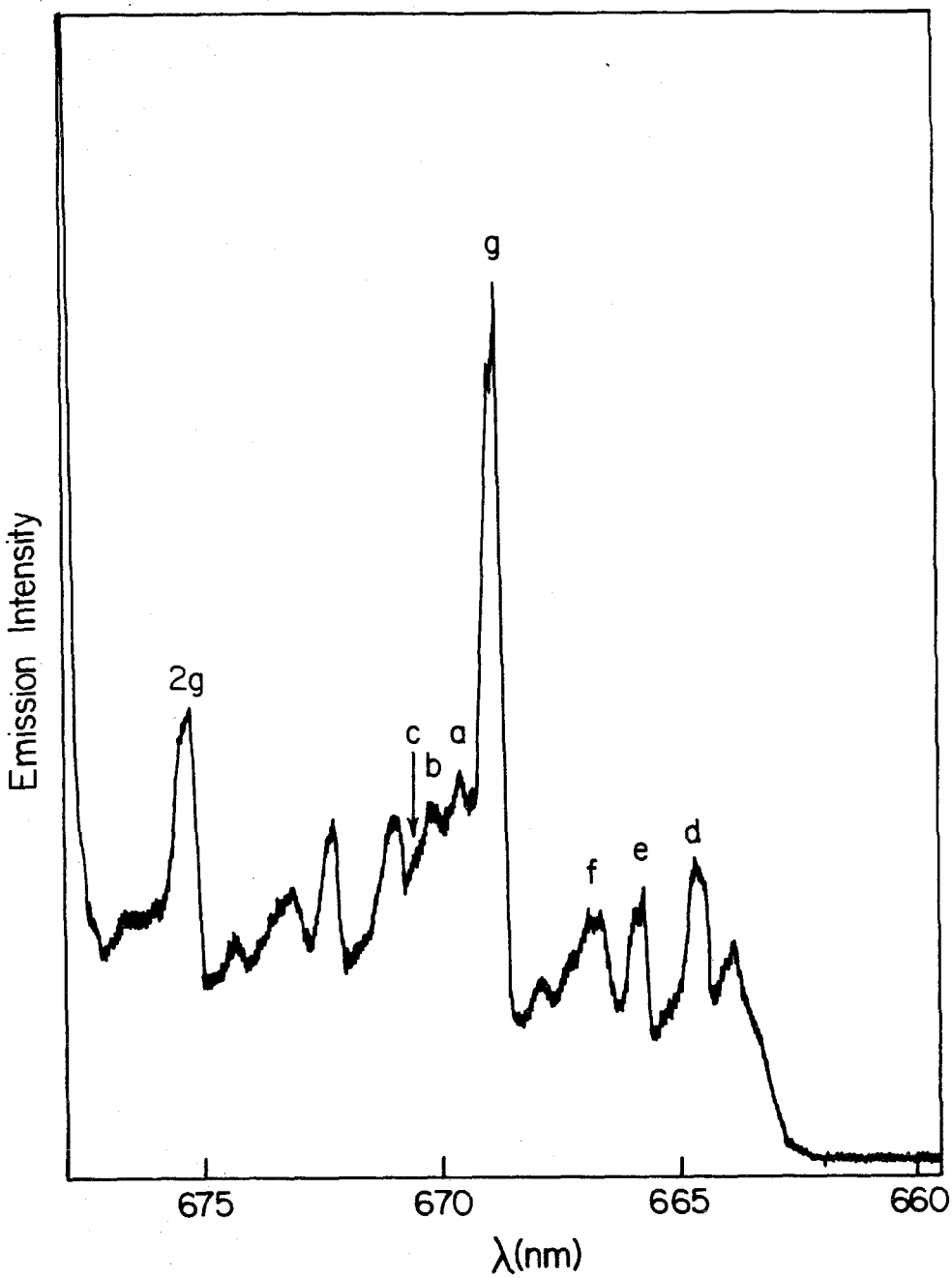
Emission Intensity
2g
c
b
a
g
f
e
d
675
670
665
660
λ(nm)

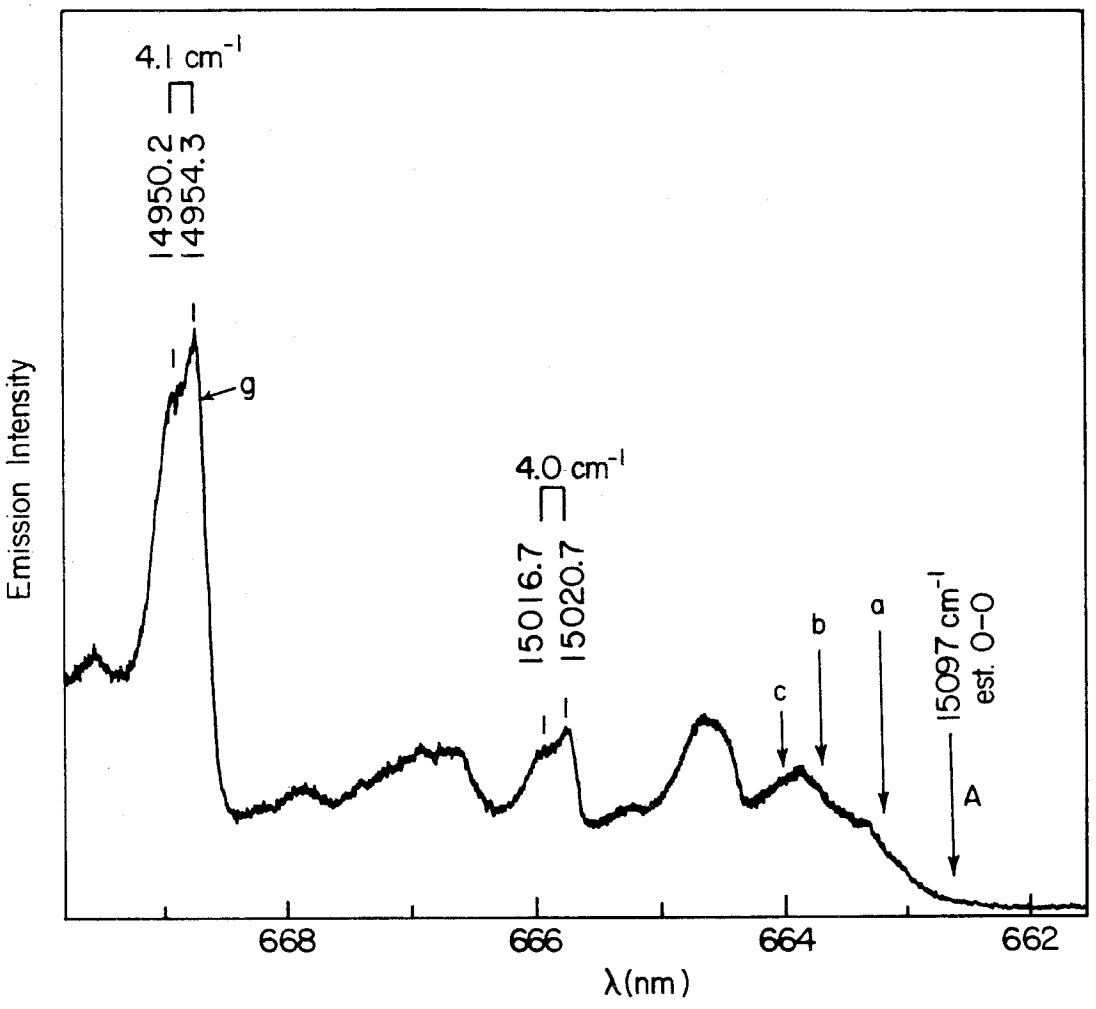
4.1 cm⁻¹
14950.2
14954.3
g
4.0 cm⁻¹
15016.7
15020.7
c
b
a
15097 cm⁻¹
est. 0-0
A
Emission Intensity
668
666
664
662
λ(nm)

Figure 10. Emission spectrum of polycrystalline $W_2Cl_4(PMe_3)_4$ at ca. 5 K (uncorrected for spectrometer response). The $\nu_1(W_2)$ progression-forming mode is identified. Fluorescence in the region of the electronic origin is strongly quenched by self-absorption.

Figure 11. Origin region of the emission spectrum of polycrystalline $W_2Cl_4(PMe_3)_4$ at ca. 5 K (uncorrected for spectrometer response). The full spectrum is shown in Figure 10.

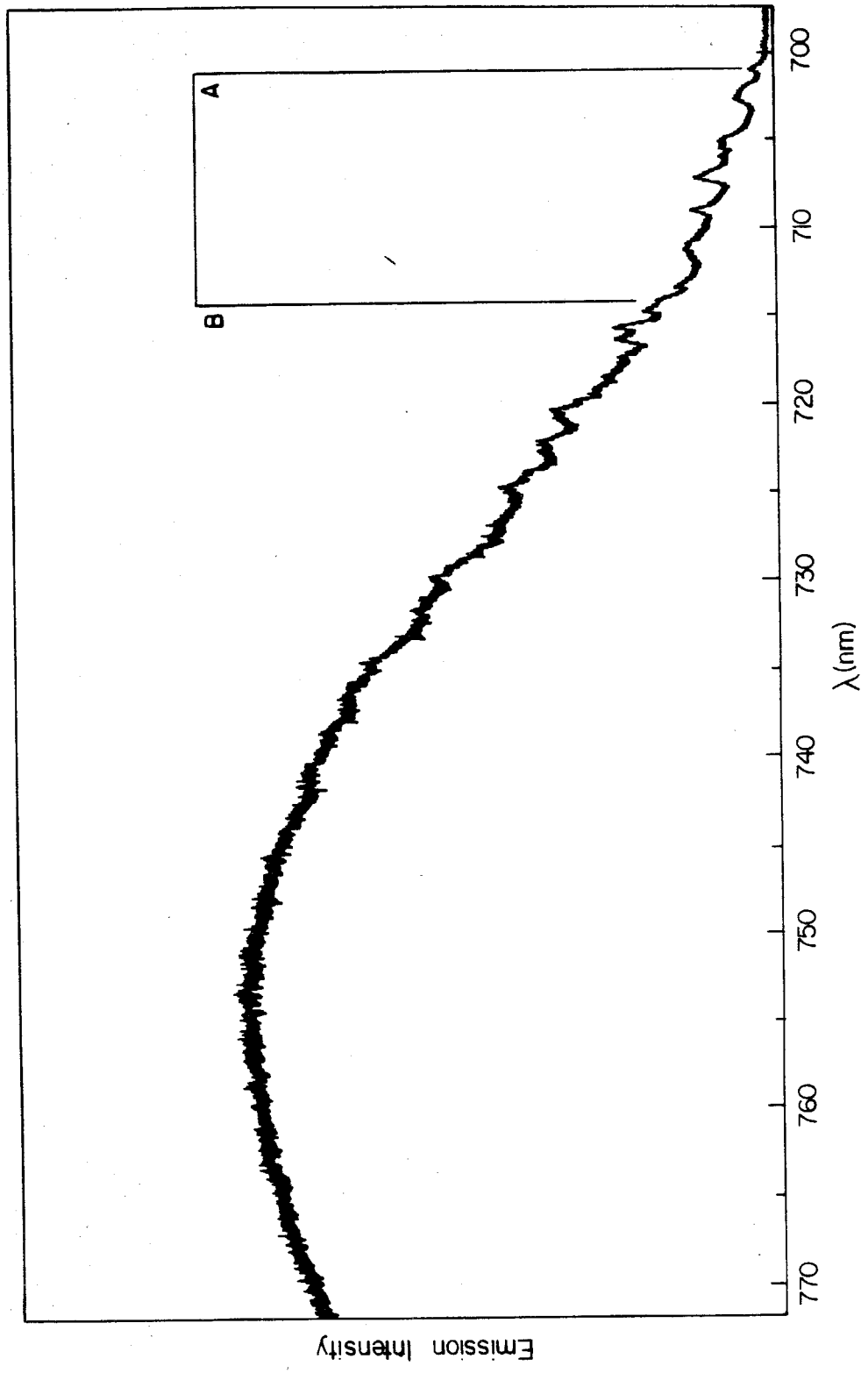
Emission Intensity
λ(nm)
700
710
720
730
740
750
760
770
A
B

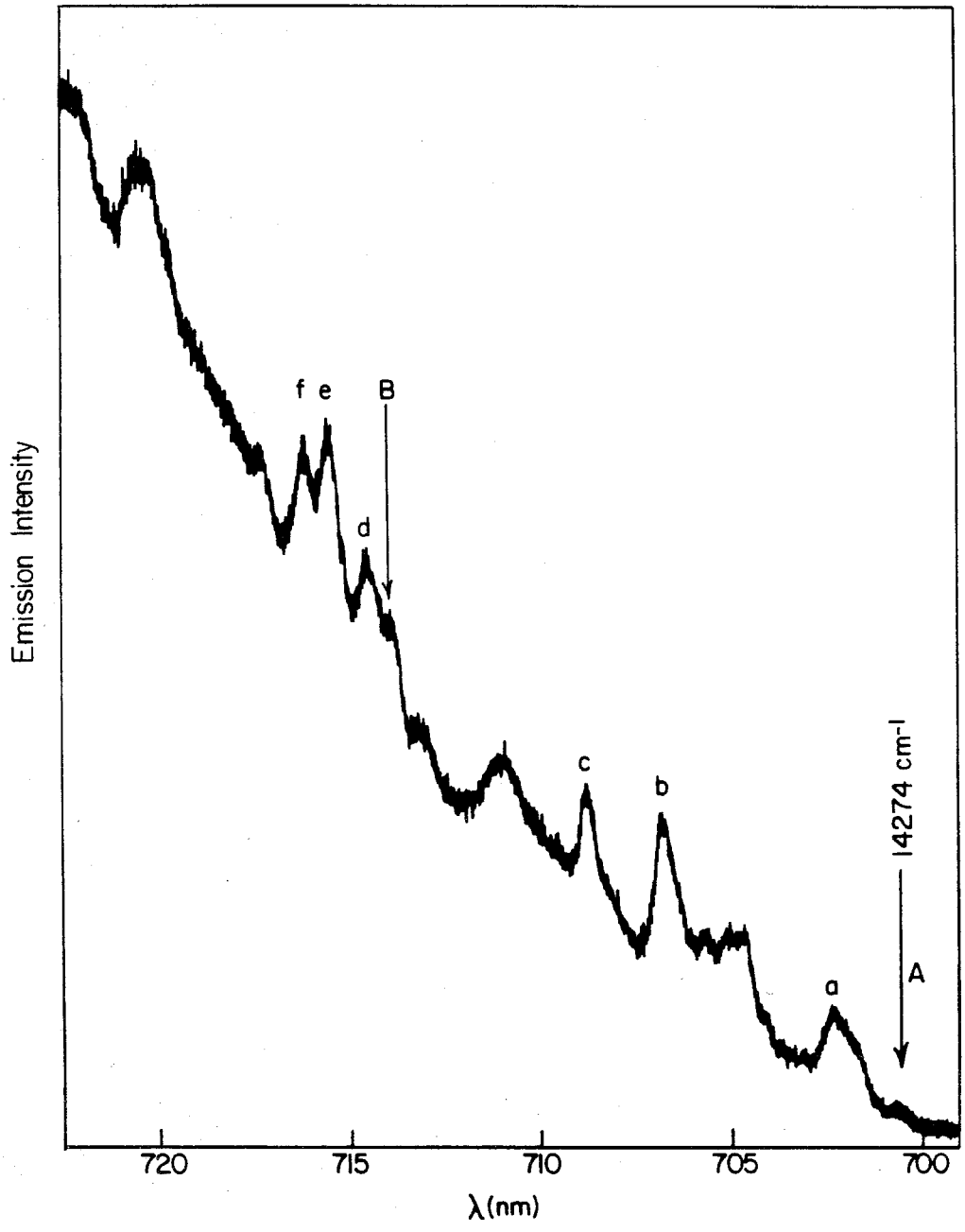
Emission Intensity
f e
B
d
c
b
a
14274 cm-1
A
720
715
710
705
700
λ(nm)

the $W_2Cl_4(PMe_3)_4$ spectrum seems to represent a continuation of the intensity trends observed in the $Mo_2X_4(PMe_3)_4$ series as the halide is changed from iodide to chloride. Specifically, the resolved progression in ν_1 is very short, with spectral congestion obscuring any significant vibronic details well before the emission band maximum. In addition, identification of the ν_1 progression is not apparent upon casual inspection, as it was for the $Mo_2X_4L_4$ complexes. The W-W stretching frequency for this complex, as determined by Raman spectroscopy, is 261 cm^{-1},[34] which places the first quantum of ν_1 in the vicinity of bands *d* and *B* (Figure 11). Of these two bands, line *B* is preferred for tentative assignment as ν_1 due to its closer frequency match with this Raman value, and, more significantly, because the energy spacings from this line to the two features centered at 722 nm are consistent with intervals for subprogressions of the prominent *b* and *c* modes. Regardless of which line is chosen, however, there are several other modes, namely *b*, *c*, *e*, and *f*, of greater intensity than ν_1; the latter two are also higher frequency than ν_1. Mode *a* (702 nm), the frequency and band shape of which closely matches that of analogous bands in $Mo_2Cl_4(PMe_3)_4$ and $Mo_2Cl_4(AsMe_3)_4$, is also more intense than the band attributable to ν_1 for $W_2Cl_4(PMe_3)_4$. This behavior is consistent with the increase in frequency and intensity, relative to ν_1, of the major subprogressions of the $Mo_2X_4L_4$ series according to I < Br < Cl.

Although a detailed discussion of the nature of the non-ν_1 vibronic progressions of the $M_2X_4L_4$ complexes will be delayed until later in this chapter, it is initially noted that the emission and resonance Raman spectra (Chapter II, Figures 2 and 3) of these species bear little resemblance to each other with respect to both the relative intensities and frequencies of the vibrational modes, with the exception of those of ν_1.

5 K Absorption Spectra.

As is observed for their emission spectra, the $^1(\delta \rightarrow \delta^*)$ bands of the $Mo_2X_4(PMe_3)_4$ series, $Mo_2Cl_4(AsMe_3)_4$, and $W_2Cl_4(PMe_3)_4$, are more highly vibronically structured at 5 K than at 77 K, and those of $Mo_2Cl_4(PR_3)_4$ (R = Et, n-Pr, n-Bu)[29,36] do not show enhanced resolution at 5 K under these conditions. Unfortunately, the large intensity of this transition (see Figure 1) prohibited the acquisition of single-crystal absorption data, and therefore of data with resolution comparable to that for emission, for all but a small portion of their band profiles. The spectra presented here are thus largely for dilute cesium halide pellets of these complexes; comparisons of analogous absorption features for these samples and for single crystals (*vide infra*) indicate that while the $M_2X_4L_4$ dimers retain their structural and molecular integrity in these pellets, inhomogeneous broadening in this host matrix completely obscures some of the lower frequency vibronic spacings. Since only a few of the higher frequency features appear as discrete peaks, discussion of the vibronic details of these spectra will necessarily be less extensive than for the emission spectra.

The 5 K absorption spectra of the $Mo_2X_4(PMe_3)_4$ series and of $Mo_2Cl_4(AsMe_3)_4$ are shown in Figures 12 and 13, respectively. Immediately noticeable is the fact that the close resemblance that these spectra bear to each other at 77 K is lost at high resolution, although both the relative intensities of the major clusters of vibronic features within each spectrum, as well as the values of $\nu_1^*(Mo_2)$, agree with those observed for their glassy matrix counterparts. An additional difference among these spectra is that the level of resolution of the spectrum of $Mo_2Cl_4(AsMe_3)_4$ is lower than that for $Mo_2Cl_4(PMe_3)_4$, even though their 5 K emission spectra are equally well-resolved.

The arrows in Figures 12 and 13 mark the locations of the 0-0 transitions

Figure 12. Absorption spectra of CsX pellets of $Mo_2X_4(PMe_3)_4$ at ca. 5 K: (a) X = Cl; (b) X = Br; (c) X = I. The arrows indicate the observed position of the emission 0-0 line of each compound (Figures 6a, 7, and 8, respectively). Two spacings (cm^{-1}) corresponding to the excited state metal-metal stretching frequencies are identified.

Figure 13. Absorption spectrum of a CsCl pellet of $Mo_2Cl_4(AsMe_3)_4$ at ca. 5 K. The arrow indicates the observed position of the emission 0-0 line (Figure 6b). Spacings (cm^{-1}) corresponding to the excited state metal-metal stretching frequency (ν_1^*(av.) = 337(7) cm^{-1}) and to lower frequency vibronic features are identified.

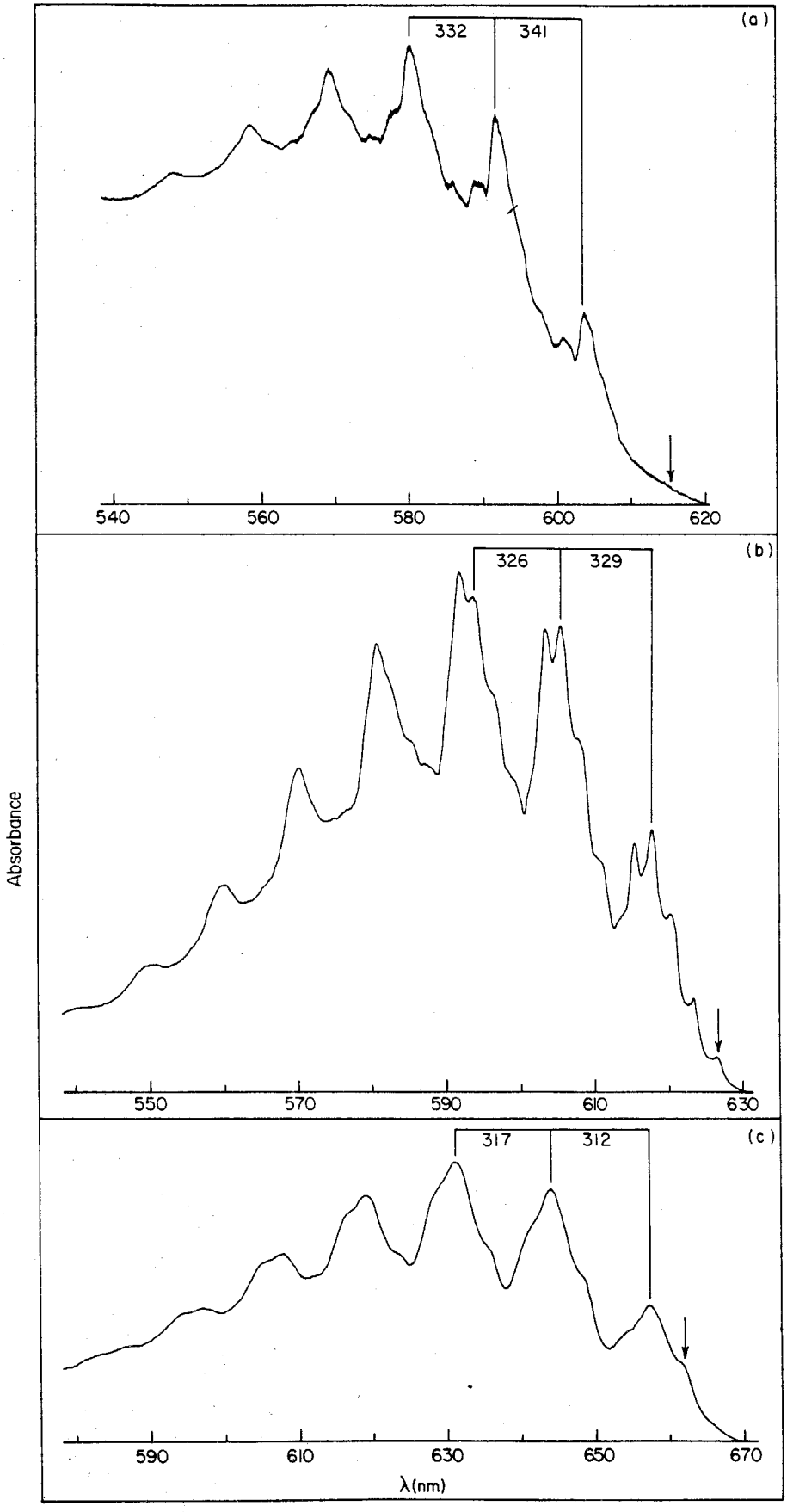
(a)
332
341
540
560
580
600
620
(b)
326
329
550
570
590
610
630
(c)
317
312
590
610
630
650
670
λ(nm)
Absorbance

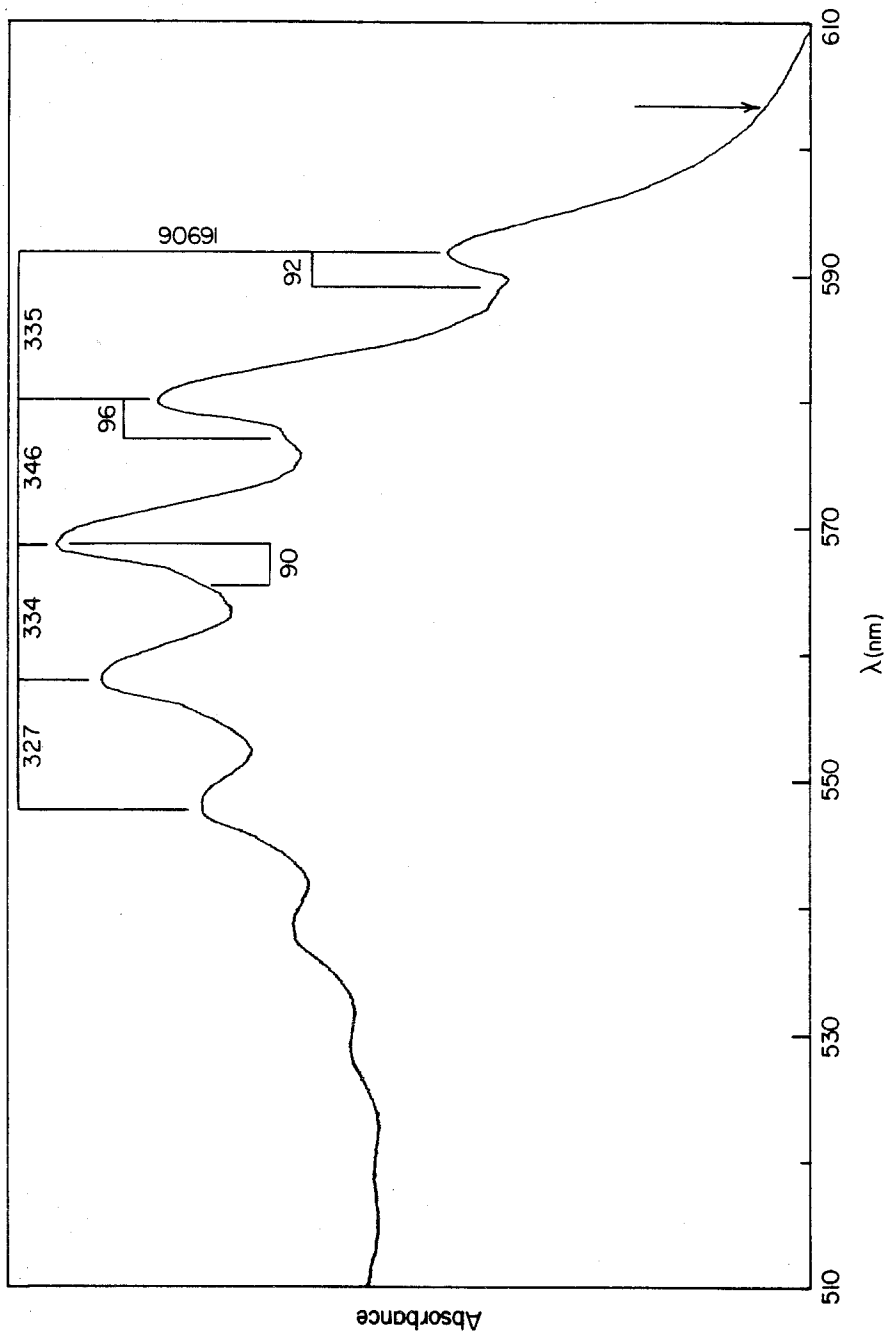
16906
92
335
96
346
90
334
327
Absorbance
λ(nm)
510
530
550
570
590
610

of the corresponding 5 K emission spectra. While the positions of these emission lines clearly coincide with the lowest energy vibronic transitions in the absorption spectra of $Mo_2Br_4(PMe_3)_4$ and $Mo_2I_4(PMe_3)_4$, there are no intense features for $Mo_2Cl_4(PMe_3)_4$ and $Mo_2Cl_4(AsMe_3)_4$ in this region, the red flanks of these spectra instead consisting of a series of weak shoulders (*vide infra*). These origin bands are sufficiently weak that they can only be resolved with clarity in spectra of single crystals of these complexes. The $\parallel$ z-polarized absorption spectra of the origin region of the $^1(\delta \rightarrow \delta^*)$ bands of $Mo_2Cl_4(PMe_3)_4$ and $Mo_2Br_4(PMe_3)_4$ are reproduced in Figure 14.[37] Examining first the spectrum of the bromide complex (Figure 14b) reveals a sharp pair of bands at the same wavelength as the lowest band of the pellet spectrum. The frequency of the lower energy of the two single-crystal bands, which is assigned as the 0-0 transition,[38] differs from the emission 0-0 line by only 3 cm^{-1} (15954 cm^{-1}; Table II).[27] The 20-cm^{-1} splitting between the 0-0 line and the weaker absorption band matches that between the emission 0-0 line and the first member of the subprogression in phonon mode *a*. The lowest energy line in the single-crystal absorption spectrum of the chloride derivative (Figure 14a), which is at the same wavelength as the lowest energy feature in the pellet spectrum of this complex (*vide infra*), lies 13 cm^{-1} from its emission counterpart (16200 cm^{-1}; Table II); the 35-cm^{-1} splitting between this absorption line and the next highest energy absorption feature again reproduces the frequency of the emission subprogression in phonon mode *a* for this compound. Further evidence for the close correspondence between the origin regions of the crystal absorption and emission spectra comes from the observation that the relative widths of the absorption 0-0 line and the band 35 cm^{-1} higher are the same as those seen for emission mode *a* and the first quanta of the other emission modes (Figure 6a).

The vibronic peak maxima and spacings of the spectra in Figure 12 are set out

Figure 14. Origin region of the $\|$ z-polarized (101 face; $\|$ b polarization) single-crystal absorption spectra of $Mo_2X_4(PMe_3)_4$ at ca. 5 K: (a) X = Cl; (b) X = Br. *Note*: the two spectra have different optical density scales.

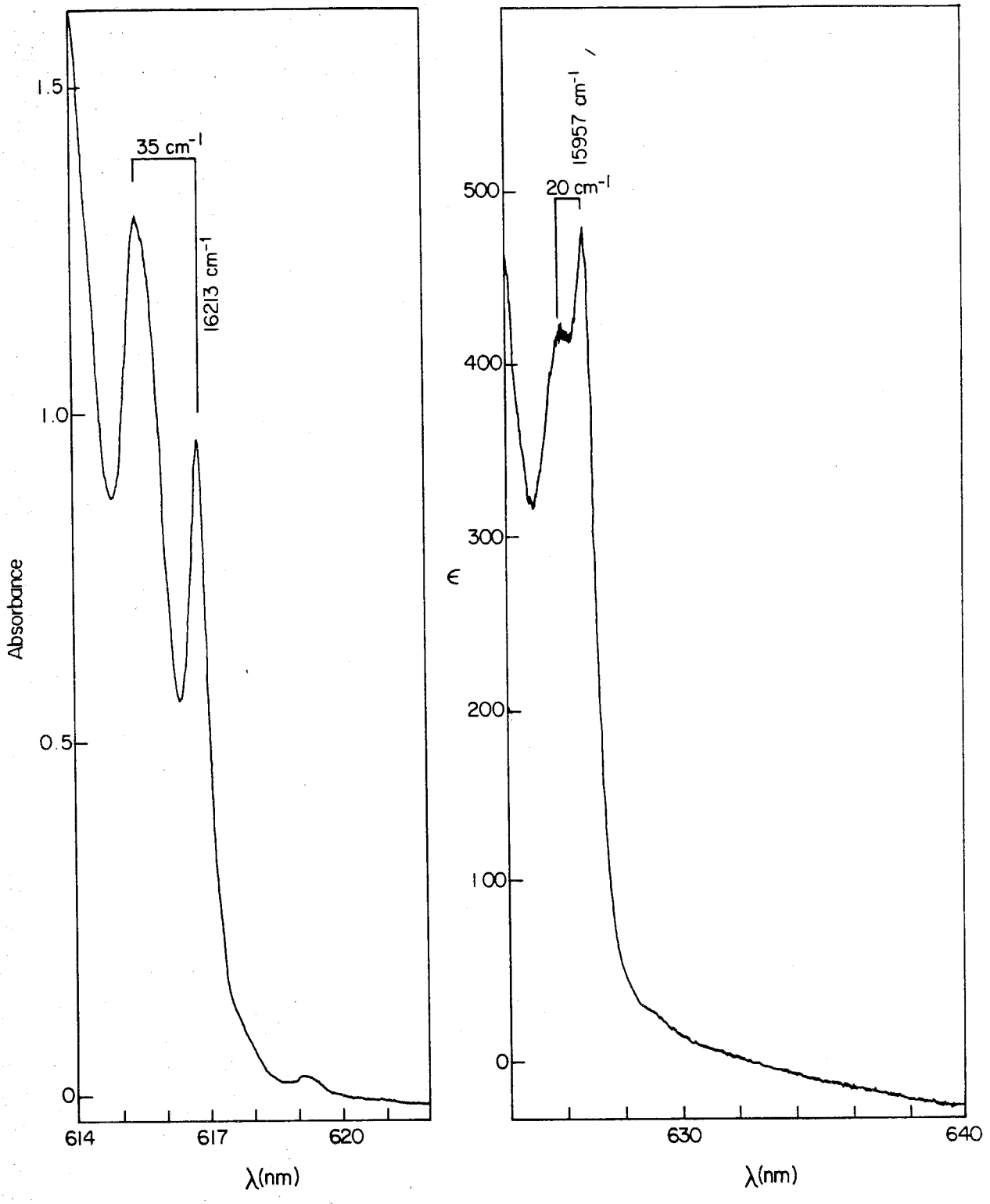
1.5
1.0
0.5
0
Absorbance
35 cm⁻¹
16213 cm⁻¹
614
617
620
λ(nm)
500
400
300
200
100
0
ε
15957 cm⁻¹
20 cm⁻¹
630
640
λ(nm)

Table III. Vibronic Peak Maxima and Spacings of the $^1(\delta \rightarrow \delta^*)$ Bands of of $Mo_2X_4(PMe_3)_4$ Complexes in CsX Pellets at 5 K.[a]

Band	ν_{max} (cm^{-1})	Spacings (cm^{-1})

$Mo_2Cl_4(PMe_3)_4$

A	16208	26	74	119	175	204	245	288	337	
a	16234									
b	16282									
c	16327									
d	16383									
e	16412	328								
f	16453		340							
g	16496									
B	16545			323		322				
*a'	16562									
b'	16622									
c'	16650									
e'	16734	339								330
	16794		327							
	16832									
C	16875			331		328				
*a"	16901									
b"	16949									
c"	16981									
	17036	337								
e"	17062									
	17167									
*	17238									
	17572	334								
	17915	343								

ν_1^* (av.) = 331(7) cm^{-1}

Table III. (continued)

$Mo_2Br_4(PMe_3)_4$

Band	ν_{max} (cm^{-1})	Spacings (cm^{-1})
A	15962	82, 325
a	16044	
b	16124	162, 329
*c	16189	
d	16250	227, 329, 323, 326, 313
B	16300	
e	16313	288, 328, 323, 326
a'	16369	
f	16393	338
b'	16453	
*c'	16518	351
d'	16578	
	16631	431
	16692	
	16717	
b"	16776	
*c"	16844	
d"	16901	
	16955	312
	17004	
	17033	
(b'")	17088	
(c'")	17167	
(d'")	17227	
	17346	
	17406	
(c'"")	17480	

ν_1^* (av.) = 326(3) cm^{-1}

Table III. (continued)

Band	ν_{max} (cm^{-1})	Spacings (cm^{-1})

$Mo_2I_4(PMe_3)_4$

	15117			
		99		
*	15216		174	
		312		310
	15291			
			298	
	15427			
*	15528			309
	15589			
		317		
	15736		322	
*	15845			308
	15911			
		308		
	16044		310	
	16153			296
	16221			
		303		
	16340			
	16456			

ν_1^* (av.) = 310(7) cm^{-1}

[a]Band frequencies marked with an asterisk correspond to the peaks labeled in Figure 12; those designated by letters are defined in Figures 15 and 16; and those designated by letters in parentheses are not given in the figures but are inferred to be members of the same vibronic progression. The quoted uncertainty in the average value of ν_1^* is the standard deviation of the spacings of the intense peaks in the corresponding spectrum.

in Table III.[39] As is indicated in this table and figure, the pattern of these features repeats itself with a frequency equal to that of $\nu_1^*(Mo_2)$. This is shown in more detail for $Mo_2Cl_4(PMe_3)_4$ and $Mo_2Br_4(PMe_3)_4$ in Figures 15 and 16, respectively, wherein the individual vibronic transitions are labeled. In light of the close correspondence between the origin regions of the single-crystal absorption and emission spectra of $Mo_2Cl_4(PMe_3)_4$ and $Mo_2Br_4(PMe_3)_4$, it is tempting to simply attribute the many features seen in their pellet absorption spectra to progressions in the excited state analogues of the ground state vibrational modes seen in their $^1(\delta^* \rightarrow \delta)$ transitions. There is one very important difference between these latter spectra and their absorption counterparts, however, that indicates that the explanation of these transitions is not as simple as one might hope: the features corresponding to the progression in ν_1 built on the electronic origin are the most intense bands in the emission spectra (bands *A*, *B*, and *C* in Figure 4), while in the absorption spectra they are quite weak, especially for $Mo_2Cl_4(PMe_3)_4$ and $Mo_2Br_4(PMe_3)_4$. Specifically, band *B* of these absorption spectra, which corresponds to the first member of the ν_1^* progression built on *A*, appears only as a weak shoulder for the latter two complexes; it is seen as a barely discernible feature on the red flank of the relatively intense band *a'* for $Mo_2Cl_4(PMe_3)_4$, and is dwarfed by the strong *c* and *d* lines for $Mo_2Br_4(PMe_3)_4$. No higher quanta in this progression are observed for the bromo compound,[40] while for the chloro derivative only one additional quantum of ν_1^* is resolved (line *C*). That band *a* of the pellet spectrum of $Mo_2Cl_4(PMe_3)_4$ should be the origin of what appears to be the most intense progression in ν_1^* is fairly surprising, given that this feature corresponds to the crystal lattice vibration identified in the single-crystal absorption and emission spectra of this complex.

In contrast to the progression built on 0-0, longer and more prominent progressions in ν_1^* are observed for origins *a*, *b*, *c*, and *e* of $Mo_2Cl_4(PMe_3)_4$, and for *b*, *c*

Figure 15. Low energy region of the absorption spectrum of a CsCl pellet of $Mo_2Cl_4(PMe_3)_4$ at ca. 5 K.

Figure 16. Low energy region of the absorption spectrum of a CsBr pellet of $Mo_2Br_4(PMe_3)_4$ at ca. 5 K.

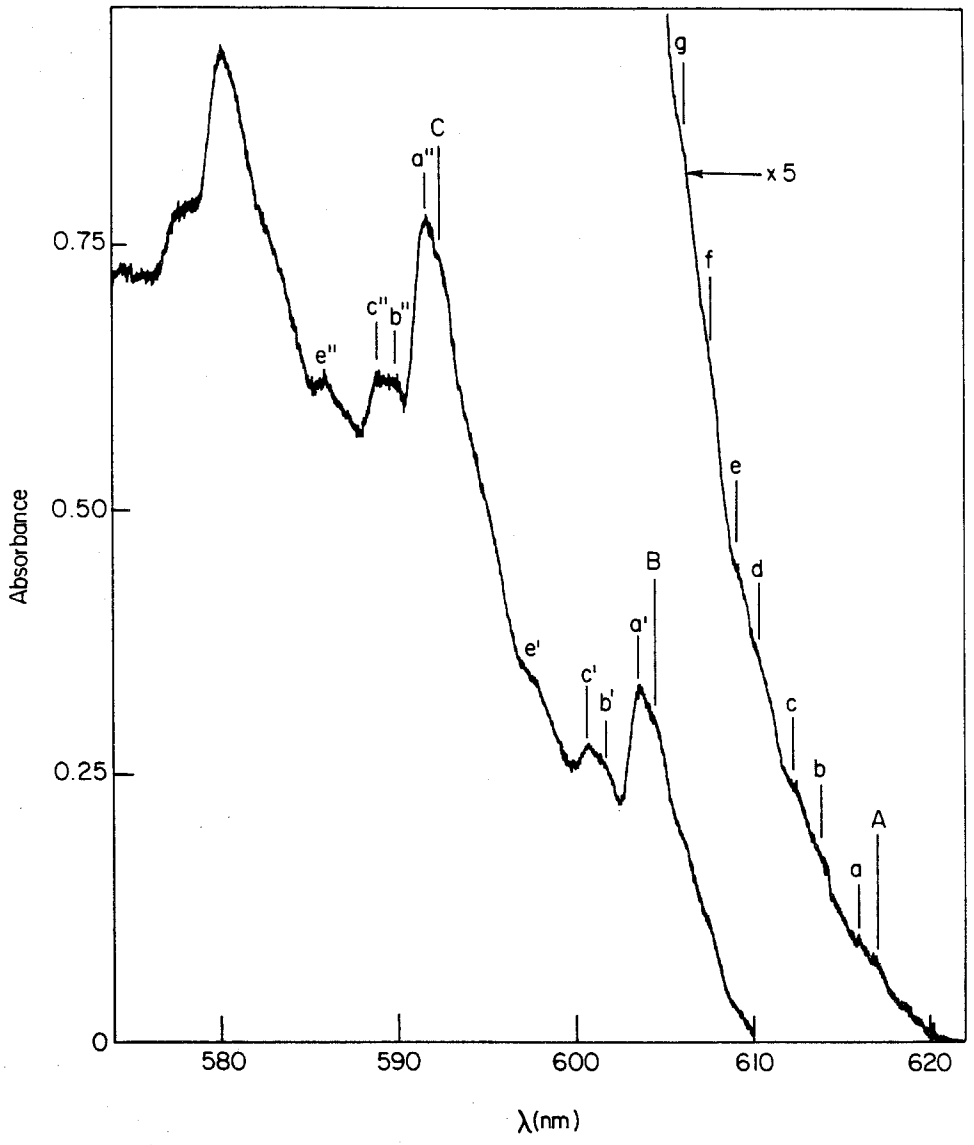
Absorbance
0.75
0.50
0.25
0
580
590
600
610
620
λ(nm)
x 5
g
f
e
d
c
b
a
A
B
a'
b'
c'
e'
C
a''
b''
c''
e''

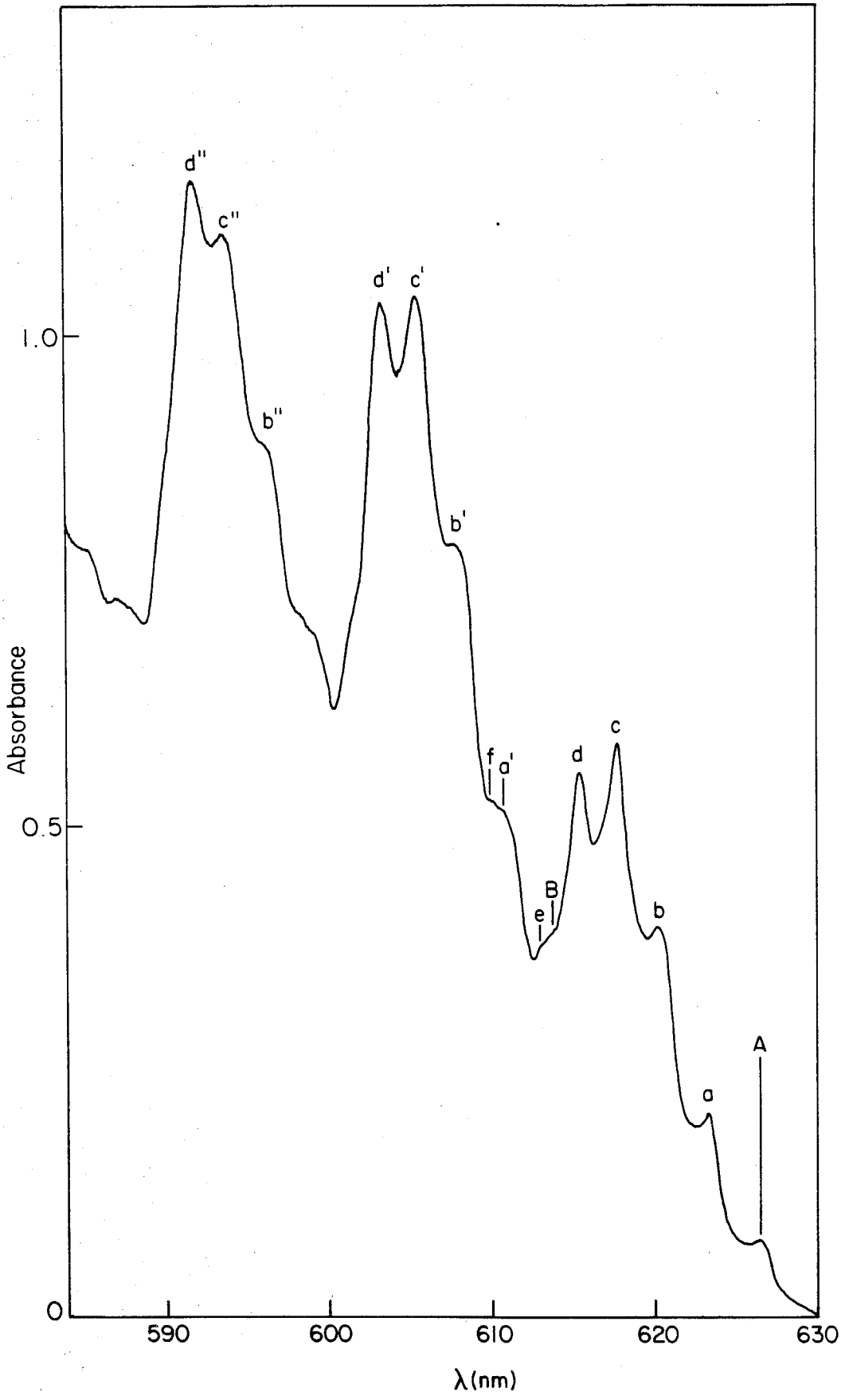
d''
c''
d'
c'
b''
b'
f
a'
d
c
B
e
b
a
A
1.0
0.5
0
Absorbance
590
600
610
620
630
λ(nm)

and d of $Mo_2Br_4(PMe_3)_4$. The intensity patterns of the progressions built on these origins are, to say the least, quite unusual, and again are significantly different from those seen in emission. Examination of the spectrum of $Mo_2Cl_4(PMe_3)_4$ (Figure 15) reveals that while the first major cluster of vibronic features (spanned by A and a') shows lines superimposed on a monotonically rising intensity background, the intensity drops very sharply between bands a' and b', rises between b' and c', drops again, and then steadily increases, as before, to band a''. To higher energy of line a'' the pattern repeats itself beginning with the sharp intensity drop between a'' and b'', except that band e'' now displays a discrete peak maximum; beyond this point, spectral congestion obscures most vibronic features.[41] Similarly sudden decreases in intensity occur within each cluster of vibronic features in the spectrum of $Mo_2Br_4(PMe_3)_4$ (Figure 16) following the transitions of the progression built on origin d. Moreover, the progression based on band c, which is the most intense feature in the cluster of peaks spanned by A and B, seems to lose intensity relative to the progression built on d at higher vibrational quanta.

The spectrum of $Mo_2Br_4(PMe_3)_4$ also displays two weak bands (e and f) possessing spacings from the 0-0 line that are greater than any ground state vibrational frequency of the $Mo_2Br_4P_4$ core of this complex. While this suggests that they might be attributable to combination bands of the lower frequency origins, neither band e nor f appears at an appropriate interval from a, b, c, or d to be part of such a progression. In fact, the most likely candidates for bands of this type, namely $c+d$, $2c$, and $2d$, are not observed at all. Viewing lines e and f as corresponding to a separate electronic origin of the $^1(\delta \rightarrow \delta^*)$ band, due to some form of sample inhomogeneity introduced by the CsBr matrix, is equally unsatisfactory. The separation of these two features (f - e) is 80 cm^{-1}, which is equal to the spacings A - a and a - b; were line e a separate electronic origin, or the first quantum of

mode *a* built on a separate electronic origin that is not observed, intense bands corresponding to *c* and *d* on this origin would be expected, but none are found.

The absorption spectrum of $Mo_2I_4(PMe_3)_4$ is much simpler than those of $Mo_2Cl_4(PMe_3)_4$ and $Mo_2Br_4(PMe_3)_4$. This is not surprising given that the decrease in the number of intense subprogressions in the emission spectra of the $Mo_2X_4(PMe_3)_4$ series according to Cl > Br > I is reflected in the absorption spectra of the chloride and bromide derivatives (Table III). Although the ν_1^* progression built on the electronic origin is still quite weak relative to those built on the other origins, as well as to those seen in emission, it appears to extend for several quanta. Because of the greater breadth of the vibronic transitions in this spectrum, however, it is unclear if the bands 99 and 174 cm^{-1} from the 0-0 line represent single origins or are actually composed of a number of closely spaced features. The progression in ν_1^* built on the former of these two modes dominates the spectrum.

Inasmuch as the emission spectrum of $W_2Cl_4(PMe_3)_4$ is considerably more complex than those of the $Mo_2X_4(PMe_3)_4$ series, it might be anticipated that the unusual effects described above for the absorption spectra of the molybdenum complexes would be even more dramatically manifested in that of the tungsten dimer. Fortunately, the absorption spectrum of $W_2Cl_4(PMe_3)_4$ (Figure 17) is poorly vibronically resolved, consisting of a series of weak but regularly spaced vibronic features; discussion of this spectrum is thus accordingly brief. As was observed for its molybdenum homologue, no prominent features are apparent near the emission 0-0 line. Concentrated CsCl pellets of this material also failed to show any lines in this region, however, and attempts at growing crystals suitable for single-crystal absorption studies were unsuccessful. That the absorption 0-0 line does lie near its emission counterpart may be inferred from noting that adding two quanta of the average ν_1^* value of 236 cm^{-1} to the position of the emission origin line (14274 cm^{-1};

Figure 17. Absorption spectrum of a CsCl pellet of $W_2Cl_4(PMe_3)_4$ at ca. 5 K. The arrow indicates the observed position of the emission 0-0 line (Figure 11). Spacings (cm^{-1}) corresponding to the excited state metal-metal stretching frequency (ν_1^*(av.) = 236(5) cm^{-1}) and to lower frequency vibronic features are identified.

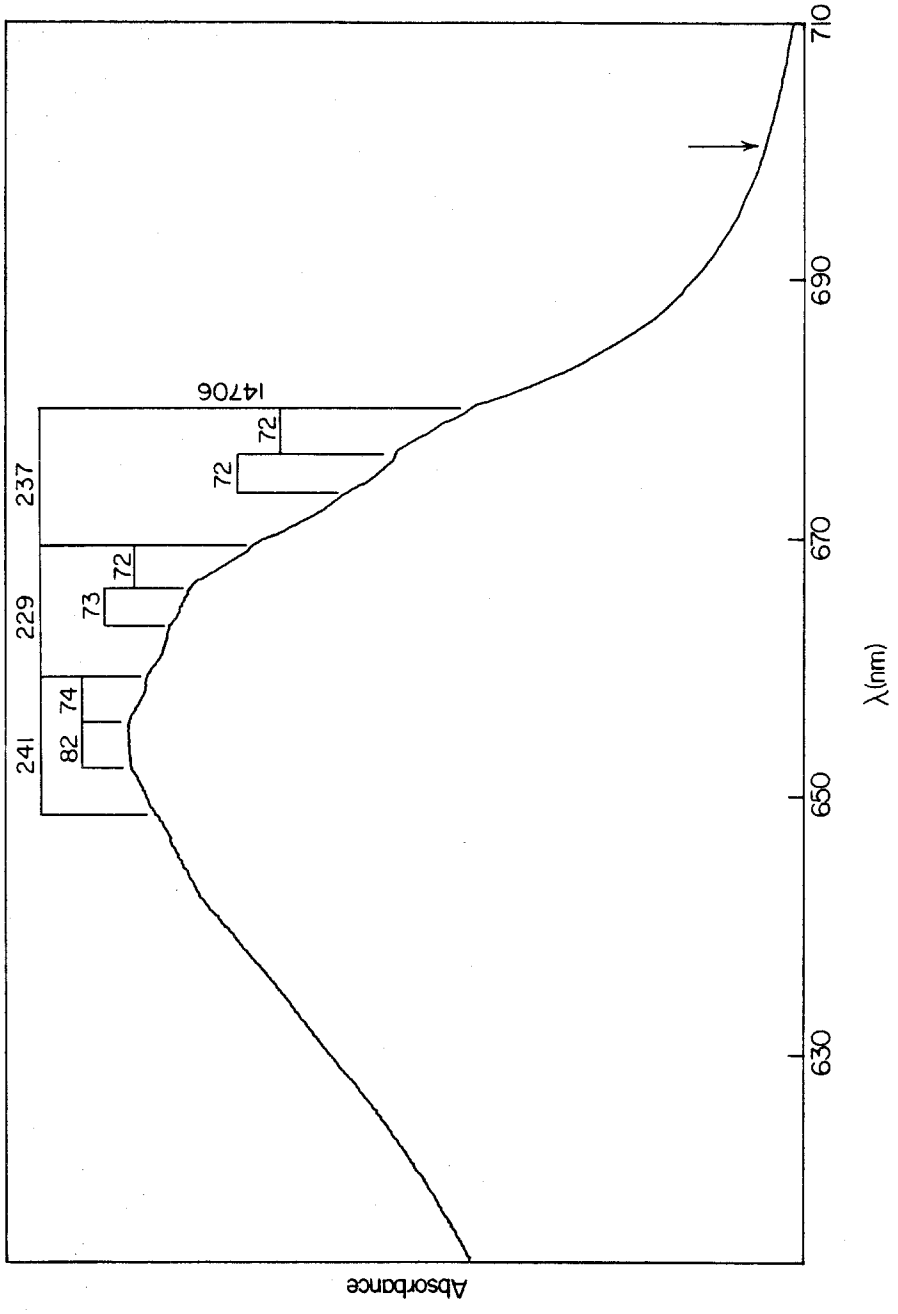
Absorbance
λ(nm)
630
650
670
690
710
1470
72
72
237
72
73
229
74
82
241

Table II) yields 14746 cm^{-1}, which differs from the position of the relatively strong absorption feature at 14778 cm^{-1} by 32 cm^{-1}; this difference agrees closely with the frequency of emission phonon mode *a* (34 cm^{-1}; Table II), upon which was built the most intense progression of ν_1^* in the spectrum of $Mo_2Cl_4(PMe_3)_4$. Moreover, the frequencies of the vibronic transitions of this progression of $W_2Cl_4(PMe_3)_4$ (14778, 15015, 15246 cm^{-1}) are nearly the same as the shoulders in the 77 K glassy matrix spectrum of this compound (14780, 15040, 15246 cm^{-1}; Table I).

A more important difference between the $^1(\delta \rightarrow \delta^*)$ transitions of the molybdenum dimers and that of $W_2Cl_4(PMe_3)_4$ is that the Franck-Condon maximum of this band for the latter complex, counting from the 0-0 line in intervals of ν_1^*, is near the 0-4 and 0-5 transitions, whereas those of the former compounds generally maximized at 0-2. Such deviations are not surprising in light of the relatively highly distorted emission band shape of the tungsten compound; its absorption profile is presumably dominated by a higher degree of spectral congestion than is found for the molybdenum complexes.

Discussion

The unprecedented vibronic resolution of the spectra of the $M_2X_4L_4$ complexes would appear to make these species ideal candidates for elucidating, for the first time, the multidimensional potential energy surfaces of the $^1[\sigma^2\pi^4\delta^2]$ and $^1[\sigma^2\pi^4\delta\delta^*]$ states of quadruply bonded dimers. As aesthetically pleasing as these spectra are at first glance, closer scrutiny reveals a number of glaring anomalies that serve to temper one's initial enthusiasm for the completion of this task. These problems, as well as some historical background on related phenomena in similar systems, are enumerated below:

1. *The absorption and emission spectra of these complexes are not mirror images of each other.* In the first photophysical and spectroscopic study of a dimer of the $M_2X_4L_4$ type ($Mo_2Cl_4(PBu^n_3)_4$),[30] assignment of the emission as $^1(\delta^* \rightarrow \delta)$ fluorescence was based on the mirror symmetry of the emission and $^1(\delta \rightarrow \delta^*)$ absorption bands and the mutual overlap of their respective 0-0 transitions, as well as the close agreement of the observed radiative rate constant with that estimated from the oscillator strength of the $^1(\delta \rightarrow \delta^*)$ transition using the Strickler-Berg formalism. This was contrasted with the behavior of the weakly emissive (in solution) $Re_2Cl_8^{2-}$ ion, the spectra of which are not mirror images, and whose radiative rate ($\sim 10^2$ s^{-1}) is four orders of magnitude lower than that calculated from $^1(\delta \rightarrow \delta^*)$. These differences between $Mo_2Cl_4(PBu^n_3)_4$ and $Re_2Cl_8^{2-}$ were attributed to the ability of the latter to rotate from its δ-bond-enforced D_{4h} ground-state geometry to the sterically favored D_{4d} geometry in the $^1(\delta\delta^*)$ excited state, which the arrangement of the bulky ligands of the former complex strongly hindered. As was shown in Chapter IV, however, the radiative rate constants of all of the complexes described in the preceding section agree very closely with those calculated from their $^1(\delta \rightarrow \delta^*)$ oscillator strengths, with the highest emission quantum yields of this class of compounds belonging to those species whose spectra deviate furthest from the mirror image relationship.[33] Thus, in contrast to $Re_2Cl_8^{2-}$, the mechanism responsible for the unprecedented "variable mirror symmetry" displayed by these complexes does not alter the dipole-allowed character of the electronic transition.

2. One of the hallmarks of the $^1(\delta \rightarrow \delta^*)$ transition is that its metal-metal-localized character is vibronically manifested as long, intense progressions in $\nu_1^*(M_2)$. *While this is clearly the progression-forming mode in the absorption spectra of these complexes, the progression in this mode based on the electronic origin is extremely weak, with the vibronic transitions in this progression beyond the*

first quantum of ν_1 being discernible only with difficulty. In a high-resolution single-crystal spectral study of the $Re_2X_8^{2-}$ (X = Cl, Br) ions, Martin *et al.* reported[42] $^1(\delta \rightarrow \delta^*)$ bands displaying intense progressions in $\nu_1^*(Re_2)$ that were preceded, at lower energy than the strong features that they assigned as the 0-0 lines, by a weak but highly structured band system that also repeated with an interval of ν_1^*:

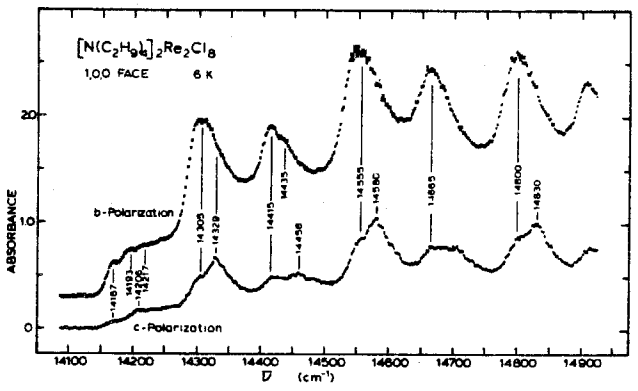

Figure 2. Polarized spectra in the low-energy region with an extended wavenumber scale for a crystal of $(TBA)_2Re_2Cl_8$ that was 2.2 μm thick at 6 K.

(reproduced from reference 42)

Because these spectra also displayed smaller spacings that were consistent with the large degree of crystallographic disorder typically found for molecules of the octahalodimetallate class, they attributed these weak absorption systems to separate electronic origins arising from a form of disorder that was not evident in the otherwise highly refined (R = 0.042) crystal structure.

Comparison of the $Re_2X_8^{2-}$ spectra with those of the $M_2X_4L_4$ systems, and particularly with those of $Mo_2Cl_4(PMe_3)_4$ and $Mo_2Br_4(PMe_3)_4$, reveals that the behavior described by Martin *et al.* is qualitatively similar to that reported here.

The crystal structures of these latter compounds are completely ordered, however, and thus any crystallographic site splittings responsible for the weak origin lines again cannot be identified by x-ray crystallography. Moreover, the polarized single-crystal absorption spectra of the $Mo_2X_4(PMe_3)_4$ complexes (Figure 14 and reference 37) show very clean molecular-z polarization of the $^1(\delta \rightarrow \delta^*)$ transition, with polarization ratios on the order of 100. It is difficult to envision any type of disorder that is consistent with this observation.

3. *The $^1(\delta^* \rightarrow \delta)$ emission bands of these complexes, the vibronic progressions of which correspond to ground-state vibrational modes, display fairly intense subprogressions in modes that are not enhanced in the resonance Raman (rR) spectra obtained upon $^1(\delta \rightarrow \delta^*)$ excitation.* Inasmuch as this is the first observation of vibronic transitions corresponding to vibrational modes other than ν_1 in the $^1(\delta^* \rightarrow \delta)$ spectra of quadruply bonded complexes, this result cannot be evaluated in the context of previous findings. It is nonetheless surprising, however, since the theory of resonance Raman requires that those totally symmetric modes that undergo displacements in the electronic excited state responsible for resonance scattering be, in turn, resonantly enhanced.[43] The only mode displaying comparable intensity in both the rR[13] and $^1(\delta^* \rightarrow \delta)$ spectra is $\nu_1(M_2)$; the others appear to obey an effective exclusion relationship between the two sets of spectra.

It is essentially impossible to interpret the above aspects of the electronic spectra of the $M_2X_4L_4$ complexes within the framework of the current portrait of their δ^2 and $^1(\delta\delta^*)$ potential energy surfaces. It is also clear that vestiges of the unusual spectroscopic behavior described in this chapter have been seen previously for other quadruply bonded complexes, and that such interpretation as was given at the time may not provide an adequate account of these effects in the present case. Therefore, before attempting to understand the obvious spectroscopic trends observed upon

perturbation of the ligands and metals of the $M_2X_4L_4$ chromophore, we will try to interpret these spectra within the Franck-Condon regime by calculating their vibronic transition positions and intensities. The specific aims of these calculations are: (*i*) to determine, in general terms, the extent to which the high-resolution spectra manifest solid state effects; (*ii*) to evaluate the interpretation of the vibronic structure of the 5 K emission spectra as being simple progressions built on a single electronic origin; and (*iii*) to calculate the corresponding absorption spectra from the Franck-Condon parameters that characterize the emission spectra, and determine those changes in these parameters that are necessary to obtain the correct fit (item **1** above).

Franck-Condon Calculations.

Although the 77 K spectra of the $M_2X_4L_4$ complexes are not as informative, from a vibronic standpoint, as their high-resolution counterparts, their simple band shapes are necessarily easier to reproduce in calculations. In light of the above discussion concerning crystallographic effects on the solid state spectra of these species, and the apparent absence of totally symmetric modes among the emission spectra subprogressions, attempting to simulate the 77 K spectra using the one vibrational mode known with certainty to be Franck-Condon-active, namely ν_1, will demonstrate which, if any, of the other vibronic transitions seen in the solid state spectra are also present in the absence of a crystal lattice, and thus which are intrinsic vibronic features of these molecules.

The best-fit[44] calculated spectra for the $Mo_2X_4(PMe_3)_4$ series, based on the parameters set out in Table IV, are shown in Figures 18 and 19. Comparison of the calculated and experimental low-resolution absorption spectra (Figure 18) shows that while the two sets of spectra look roughly similar in each instance, the relative intensities of the vibronic transitions, and the extent to which the spectrum is filled

Table IV. Parameters for Franck-Condon Calculations of Low-Resoluton $Mo_2X_4(PMe_3)_4$ Spectra.[a]

Figure	Compound	Mode	Initial Freq.	Final Freq.	S	E_{0-0}	FWHM (Gaussian)
18a	$Mo_2Cl_4(PMe_3)_4$	ν_1	355	335	2.65	16480	280
19a	$Mo_2Cl_4(PMe_3)_4$	ν_1	335	355	4.50	16290	375
18b	$Mo_2Br_4(PMe_3)_4$	ν_1	355	340	2.45	16120	250
19b	$Mo_2Br_4(PMe_3)_4$	ν_1	340	355	3.30	16040	300
18c	$Mo_2I_4(PMe_3)_4$	ν_1	345	320	2.40	15160	225
19c	$Mo_2I_4(PMe_3)_4$	ν_1	320	345	2.30	15110	225
21	$Mo_2I_4(PMe_3)_4$	ν_1	310[b]	343[c]	2.30	15097	150
		g	145[d]	145[d]	0.45		

[a]All parameters except S are given in cm^{-1}; values of ν_1 and E_{0-0} are taken from Table I unless specified otherwise.

[b]Table III.

[c]Chapter II, Table V.

[d]Table II

Figure 18. Single-mode (ν_1^*) Franck-Condon fit to the low-resolution absorption spectra of $Mo_2X_4(PMe_3)_4$, based on the parameters set out in Table IV: (a) X = Cl; (b) X = Br; (c) X = I. Experimentally observed spectra are represented by dotted lines.

Figure 19. Single-mode (ν_1) Franck-Condon fit to the low-resolution emission spectra of $Mo_2X_4(PMe_3)_4$, based on the parameters set out in Table IV: (a) X = Cl; (b) X = Br; (c) X = I. Experimentally observed spectra are represented by dotted lines.

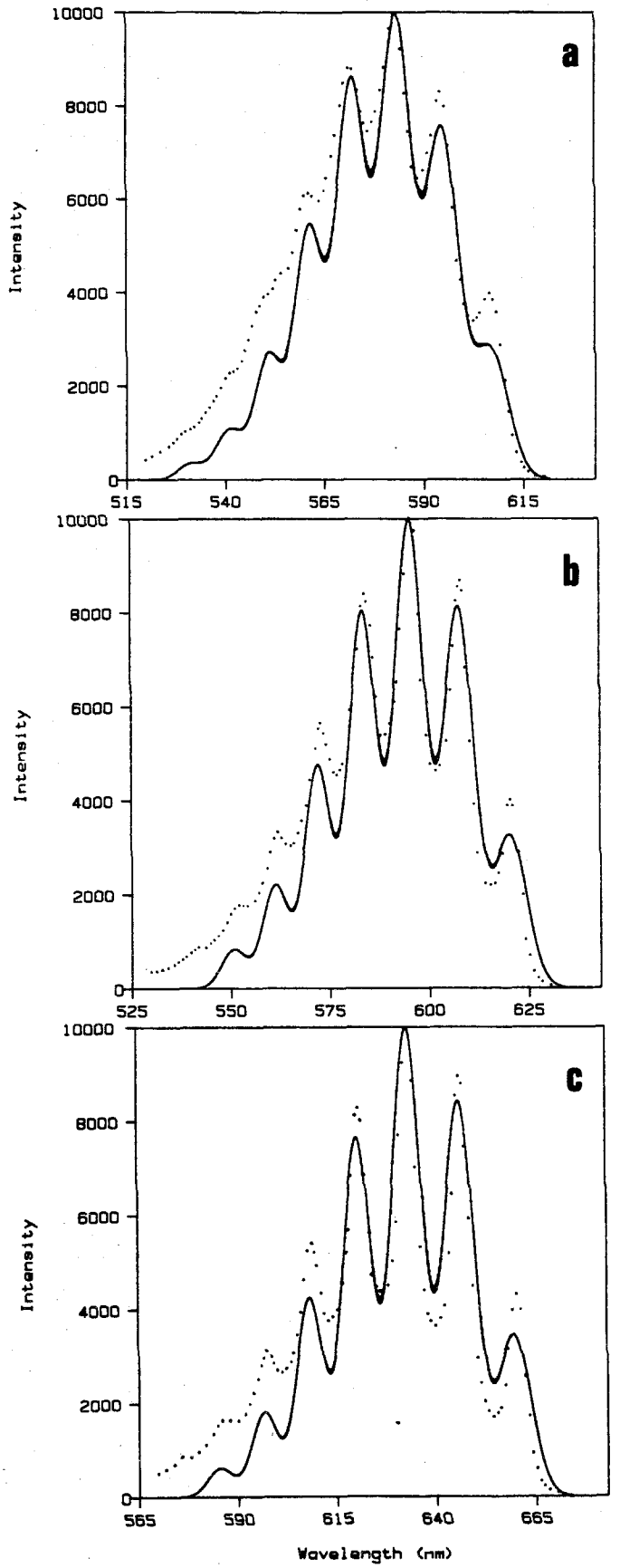
a
b
c
Intensity
Intensity
Intensity
10000
8000
6000
4000
2000
0
515
540
565
590
615
525
550
575
600
625
565
590
615
640
665
Wavelength (nm)

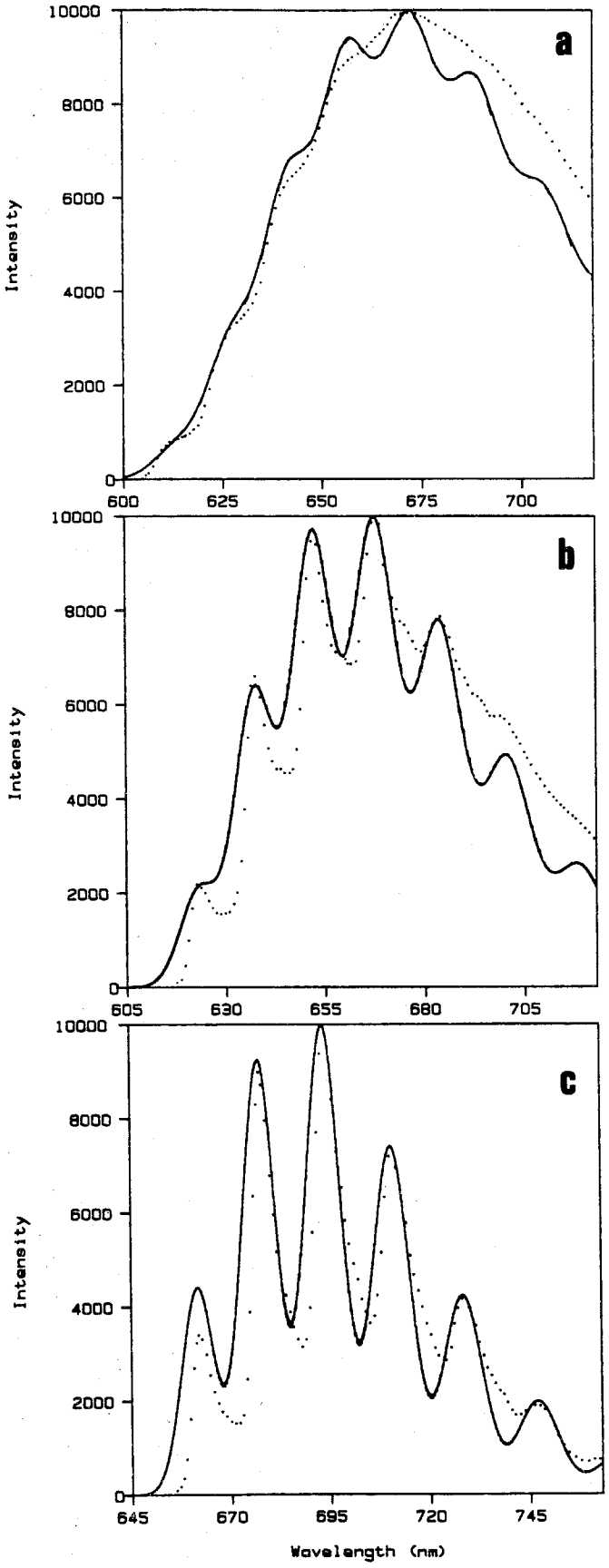
a
b
c
Intensity
Intensity
Intensity
10000
8000
6000
4000
2000
0
600
625
650
675
700
605
630
655
680
705
645
670
695
720
745
Wavelength (nm)

in by the overlap of these transitions, cannot be simultaneously reproduced by the single-mode fit, *i. e.*, no combination of Huang-Rhys factor (S) and Gaussian fwhm for ν_1 simulates the band profile. For example, although the experimental intensity pattern of $Mo_2Cl_4(PMe_3)_4$ ($I_{0-2} > I_{0-3} > I_{0-1}$, etc.) is reproduced by the calculation, the calculated intensities of the vibronic transitions to both higher and lower energy of the 0-2 Franck-Condon maximum are weaker than are experimentally observed. Changing the Huang-Rhys factor will not improve this situation; decreasing S will provide a better fit of 0-0 and 0-1 but will result in all quanta higher than 0-2 being weaker than they already are, while increasing S will decrease the 0-0 and 0-1 intensities further. Moreover, the line width that best simulates the minimum intensity between the 0-1 and 0-2 and the 0-2 and 0-3 transitions results in the 0-0 band being a shoulder rather than a discrete peak. Similar defects are apparent in the calculated spectra of $Mo_2Br_4(PMe_3)_4$ and $Mo_2I_4(PMe_3)_4$.

The deviations of the best-fit calculated emission spectra from the experimental spectra (Figure 19) are less obvious than are those for absorption, but they nonetheless result in inadequate reproductions. Specifically, while the positions and intensities of most of the vibronic transitions in these spectra are fit fairly well, their band shapes are clearly not Gaussian. A striking example of this is seen for $Mo_2I_4(PMe_3)_4$, for which the calculated spectrum gives the correct positions of the vibronic intensity maxima but fails to give the correct minima. Although the fit to the spectrum of $Mo_2Cl_4(PMe_3)_4$ does not suffer from this problem to the same extent, the width of the observed lines near the emission maximum cannot be simulated without those near the origin being completely washed out. This breakdown of the single-mode fit of the emission spectra was anticipated, of course, by the experimental emission spectrum of $Mo_2Br_4(PMe_3)_4$, which shows a weak shoulder at an interval that matches the frequency of mode *e* in the solid state spectrum. That the

analogous vibronic side bands in the solid state spectra of the other $Mo_2X_4(PMe_3)_4$ complexes are also present in the absence of the crystal lattice is indicated by the fact that the decrease in the best-fit S and fwhm parameters according to Cl > Br > I (Table IV) is consistent with the decrease in intensity and frequency of the most intense emission subprogression in the high resolution spectra.

The extent to which the single-mode Franck-Condon calculations failed to fit the simple low resolution spectra of the $Mo_2X_4(PMe_3)_4$ series indicates that the intense, higher frequency "non-ν_1" features in both the high-resolution absorption and emission spectra of these complexes are intrinsic vibronic origins. With this information in hand, we now attempt to simulate the behavior of these modes in the high-resolution emission spectra. Because our current programs are limited to simulating progressions for only three Franck-Condon-active vibrational modes, the high degree of congestion displayed by the spectra of these complexes cannot be reproduced accurately, and thus all of the following spectra will be more highly resolved at energies far from the electronic origin than are the experimental spectra. The calculated emission spectrum of $Mo_2I_4(PMe_3)_4$, shown in Figure 20a for modes ν_1, g, and e and the parameters set out in Table V, is in line with this anticipation; the vibronic resolution does not wash out at all, in contrast to the experimental observation (Figure 4c), when the experimental line widths of the emission origin region (Figure 8) are used in the calculation. Overriding this shortcoming, however, is the fact that each of the calculated bands has a corresponding feature in the experimental spectrum at roughly the same energy and intensity (when the underlying emission intensity[45] is accounted for). The most obvious success of this calculation is the reproduction of the long progressions in ν_1 and g; the sizeable Huang-Rhys factor for the latter mode (Table V) indicates that there is a considerable distortion along this normal coordinate in the $^1(\delta\delta^*)$ excited state, in addition

Table V. Parameters for Franck-Condon Calculations of the High-Resolution Emission Spectra of $Mo_2X_4(PMe_3)_4$ Compounds.[a]

Figure	Compound	Vibrations				Origins		FWHM	
		Mode	initial freq.	final freq.	S	Energy (mode)	relative intensity	Gaussian	Lorentzian
20a	$Mo_2I_4(PMe_3)_4$	ν_1	310[b]	343	2.00	15097	1.00	3	1.5
		g	145	145	0.65	15093	0.75		
		e	77	77	0.20				
20b	$Mo_2I_4(PMe_3)_4$	ν_1	310[b]	343	2.00	15097	1.00	3	1.5
		g	145	145	0.65	15093	0.75		
		e	77	77	0.20	15078(*a*)	0.12		
						15065(*b*)	0.09		
						15057(*c*)	0.05		
						15046(*d*)	0.20		
						15001(*f*)	0.17		
20c	$Mo_2I_4(PMe_3)_4$	*g*	145	145	0.65	15097	1.0	3	1.5
		e	77	77	0.20	15093	0.75		
		d	48	48	0.20	15078(*a*)	0.12		
						15065(*b*)	0.09		
						15057(*c*)	0.05		
						15001(*f*)	0.17		
						14748(ν_1)	2.00		
20d	$Mo_2I_4(PMe_3)_4$	---------- Same as Figure 20b ----------						12	6
22a	$Mo_2Br_4(PMe_3)_4$	ν_1	326[b]	352	2.90	15954	1.00	4	3
		e	172	172	0.70				
		d	92	92	0.60				
22b	$Mo_2Br_4(PMe_3)_4$	ν_1	326	352	2.90	15954	1.00	4	3
		e	172	172	0.70	15934(*a*)	0.16		
		d	92	92	0.60	15918(*b*)	0.10		
						15892(*c*)	0.10		
						15739(*f*)	0.20		
						15624(*g*)	0.06		
22c	$Mo_2Br_4(PMe_3)_4$	---------- Same as Figure 22b ----------						12	10
23a	$Mo_2Cl_4(PMe_3)_4$	*b*	91	91	0.85	16200	1.00	10	0
		c	124	124	0.85				
		d	285	285	0.80				
23b	$Mo_2Cl_4(PMe_3)_4$	ν_1	331[b]	355	3.50	16200	1.00	10	0
		b	91	91	0.85				
		d	285	285	0.80				

[a]All values except S are given in cm^{-1}. Experimental parameters are taken from Table II, except as noted. [b]Table III.

Figure 20. Franck-Condon fit to the high-resolution emission spectrum of $Mo_2I_4(PMe_3)_4$, based on the parameters set out in Table V: (a) three mode calculation (ν_1, g, and e) using the experimental line widths taken from Figure 8; (b) same as spectrum (a) except modes a, b, c, d, and f are added as false electronic origins; (c) comparison of the origin regions of spectrum (b) and Figure 8 (the intensity of the calculated spectrum has been reduced to 0.6 times that of the experimental spectrum); (d) same as spectrum (b) with broader lines.

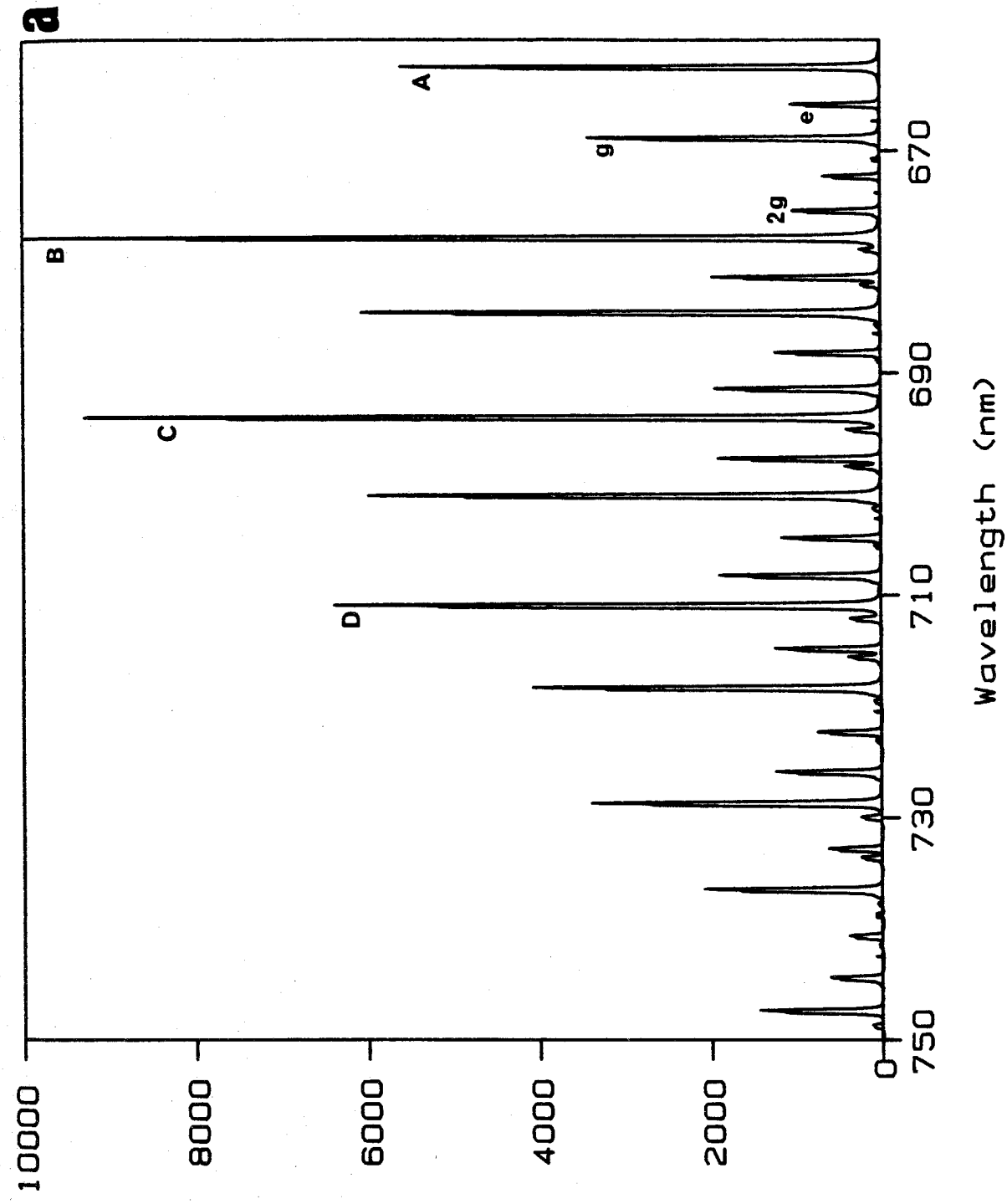
a
A
B
C
D
g
2g
e
10000
8000
6000
4000
2000
0
750
730
710
690
670
Wavelength (nm)

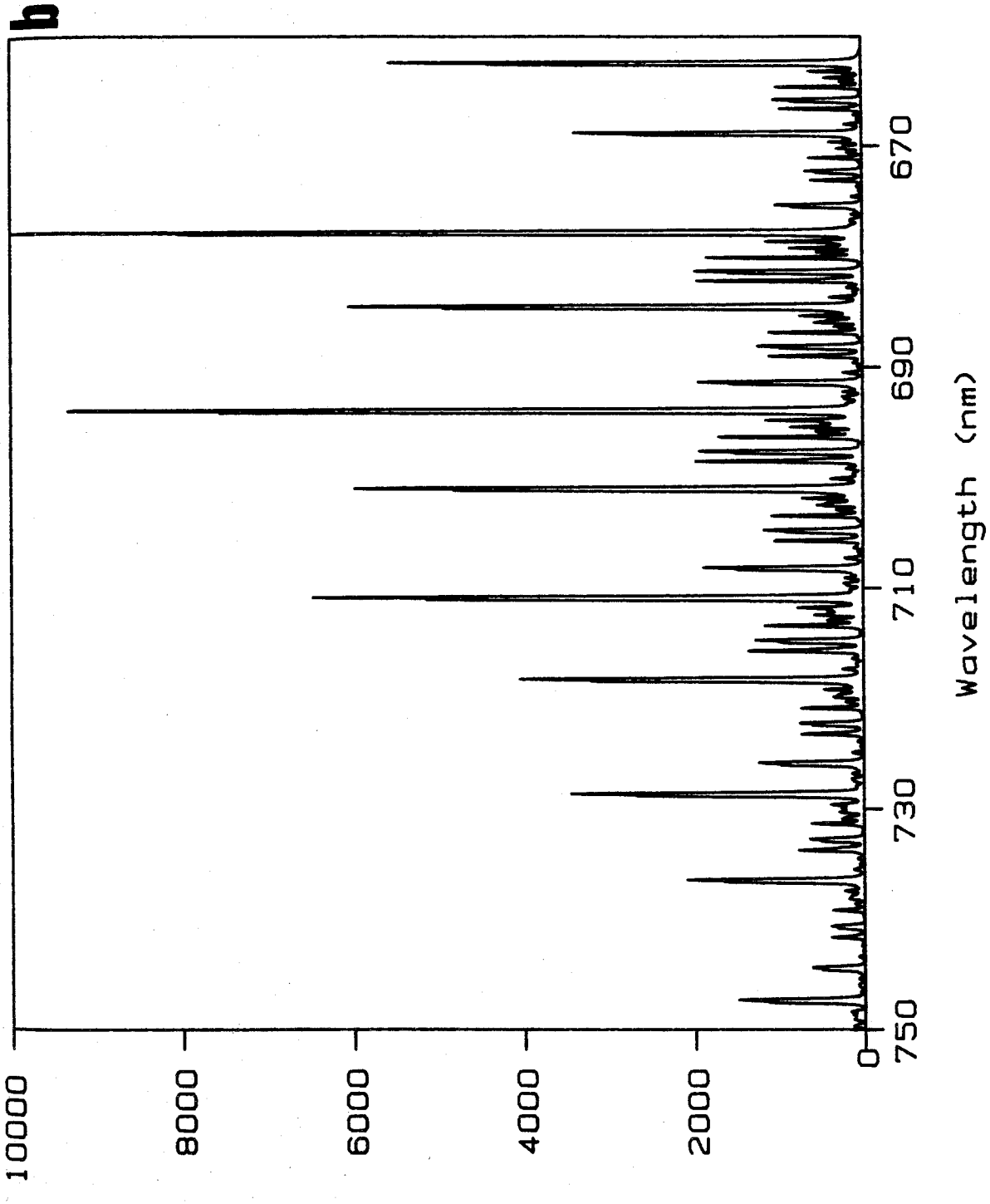
b
10000
8000
6000
4000
2000
0
750
730
710
690
670
Wavelength (nm)

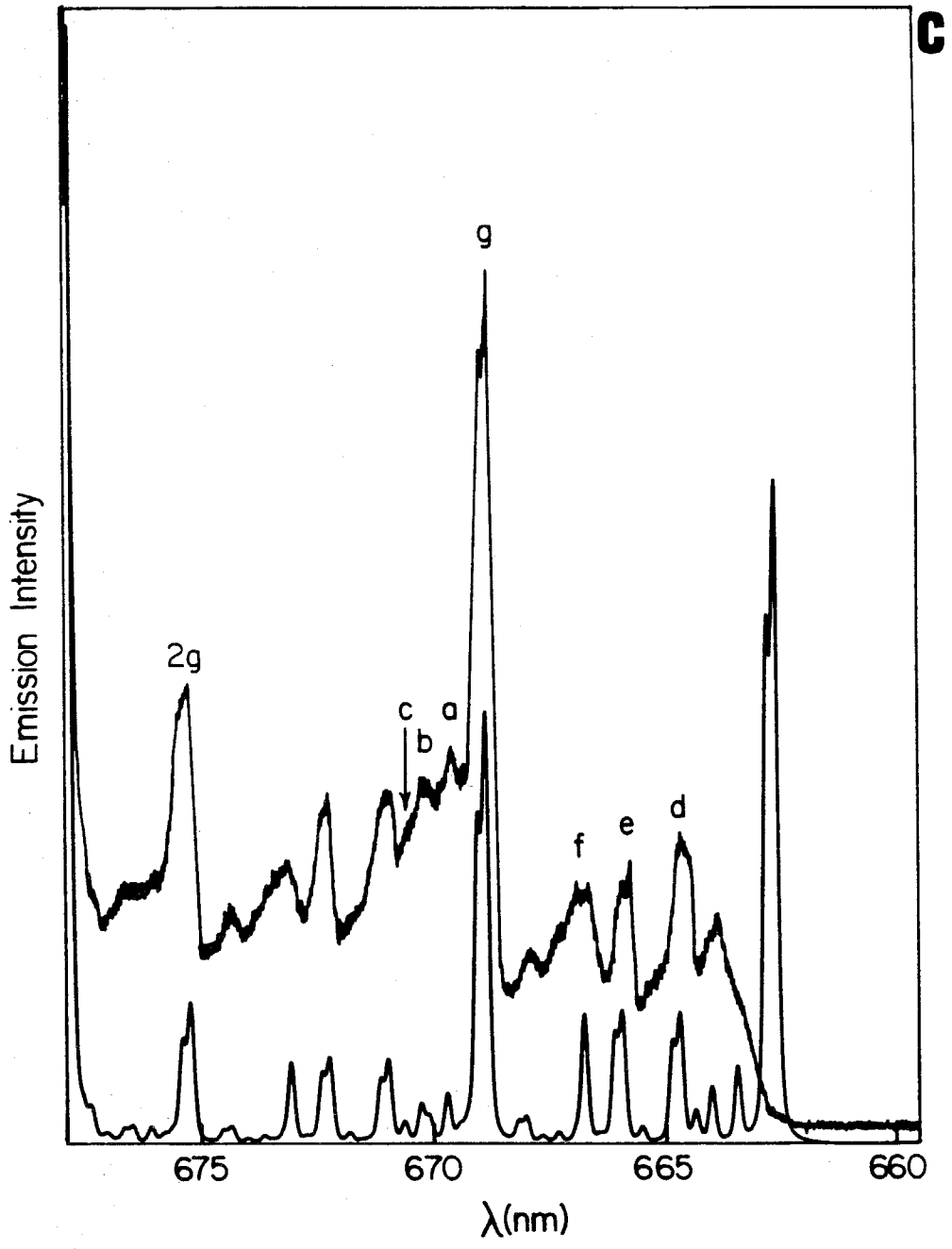
C
g
2g
c
b
a
f
e
d
Emission Intensity
675
670
665
660
λ(nm)

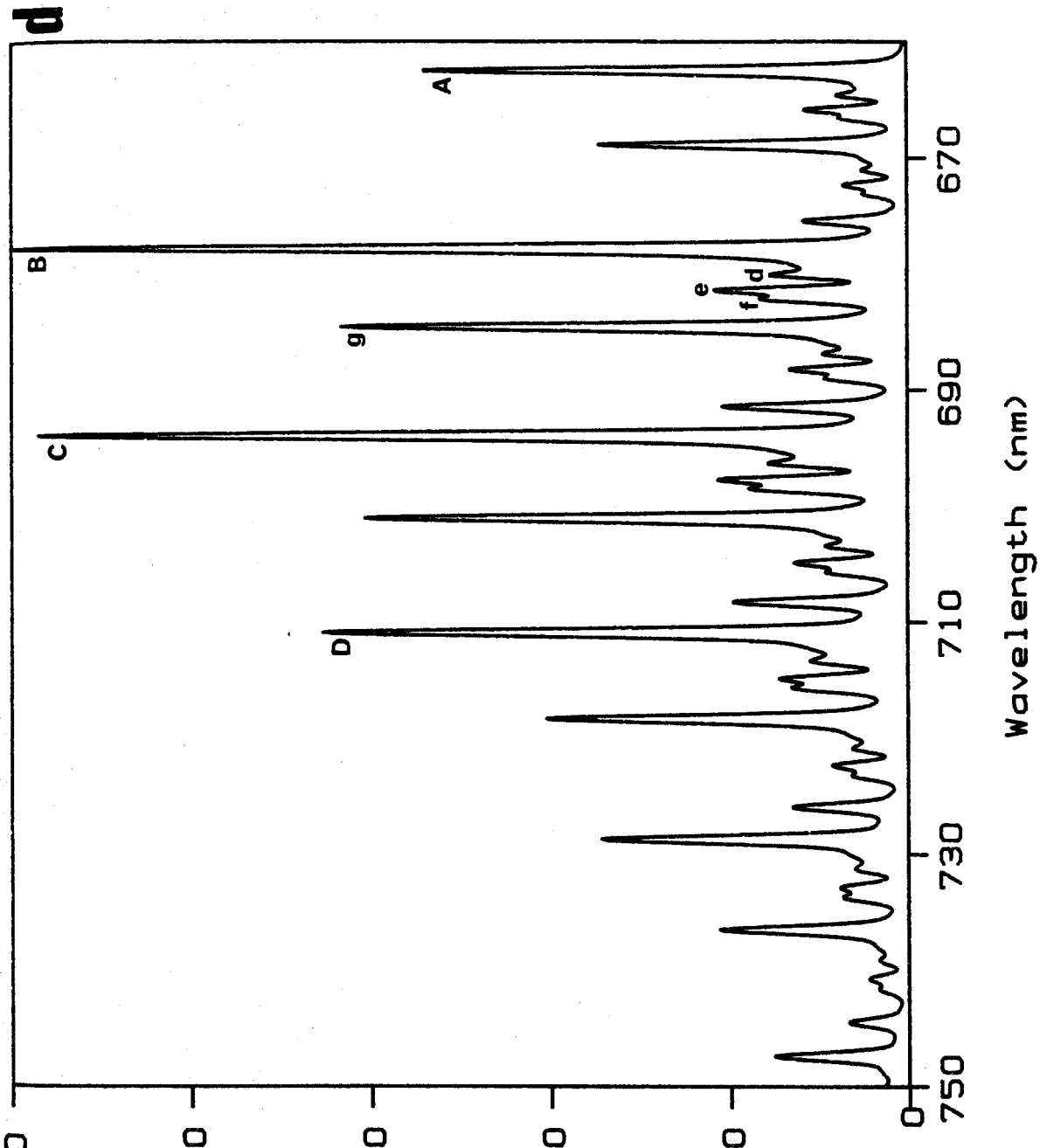
d
A
B
C
D
e
f
d
g
10000
8000
6000
4000
2000
0
750
730
710
690
670
Wavelength (nm)

to the well established elongation of the metal-metal bond. At higher quanta of the ν_1 progression, the calculation shows that the features attributable to $n\nu_1 + g$ (where n is the quantum number of the vibronic transition) are of comparable intensity to the $(n + 1)\nu_1$ bands, resulting in a smooth drop in the intensity of the prominent transitions to lower energy of band C; comparison to experiment shows that this is indeed the case. The origin of the progressive broadening of all vibronic transitions of the experimental spectrum at higher quanta is also revealed by this calculation: for each $n\nu_1$ transition there is a line corresponding to $(n - 1)\nu_1 + 2g + e$ only 24 cm^{-1} to lower energy, the intensity of which increases relative to that of $n\nu_1$ with increasing n. Similarly, there is a band corresponding to $(n - 1)\nu_1 + 3g$ only 15 cm^{-1} to the red of the $n\nu_1 + e$ lines.

Because the three-mode Franck-Condon calculation showed only a trace of the spectral congestion that is observed experimentally, any attempts to generate the underlying emission intensity would require the use of line widths far in excess of those used in the previous calculation. This congestion can be mimicked, however, by introducing the five remaining Franck-Condon-active vibrational modes of $Mo_2I_4(PMe_3)_4$ as false electronic origins, with energies equal to the position of the first quantum of that mode built on the 0-0 line, and intensities, relative to that of the true electronic origin, equal to their Huang-Rhys factor. The result of this calculation is shown in Figure 20b, where the experimental line widths from Figure 8 have again been used. Although the number of lines is still far short of what would be generated by a calculation in which all eight vibrations were treated correctly, this figure does give an indication of the degree of vibronic complexity encountered far from the origin. A comparison of the origin regions of the calculated and experimental intensity patterns is reproduced in Figure 20c. Close examination reveals that virtually every observed vibronic transition, including weak shoulders

and other subtle features, has a counterpart in the calculated version.[46]

A simple attempt at reproducing the degree to which the spectrum of $Mo_2I_4(PMe_3)_4$ is filled in at higher quanta is shown in Figure 20d, which uses the same parameters as the preceding false origin spectra with the exception of line width. Immediately obvious is the fact that the resolution of virtually every weak feature seen in the calculated line spectrum is lost. Although this results in poor agreement between the origin regions of the observed and calculated spectra, comparison of the region between bands *B* and *C* reveals that the fine structure of both spectra collapses to a similar pattern. Specifically, mode *d* built on *B* and *B* + *g* appears as a spike on the red flank of these bands, while bands *e* and *f* merge to give an asymmetric doublet. Also noteworthy is the fact that band *C* of the calculated spectrum has increased in intensity by ~5% relative to that of the line spectra of Figures 20a and 20b; this shift is in the correct direction for producing the observed Franck-Condon maximum when the underlying emission intensity is increased to the experimentally observed value of ~4000 (in the intensity units of Figure 20d) by further broadening the lines. At this latter level of resolution, however, all features are obscured with the exception of the ν_1 progression and the first members of the *g* subprogressions.

In principle, greatly broadening the lines of the best-fit high-resolution calculation should yield an emission intensity profile resembling that observed in 2-methylpentane at 77 K. Using only the ν_1 and *g* modes and the parameters in Table V did not reproduce this spectrum, however. Instead, the values of S for ν_1 and *g* had to be increased and decreased, respectively, relative to their values for the 5 K spectra; the resulting spectrum, shown in Figure 21 for the parameters set out in Table IV, provides a much more reasonable reproduction of the observed intensity profile than did the single-mode fit. The slight differences between the two spectra

Figure 21. Two mode (ν_1 and g) Franck-Condon fit to the low-resolution emission spectrum of $Mo_2I_4(PMe_3)_4$, based on the parameters given in Table IV. Experimentally observed spectrum is represented by the dotted line.

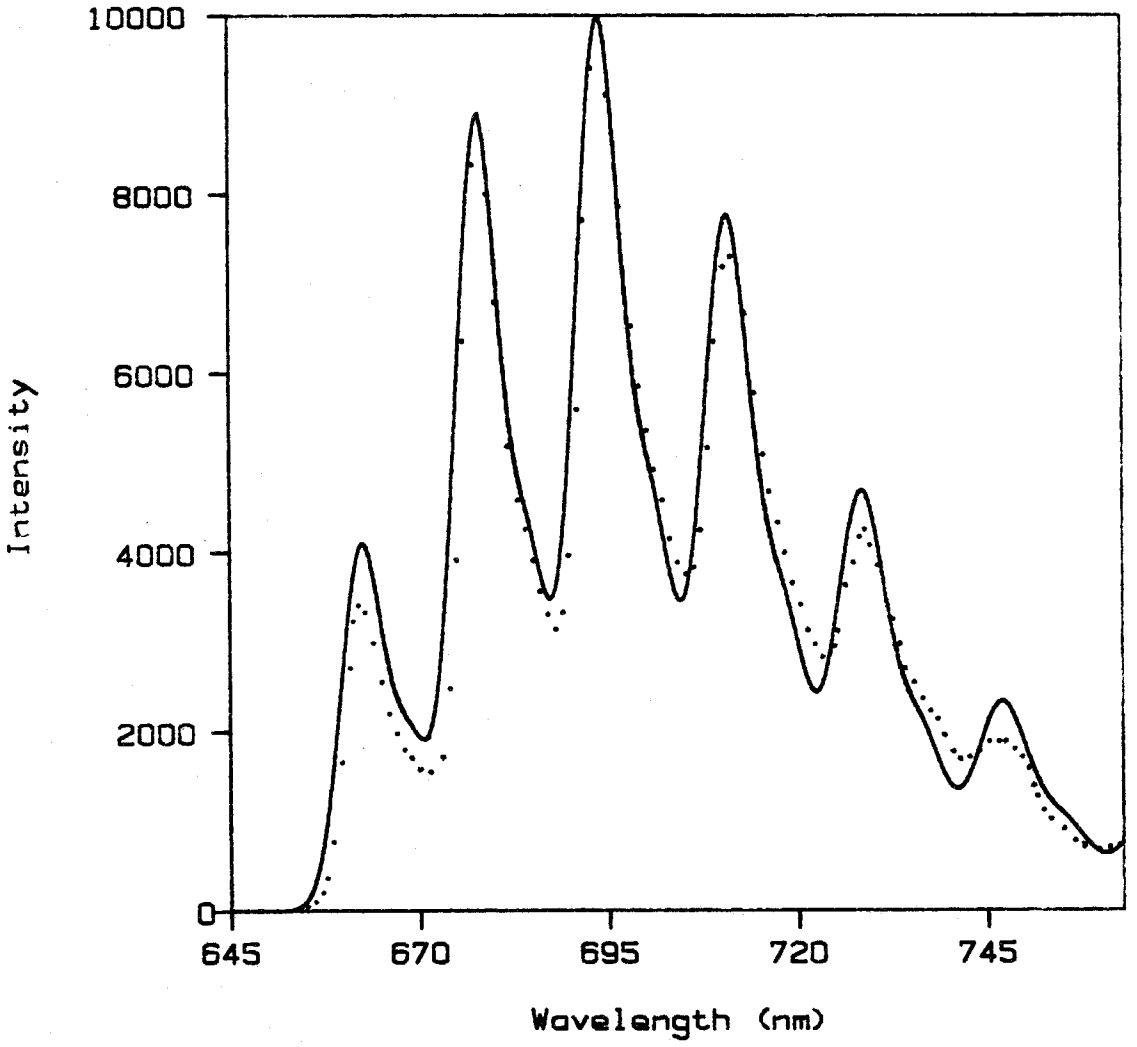
10000
8000
6000
4000
2000
0
Intensity
645
670
695
720
745
Wavelength (nm)

are probably due to the neglect of the other vibrational modes observed at high resolution; their inclusion would result in the filling in of the low energy tail of the calculated spectrum. That the Huang-Rhys factors for the ν_1 and g modes should be slightly different in the crystalline and frozen solution phases is not difficult to understand since any molecular distortion is subject to a restoring force by the surrounding environment; this is likely to differ between the two phases.

In light of the close similarities between the calculated and observed high- and low-resolution emission spectra of $Mo_2I_4(PMe_3)_4$ noted above, it is reasonable to suggest that the Franck-Condon calculations employed here would nearly perfectly reproduce the experimental spectrum in all respects if they were not limited to three vibrational modes. We will now show that the same basic conclusion can be reached for the emission spectra of $Mo_2Br_4(PMe_3)_4$, $Mo_2Cl_4(PMe_3)_4$, and $Mo_2Cl_4(AsMe_3)_4$. Because the subprogressions of these species possess greater intensity, relative to ν_1, than do the non-ν_1 vibronic transitions in $Mo_2I_4(PMe_3)_4$, spectral congestion is more severe and the limitations of our calculations will result in reproductions of the observed intensity profiles that are correspondingly poorer.[47]

The three-mode Franck-Condon calculation of the emission spectrum of $Mo_2Br_4(PMe_3)_4$ using modes ν_1, e, and d and the parameters given in Table V, is shown in Figure 22a. As was observed for $Mo_2I_4(PMe_3)_4$, the long progressions in these modes that are experimentally observed are faithfully reproduced by Franck-Condon theory.[48] In addition to accurately simulating the origin region both with respect to the position and line width of these three modes, this calculation also indicates that at high $n\nu_1$, the $(n - 1)\nu_1 + e$ lines become of comparable intensity, thus resulting in the sawtooth pattern observed experimentally beyond the emission maximum. In spite of the limitations of this calculation, vestiges of spectral congestion are also observed. Comparison of the widths of the bases of the bands between

Figure 22. Franck-Condon fit to the high-resolution emission spectrum of $Mo_2Br_4(PMe_3)_4$, based on the parameters set out in Table V: (a) three-mode calculation (ν_1, e, and d) using the experimental line widths taken from Figure 7; (b) same as spectrum (a) except modes a, b, c, f, and g are added as false electronic origins; (c) same as spectrum (b) with broader lines.

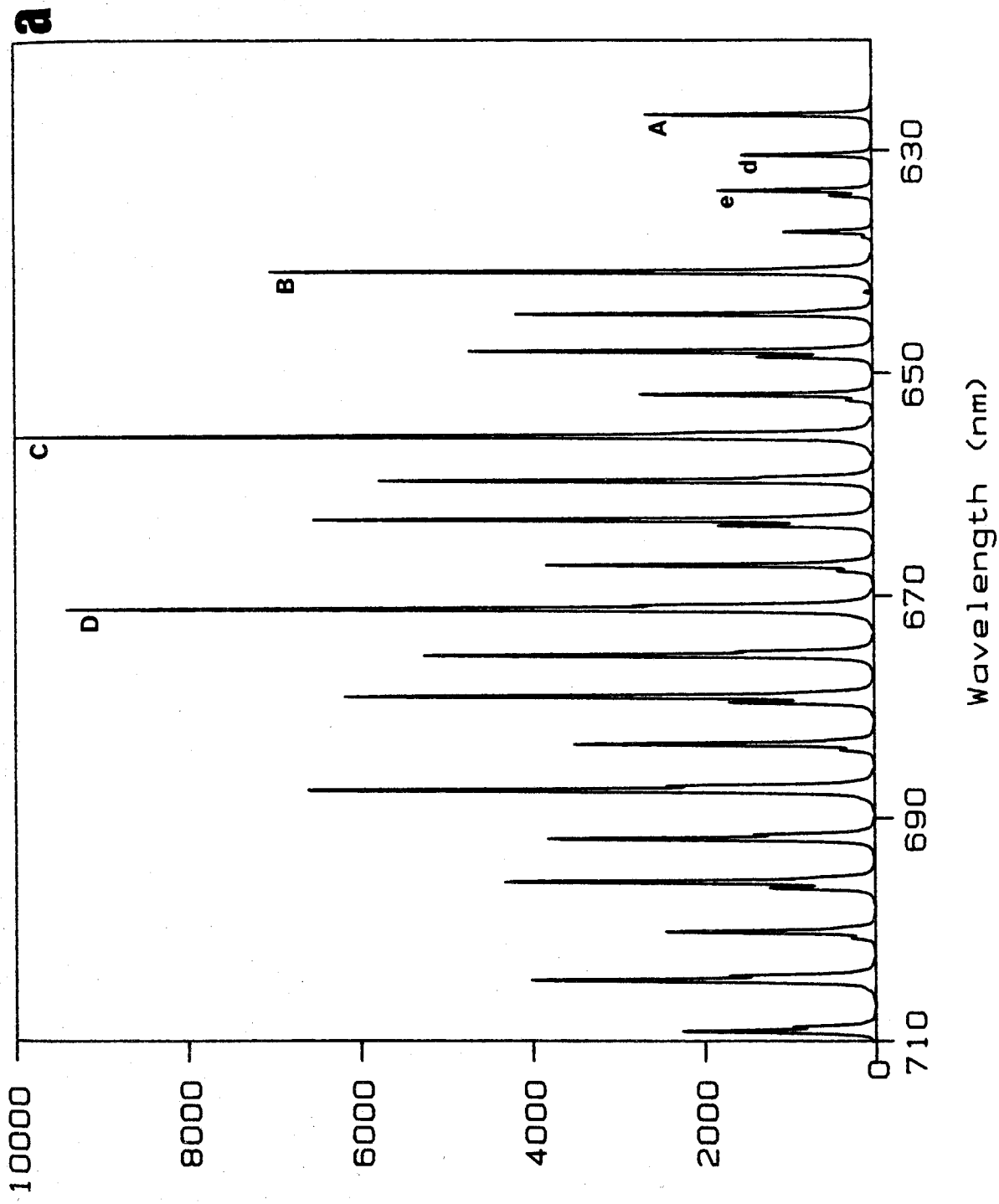
a
10000
8000
6000
4000
2000
0
710
690
670
650
630
Wavelength (nm)
A
B
C
D
d
e

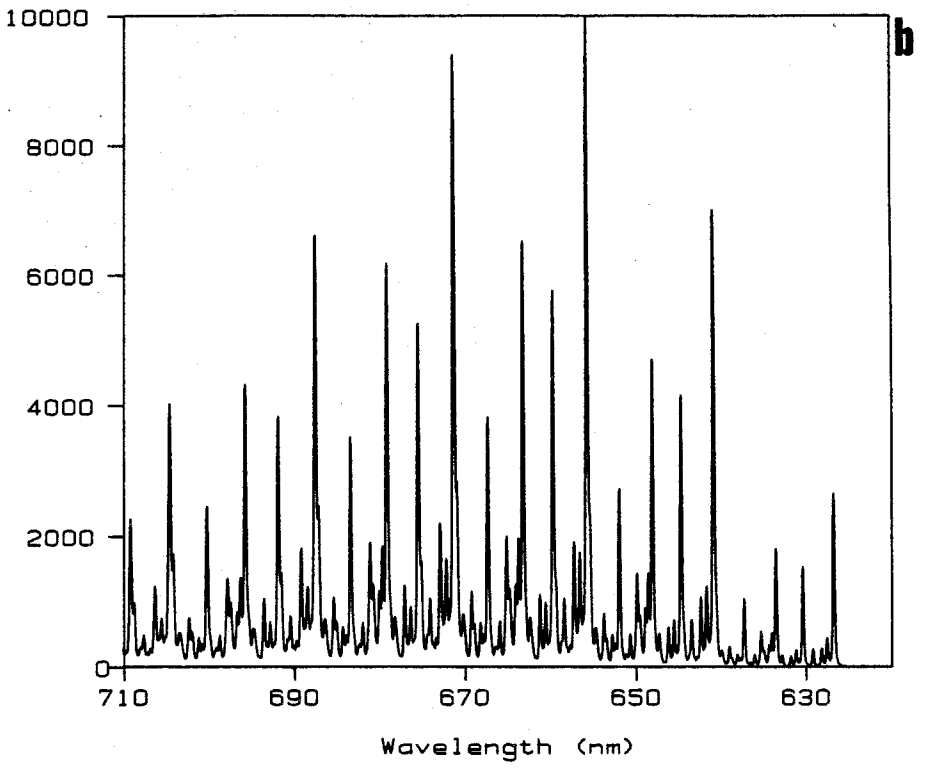
b
10000
8000
6000
4000
2000
0
710
690
670
650
630
Wavelength (nm)

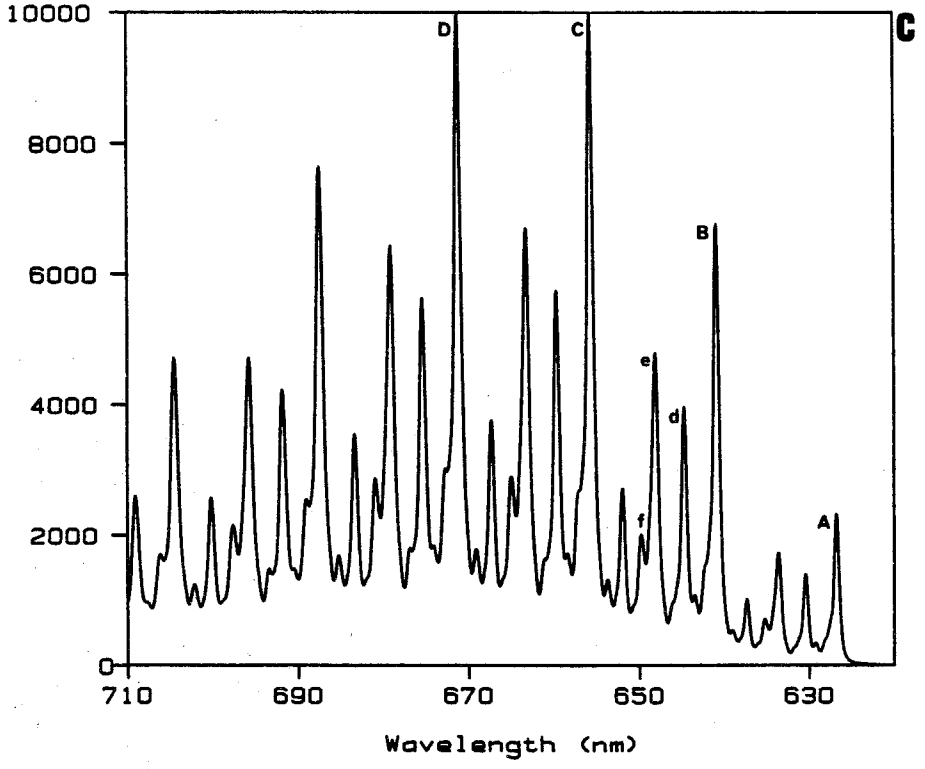
c
D
C
B
e
d
f
A
10000
8000
6000
4000
2000
0
710
690
670
650
630
Wavelength (nm)

690 - 710 nm to those near the origin line shows that they increase with wavelength. This broadening of the $n\nu_1$ transitions, which is observed experimentally, is due to the $(n - 1)\nu_1 + 2e$ (located at $n\nu_1$ - 8 cm^{-1}) and $(n - 1)\nu_1 + e + 2d$ (located at $n\nu_1 + 4$ cm^{-1}) bands; the former appears as a distinct notch on the high energy side of band *D*. Introducing modes *a*, *b*, *c*, *f*, and *g* as false origins results in an extraordinarily complex line spectrum (Figure 22b). The most notable aspect of this calculation, in the context of the spectral congestion of the experimental spectrum, is that there is nonzero emission intensity at all wavelengths, even with this narrow line width. Broadening these lines slightly (Table V) gives the spectrum shown in Figure 22c. As was observed for $Mo_2I_4(PMe_3)_4$, the vibronic resolution of Figure 22b is rapidly lost with increasing line width, but the collapse of vibronic fine structure yields similar intensity patterns in both the experimental and calculated spectrum. Comparing the region between bands *B* and *C* in these spectra shows that each major transition in this region contains a notch on their red flanks resulting from phonon modes *a*, *b*, and *c*, with the $B + e$ transition also showing a moderately intense side band due to mode *f*.

Two three-mode Franck-Condon calculations of the emission spectrum of $Mo_2Cl_4(PMe_3)_4$ are displayed in Figure 23.[49] Because this spectrum contains three subprogressions with relatively large Huang-Rhys factors, combinations and pure progressions of these modes extend over a sizeable frequency range. As seen in Figure 23a, where only modes *b*, *c*, and *d* are fit, 16 bands that possess at least 20 % of the intensity of the origin line are generated, and span a range of nearly 800 cm^{-1}. Figure 23b reveals the complex pattern that results from fitting ν_1 in addition to two of the above modes. The distinct notch on the low energy side of $n\nu_1$ that gains intensity with increasing *n* in the experimental spectrum is seen to be a result of $(n - 1)\nu_1 + b + d$, which overtakes the $n\nu_1$ band in intensity by line

Figure 23. Three-mode Franck-Condon fits to the high-resolution emission spectrum of $Mo_2Cl_4(PMe_3)_4$, based on the parameters set out in Table V: (a) spectrum generated by fitting modes *b*, *c*, and *d* (the arrows indicate the position of the first (*B*) and second (*C*) quanta of the ν_1 progression built on *A*); (b) spectrum generated by fitting modes ν_1, *b*, and *d*.

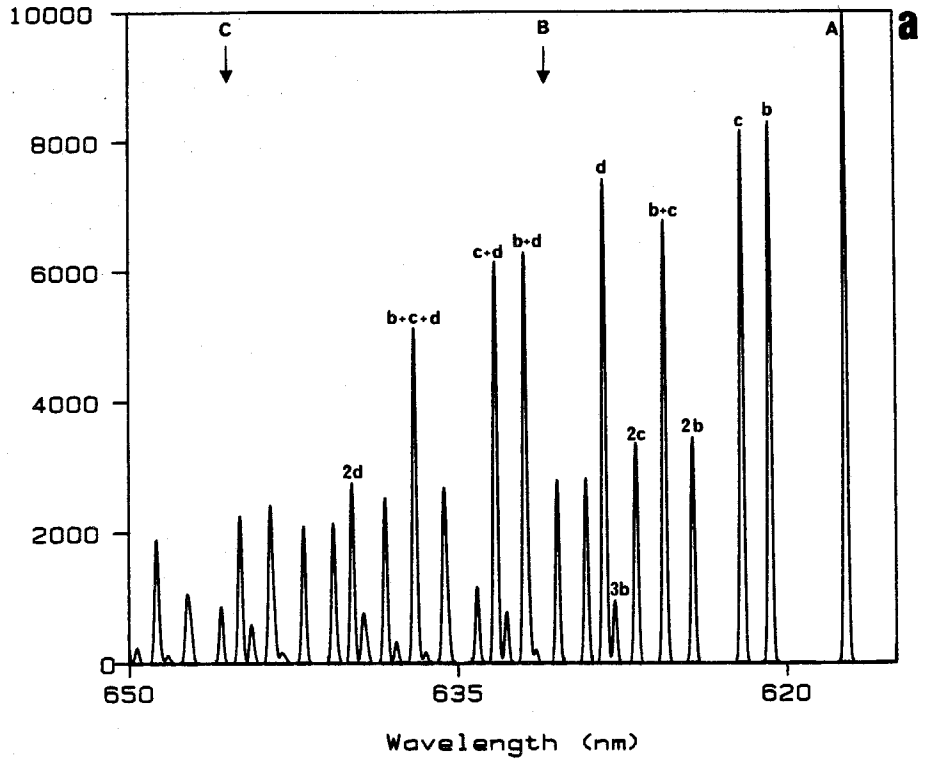
a
10000
8000
6000
4000
2000
0
650
635
620
Wavelength (nm)
C
B
A
c
b
d
b+c
c+d
b+d
b+c+d
2d
2c
2b
3b

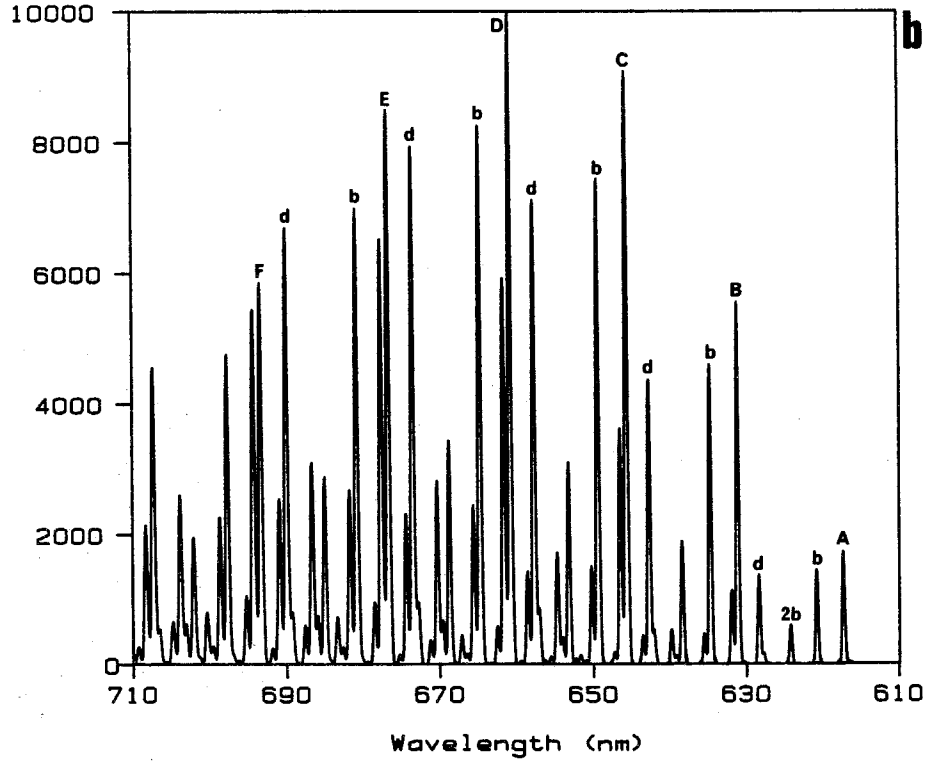
b
10000
8000
6000
4000
2000
0
710
690
670
650
630
610
Wavelength (nm)
D
C
E
B
A
F
d
b
2b

F.

With regard to the low-resolution emission spectrum of $Mo_2Cl_4(PMe_3)_4$, we note that its distinctive staircase profile is attributable to the comparable intensity of the *b*, *c*, *b* + *c*, and *d* lines, shown in Figure 23a, that fill in the region between quanta of ν_1. Since the emission spectra of the other phosphine derivatives of this complex, namely $Mo_2Cl_4(PR_3)_4$ (R = Et, n-Pr, n-Bu) are not well resolved at low temperature, firm comparisons between them cannot be made. It nevertheless seems quite unlikely that the variable band shape seen across this series (Figure 2) is the result of large changes in S for ν_1, particularly in light of the single-mode Franck-Condon calculations discussed earlier, but rather reflects a decrease in S with larger phosphines for modes *b*, *c*, and *d*, which are likely to be vibronically active (perhaps with slightly different frequencies) for all of these species.

Having successfully interpreted the high- and low-resolution emission spectra of the $Mo_2X_4(PMe_3)_4$ series within the Franck-Condon framework, we now turn our attention to their absorption spectra. One difficulty associated with this task that was not encountered for the more highly resolved emission spectra is the differentiation of vibronic origins from combination bands and other features. The approach employed here for the identification of these bands is to draw comparisons between the frequencies of the emission subprogressions possessing large Huang-Rhys factors and those of the intense vibronic origins listed in Table III.

The absorption spectrum of $Mo_2I_4(PMe_3)_4$ is dominated by progressions in ν_1^* built on an intense origin 99 cm^{-1} higher in energy than the electronic origin, which we adopt as the excited state analogue of emission mode *g* (145 cm^{-1}; S = 0.65), and a weaker, broader shoulder 174 cm^{-1} above 0-0. The best-fit Franck-Condon calculation of this spectrum, using only the 99-cm^{-1} and ν_1^* modes and the parameters set out in Table VI, is shown in Figure 24. Because the absorption

Table VI. Parameters for Franck-Condon Calculations of the High-Resolution Absorption Spectra of $Mo_2X_4(PMe_3)_4$ Complexes.[a]

Figure	Compound	Vibrations		S	E_{0-0}[b]	FWHM		
		initial frequency (band)[b]	final frequency (band)[c]			Gaussian	Lorentzian	
24	$Mo_2I_4(PMe_3)_4$	343 (ν_1)	310 (ν_1^*)	2.20	15097	85	(broad)	0
		145 (*g*)	99 (*a*)	1.70		5	(line)	0
25a	$Mo_2Br_4(PMe_3)_4$	172 (*e*)	162 (*b*)	3.60	15962	45		20
		92 (*d*)	80 (*a*)	2.70				
25b	$Mo_2Br_4(PMe_3)_4$	352 (ν_1)	326 (ν_1^*)	2.20	15962	5		0
		172 (*e*)	162 (*b*)	3.60				
		92 (*d*)	80 (*a*)	2.70				

[a]All values except S are in cm^{-1}. [b]Table II. [c]Table III.

Figure 24. Franck-Condon fit to the high-resolution absorption spectrum of $Mo_2I_4(PMe_3)_4$, based on the parameters set out in Table V.

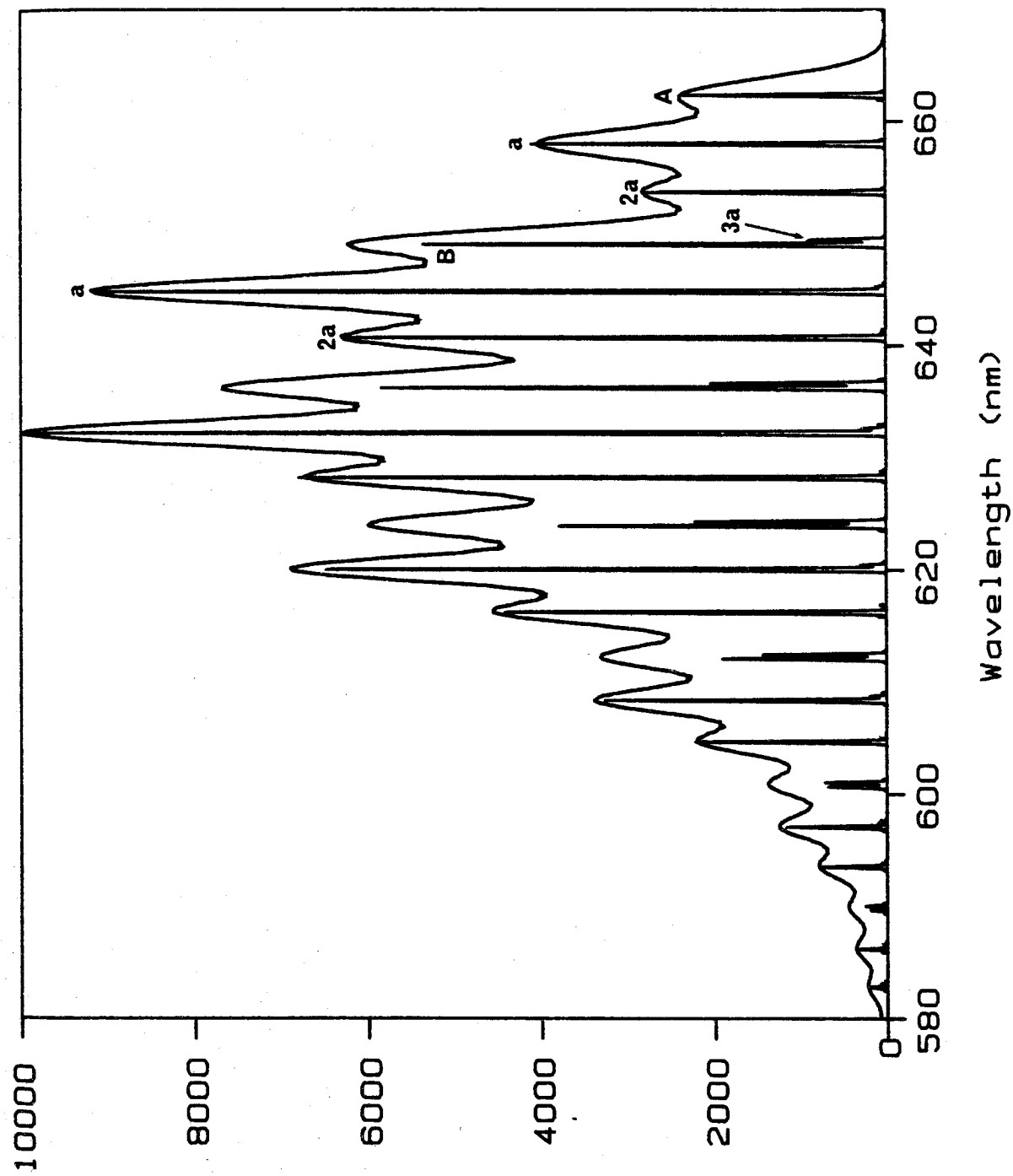
10000
8000
6000
4000
2000
0
580
600
620
640
660
Wavelength (nm)
a
2a
B
a
2a
3a
A

band is not a mirror image of the emission spectrum, it cannot be fit by simply correcting the best-fit emission Huang-Rhys factors for the ground state/excited state frequency differences, as borne out by the fact that S for the 99-cm^{-1} mode is quite a bit larger than that estimated from that of emission mode g.[50] Examining the first cluster of vibronic transitions ($650 < \lambda < 660$ nm) shows that the basic three band pattern of the experimental spectrum is reproduced. Considering the number of Franck-Condon-active modes observed in the emission spectrum of this complex that have been neglected in this calculation, it seems reasonable that the broad 174-cm^{-1} feature of the observed spectrum is composed of the second quantum of the 99-cm^{-1} mode (labeled $2a$ in Figure 24) and these other modes, which, because of the intensity of a, fill in the region between a and $2a$ to a greater extent than that between A and a. Beyond the first cluster of bands, the calculation also correctly simulates the relative intensities of the $B + a$ and $B + 2a$ bands both with respect to each other as well as relative to their counterparts built on A. As seen from the superimposed line spectrum, the intensities of these vibronic transitions are composed of nearly pure a and $2a$ character. In contrast, the calculation cannot reproduce the relative intensities of the first member of the three band pattern starting with band B. Experimentally, this $n\nu_1^*$ progression is observed to lose intensity relative to $n\nu_1^* + a$ and $n\nu_1^* + 2a$ as n increases, while the calculated spectrum indicates the converse to be true. This is due to the fact that this feature is composed not only of the ν_1^* progression built on A ($n\nu_1^*$), but also of $(n - 1)\nu_1^* + 3a$, with the intensity of this latter line overtaking that of the former by 600 nm. If the $(n - 1)\nu_1^* + 3a$ line did not contribute to the intensity of this feature, its intensity, as indicated by the superimposed line spectrum, would be roughly correct. Unfortunately, decreasing the Huang-Rhys factor of this progression to provide this effect destroys what is otherwise a good fit to the $n\nu_1^* + a$ and $n\nu_1^* + 2a$ bands.

Turning now to the absorption spectrum of $Mo_2Br_4(PMe_3)_4$, the problem of identifying the modes is more complicated due to the presence of four strong bands within the region spanned by *A* and *B* in Figure 16. Since all of these are quite a bit more intense than the 0-0 line, and thus would all possess much larger Huang-Rhys factors than any of the non-ν_1 modes observed in emission, it seems reasonable, by analogy to the discussion for $Mo_2I_4(PMe_3)_4$, that the frequency of these modes should be lower in the excited state than the ground state. Absorption features *a* (80 cm^{-1}) and *b* (162 cm^{-1}) are thus reasonable assignments for the excited state analogues of emission modes *d* (91 cm^{-1}) and *e* (172 cm^{-1}), respectively. In keeping with the observation of a lack of mirror symmetry between the two bands, the emission parameters do not adequately fit the absorption spectrum of this complex. Increasing S substantially for both modes to provide a fit to their first quanta built on 0-0 leads to the spectrum shown in Figure 25a. The obvious inconsistency of this calculation with experiment is that the resulting progressions predicted from these Huang-Rhys factors are long, maximizing at 0-8 or 0-9, and extremely intense; scaling up the lower curve in Figure 25a to match intensities with bands *a* and *b* results in the Franck-Condon maximum of the progression built on *A* being roughly three times more intense than band *d''* of the experimental spectrum. Additionally fitting the progression in ν_1^* built on the electronic origin results in the spectrum shown in Figure 25b. Unlike the situation found for $Mo_2I_4(PMe_3)_4$, where Franck-Condon theory was unable to reconcile only one aspect of the observed absorption intensity profile, the calculated spectrum of $Mo_2Br_4(PMe_3)_4$ is a failure that crosses all boundaries. As was noted in the Results section when this spectrum was first discussed, the intensity drops sharply following the ν_1^* progression built on origin *d*; ***Franck-Condon theory simply cannot account for this behavior within the harmonic potential energy surface regime.***

Figure 25. (a) Franck-Condon fit (- - -) to modes *a* and *b* of the high-resolution absorption spectrum of $Mo_2Br_4(PMe_3)_4$ (upper curve), based on the parameters set out in Table V. The lower curve is the full calculated spectrum, with intensity 0.2 times that of the dashed line. (b) Franck-Condon fit to modes *a*, *b*, and ν_1^*, based on the parameters set out in Table V. The position of the 0-0 line (*A*) is indicated.

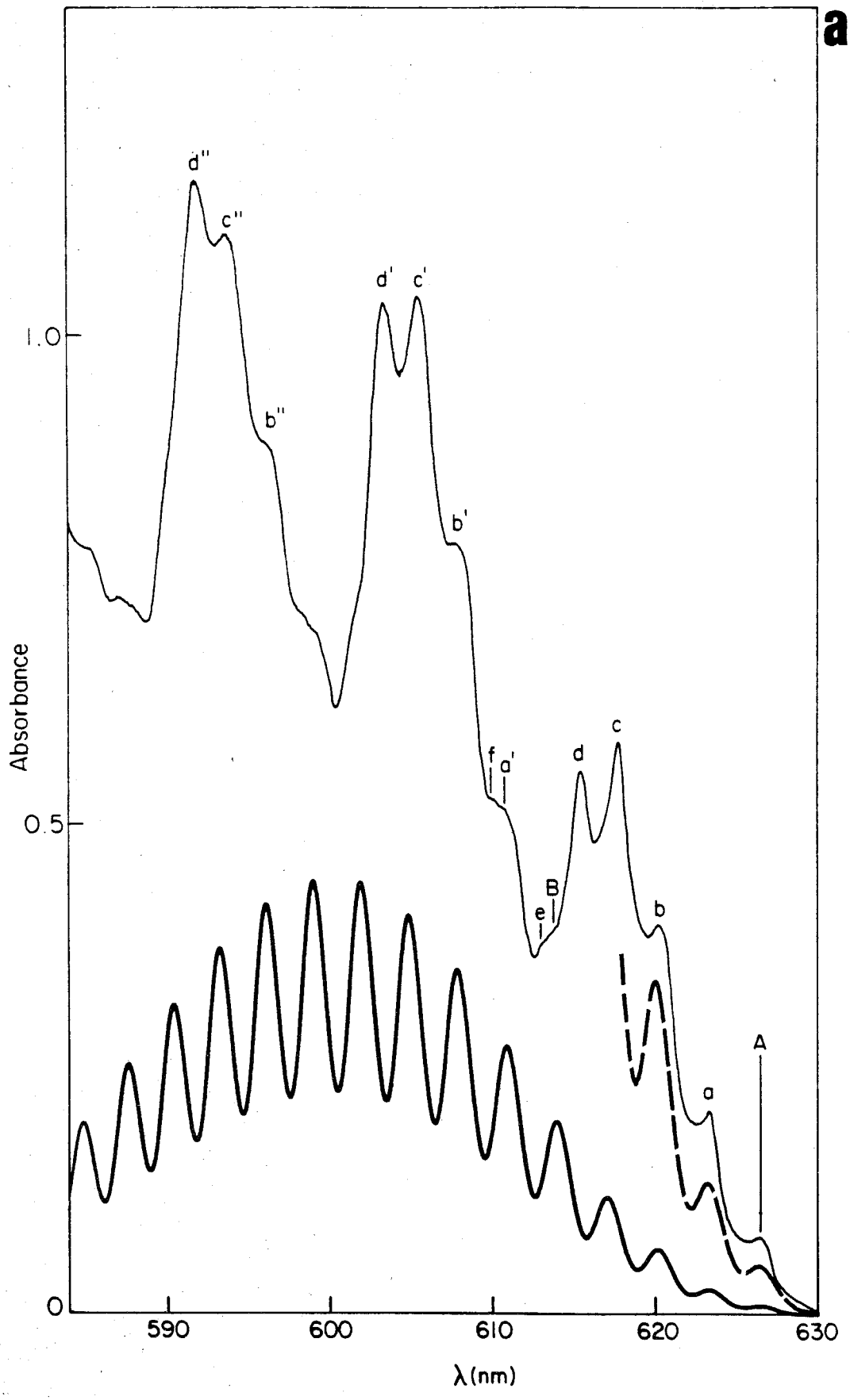
a
d''
c''
b''
d'
c'
b'
f
a'
d
c
B
e
b
a
A
1.0
0.5
0
Absorbance
590
600
610
620
630
λ(nm)

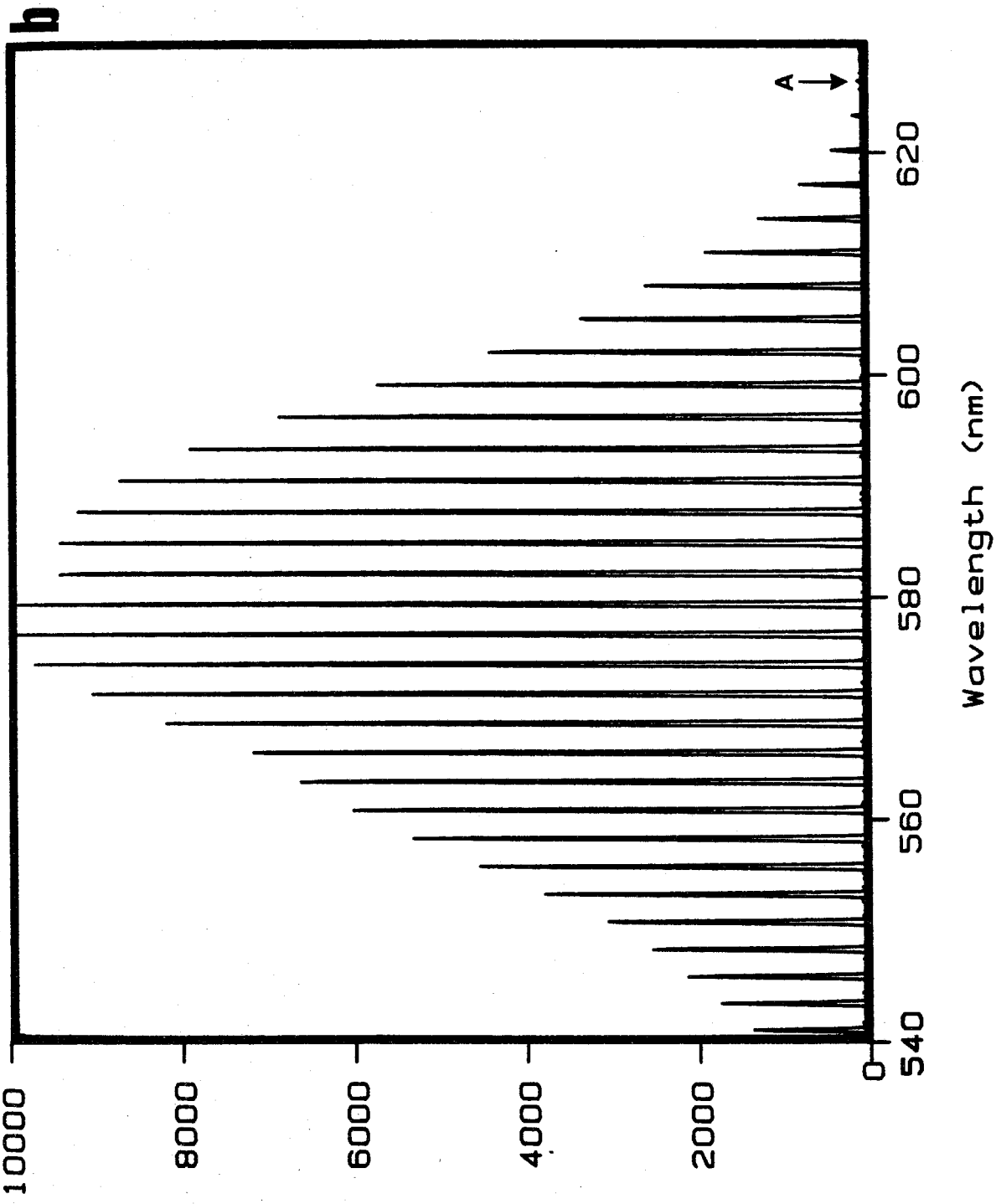
b
A
10000
8000
6000
4000
2000
0
540
560
580
600
620
Wavelength (nm)

If we take *a* and *b* to be the excited state analogues of emission modes *d* and *e*, then absorption bands *c* and *d* must correspond to members of their truncated progressions, even though, as noted, band *c* is slightly weaker than predicted, and band *d* dramatically weaker. The reason that these features were not identified as such when these spectra were presented in the Results section is that their frequencies are in poor agreement with such an assignment. It thus appears that the progressions in *a* and *b* are not only weaker than predicted, but that they also display a marked anharmonicity.

The aspects of the absorption spectrum of $Mo_2Br_4(PMe_3)_4$ that result in its marked deviation from the Franck-Condon regime are greatly magnified in the spectrum of $Mo_2Cl_4(PMe_3)_4$. Given the extremely weak 0-0 line of this complex, it is obvious that its intensity profile is simply unfittable. Despite the failure encountered in the calculation of the absorption spectra of these systems, it should be noted that they display the same qualitative ordering of the Huang-Rhys factors of their subprogressions as was seen for emission, namely $S(X = Cl) > S(Br) > S(I)$, and that this trend parallels the decreasing extent to which Franck-Condon theory breaks down for the $Mo_2X_4(PMe_3)_4$ series.

Assignment of the Vibronic Subprogressions in Absorption and Emission. The Nature of the $^1(\delta\delta^*)$ Potential Energy Surface.

The ability of Franck-Condon theory to fit the high-resolution emission spectra of the $Mo_2X_4(PMe_3)_4$ complexes, and its unequivocal failure to do the same for their absorption spectra, indicates that the potential energy surfaces of the states between which these transitions occur are far more complex than has previously been assumed. The results of these calculations also raise a question that has been avoided until now: Along which normal coordinates, besides ν_1, are these molecules distorting in the $^1(\delta\delta^*)$ excited state? The Huang-Rhys factors for these other

modes are large enough that such distortions are sizeable.

Given the discussion in Chapter II regarding the coupling of the metal-metal stretching mode to other totally symmetric modes, such as metal-ligand stretches and metal-metal-ligand deformations, one might expect some Franck-Condon activity for these modes in the $^1(\delta \rightarrow \delta^*)$ and $^1(\delta^* \rightarrow \delta)$ transitions as a result of the elongation of the metal-metal bond in the $^1(\delta\delta^*)$ state. More specifically, the strong dependence of the energy and intensity of the $^1(\delta \rightarrow \delta^*)$ transition on the nature of the halide ligand suggests that one reasonable candidate would be the symmetric metal-halide stretch, $a_1\nu_2$(MX). It was pointed out earlier in this chapter that there appears to be poor agreement between the emission and resonance Raman spectra, however, and the data presented in Table VII support this assertion. Comparing the frequency of the highest energy intense subprogression in the emission spectra of the $Mo_2X_4(PMe_3)_4$ series with those of $a_1\nu_2$ shows that while the differences are small, they lie outside the uncertainty range defined by the difference in the Raman and emission frequencies of ν_1. The lower frequency emission subprogressions show a similar disagreement with the rR data. In contrast, the frequencies of modes *b*, *c*, *d* of $Mo_2Cl_4(PMe_3)_4$ are in excellent agreement with lines observed in its far-infrared spectrum. The one firm assignment that can be made for these emission modes is that *d* is attributable to the asymmetric analogue of the $a_1\nu_2$ vibration, namely $b_2\nu$(MoCl):

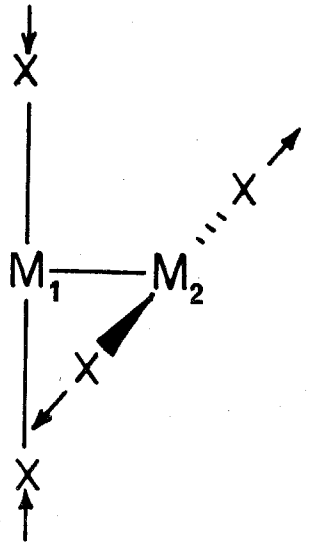

Similar comparisons for $Mo_2Cl_4(AsMe_3)_4$, whose emission spectrum strongly resembles that of $Mo_2Cl_4(PMe_3)_4$, shows that mode *b* again matches up well with an infrared-active band, although the $b_2\nu$(MoCl) mode is 8 cm^{-1} lower than the emission mode *d* for this compound. Given the similarly large difference in frequency between the emission and Raman values of ν_1, it is reasonable that the assignment of *d* as this b_2 mode is correct, with its shift to higher frequency in emission being due to the higher degree of spectral congestion seen for this compound relative to $Mo_2Cl_4(PMe_3)_4$ (*vide supra*). While analogous far-infrared data are not available for $Mo_2Br_4(PMe_3)_4$ and $Mo_2I_4(PMe_3)_4$, it is noted that the frequency of mode *e* of the former compound differs from that of $a_1\nu_2$(MoBr) by roughly the same amount as $b_2\nu$(MoCl) does from $a_1\nu_2$(MoCl), and a similar assignment thus appears to be in order. The frequency of emission mode *g* of $Mo_2I_4(PMe_3)_4$, in contrast, is much higher than that of $a_1\nu_1$(MoI); this discrepancy is probably due to the fact that the coupling between ν_1 and ν_2 increases according to Cl < Br < I, as indicated by the sensitivity of ν_1 to the nature of X. Since the b_2 vibration is not coupled to any mode to the same extent, its frequency difference relative to ν_2 is likely to display a halide dependence.

The assignment of molecular-*z*-polarized nontotally symmetric vibrational modes in the electronic spectra of the $Mo_2X_4L_4$ complexes indicates that the D_{2d} symmetry of the ground state is *not* preserved upon $^1(\delta \rightarrow \delta^*)$ excitation. While such distortions provide a mechanism by which the mirror symmetry relationship between absorption and emission spectra can be violated, this fact by itself does not explain the gross deviations of the absorption spectra of these complexes from Franck-Condon theory, nor does it indicate why the progressions in ν_1 built on the electronic origin are so weak while those in emission are quite strong.

Table VII. Selected Ground-State Vibrational Frequencies from the Emission, Resonance Raman, and Far-Infrared Spectra of $Mo_2X_4L_4$ Complexes.[a]

Complex	Emission[b]		Raman[c]		$\Delta\nu$	Far-IR[b]	
	ν	band	ν	mode		ν	mode
$Mo_2Cl_4(PMe_3)_4$	359	ν_1	355	ν_1	4	285	$b_2\nu$ (MoCl)
	285	*d*	274	ν_2		122	
	124	*c*	234	ν_3		87	
	91	*b*					
$Mo_2Cl_4(AsMe_3)_4$	367	ν_1	356	ν_1	11	288	$b_2\nu$ (MoCl)
	296	*d*	278	ν_2		111	
	115	*c*	217	ν_3		89	
	80	*b*					
$Mo_2Br_4(PMe_3)_4$	358	ν_1	352	ν_1	6		
	215	*f*	235	ν_3			
	172	*e*	159	ν_2			
	92	*d*					
$Mo_2I_4(PMe_3)_4$	347	ν_1	343	ν_1	4		
	145	*g*	248	ν_3			
			105	ν_2			

[a]Frequencies are in cm^{-1}. [b]Table II. [c]Chapter II, Table V.

To recapitulate the findings of the Franck-Condon calculations, the absorption spectra of the $Mo_2X_4(PMe_3)_4$ compounds showed progressions built on the origin that either appeared anomalously weak ($Mo_2I_4(PMe_3)_4$) or were abruptly truncated ($Mo_2Cl_4(PMe_3)_4$, $Mo_2Br_4(PMe_3)_4$) near the position of the first quantum of ν_1^*. In addition, the progressions of the *a* and *b* modes of $Mo_2Br_4(PMe_3)_4$, both of which we have now assigned as nontotally symmetric modes, became quite anharmonic before stopping altogether, some five quanta short of its calculated vibronic maximum. This behavior is not consistent with transitions between harmonic potential energy surfaces of the type depicted in Figure 26, but rather is reminiscent of the situation found near the dissociative limit of an anharmonic potential energy surface. The spacings of the vibronic peaks of a progression decrease rapidly near this limit, and concomitantly loses intensity. Because the $[\sigma^2\pi^4]$ triple-bond core of quadruply bonded dimers remains intact in the $^1(\delta\delta^*)$ state, however, the dissociative limit of its potential energy surface lies tens of thousands of wavenumbers above the lowest vibrational level, whereas the progressions observed within each cluster of vibronic transitions in the $^1(\delta \rightarrow \delta^*)$ bands of the $M_2X_4L_4$ complexes die out within a few hundred wavenumbers of their origins.

The only potential energy surface that provides the correct combination of the bound character of the $^1(\delta\delta^*)$ state, as well as the possibility for spectroscopic behavior similar to that seen near the dissociative limit, is a double well of the type shown in Figure 27. What allows this surface to be invoked in the present case is the presence of nontotally symmetric excited state distortions. The interpretation of this surface from the standpoint of the $b_2\nu(MX)$ mode depicted in the preceding inset is that the left well represents the case in which the halide atoms bonded to M_1 are moving toward the metal and those on M_2 are moving away, while the right well represents the opposite motions of these ligands. The separation of the two minima

Figure 26. Harmonic potential energy surfaces of the δ^2 and $^1(\delta\delta^*)$ states along the metal-metal coordinate.

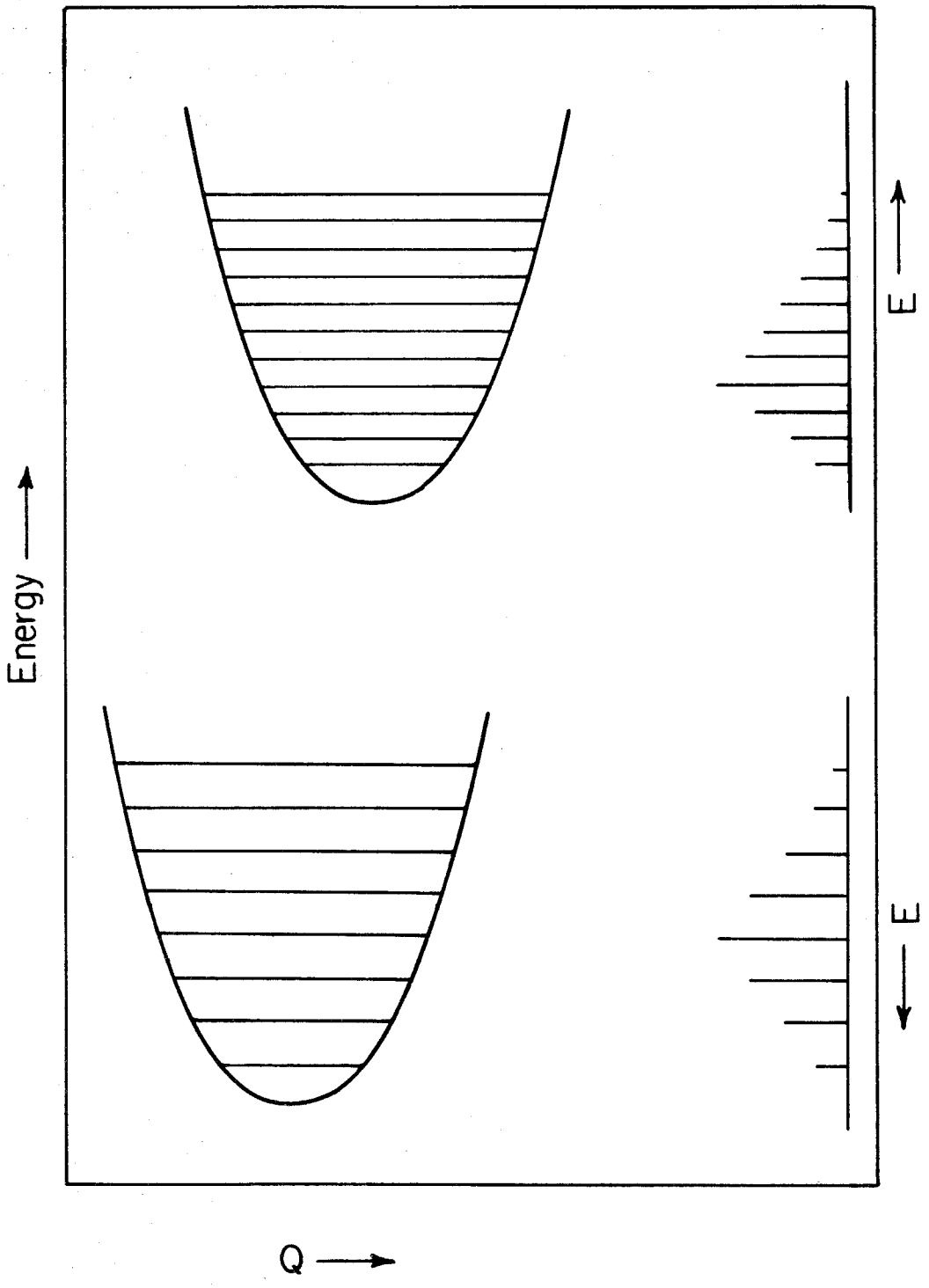
Energy
Q
E
E

Figure 27. Proposed $^1(\delta\delta^*)$ potential energy surface along a nontotally symmetric coordinate.

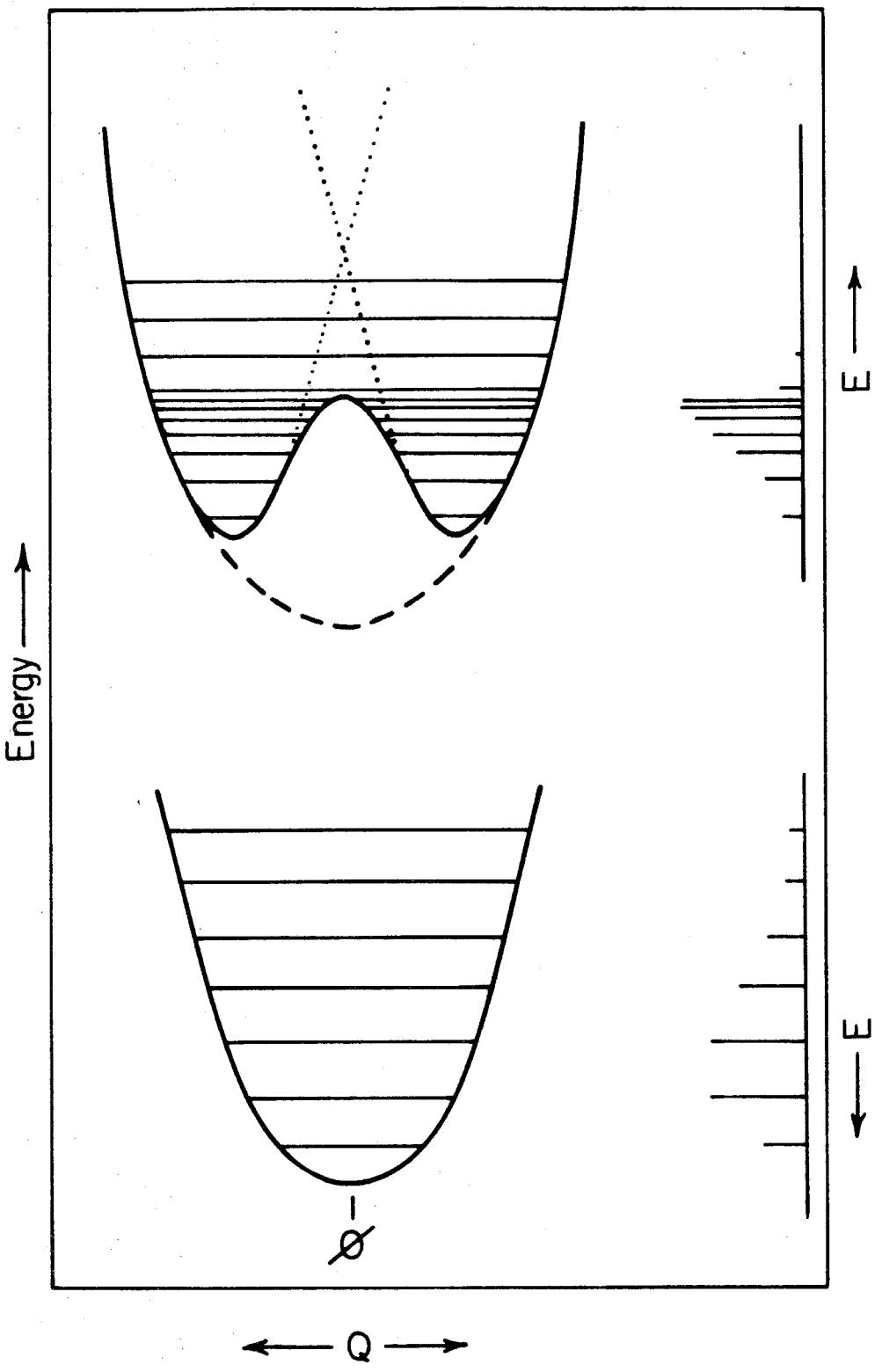
Energy
E
E
Q

along the b_2 coordinate is related to the magnitude of this nontotally symmetric distortion, as measured by the Huang-Rhys factor, while the height of the barrier is a measure of the stabilization of this distorted state relative to that in which the ground state symmetry is preserved. The symmetries of the δ^2 and $^1(\delta\delta^*)$ states in this case are D_{2d} and C_{2v}, respectively; these are entirely consistent with the dipole-allowed character of $^1(\delta \rightarrow \delta^*)$ and $^1(\delta^* \rightarrow \delta)$, as well as the molecular-z-polarization of both bands, since the B_2 symmetry of the $^1(\delta\delta^*)$ state in D_{2d} symmetry converts to A_1 in C_{2v}, with preservation of the unique z axis. It must be emphasized that this potential energy surface is only valid for distortions along such a nontotally symmetric coordinate, and that the surfaces shown in Figure 26 still provide the correct description of this state along symmetric coordinates such as $\nu_1(M_2)$.

The double-well surface invoked for the $^1(\delta\delta^*)$ state adequately accounts for the general spectroscopic behavior of the $M_2X_4L_4$ complexes. For emission, which occurs from the lowest vibrational level of the two upper surface minima, the spectra should resemble that of the harmonic surfaces shown in Figure 26, a fact that is consistent with the spectra of these complexes being entirely amenable to interpretation within the Franck-Condon regime. On the other hand, the absorption spectrum will initially mirror the intensity profile of its emission counterpart, as borne out by the similarity of the origin regions of the emission and single-crystal absorption spectra of $Mo_2Cl_4(PMe_3)_4$ and $Mo_2Br_4(PMe_3)_4$, but the progressions will quickly become anharmonic as the barrier is approached. Above the barrier, the surface along this coordinate will resemble that shown by the dashed line below the two minima. This latter surface is not displaced at all along this coordinate relative to the ground state, resulting in Huang-Rhys factors of zero for the modes associated with it; their vibronic progressions will thus be truncated at the barrier.

For the $Mo_2X_4L_4$ complexes, the energy of this barrier relative to the bottom of the well must be on the order of one quantum of ν_1^*, thus accounting for the extreme weakness of this mode built on the electronic origin. That progressions in ν_1^* built on the higher energy vibronic origins are more intense than that built on 0-0 is consistent with the fact that above the barrier there is no longer a distortion along this nontotally symmetric coordinate, and thus these progressions behave according to the harmonic potential energy surface associated with the metal-metal stretching coordinate.

In addition to accounting for the spectroscopic behavior of the $M_2X_4L_4$ chromophore in a general sense, the double well description of the $^1(\delta\delta^*)$ state also allows for the interpretation of the specific trends observed upon perturbation of the coordination sphere of this class of compounds. It was noted that the Huang-Rhys factor for the now-assigned $b_2\nu$(MoX) vibrations of the spectra of the $Mo_2X_4(PMe_3)_4$ series decreased according to Cl > Br > I, thus indicating an increasingly smaller distortion along this coordinate. This is consistent with the fact that as the halide ligands move toward the metal, as shown in the preceding inset for M_1, they come into closer contact with the bulky trimethylphosphine ligands that they are adjacent to in the *cis*-MX_2L_2 fragment. This steric repulsion is likely to increasingly hinder the extent of distortion with larger halide ligands. The lower double-well barrier that results from this restricted motion would seem to account for the improvement in the fit to the absorption spectrum of $Mo_2I_4(PMe_3)_4$ relative to that of $Mo_2Br_4(PMe_3)_4$ and $Mo_2Cl_4(PMe_3)_4$. That such steric contacts are important in determining the geometries of these complexes is indicated by their structural data, which display increasing Mo-P bond lengths and Mo-Mo-P and Mo-Mo-X bond angles according to Cl < Br < I.

This concept of the excited state geometry being under steric control similarly

allows the intensity profiles of the emission spectra of the $Mo_2Cl_4(PR_3)_4$ (R = Me, Et, n-Pr, n-Bu) series and of $Mo_2Cl_4(AsMe_3)_4$ to be rationalized. Specifically, the band shapes of the isoenergetic $^1(\delta^* \rightarrow \delta)$ transitions of the $Mo_2Cl_4(PR_3)_4$ dimers are quite sensitive to the nature of R, with the Franck-Condon calculations indicating this to be the result of a decrease in the Huang-Rhys factors of the nontotally symmetric subprogressions along the series $PMe_3 \rightarrow PBu^n_3$, while substitution of the ligating atom of the neutral ligand has no such effect on band shape, as seen for $Mo_2Cl_4(PMe_3)_4$ and $Mo_2Cl_4(AsMe_3)_4$. Thus, while the extent of the distortion along $b_2\nu$(MoCl) is nearly equivalent for $Mo_2Cl_4(PMe_3)_4$ and $Mo_2Cl_4(AsMe_3)_4$ because of the similarity of the cone angles of the EMe_3 ligands, it changes as an inverse function of steric bulk for $Mo_2Cl_4(PR_3)_4$ according to $PMe_3 > PEt_3 > PPr^n_3 \sim PBu^n_3$. Finally, the fact that the Huang-Rhys factors for the emission subprogressions of $W_2Cl_4(PMe_3)_4$ are larger than those for the analogous $Mo_2Cl_4L_4$ complexes is presumably a reflection of the longer metal-metal distance in this compound. This expansion along the M-M coordinate results in an increase in the X-M-P bond angles of the MX_2P_2 fragment relative to the molybdenum species, thus allowing greater inward displacements of the halide.

Although the foregoing discussion indicates that the spectroscopic data and the double-well description of the excited state form an internally consistent portrait of the transitions between the $^1(\delta\delta^*)$ state and the ground state, it does not provide an answer to the single most basic question raised by these spectra: Why does the $^1(\delta\delta^*)$ state generate molecular distortions along nontotally symmetric coordinates at all? As was pointed out in the introduction to this thesis and emphasized in subsequent chapters, the $^1(\delta\delta^*)$ state is ionic in nature, in contrast to the covalent $^1(\delta^2)$ and $^3(\delta\delta^*)$ states. One property of such an excited state is that it is potentially subject to the phenomenon of sudden polarization,[51] whereby the two-center

resonance of the excited-state electron pair is disrupted by a nontotally symmetric distortion to yield an asymmetric wavefunction in which the pair is partially or completely localized on one of the two centers, thus generating a net dipole. That prominent progressions in the $b_2\nu(MoX)$ vibration should be displayed by the $^1(\delta \rightarrow \delta^*)$ and $^1(\delta^* \rightarrow \delta)$ transitions of these complexes is entirely consistent with this sudden polarization scenario:

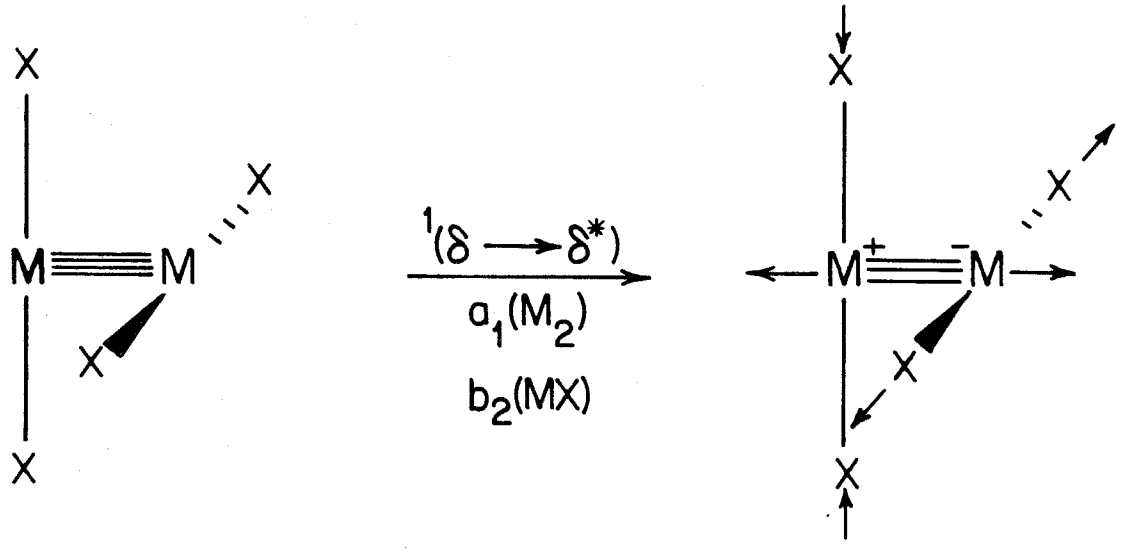

The movement of the electronegative halide ligands toward the left metal center and away from the right one results in the formation, from the M(II)-M(II) ground state, of a polar excited state possessing some M(I)-M(III) character. The fact that the spectroscopic data indicate the barrier to be only a few hundred wavenumbers high suggests that the charge localization on one center is less than total.

In light of our findings for the $M_2X_4L_4$ complexes, we now reconsider, in closing, the interpretation by Huang and Martin[42] of the $^1(\delta \rightarrow \delta^*)$ band of $Re_2Cl_8^{2-}$. The essential details of their conclusions, as well as reproductions of their absorption spectra, were given at the outset of the Discussion section. Central to this reinterpretation is the 5 K emission spectrum of this complex, which is shown in Figure

Figure 28. Emission spectrum of polycrystalline $(TBA)_2Re_2Cl_8$ at ca. 5 K (uncorrected for spectrometer response). The ν_1 and ν_2 progressions, the corrected emission band maximum, and the frequency of the 0-0 line are indicated.

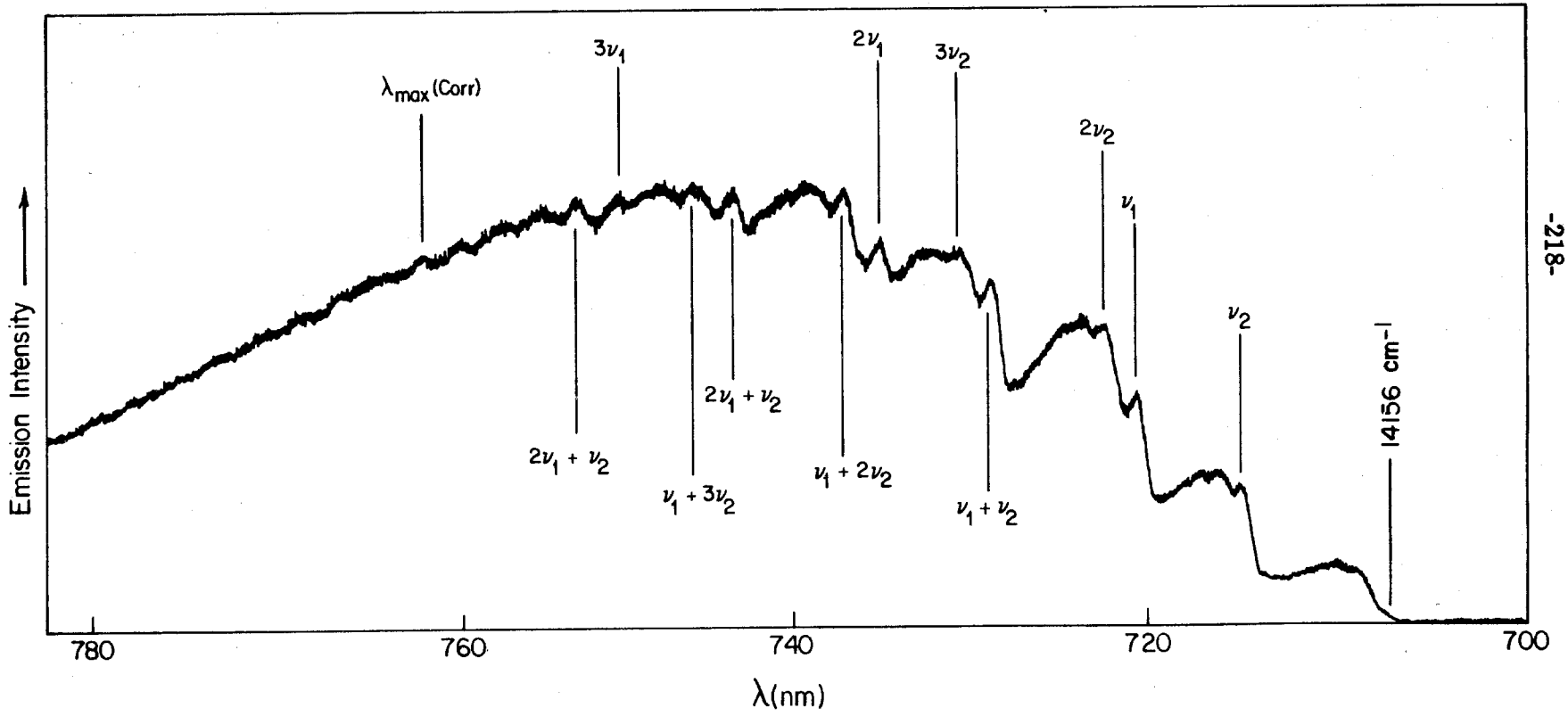
λ_{max}(Corr)
$3\nu_1$
$2\nu_1$
$3\nu_2$
$2\nu_2$
ν_1
ν_2
$2\nu_1 + \nu_2$
$\nu_1 + 3\nu_2$
$2\nu_1 + \nu_2$
$\nu_1 + 2\nu_2$
$\nu_1 + \nu_2$
14156 cm^{-1}
Emission Intensity
780
760
740
720
700
λ(nm)

28. Progressions in three vibrational modes are apparent: a 277-cm^{-1} progression-forming mode, which is assigned as $\nu_1(Re_2)$, a 156-cm^{-1} mode, labeled ν_2 in this figure, and a 25-cm^{-1} phonon mode. There are two strong analogies between this spectrum and the emission spectra of the $M_2X_4L_4$ complexes: first, the positions and intensities of the vibronic transitions within this spectrum can be fit by Franck-Condon calculations (not shown) of the type already outlined in this chapter; and second, the prominent ν_2 mode does not appear in the resonance Raman spectrum of this complex, but rather is in good agreement with an unassigned nontotally symmetric vibration at 154 cm^{-1} in the infrared spectrum of this complex.[52] Comparison of the emission spectrum with the $^1(\delta \rightarrow \delta^*)$ transition reveals that while the two bands are not mirror images, the lowest energy feature in absorption is only 11 cm^{-1} higher than the emission 0-0. Built on this weak origin is a weak cluster of phonon side bands that mirrors that seen in emission, as well as a progression in a 135-cm^{-1} mode, which we take to be the excited state analogue of the ν_2 emission mode. Despite the fact that its Huang-Rhys factor is quite large ($S \sim 3$), this latter progression extends for only two quanta, the second of which is extremely weak. The absorption spectrum of $Re_2Cl_8^{2-}$ thus appears to suffer from the same breakdown of Franck-Condon theory as did those of the $M_2X_4L_4$ complexes.

The close analogies between the spectroscopic behavior detailed in this chapter and that encountered for $Re_2Cl_8^{2-}$ suggest that the sudden polarization description of the $^1(\delta\delta^*)$ state of the $M_2X_4L_4$ complexes, and the double-well potential energy surface that this regime necessitates, are also applicable to the rhenium compound. For this system, it appears that an $a_{2u}\delta(MX_4)$ deformation is a very effective mode for lowering the D_{4h} symmetry of the ground state to C_{4v} in the polar excited state, and we suggest that this is a reasonable assignment for the 156-cm^{-1} emission mode:

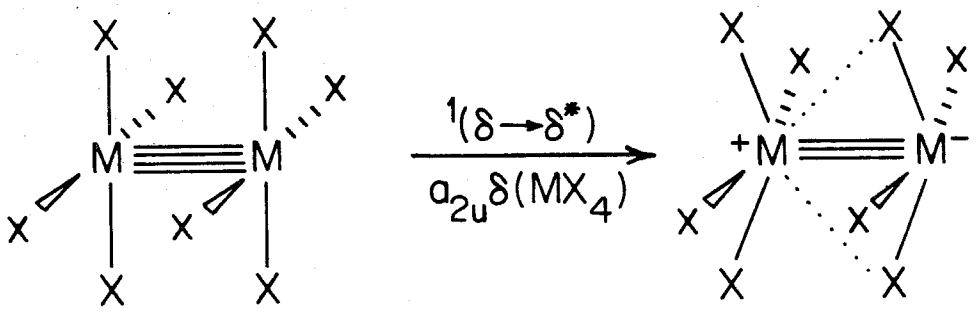

Similar frequency modes were seen for the $Mo_2X_4L_4$ complexes in absorption and emission, *e.g.*, emission modes *b* and *c* of $Mo_2Cl_4(PMe_3)_4$. Unlike the phosphine complexes, a ν(ReCl) mode is not resolved for $Re_2Cl_8^{2-}$ in either its absorption or emission spectrum, although spectral simulations suggest that it may be present but only poorly resolved. Since the $^1(\delta\delta^*)$ potential energy surface of $Re_2Cl_8^{2-}$ does not prevent torsional distortion, as we noted earlier, the excited state distortions are undoubtedly somewhat different from those of the $M_2X_4L_4$ systems.

It would appear that the ionic description of the $^1(\delta\delta^*)$ state detailed here should be general for the quadruple bond class, with the restriction that steric constraints upon distortion may have profound effects upon the extent of excited state charge localization. It is likely that such steric constraints account for the relative simplicity of the vibronic structure in the $^1(\delta \rightarrow \delta^*)$ transitions of ligand-bridged compounds[8] such as $Mo_2(O_2CCH_3)_4$.[53]

References and Notes

1. Cowman, C. D.; Gray, H. B. *J. Am. Chem. Soc.* **1973**, *95*, 8177-8178.
2. Cotton, F. A.; Walton, R. A. "Multiple Bonds Between Metal Atoms"; Wiley: New York, 1982; chapter 8. Trogler, W. C.; Gray, H. B. *Acc. Chem. Res.* **1978**, *11*, 232-239.
3. Sattelberger, A. P.; Fackler, J. P. *J. Am. Chem. Soc.* **1977**, *99*, 1258-1259.
4. Manning, M. C.; Trogler, W. C. *J. Am. Chem. Soc.* **1983**, *105*, 5311-5320.
5. Campbell, F. L., III; Cotton, F. A.; Powell, G. L. *Inorg. Chem.* **1985**, *24*, 177-181.
6. Trogler, W. C.; Solomon, E. I.; Trajberg, I.; Ballhausen, C. J.; Gray, H. B. *Inorg. Chem.* **1977**, *16*, 828-836.
7. Cotton, F. A.; Fanwick, P. E. *J. Am. Chem. Soc.* **1979**, *101*, 5252-5255.
8. Martin, D. S.; Newman, R. A.; Fanwick, P. E. *Inorg. Chem.* **1979**, *18*, 2511-2520.
9. Cotton, F. A. *Chem. Soc. Rev.* **1983**, *12*, 35-51.
10. Yoo, C.-S.; Zink, J. I. *Inorg. Chem.* **1983**, *22*, 2474-2476.
11. Cotton, F. A.; Martin, D. S.; Webb, T. R.; Peters, T. J. *Inorg. Chem.* **1976**, *15*, 1199-1201.
12. A preliminary account of this work has been published: Hopkins, M. D.; Gray, H. B. *J. Am. Chem. Soc.* **1984**, *106*, 2468-2469.
13. Chapter II.
14. Glicksman, H. D.; Hamer, A. D.; Smith, T. J.; Walton, R. A. *Inorg. Chem.* **1975**, *15*, 2205-2209.
15. San Filippo, J., Jr.; Sniadoch, H. J.; Grayson, R. L. *Inorg. Chem.* **1974**, *13*, 2121-2130.

16. Green, M. L. H.; Parkin, G.; Bashkin, J.; Fail, J.; Prout, K. *J. Chem. Soc., Dalton Trans.* **1982**, 2519-2525.

17. Schrock, R. R.; Sturgeoff, L. G.; Sharp, P. R. *Inorg. Chem.* **1983**, *22*, 2801-2806. Sharp, P. R.; Schrock, R. R. *J. Am. Chem. Soc.* **1980**, *102*, 1430-1431.

18. Barder, T. J.; Walton, R. A. *Inorg. Chem.* **1982**, *21*, 2510-2511.

19. Brencic, J. V.; Cotton, F. A. *Inorg. Chem.* **1970**, *9*, 351-353.

20. Luck, R. L.; Morris, R. H. *J. Am. Chem. Soc.* **1984**, *106*, 7978-7979.

21. Rice, S. F.; Gray, H. B. *J. Am. Chem. Soc.* **1983**, *105*, 4571-4575.

22. Parker, C. A.; Rees, W. T. *Analyst* **1960**, *85*, 587-600.

23. Winkler, J. R.; Gray, H. B. *Inorg. Chem.* **1985**, *24*, 346-355.

24. Cotton, F. A.; Extine, M. W.; Felthouse, T. R.; Kolthammer, B. W. S.; Lay, D. G. *J. Am. Chem. Soc.* **1981**, *103*, 4040-4045.

25. Yersin, H.; Otto, H.; Zink, J. I.; Gliemann, G. *J. Am. Chem. Soc.* **1980**, *102*, 951-955.

26. Steinfeld, J. I. "Molecules and Radiation"; MIT Press: Cambridge, Massachusettes, 1974; p. 24.

27. While the coincidence of absorption and emission 0-0 lines would appear to be a fairly routine observation, it has not been so in previous spectroscopic studies of quadruply bonded dimers. Specifically, $^1(\delta \rightarrow \delta^*)/^1(\delta^* \rightarrow \delta)$ 0-0 energy gaps of 600 - 1000 cm^{-1} have been reported for compounds of the $M_2(mhp)_4$ (M = Mo, W) type,[4] while the energy gap between the emission origin line and that of the $^1(\delta \rightarrow \delta^*)$ transition for $K_4Mo_2Cl_8$ is 600 cm^{-1}.[28]

28. Fraser, I. F.; Peacock, R. D. *Chem. Phys. Lett.* **1983**, *98*, 620-623.

29. Spectrum not shown. Hopkins, M. D., unpublished results.

30. Miskowski, V. M.; Goldbeck, R. A.; Kliger, D. S.; Gray, H. B. *Inorg. Chem.* **1979**, *18*, 86-89.

31. Fanwick, P. E.; Martin, D. S.; Cotton, F. A.; Webb, T. R. *Inorg. Chem.* **1977**, *16*, 2103-2106.

32. The previous claim[30] that the absorption and emission spectra of $Mo_2Cl_4(PBu^n_3)_4$ were mirror images, as well as the small differences between the spectrum of this compound presented in Figure 2d and that shown in reference 30, may be the result of experimental difficulties associated with the low-red-sensitivity detector used in the earlier study.

33. Chapter IV. Zietlow, T. C.; Hopkins, M. D.; Gray, H. B. *J. Solid State Chem.* **1985**, *57*, 112-119.

34. The Raman spectrum of $W_2Cl_4(PMe_3)_4$, obtained under nonresonance conditions (λ_{ex} = 530.9 nm; see Chapter II, Figure 6) of a polycrystalline solid at ca. 20 K, displays lines at the following frequencies (cm^{-1}): 122 m, 161 m, 226 w, 261 s ($\nu_1(W_2)$), 270 sh, 288 w, 300 m, 312 w. A value of ν_1 = 260(10) cm^{-1} has been reported for the related $W_2Cl_4(PBu^n_3)_4$ dimer.[17]

35. The crystal structure of $Mo_2I_4(PMe_3)_4$ ($P2_1/c$)[13] places the Mo-Mo axes at angles of 57° to the unique *b* crystal axis; with Z = 4, a factor group analysis predicts that a molecular-*z*-polarized transition should give rise to two electronic transitions polarized parallel and perpendicular to *b*. In contrast, the structures of $Mo_2Cl_4(PMe_3)_4$[24] and $Mo_2Br_4(PMe_3)_4$[13] ($C2/c$) place molecular-*z* rigorously parallel to *b*; a molecular-*z*-polarized excitation yields only one crystal transition that carries any intensity.

36. Cowman, C. D.; Trogler, W. C.; Gray, H. B. *Isr. J. Chem.* **1976/77**, *15*, 308-310.

37. The $\perp$ *z*-polarized $^1(\delta \rightarrow \delta^*)$ spectra of these complexes, as well as polarized single-crystal spectra of their higher energy absorption bands, are presented in Appendix II.

38. The broad, weak features that appear on the low-energy flanks of the assigned 0-0 transitions bay be due to sample inhomogeneities generated by the crystal mounting procedure. These anomalous bands are also present in the $\perp z$-polarized single-crystal spectra.[37]

39. The vibronic peaks are labeled alphabetically according to their spacing from the origin. Transitions corresponding to the same vibrational mode in absorption and emission may thus have different labels.

40. Reference to Table III reveals, in fact, that the spacing of line *B* from the 0-0 line lies well outside the narrow range spanned by those of the progressions built on other origins; its assignment must be regarded as tentative given the low intensity of this feature.

41. Comparable behavior, albeit at lower resolution, is seen for $Mo_2Cl_4(AsMe_3)_4$, the spectrum of which (Figure 13) displays a distinct shoulder adjacent to each broad vibronic transition, but only a smoothly increasing intensity profile near the electronic origin. The spacing of this shoulder from the strong bands ($\sim$93 cm^{-1}) is roughly equal to the average frequency of lines *b* (74 cm^{-1}) and *c* (119 cm^{-1}) of $Mo_2Cl_4(PMe_3)_4$.

42. Huang, H. W.; Martin, D. S. *Inorg. Chem.* **1985**, *24*, 96-101.

43. Clark, R. J. H.; Stewart, B. *Struct. Bonding* **1979**, *36*, 1-80.

44. The term "best fit" implies, in the case of the single-mode calculations only, the calculated spectrum that best simulates the overall appearance of the experimental spectrum with respect to the degree of resolution and the rough intensity pattern of the vibronic transitions. The intensity ratios of the vibronic transitions in these spectra may not be the same as those observed experimentally, however.

45. By "underlying emission intensity" we mean the emission intensity above the

baseline and below the minima between the vibronic transitions, namely that which is formed by the collapse of vibronic fine structure to give an unstructured background; it does not imply that there is a second emission band beneath $^1(\delta^* \rightarrow \delta)$.

46. The noteable exception to this, of course, is the region near the 0-0 line, which is self-absorbed.

47. It is for this reason that no attempt will be made to fit the extremely complex emission spectrum of $W_2Cl_4(PMe_3)_4$, although we contend that our conclusions for the molybdenum complexes also apply to this species.

48. Whereas the background emission intensity of $Mo_2I_4(PMe_3)_4$ could be deconvoluted in order to obtain estimates of Huang-Rhys factors, the degree of spectral congestion for $Mo_2Br_4(PMe_3)_4$ and $Mo_2Cl_4(PMe_3)_4$ make this procedure prohibitive in these cases. This will generally result in the overestimation of S for high-frequency modes, specifically ν_1, while those of the subprogressions are fairly accurate for all complexes.

49. The similarity of the emission spectra of $Mo_2Cl_4(PMe_3)_4$ and $Mo_2Cl_4(AsMe_3)_4$ makes the following discussion equally applicable to the latter compound.

50. $S_{abs}/S_{em} = \nu_{g.s.}/\nu_{e.s.}$

51. Chapter I. Benard, M.; Veillard, A. *Chem. Phys. Lett.* **1982**, *90*, 160-165.

52. Clark, R. J. H.; Stead, M. J. *Inorg. Chem.* **1983**, *22*, 1214-1220. Bratton, W. K.; Cotton, F. A.; Debeau, M.; Walton, R. A. *J. Coord. Chem.* **1971**, *1*, 121-131.

53. The medium dependence of the spectroscopic properties of $Mo_2Cl_4(PMe_3)_4$ is interesting in light of the sudden polarization invoked here. Specifically, it was noted in Chapter IV that the $^1(\delta \rightarrow \delta^*)$ and $^1(\delta^* \rightarrow \delta)$ bands of $Mo_2Cl_4(PMe_3)_4$ shifted in opposite directions as a function of solvent polar-

ity, with the Stokes shift increasing with increasing polarity. This shift of the Franck-Condon maximum is consistent with an increase in the Huang-Rhys factors of one or more vibronically active modes. One reasonable explanation of this phenomenon is polar solvents contribute to the stabilization of the sudden polarized excited state; the Huang-Rhys factors for the nontotally symmetric modes would increase, yielding more intense progressions and a shifted band maximum. It is not clear how such enhanced stabilization would increase the rate of nonradiative decay, however, since all complexes of the $Mo_2Cl_4(PR_3)_4$ type display the same low temperature lifetime, regardless of ligand or medium.

CHAPTER VI

Reactivity of the $^1(\delta\delta^*)$ State

Introduction

Many oxidation-reduction reactions of central importance in chemistry and biology involve the transfer of two or more electrons. The long-standing interest of this research group in polynuclear transition metal clusters as photoredox catalysts was initially motivated by the fact that these systems provide both the multielectron source and the available metal binding sites to facilitate such transformations.[1-4] We have demonstrated the ability of several classes of metal clusters to undergo photoinduced two-electron transfers, resulting, for example, in the production of molecular hydrogen from protons,[3,4] or in the oxidative addition of an activated organic substrate to the dimetal unit.[5,6] In the cases we have scrutinized most closely, however, the mechanism by which these reactions occur involves either two consecutive electron transfer events, the first of which takes place from the electronically excited cluster and the second from a one-electron oxidized derivative of the cluster ground state,[6] or atom abstraction.[7] While such mechanisms are suitable for carrying out a number of useful multielectron redox reactions, there are other important processes, such as proton-transfer or the oxidative addition of unsaturated organic molecules, which could require a concerted two-electron change.

The relatively long lifetimes of the $^1(\delta\delta^*)$ states of many complexes of the $M_2X_4L_4$ type in fluid solution[8] suggest that these species should be capable of participating in bimolecular photochemical electron-transfer reactions. While one potential mode of reactivity involves simple one-electron-transfer quenching of this excited state, as has been shown previously for $Re_2Cl_8^{2-}$,[9] a novel mechanistic course with implications for concerted two-electron transfer can be envisioned upon consideration of the ionic character of the $^1(\delta\delta^*)$ state:

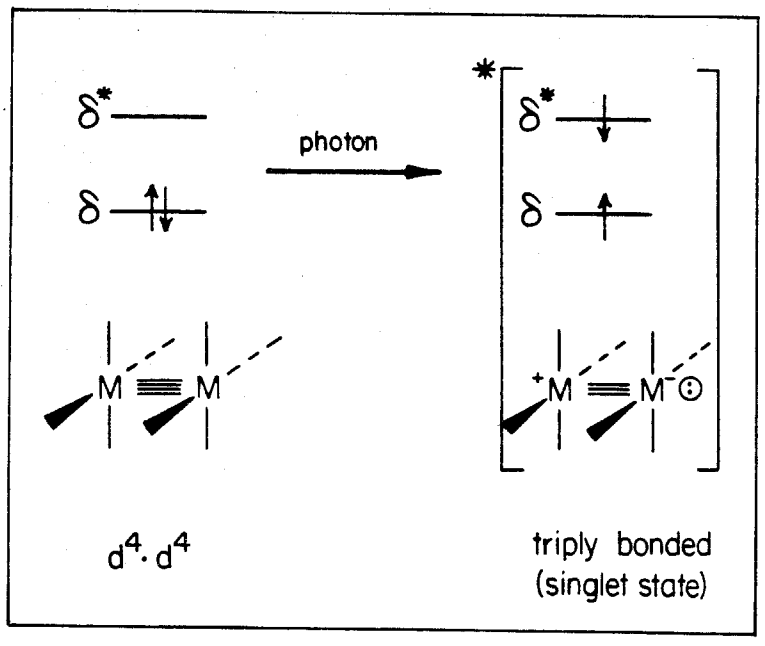

Viewed from the standpoint of chemical reactivity, the sudden polarization of the $^1(\delta\delta^*)$ state generates a highly localized, conjugate Lewis acid-base pair, potentially suitable for interaction with nucleophiles and electrophiles, respectively. One might intuitively expect that the reactivity of this excited state acid-base pair should be enhanced relative to its ground state counterpart, namely the LUMO-HOMO pair, by some factor proportional to the $^1(\delta \rightarrow \delta^*)$ transition energy. Our interest in the excited state electron transfer reactions of metal clusters led us to investigate this avenue of photochemical reactivity for the $M_2X_4L_4$ dimers. The results of this study are reported herein.

Experimental Section

Materials.

Benzene and tetrahydrofuran (Burdick & Jackson) were dried by standard

methods, degassed with a minimum of five freeze-pump-thaw cycles on a high-vacuum manifold (limiting pressure $< 10^{-3}$ torr), and stored under vacuum with sodium metal/benzophenone. Immediately prior to use, dimethylacetylenedicarboxylate (Aldrich) was vacuum distilled and degassed with five freeze-pump-thaw cycles, and hydrogen chloride (Matheson) was degassed with three freeze-pump-thaw cycles and passed through a -20°C trap to remove water. All other chemicals were of reagent grade or comparable quality and were used as received. The complexes $Mo_2X_4(PMe_3)_4$ (X = Cl, Br),[10] $Mo_2Cl_4(PR_3)_4$ (R = Et, n-Pr, n-Bu),[11] and $W_2Cl_4(PBu^n_3)_4$[12] were prepared according to existing procedures; satisfactory carbon and hydrogen elemental analyses were obtained for each.

Electrochemical Measurements.

Cyclic voltammograms were obtained with a Princeton Applied Research model 175 universal programmer and a model 173 potentiostat/galvanostat, with glassy carbon working, Ag-wire auxiliary, and saturated calomel (SCE) reference electrodes. Measurements were made of deoxygenated dichloromethane solutions (0.1 M n-Bu_4NPF_6) contained in a standard H-cell.

Photolysis Experiments.

Time-course photolysis experiments were performed on solutions prepared on a vacuum line in a vessel consisting of a 10 mL round bottom flask, a 1 cm pathlength quartz spectral cell, and a teflon high-vacuum stopcock. Solvent was bulb-to-bulb distilled into the evacuated cell from the appropriate storage flask, followed, in the dark, by the addition of substrate by bulb-to-bulb distillation. A 1000 W high-pressure Hg/Xe lamp equipped with Corning cut-off filters was employed as the light source in these experiments. Spectrophotometric monitoring of both photolysis and thermal-blank experiments was performed with a Hewlett-Packard 8450A spectrometer.

The compound $(Me_3PH)_3[Mo_2(\mu\text{-}H)Cl_8]$ was prepared photochemically by the following method. A septum-stoppered Schlenk tube charged with $Mo_2Cl_4(PMe_3)_4$ (0.12 g) was purged with argon, and 75 mL of dry, deoxygenated benzene was added *via* cannula. The resulting dark blue-red dichroic solution was purged with argon for 20 min, followed by hydrogen chloride for 3 min. The flask was placed in a part of the room that was partially shielded from the overhead fluorescent lamps and left undisturbed for 5 d, at which point the solution was pale blue and the flask contained a large amount of a microcrystalline orange-brown precipitate. The contents of the flask were filtered in air (*caution*: this should be performed in a fume hood due to the liberation of one equivalent of PMe_3 in the course of the photoreaction and the presence of residual HCl), and the solid washed with benzene (to remove unreacted $Mo_2Cl_4(PMe_3)_4$), hexane, benzene again, and *i*-propanol, and dried *in vacuo*. Anal. Calcd. (found) for $C_9H_{31}P_3Cl_8Mo_2$: C, 15.27 (15.41); H, 4.41 (4.10).

Results and Discussion

One-electron Redox Chemistry of the $^1(\delta\delta^*)$ State.

Following the observation of electron-transfer quenching of the emissive excited state of $Ru(bpy)_3^{2+}$ by Gafney and Adamson in 1972,[13] the ability of the luminescent excited states of transition metal complexes to act as more potent oxidants and reductants than their ground states has been extensively documented. Much of this interest has been fueled by the potential use of such systems as photochemical sensitizers in solar energy storage schemes, *e.g.*, the photodissociation of water with visible light; the aforementioned ruthenium complex has been referred to in this regard as "an inorganic substitute for chlorophyll-*a* in *in vitro* photosynthesis."[14]

Less alchemically oriented studies in this area have been directed toward the activation of organic substrates through photoinduced oxidative addition,[6,7b] while along theoretical lines the investigation of the kinetics of excited state electron-transfer processes has played a prominent role.[15]

It has previously been demonstrated that d^4-d^4 complexes of the $M_2X_4L_4$ type can undergo reversible one-electron oxidations (d^3-d^4) and reductions (d^5-d^4) at electrodes.[12,16,17] From these measurements and the spectroscopic results detailed in Chapter V, the one-electron redox potentials of the $^1(\delta\delta^*)$ states of these systems can be estimated (Table I), as shown schematically in the following diagram (electrode potential *vs.* SCE in tetrahydrofuran solution):

Modified Latimer Diagram
of $Mo_2Cl_4(PMe_3)_4$

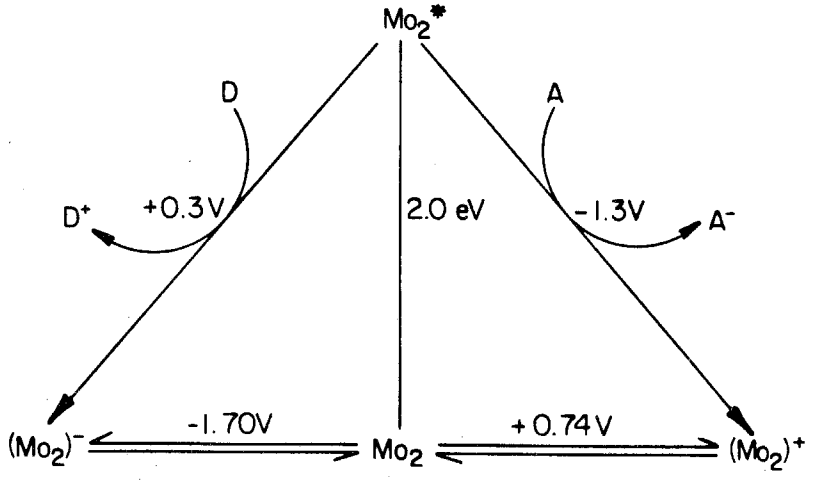

Because of the sensitivity of the redox couples of these complexes to both the nature of the metal and of ligands X and L, a wide variety of photochemical electron-transfer reagents are available within the $M_2X_4L_4$ class ranging from very powerful

Table I. Ground State and Excited State Redox Potentials of $M_2X_4L_4$ Dimers.[a]

Compound	δ^2			$^1(\delta\delta^*)$			
	$E_{\frac{1}{2}}$(ox)[b] THF	$E_{\frac{1}{2}}$(ox)[c] CH_2Cl_2	$E_{\frac{1}{2}}$(red)[b] THF	E_{0-0}[d] (eV)	$E_{\frac{1}{2}}$(ox) THF	$E_{\frac{1}{2}}$(ox) CH_2Cl_2	$E_{\frac{1}{2}}$(red) THF
$Mo_2Cl_4(PMe_3)_4$	+0.74	+0.47	-1.70	2.01	-1.27	-1.54	+0.31
$Mo_2Cl_4(PEt_3)_4$	+0.67	+0.35	-1.81	f	-1.34	-1.66	+0.20
$Mo_2Cl_4(PPr^n_3)_4$	+0.65	+0.38	-1.89	f	-1.36	-1.63	+0.12
$Mo_2Cl_4(PBu^n_3)_4$	+0.65	+0.31	-2.00	f	-1.36	-1.70	+0.01
$Mo_2Cl_4(AsMe_3)_4$	----	----	-1.60	2.06	----	----	+0.46
$Mo_2Br_4(PMe_3)_4$	+0.87	+0.59	-1.48	1.98	-1.11	-1.39	+0.50
$Mo_2Br_4(PEt_3)_4$	+0.76[e]	----	-1.59[e]	f	-1.22	----	+0.39
$Mo_2I_4(PMe_3)_4$	+0.88	----	-1.28	1.87	-0.99	----	+0.59
$W_2Cl_4(PMe_3)_4$	+0.15	----	-1.93	1.77	-1.62	----	-0.16
$W_2Cl_4(PBu^n_3)_4$	+0.04[g]	-0.32	-2.16[g]	f	-1.73	-2.09	-0.39

[a]All potentials are referenced to the saturated calomel electrode at 25°C (0.1 M $(n\text{-}C_4H_9)_4N[PF_6]$), except as noted. [b]Ref. 17. [c]This work. [d]Chapter V. [e]Recorded at 0°C. [f]Assumed to be identical to congener listed above. [g]Ref. 12.

reductants ($E^{*/+} \sim$ -2.1 V) to moderate oxidants ($E^{*/-} \sim$ +0.6 V). Although no attempt was made in this study to utilize these properties for either carrying out photochemical transformations of substrates or evaluating the driving-force dependence of electron-transfer kinetics, these systems are clearly of potential interest in both of these regards and merit further study.[18]

Two-electron Redox Chemistry of the $^1(\delta\delta^*)$ State. Excited State Acid-Base Chemistry.

Although quadruply metal-metal bonded dimers have been used previously as photoredox agents, these reactions involved either short-wavelength (UV) photolysis,[5,19,20] resulting in a mononuclear or other high energy intermediate,[21] or utilization of the enhanced one-electron redox chemistry of the $^1(\delta\delta^*)$ excited state.[9] Because of the facility with which these processes can occur, experiments designed to exploit the ionic nature of the $^1(\delta\delta^*)$ state for concerted two-electron transfer must include conditions in which these potentially competing side reactions would be highly unfavorable. This is desirable not only from the standpoint of simplifying product distributions, but also for the purpose of mechanistic interpretation.

The introduction of hydrogen chloride to a degassed benzene solution of $Mo_2Cl_4(PMe_3)_4$ results in an immediate, visible diminution of the intense red luminescence normally observable from this species. While such solutions are stable in the absence of light for a period of greater than one month, irradiation within the $^1(\delta \rightarrow \delta^*)$ absorption envelope of $Mo_2Cl_4(PMe_3)_4$ ($\lambda_{ex} > 525$ nm) rapidly produces the spectral changes displayed in Figure 1. For solutions that are relatively dilute in $Mo_2Cl_4(PMe_3)_4$, such as the one shown here (65 μM), isosbestic behavior (λ = 524, 644 nm) is maintained up to virtually quantitative conversion. The same spectral changes are also initially seen for more concentrated solutions, but this is followed by the loss, at higher conversion levels, of isosbestic points in the spectrum

Figure 1. Electronic absorption spectral changes during irradiation ($\lambda_{ex} > 525$ nm) of $Mo_2Cl_4(PMe_3)_4$ in C_6H_6/HCl (1 atm) solution at room temperature.

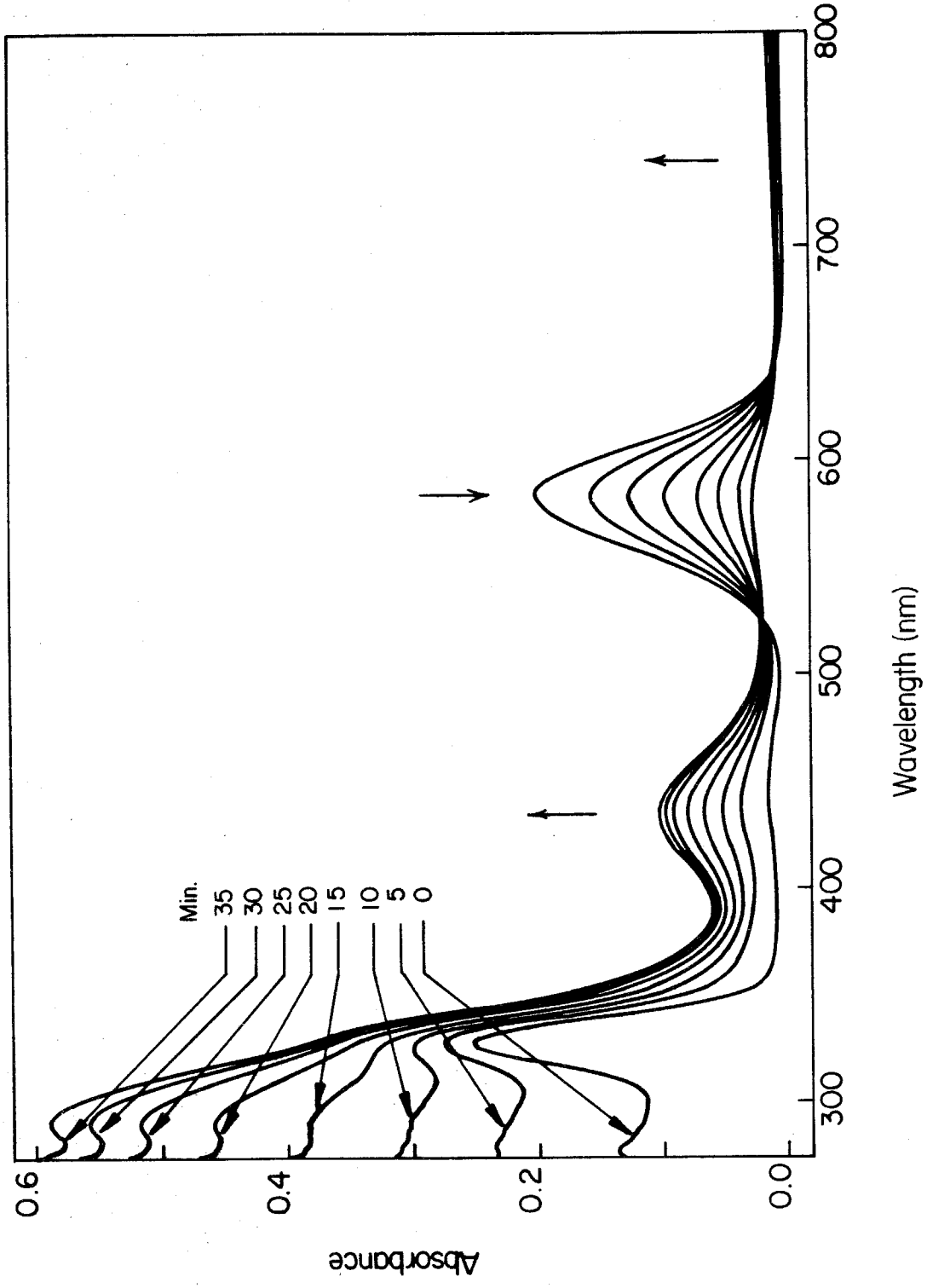
Min.
35
30
25
20
15
10
5
0
0.6
0.4
0.2
0.0
Absorbance
300
400
500
600
700
800
Wavelength (nm)

and the concomitant production of an orange-brown precipitate. Crystals of this material grown slowly by irradiation in indirect room light of a 2.5 mM solution of $Mo_2Cl_4(PMe_3)_4$ in HCl-saturated benzene analyzed for the two-electron-oxidized, Mo_2(III,III) species $(Me_3PH)_3[Mo_2(\mu\text{-}H)Cl_8]$. The absorption spectrum of this material in acetonitrile solution is very similar to that of the photoproduct shown in Figure 1, and is also in excellent agreement with that reported for the Et_3PH^+ [22] and Rb^+ [20] salts of this compound.

The overall stoichiometry of the reaction described above is:

$$Mo_2Cl_4(PMe_3)_4 + 4HCl \rightarrow (Me_3PH)_3[Mo_2(\mu\text{-}H)Cl_8] + PMe_3$$

Given the number of bonds that are made and broken during the course of this reaction, it seems quite reasonable that the final product is derived from some relatively thermally unstable intermediate that is produced in the initial excited state quenching reaction. Mechanistic considerations of the photochemical portion of this pathway from both the standpoint of the potential reactivity of the substrate and the nature of the excited state are inconsistent with any previously reported quenching scheme. Specifically, neither homolytic cleavage of the H-Cl bond nor outer-sphere one-electron reduction are energetically feasible processes for hydrogen chloride under these conditions. Furthermore, population of the $^1(\delta\delta^*)$ state does not result in the labilization of metal-ligand bonds, thus ruling out the possibility of photosubstitution. Instead, the quenching of the $^1(\delta\delta^*)$ state of $Mo_2Cl_4(PMe_3)_4$ by HCl appears to be associated with the acid-base character of both the excited state and the substrate. Shown in Figure 2 are two quenching pathways that lead to viable products of the photochemical step of the overall reaction. Both of these potential quenching processes are unprecedented for transition metal complexes in that they involve excited state proton-transfer directly at a basic metal center, and thus are formally concerted two-electron oxidation reactions.[23,26] The funda-

Figure 2. Possible proton transfer mechanisms for the quenching of the $^1(\delta\delta^*)$ excited state of $Mo_2Cl_4(PMe_3)_4$ by HCl.

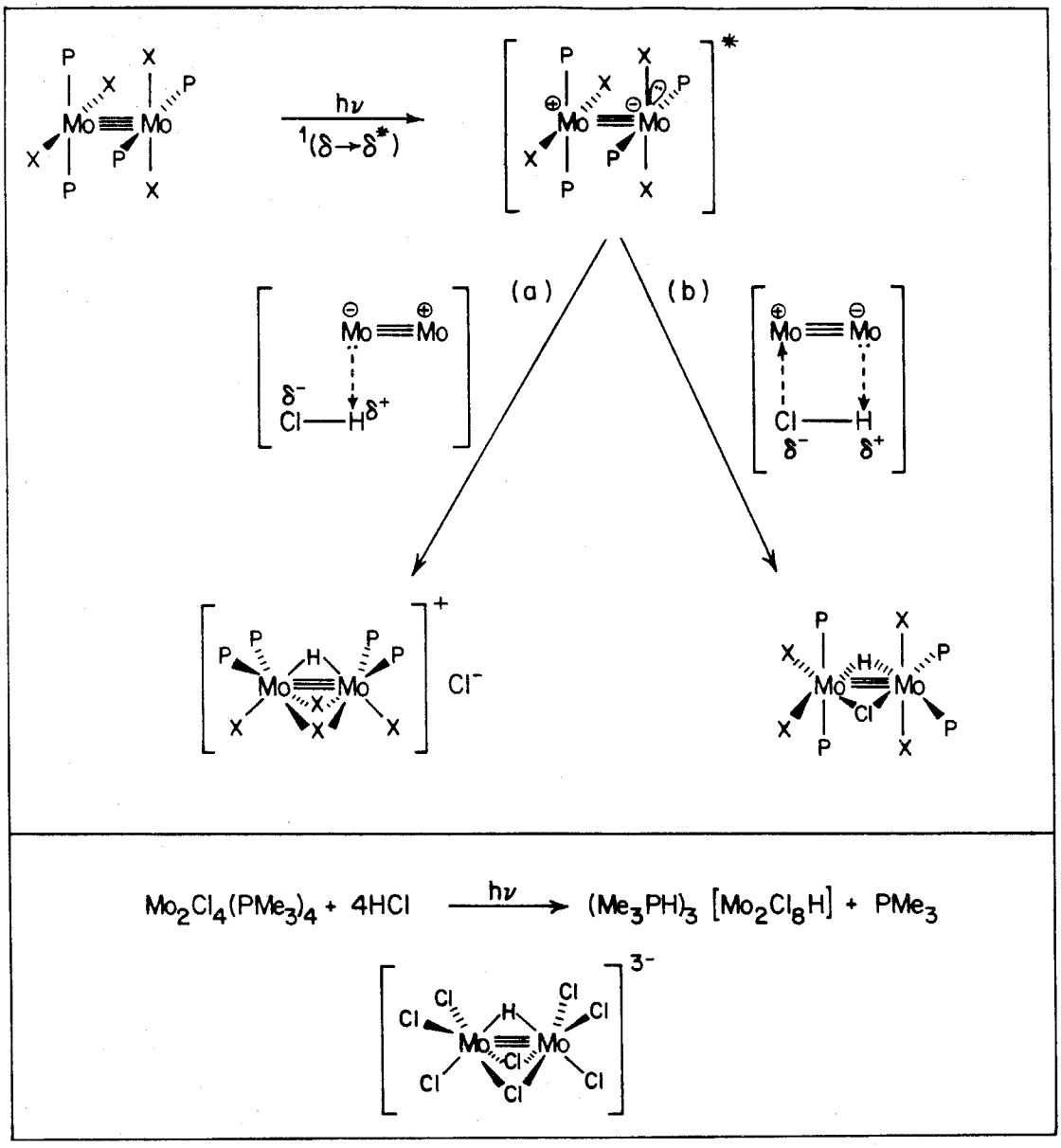

$$Mo_2Cl_4(PMe_3)_4 + 4HCl \xrightarrow{h\nu} (Me_3PH)_3\,[Mo_2Cl_8H] + PMe_3$$

mental difference between the two processes is that reaction *b* may be additionally driven by the electrophilicity of the conjugate Lewis acid site of the dimetal unit. Although no attempt was made to experimentally determine the more plausible of these mechanisms through the correlation of emission quenching rates with the nucleophilicity of the conjugate base X^- (*e.g.*, $k_q(HCl)$ *vs.* $k_q(HO_3SCF_3)$), comparisons of this two-electron oxidation chemistry to the excited state one-electron redox potentials of $Mo_2Cl_4(PMe_3)_4$ suggest that the $^1(\delta\delta^*)$ state of this species is likely to be a more powerful Lewis base than acid, since, at a crude level of approximation, pK_b^* and pK_a^* should roughly scale with $E^{*/+}$ (-1.3 V) and $E^{*/-}$ (+0.3 V) (Table I), respectively. The addition of weakly basic Cl^- to the relatively weak Lewis acid site of the dimetal unit, as shown in pathway *b*, is thus probably less thermodynamically favored than proton addition to the photogenerated lone pair. Steric considerations also point to the primacy of proton transfer in the quenching process. As is illustrated in Figure 3, access to the redox-active orbitals (*i.e.*, those of δ-symmetry) of dimers of this type is strongly hindered for all but the smallest of substrates; a photoinduced pericyclic oxidative addition of the type depicted in reaction *b* would have a very sizeable kinetic barrier relative to reaction *a*. Taken together, these arguments strongly support the notion that the Mo-H bond found in the final product of this reaction is formed by the interaction of the $^1(\delta\delta^*)$ state with a proton in an acid-base fashion.

An important question in transition metal photochemistry, particularly with respect to energy storage, and one that will be briefly considered in closing for the reaction of $Mo_2Cl_4(PMe_3)_4$ with HCl, is whether the enhanced reactivity of an excited state relative to that of the ground state for a given transformation is the result of a lowering of the thermodynamic barrier along the reaction coordinate, or instead the kinetic barrier. While this is difficult to ascertain for the photochem-

Figure 3. Space-filling model of $Mo_2Br_4(PMe_3)_4$, drawn by ORTEP (see Chapter II, Figure 1), showing the covalent radii of all atoms.

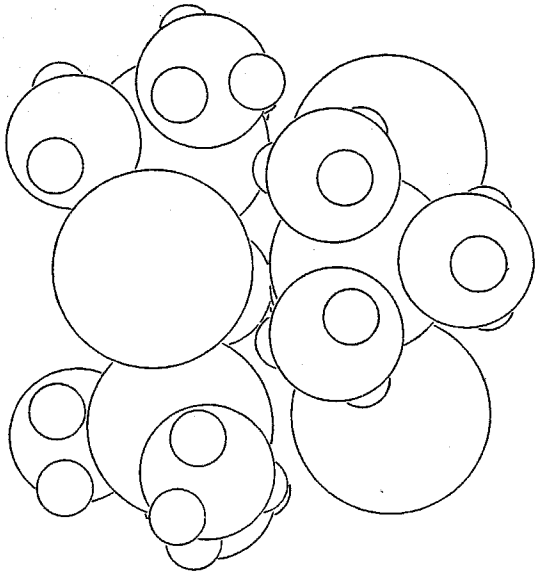

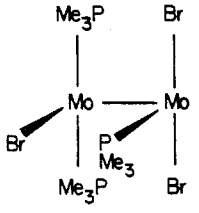
Me3P
Br
Mo
Mo
Br
P
Me3
Me3P
Br

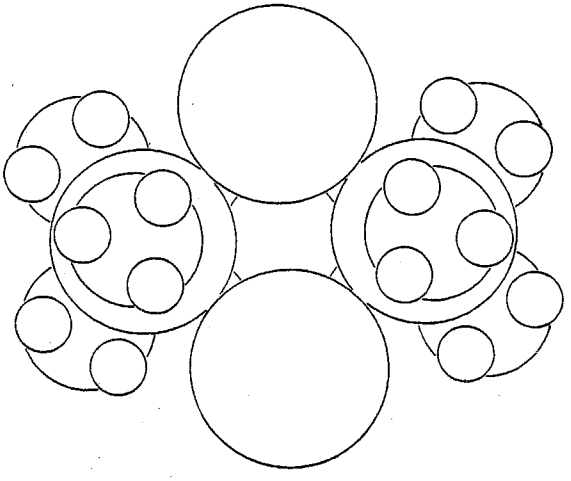

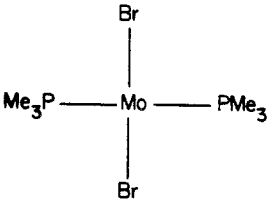
Br
Me3P
Mo
PMe3
Br

ical step of this reaction since the properties of the thermally unstable product, *viz.* $[Mo_2(\mu\text{-}H)Cl_4(PMe_3)_4]^+$, are largely unknown,[27] one experiment relevant to determining the stability of this species relative to that of $Mo_2Cl_4(PMe_3)_4$ was performed. Addition of tetrahydrofuran at room temperature to a solid containing a relatively high percentage of the product of the photoreaction resulted in the production of $Mo_2Cl_4(PMe_3)_4$ and HCl,[28] as summarized below:

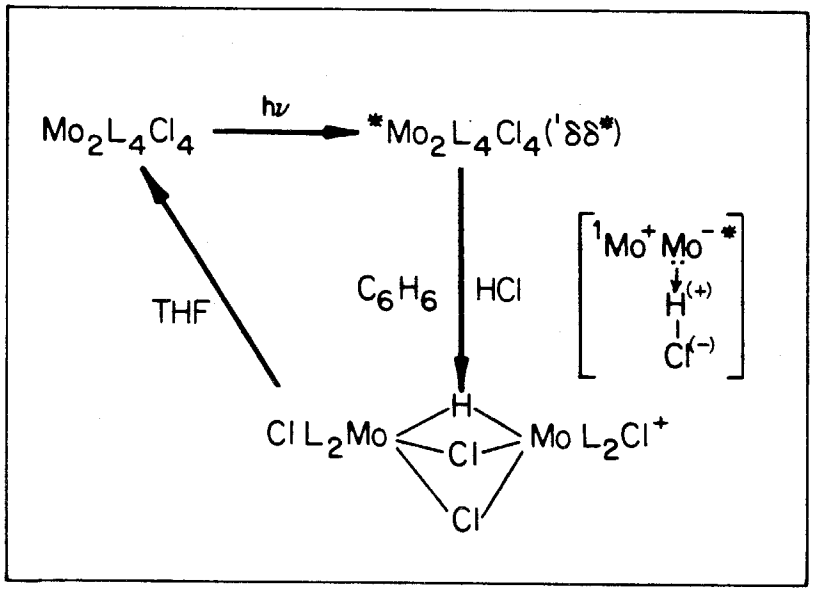

The fact that the reductive deprotonation of the Mo_2(III,III)-hydride complex occurs with such facility with as weak a base as THF may indicate that the photoproduct possesses considerable kinetic stability relative to $Mo_2Cl_4(PMe_3)_4$ and HCl in benzene, and thus that population of the $^1(\delta\delta^*)$ state drives a reaction that is thermodynamically uphill for the the ground state. While an alternative, and much less interesting, explanation for this back-reaction lies in the more favorable heat of solvation of HCl in tetrahydrofuran relative to benzene, consideration of the geometry of the $^1(\delta\delta^*)$ state is not intuitively inconsistent with the former possibility. Specifically, the geometric distortions that occur in the $^1(\delta\delta^*)$ state do not relieve the high degree of steric congestion possessed by the the ground state

structure,[31] and thus the photochemical pathway does not, from this standpoint, lower the kinetic barrier to reaction. Needless to say, elucidation of the finer details of the thermodynamics of the acid-base photochemistry of these systems will require much additional study.

References and Notes

1. Nocera, D. G.; Maverick, A. W.; Winkler, J. R.; Che, C.-M.; Gray, H. B. *A. C. S. Symp. Ser.* **1983**, *211*, 21-33.
2. Maverick, A. W.; Che, C.-M.; Nocera, D. G.; Winkler, J. R.; Gray, H. B. *Plenary Lectures 4th Intl. Conf. Photochem. Conv. and Stor. of Solar Energy, Israel* **1982**.
3. Gray, H. B.; Maverick, A. W. *Science* **1981**, *214*, 1201-1205.
4. Maverick, A. W.; Gray, H. B. *Pure Appl. Chem.* **1980**, *52*, 2339-2348.
5. Trogler, W. C.; Gray, H. B. *Nouv. J. Chim.* **1977**, *1*, 475-477.
6. Caspar, J. V.; Gray, H. B. *J. Am. Chem. Soc.* **1984**, *106*, 3029-3030.
7. *a.* Roundhill, D. M. *J. Am. Chem. Soc.* **1985**, *107*, 4354-4356. *b.* Marshall, J. L.; Stiegman, A. E.; Gray, H. B. *Adv. Chem. Ser.*, in press.
8. Chapter IV.
9. *a.* Nocera, D. G.; Gray, H. B. *J. Am. Chem. Soc.* **1981**, *103*, 7349-7350. *b.* Nocera, D. G.; Gray, H. B. *Inorg. Chem.* **1984**, *23*, 3686-3688.
10. Chapter II.
11. Glicksman, H. D.; Hamer, A. D.; Smith, T. J.; Walton, R. A. *Inorg. Chem.* **1975**, *15*, 2205-2209.
12. Schrock, R. R.; Sturgeoff, L. G.; Sharp, P. R. *Inorg. Chem.* **1983**, *22*, 2801-2806.
13. Gafney, H. D.; Adamson, A. W. *J. Am. Chem. Soc.* **1972**, *94*, 8238-8239.
14. Kalyanasundaram, K. *Coord. Chem. Rev.* **1982**, *46*, 159-244.
15. Balzani, V.; Bolletta, F.; Gandolfi, M. T.; Maestri, M. *Top. Curr. Chem.* **1978**, *75*, 1-64.
16. Zietlow, T. C.; Klendworth, D. D.; Nimry, T.; Salmon, D. J.; Walton, R. A.

Inorg. Chem. **1981**, *20*, 947-949.

17. *a.* Zietlow, T. C. *Ph. D. Thesis*, California Institute of Technology, Pasadena, CA, 1985, ch. 8. *b.* Zietlow, T. C., unpublished results. *c.* Ouyang, J.; Zietlow, T. C.; Hopkins, M. D.; Fan, F.-R. F.; Gray, H. B.; Bard, A. J. *J. Phys. Chem.* **1986**, in press.
18. An interesting preliminary result is that $W_2Cl_4(PBu^n_3)_4$ is very photosensitive in dichloromethane solution. Attempts to acquire its emission lifetime in this solvent led to a change in color of the solution from light to dark green; extended photolysis in room light (2 weeks) resulted in a deep red solution (possibly $W_2Cl_6(PBu^n_3)_4$).[12]
19. Erwin, D. K.; Geoffroy, G. L.; Gray, H. B.; Hammond, G. S.; Solomon, E. I.; Trogler, W. C.; Zagars, A. A. *J. Am. Chem. Soc.* **1977**, *99*, 3620-3621.
20. Trogler, W. C.; Erwin, D. K.; Geoffroy, G. L.; Gray, H. B. *J. Am. Chem. Soc.* **1978**, *100*, 1160-1163.
21. Geoffroy, G. L.; Gray, H. B.; Hammond, G. S. *J. Am. Chem. Soc.* **1974**, *96*, 5565-5566.
22. Pierce, J. L.; DeMarco, D.; Walton, R. A. *Inorg. Chem.* **1983**, *22*, 9-12.
23. It is important to differentiate the excited state acid-base chemistry proposed here for the $^1(\delta\delta^*)$ state of $Mo_2Cl_4(PMe_3)_4$ from that observed in other transition metal systems. Previous studies[24] have focused on the emissive MLCT states of species in which the ligand that is formally reduced[25] in the excited state is derivatized with a pendant base, thus allowing luminescence quenching *via* proton transfer:

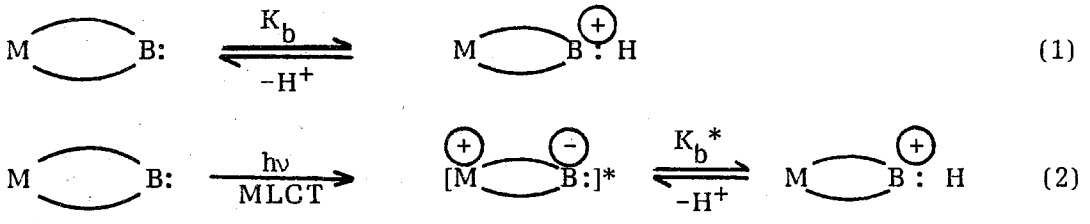

The metal center in these cases acts solely as a sensitizer of the acid-base chemistry of the organic ligand and does not participate in any net reaction, nor does it display any enhanced acid-base reactivity as a result of excitation.

24. *a.* Giordano, P. J.; Bock, C. R.; Wrighton, M. S. *J. Am. Chem. Soc.* **1978**, *100*, 6960-6965. *b.* Crutchley R. J.; Kress, N.; Lever, A. B. P. *J. Am. Chem. Soc.* **1983**, *105*, 1170-1178.

25. Bradley, P. G.; Kress, N.; Hornberger, B. A.; Dallinger, R. F.; Woodruff, W. H. *J. Am. Chem. Soc.* **1981**, *103*, 7441-7446.

26. It should be noted that $[Mo_2(\mu\text{-}H)X_8]^{3-}$ has been proposed as an intermediate in the net-two-electron photooxidation of $Mo_2X_8^{4-}$ (X = Cl, Br) by aqueous HX to $Mo_2(\mu\text{-}OH)_2(aq)^{4+}$ and H_2.[20] This reaction occurs with appreciable quantum yields only upon high-energy irradiation, however, and it was specifically noted in this study that no reaction was observed upon excitation into the $^1(\delta \rightarrow \delta^*)$ band. Since the nature of the reactive excited state is unknown, a mechanism for the formation of the intermediate in this system is not available.

27. There have been no reports of phosphine-substituted derivatives of $[Mo_2(\mu\text{-}H)Cl_8]^{3-}$.

28. The conditions of this experiment were such that the concentration of $[Mo_2(\mu\text{-}H)Cl_4(PMe_3)_4]^+$ was maximized relative to that of $[Mo_2(\mu\text{-}H)Cl_8]^{3-}$ or other chloride-substituted intermediates in its thermal decomposition pathway. Specifically, a benzene solution that was very dilute in both $Mo_2Cl_4(PMe_3)_4$ and HCl was rapidly photolyzed to near completion and the volatile contents immediately removed under vacuum. Addition of tetrahydrofuran to the remaining light brown residue produced a pale gold solution and an insoluble yellow oil. Within a few minutes, the flask containing this mixture became warm to the touch and the solution acquired a distinct greenish tinge. Spec-

trophotometric monitoring of this reaction revealed a rapid, quantitative conversion (based on the disappearance of the initially visible absorption bands) of the solution phase to $Mo_2Cl_4(PMe_3)_4$; irradiation of the flask with a mineral lamp produced the intense red luminescence characteristic of this species. The yellow oil, which presumably consisted of the THF-insoluble $(Me_3PH)_3[Mo_2(\mu\text{-}H)Cl_8]$ complex, appeared to remain unchanged over this time period, as it also did when this compound was dissolved in 1:1 acetonitrile:tetrahydrofuran in a separate experiment.[29]

29. Previous work has shown that while $[Mo_2(\mu\text{-}H)Cl_8]^{3-}$ undergoes a similar base-induced reductive elimination/deprotonation, more forcing conditions are required than are needed for its phosphine-substituted derivatives: the complex $Mo_2Cl_4py_4$ can be produced from $Cs_3Mo_2(\mu\text{-}H)Cl_8$ upon refluxing the latter in neat pyridine for 4h.[30]

30. San Filippo, J., Jr.; King, M. A. S. *Inorg. Chem.* **1976**, *15*, 1228-1232.

31. Chapter V.

APPENDICES

APPENDIX I

Heavy Atom Parameters and Additional Bond Distances and Angles of $Mo_2Br_4(PMe_3)_4$ and $Mo_2I_4(PMe_3)_4$

Table I. Additional Bond Distances and Bond Angles of $Mo_2Br_4(PMe_3)_4$[a]

Bond Distances

Atom	Atom	Distance (Å)
P1	C1	1.813(8)
P1	C2	1.802(7)
P1	C3	1.831(7)
P2	C4	1.821(7)
P2	C5	1.813(7)
P2	C6	1.808(7)

Bond Angles

Atom	Atom	Atom	Angle (deg)
P1	Mo1	Br1	84.92(4)
P1'			85.04(4)
P2	Mo2	Br2	85.00(4)
P2'			84.85(4)
Br1'	Mo1	Br1	132.70(3)
P1'		P1	154.80(6)
Br2'	Mo2	Br2	113.31(3)
P2'		P2	154.19(6)
C1	P1	Mo1	119.1(2)
C2			119.7(2)
C3			107.7(2)
C2		C1	103.1(3)
C3			103.0(3)
C3		C2	101.8(3)
C4	P2	Mo2	107.5(2)
C5			118.4(2)
C6	P1		120.1(2)
C5		C4	102.4(3)
C6	P2		102.6(3)
C6		C5	103.5(3)

[a] A prime indicates an atom related by a symmetry operation to those whose coordinates are given in Chapter 2, Table II.

Table II. Additional Bond Distances and Bond Angles of $Mo_2I_4(PMe_3)_4$

Bond Distances

Atom	Atom	Distance (Å)
P1	C11	1.802(10)
	C12	1.806(11)
	C13	1.812(12)
P2	C21	1.813(10)
	C22	1.813(9)
	C23	1.809(9)
P3	C31	1.816(9)
	C32	1.813(10)
	C33	1.807(9)
P4	C41	1.821(12)
	C42	1.822(12)
	C43	1.813(11)

Bond Angles (deg.)

Atom	Atom	Atom	Angle (deg)
I1	Mo1	P1	83.7(1)
		P2	84.3(1)
I2		P1	84.9(1)
		P2	84.2(1)
I3	Mo2	P3	83.7(1)
		P4	84.4(1)
I4		P3	84.4(1)
		P4	84.8(1)
I1	Mo1	I2	129.8(1)
P1		P2	152.9(1)
I3	Mo2	I4	129.7(1)
P3		P4	153.1(1)
Mo1	P1	C11	119.2(3)
		C12	119.6(4)
		C13	109.9(4)
	P2	C21	109.9(3)
		C22	118.9(3)
		C23	119.4(3)
Mo2	P3	C31	119.8(3)
		C32	108.8(3)
		C33	119.4(3)
	P4	C41	119.8(4)
		C42	107.9(4)
		C43	120.0(4)

Table II. (continued)

Bond Angles (deg.)

Atom	Atom	Atom	Angle (deg)
C11	P1	C12	102.9(5)
		C13	101.2(5)
C12		C13	101.2(5)
C21	P2	C22	102.0(4)
		C23	100.0(4)
C22		C23	103.8(4)
C31	P3	C32	102.2(4)
		C33	102.8(4)
C32		C33	101.2(4)
C41	P4	C42	103.0(5)
		C43	102.3(5)
C42		C43	101.2(5)

Table III. Heavy Atom Parameters for $Mo_2Br_4(PMe_3)_4$[a]

Atom	x	y	z	U_{eq}[b]
Mo1	0	3321(.7)	1/4	296(2)
Mo2	0	1057(.7)	1/4	295(2)
Br1	-1085(.3)	4410(.7)	1184(.4)	528(2)
Br2	-865(.3)	-20(.7)	3166(.4)	501(2)
P1	930(1)	3915(2)	1803(1)	468(4)
P2	-1159(1)	452(1)	1109(1)	427(4)
C1	1970(4)	3391(8)	2320(5)	752(19)
C2	653(4)	3416(7)	723(4)	664(17)
C3	986(4)	5858(7)	1752(4)	721(20)
C4	-1234(4)	-1482(7)	1032(4)	736(22)
C5	-2157(3)	969(7)	956(4)	593(17)
C6	-1123(4)	946(7)	128(4)	632(19)

[a] All coordinates except Mo1(z) and Mo2(z) have been multiplied by 10^4.

[b] $U_{eq} = \frac{1}{3} \sum_i \sum_j [u_{ij} (a_i^* \cdot a_j^*) (\vec{a}_i \cdot \vec{a}_j)]$. $\sigma(U_{eq}) = \frac{1}{\sqrt{6}} \left\langle \frac{\sigma(U_{ii})}{U_{ii}} \right\rangle U_{eq}$.

Table IV. Heavy Atom Parameters for $Mo_2I_4(PMe_3)_4$.[a]

Atom	x	y	z	Ueq[b]
Mo1	24236(3)	54200(5)	31439(3)	353(1)
Mo2	24984(4)	43378(5)	21007(4)	374(1)
I1	17014(3)	77093(5)	27795(4)	597(1)
I2	30622(4)	43187(7)	46411(3)	769(2)
I3	38846(3)	46813(6)	15815(4)	722(2)
I4	11813(4)	28232(6)	14775(4)	747(2)
P1	37478(12)	66797(25)	34863(14)	643(6)
P2	10519(11)	47846(19)	33810(13)	488(5)
P3	18449(13)	57340(20)	8782(12)	518(5)
P4	32035(17)	23420(21)	27568(15)	700(6)
C11	3916(6)	7787(9)	2745(6)	6.5(2)
C12	4712(6)	5887(10)	3811(7)	7.1(3)
C13	3794(7)	7670(10)	4369(7)	7.8(3)
C21	887(5)	5611(9)	4263(6)	5.8(2)
C22	128(5)	5127(8)	2587(5)	5.3(2)
C23	907(5)	3207(9)	3679(6)	5.7(2)
C31	786(5)	6180(9)	691(5)	5.7(2)
C32	1849(6)	4927(10)	-68(6)	6.5(2)
C33	2333(5)	7176(8)	744(5)	5.3(2)
C41	4239(7)	2407(11)	3416(7)	8.3(3)
C42	3292(7)	1317(11)	1922(7)	7.8(3)
C43	2708(6)	1331(11)	3336(6)	7.6(3)

[a] Coordinates of Mo, I, and P have been multiplied by 10^5. Coordinates of C and Ueq have been multiplied by 10^4.

[b] $Ueq = 1/3 \sum_i \sum_j [U_{ij}(a_i^* \cdot a_j^*)(\vec{a}_i \cdot \vec{a}_j)]$; $\sigma(Ueq) = \frac{1}{\sqrt{6}} \left\langle \frac{\sigma(U_{ii})}{U_{ii}} \right\rangle$ Ueq

APPENDIX II

Electronic Transitions to the Higher Energy Excited States of $M_2X_4L_4$ Complexes

Figure 1. $\perp$ z-polarized single-crystal absorption spectra of $Mo_2X_4(PMe_3)_4$ in the region of their $^1(\delta \rightarrow \delta^*)$ transition at ca. 5 K: (a) X = Cl; (b) X = Br. The arrows indicate the positions of the 0-0 transitions observed in $\parallel$ z-polarization (see Chapter V, Figure 14).

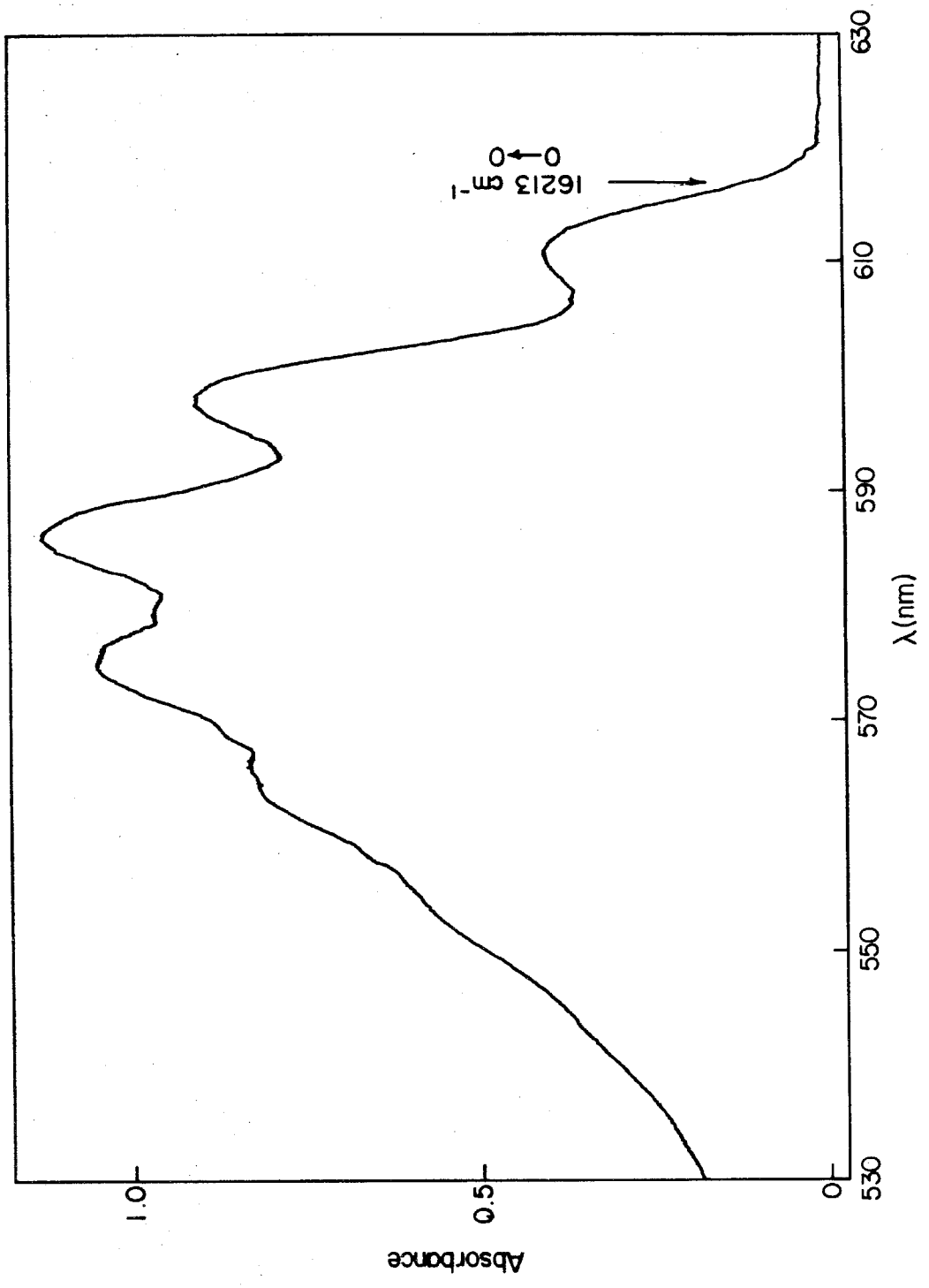
16213 cm⁻¹
0←0
Absorbance
1.0
0.5
0
530
550
570
590
610
630
λ(nm)

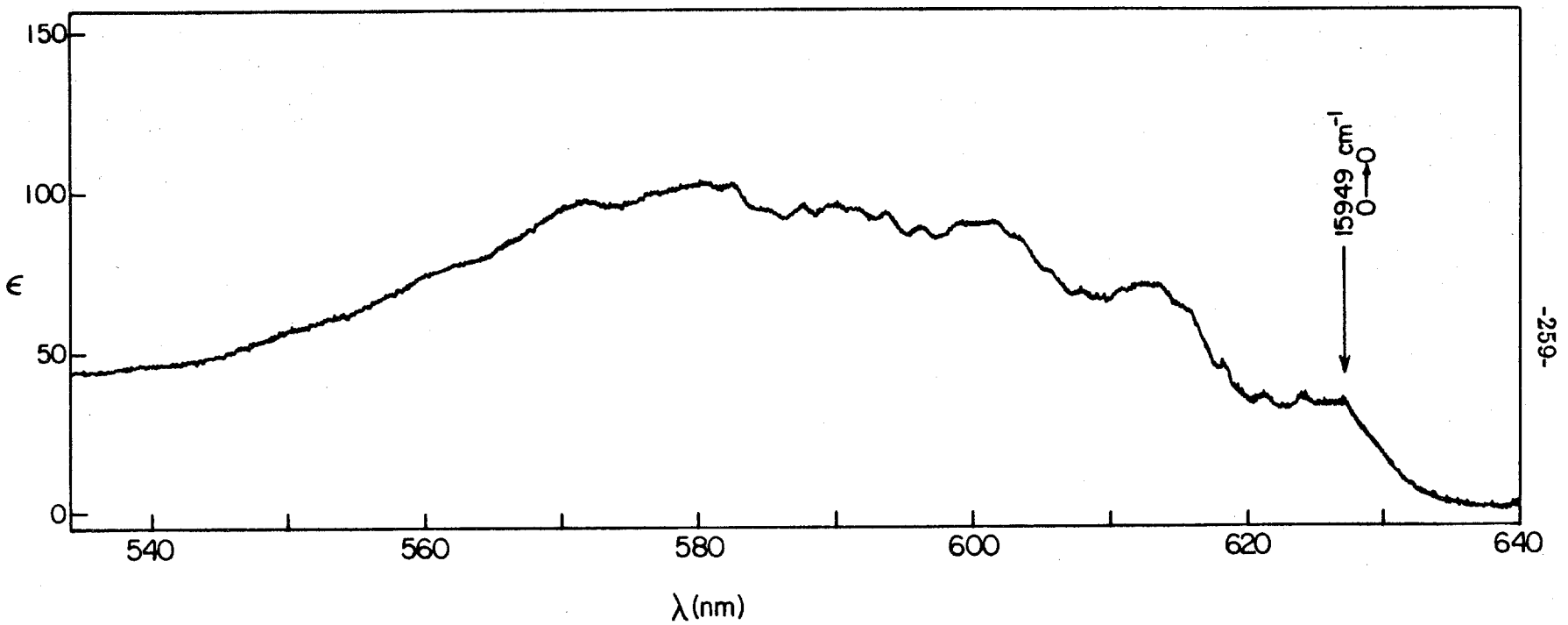
150
100
50
0
ε
540
560
580
600
620
640
λ(nm)
15949 cm⁻¹
0→0

Figure 2. Polarized single-crystal absorption spectra of $Mo_2Cl_4(PMe_3)_4$: (a) T = 300 K; (b) T = 5 K. The $\parallel z$ spectrum in (a) is offset from the $\perp z$ spectrum by 0.06 optical density units. The dashed line is the calculated isotropic spectrum ($\epsilon_{iso} = 1/3(\epsilon_z + 2\epsilon_{x,y})$) with the $\perp z$ baseline.

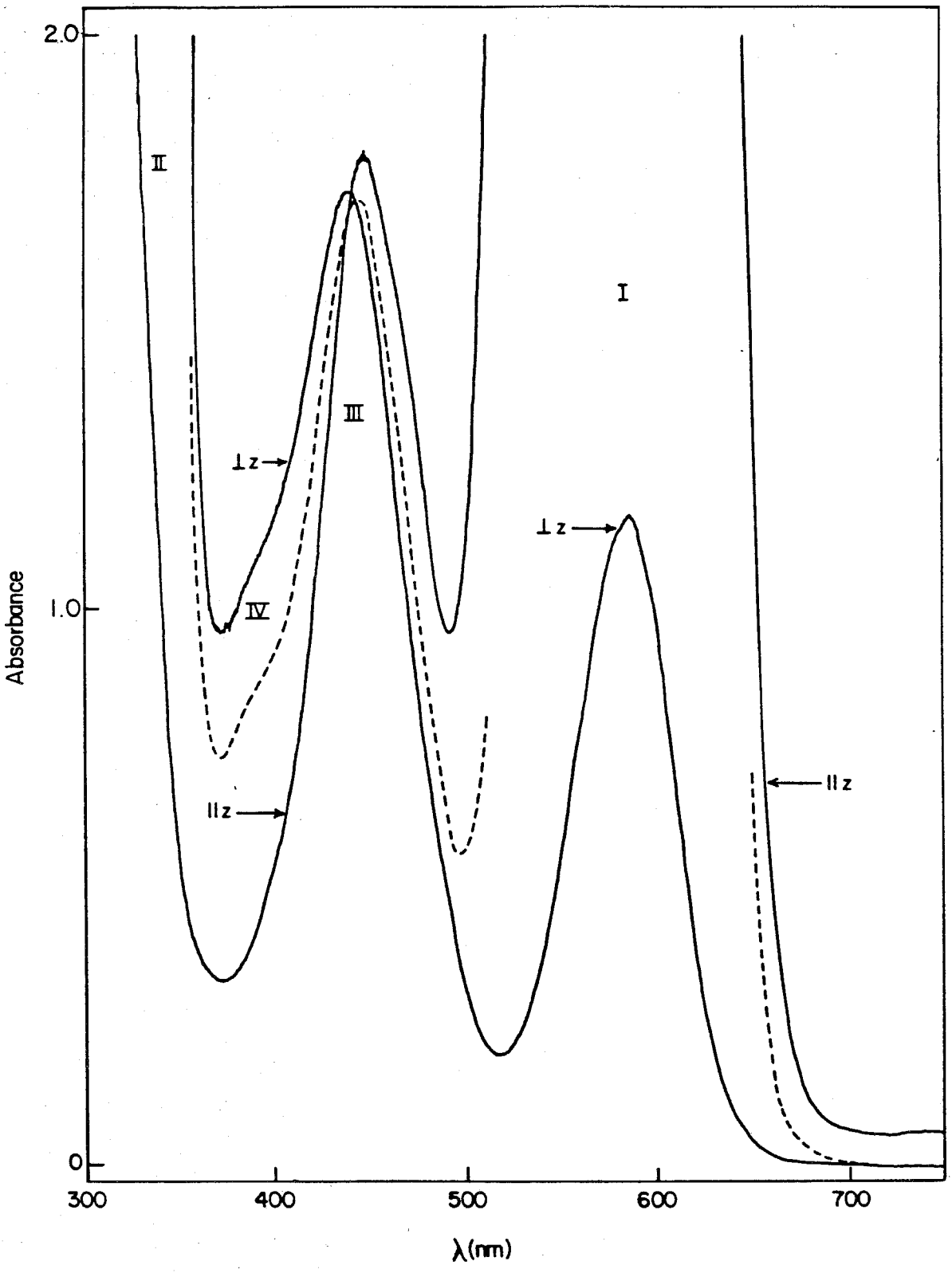
2.0
1.0
0
Absorbance
300
400
500
600
700
λ(nm)
II
III
IV
I
⊥z
⊥z
∥z
∥z

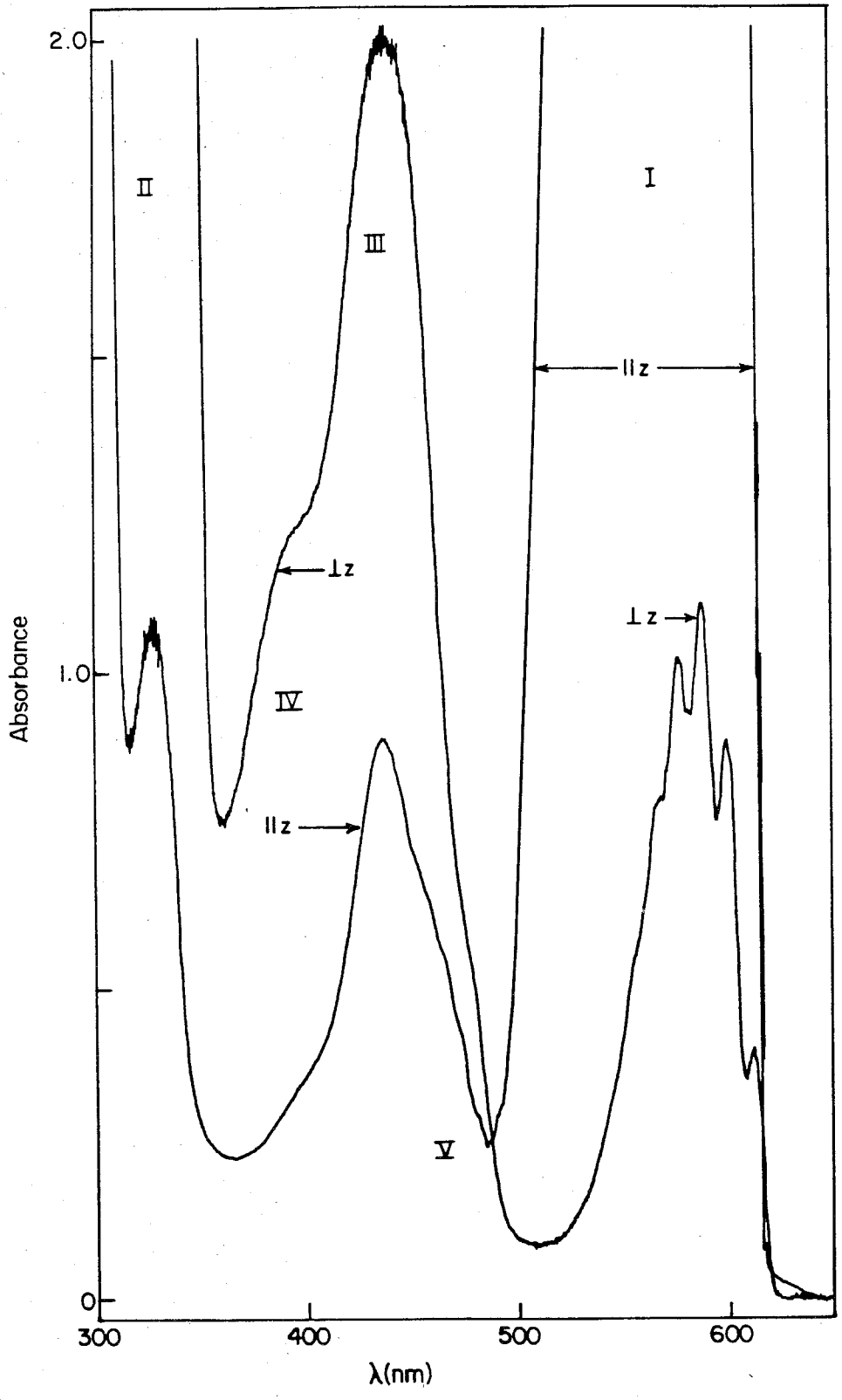
2.0
1.0
0
Absorbance
II
III
I
IV
V
⊥z
∥z
∥z
⊥z
300
400
500
600
λ(nm)

Figure 3. Polarized single-crystal absorption spectra of $Mo_2Br_4(PMe_3)_4$: (a) T = 300 K. (b) T = 40 K. The dashed line is the calculated isotropic spectrum ($\epsilon_{iso} = 1/3(\epsilon_z + 2\epsilon_{x,y})$).

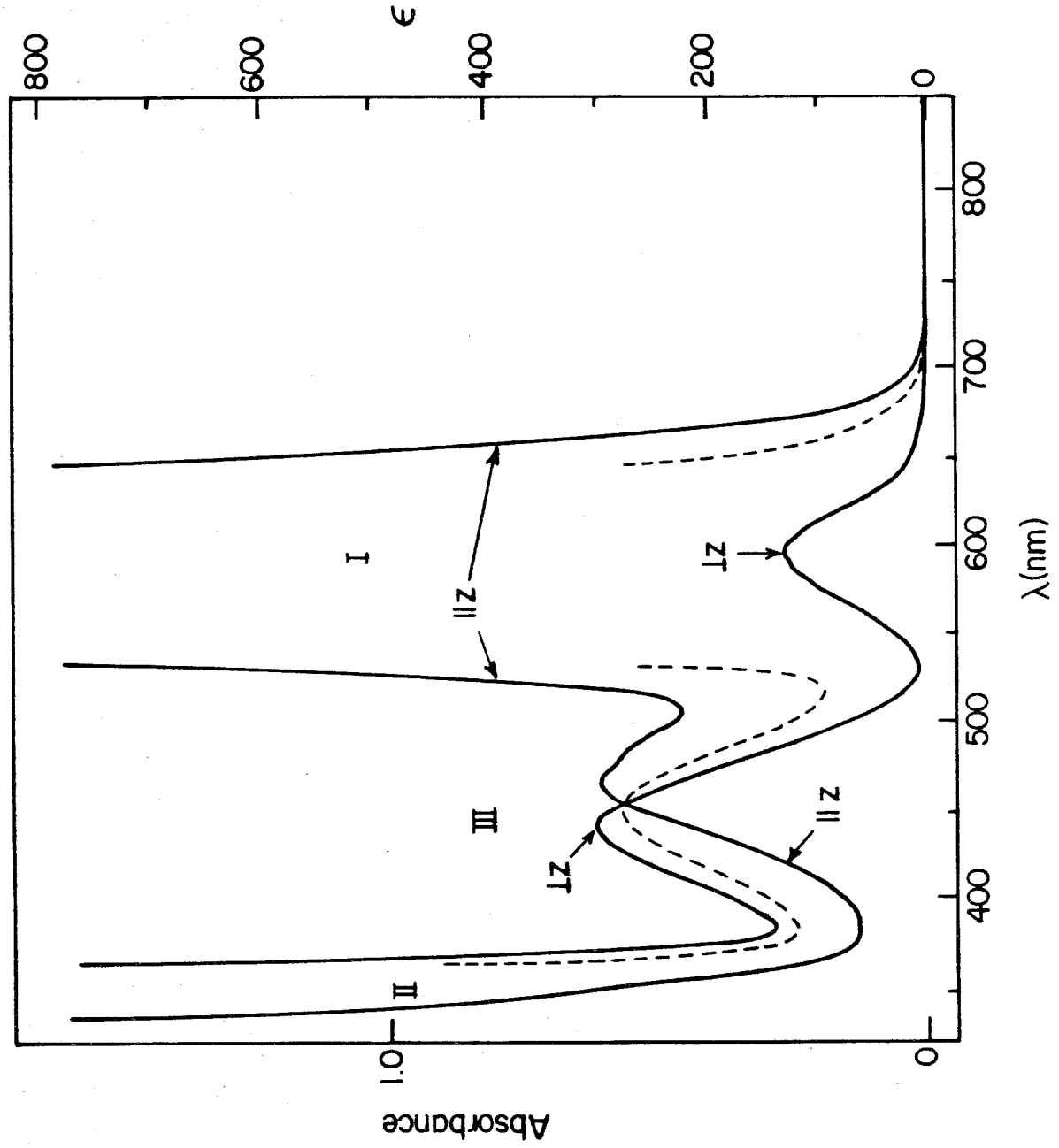
800
600
400
200
0
ε
Absorbance
1.0
0
II
I
III
z∥
z⊥
z⊥
z∥
400
500
600
700
800
λ(nm)

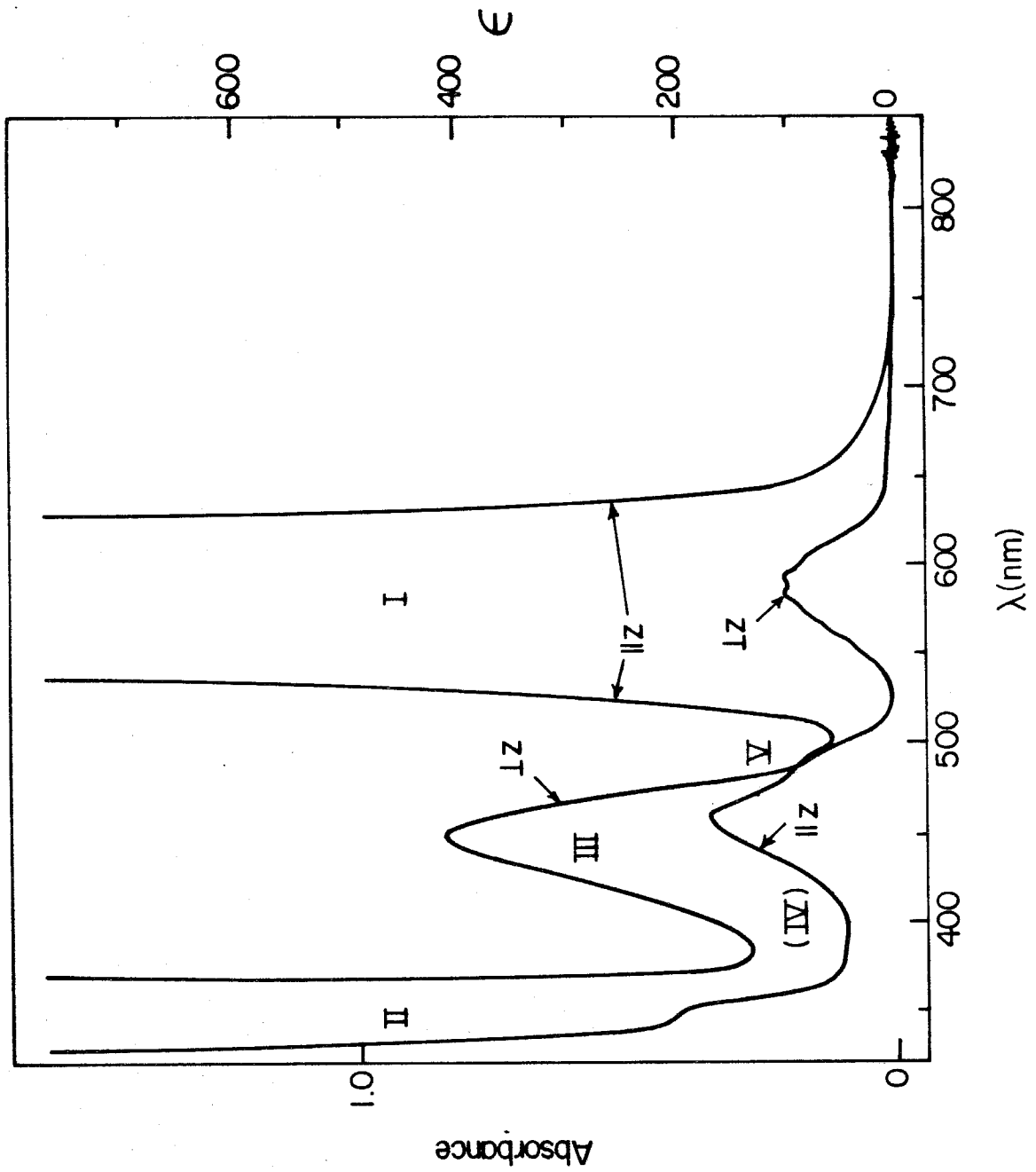
ε
600
400
200
0
800
700
600
500
400
λ(nm)
Absorbance
0.1
0
I
II
III
IV
(IV)
z∥
z⊥
z⊥
z∥

Figure 4. $\|$ z-polarized single-crystal absorption spectra of $Mo_2X_4(PMe_3)_4$ in the region of bands III and V at ca. 5 K (see Figures 2 and 3): (a) X = Cl; (b) X = Br. The average metal-metal stretching frequencies of band V for $Mo_2Cl_4(PMe_3)_4$ and $Mo_2Br_4(PMe_3)_4$ are 349 and 328 cm^{-1}, respectively. By comparison, these frequencies for the δ^2 (Chapter II, Table V) and $^1(\delta\delta^*)$ (Chapter V, Table III) states of $Mo_2Cl_4(PMe_3)_4$ are 355 and 331 cm^{-1}, and those of $Mo_2Br_4(PMe_3)_4$ are 352 and 326 cm^{-1}, respectively.

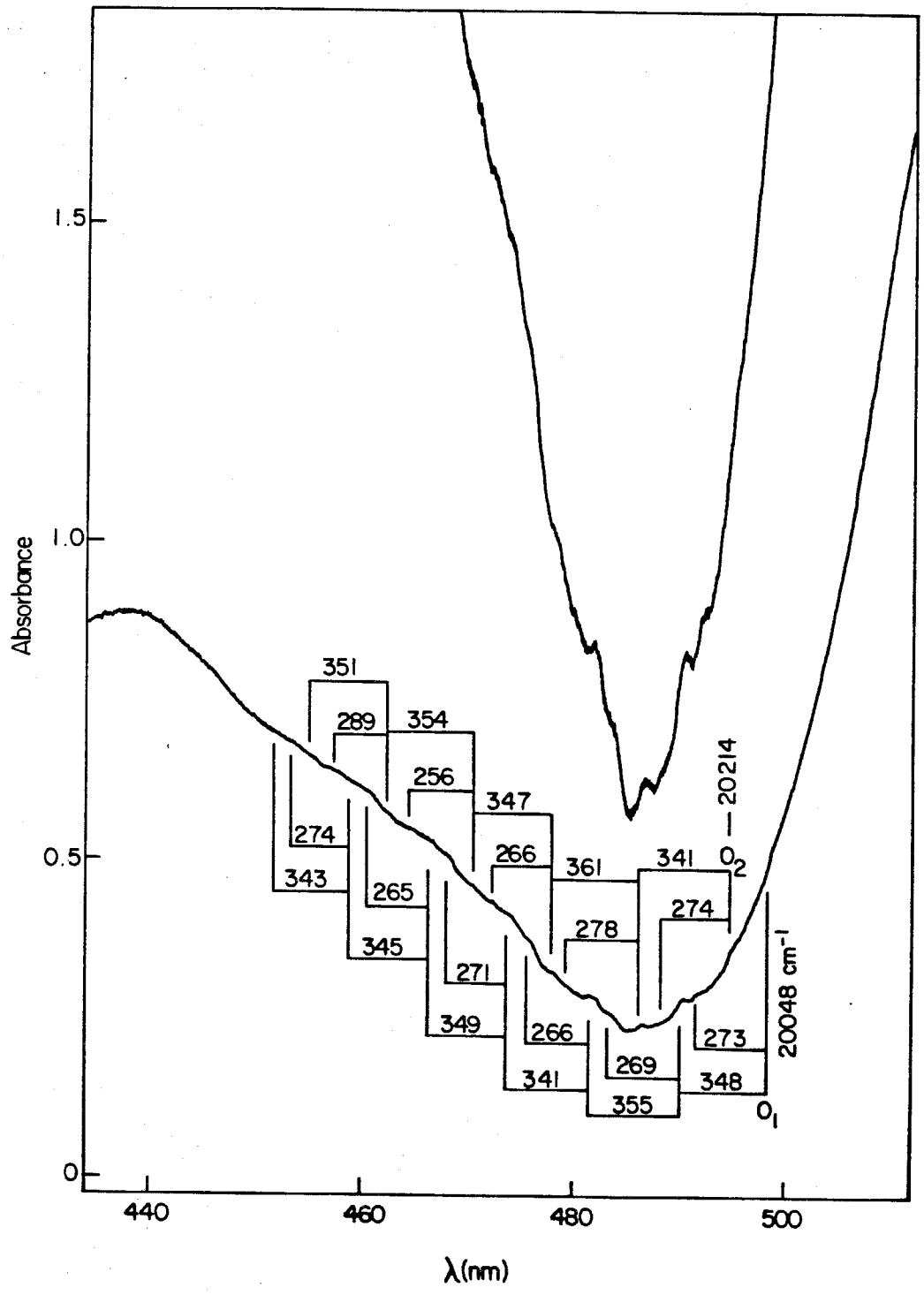
1.5
1.0
0.5
0
Absorbance
440
460
480
500
λ(nm)
351
289
354
256
347
274
266
361
341
O2
343
265
278
274
345
271
349
266
273
269
348
341
355
O1
20214
20048 cm-1

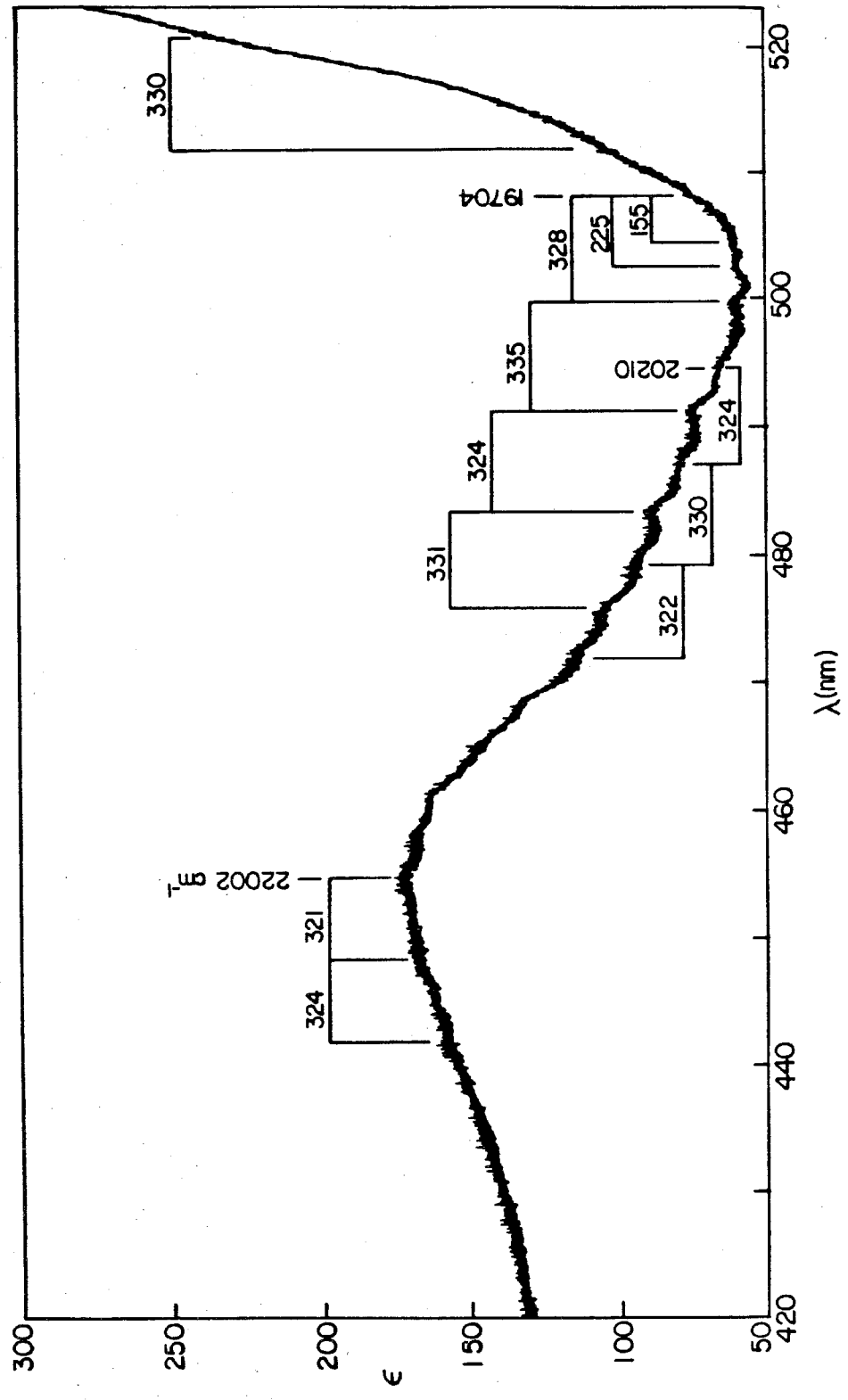
300
250
200
150
100
50
ε
420
440
460
480
500
520
λ(nm)
22002 $^1T_{1g}$
324
321
19704
328
225
155
20210
335
324
331
330
322
330

Figure 5. Absorption spectra of $M_2X_4(PMe_3)_4$ in 2-methylpentane at 77 K in the region between bands I and II: (a) M = Mo, X = I; (b) M = W, X = Cl.

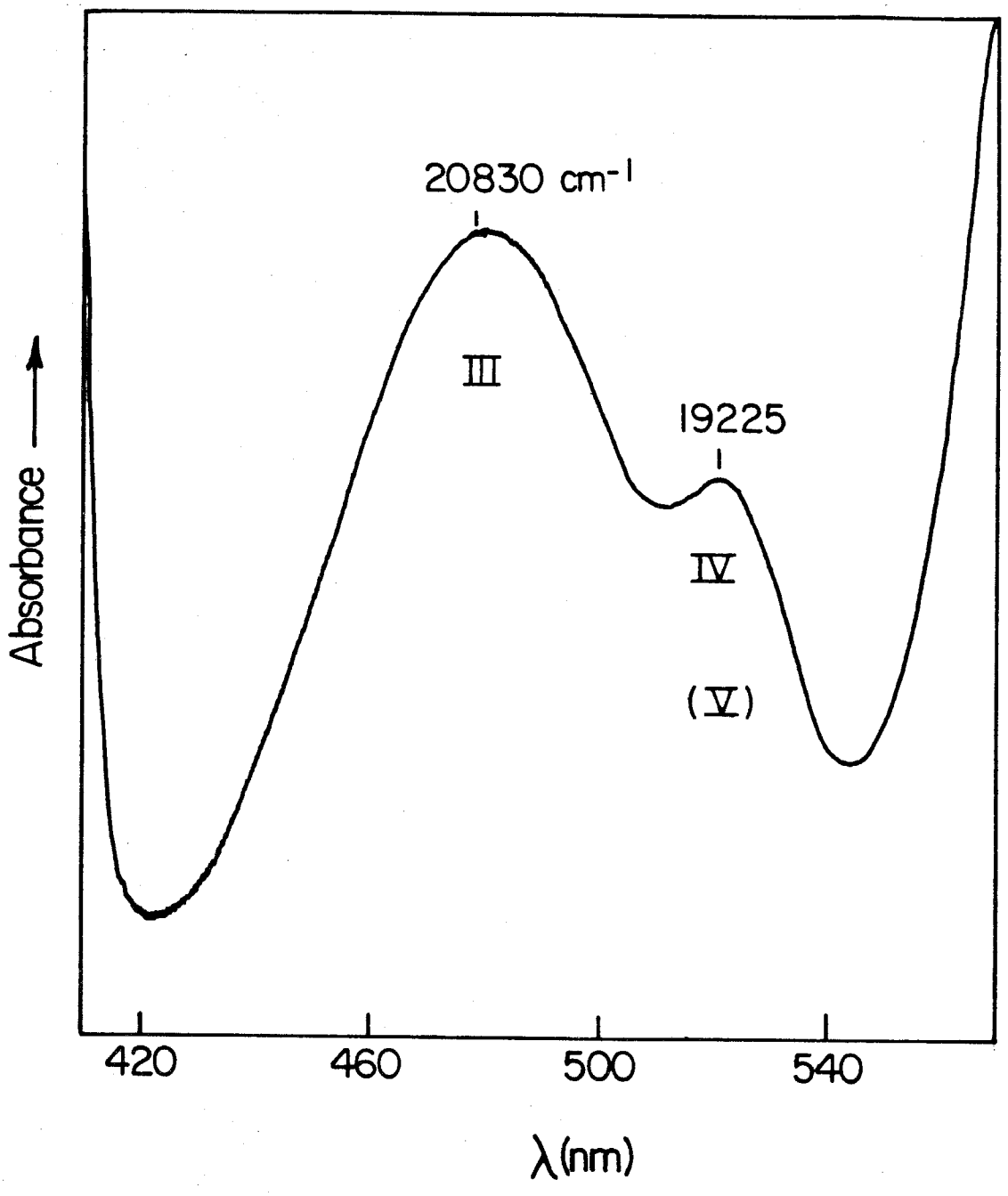
20830 cm-1
III
19225
IV
(V)
Absorbance
420
460
500
540
λ(nm)

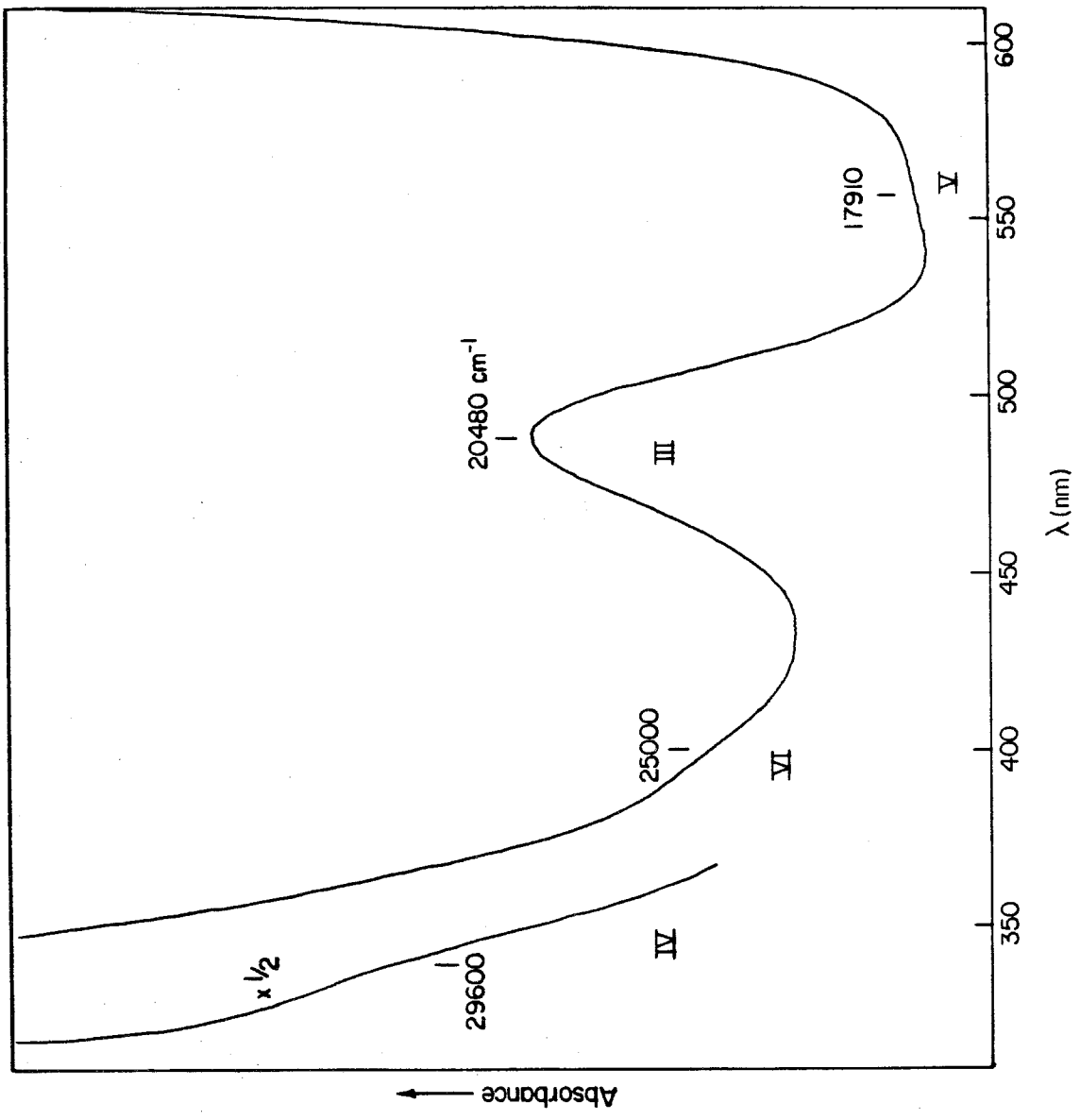
Absorbance
λ (nm)
350
400
450
500
550
600
17910
20480 cm⁻¹
25000
29600
x ½
I
II
III
IV

Figure 6. Absorption spectrum of a CsBr pellet of $Mo_2Br_4(PMe_3)_4$ at ca. 5 K in the region of band II ($\sigma(MoP) \rightarrow \delta^*(Mo_2)$; Chapter II). The ground-state molybdenum-phosphorous stretching frequency is $a_1\nu_1(MoP)$ = 235 cm^{-1} (Chapter II, Table V).

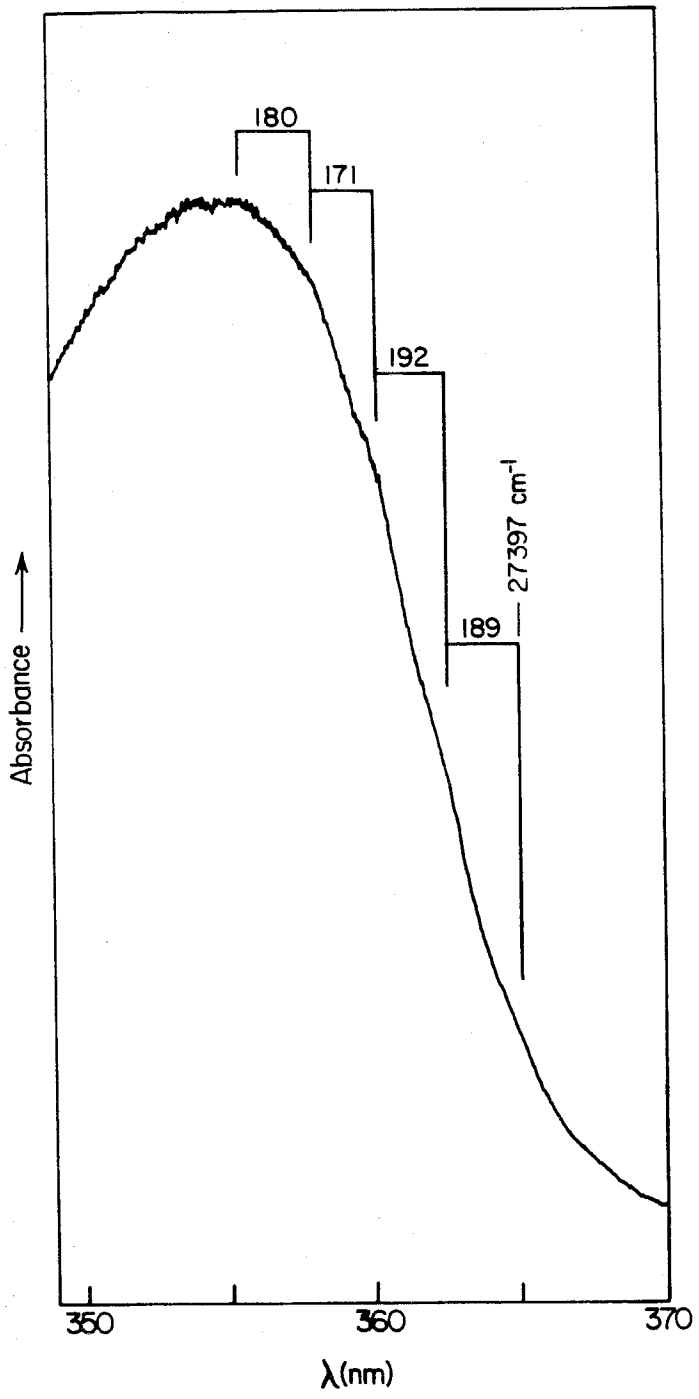
180
171
192
189
27397 cm⁻¹
Absorbance
350
360
370
λ(nm)

Figure 7. Tentative assignments of the electronic transitions of $M_2X_4(PMe_3)_4$. For a more detailed discussion of bands I and II, see Chapters V and II, respectively. The $\pi \rightarrow \delta^*$ assignment for band III is based on analogous assignments for similarly polarized bands of the $Mo_2(SO_4)_4^{4-/3-}$ and $Mo_2(HPO_4)_4^{2-}$ ions (Appendix IV). The $\sigma \rightarrow \delta^*$ assignment for band V is derived from recent theoretical (Manning, M. C.; Holland, G. F.; Ellis, D. E.; Trogler, W. C. *J. Phys. Chem.* **1983**, *87*, 3083-3088; Ziegler, T. *J. Am. Chem. Soc.* **1984**, *106*, 5901-5908; Ziegler, T. *ibid.* **1985**, *107*, 4453-4459) and photoelectron spectroscopic (Root, D. R.; Blevins, C. H.; Lichtenberger, D. L.; Sattelberger, A. P.; Walton, R. A. *J. Am. Chem. Soc.* **1985**, *108*, 953-959) evidence that the σ and π metal-metal bonding levels are in close energetic proximity; the essentially nonbonding nature of $\sigma(M_2)$ is indicated by the closeness of the metal-metal stretching frequency of the $[\sigma\pi^4\delta^2\delta^*]$ and $[\sigma^2\pi^4\delta\delta^*]$ states (Figure 4).

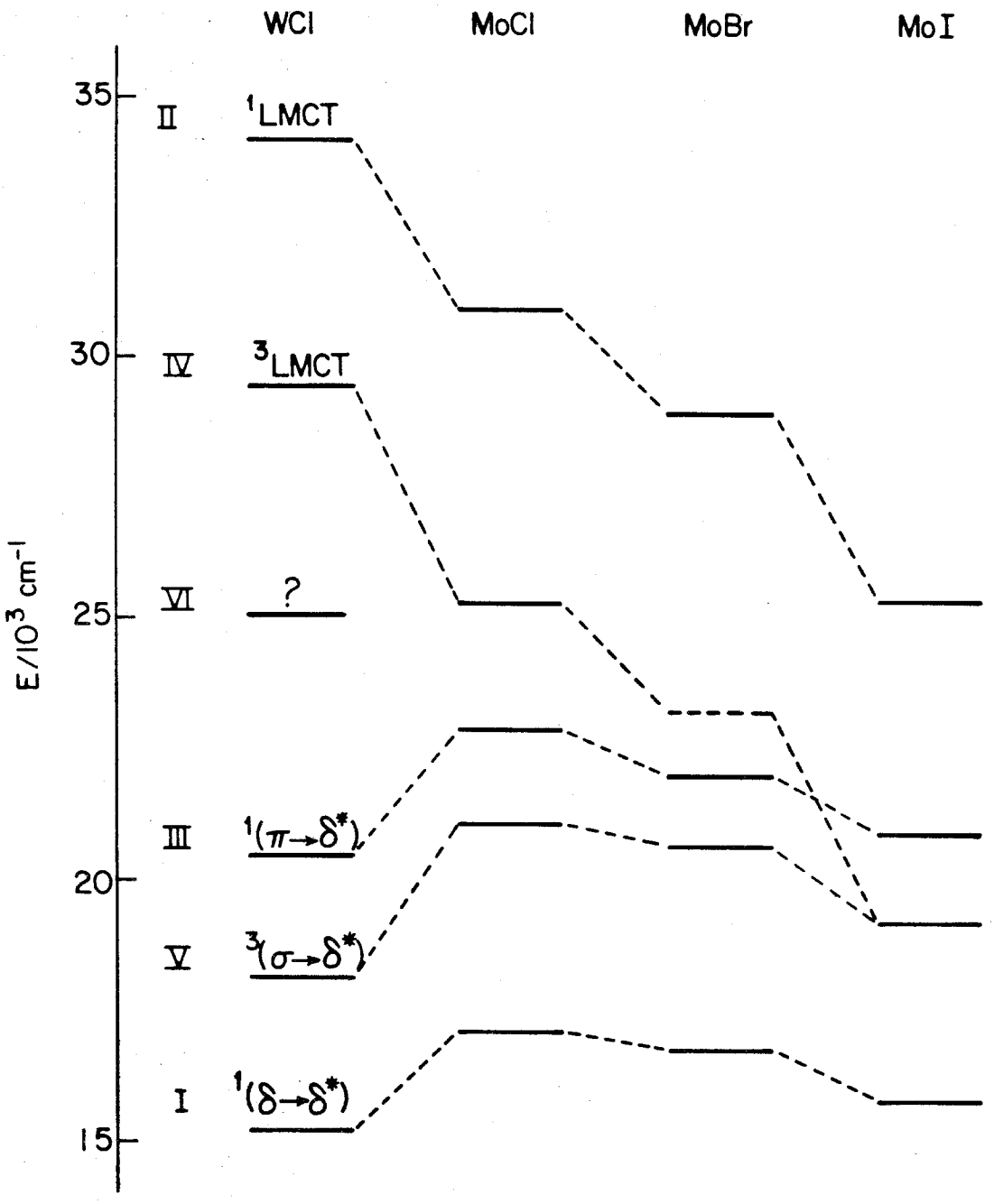
WCl
MoCl
MoBr
MoI
35
30
25
20
15
E/10³ cm⁻¹
II
IV
VI
III
V
I
¹LMCT
³LMCT
?
¹(π→δ*)
³(σ→δ*)
¹(δ→δ*)

APPENDIX III

The $\delta \rightarrow \delta^*$ Transitions of $Mo_2(O_2CPr^n)_4{}^{0/+}$

Figure 1. The $\delta \rightarrow \delta^*$ transitions of $Mo_2(O_2CPr^n)_4^{0/+}$: (a) $Mo_2(O_2CPr^n)_4$ in 2-methyltetrahydrofuran at 77 K (prepared according to the standard method: McCarley, R. E.; Templeton, J. L.; Colburn, T. J.; Katovic, V.; Hoxmeier, R. J. *Adv. Chem. Ser.* **1975**, *150*, 318-334); (b) $Mo_2(O_2CPr^n)_4^+$ in acetonitrile at ca. 235 K (generated *in situ* by chemical oxidation of $Mo_2(O_2CPr^n)_4$ with $NOPF_6$ at 0°C). *Note*: the two spectra are not on the same absorbance scale. The average values of the excited-state metal-metal stretching frequencies of the $^1[\sigma^2\pi^4\delta\delta^*]$ and $^2[\sigma^2\pi^4\delta^*]$ states of $Mo_2(O_2CPr^n)_4^{0/+}$ are ca. 365 and 335 cm^{-1}, respectively. By comparison, the ground-state metal-metal stretching frequency of $Mo_2(O_2CCH_3)_4$ is $\nu_1 = 406$ cm^{-1} (Hutchinson, B.; Morgan, J.; Cooper, C. B., III; Mathey, Y.; Shriver, D. F. *Inorg. Chem.* **1979**, *18*, 2048-2049).

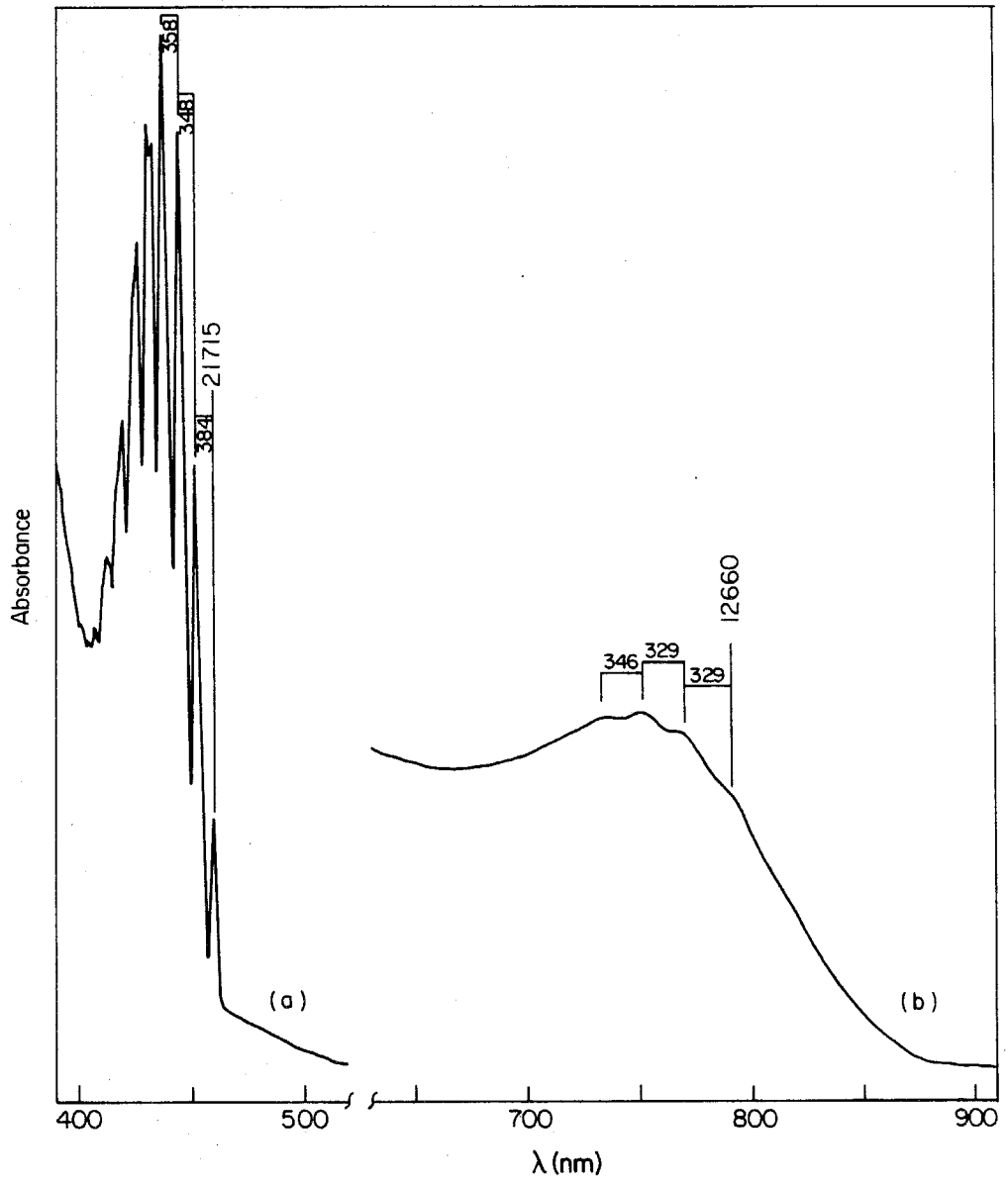
Absorbance
21715
384
348
358
12660
346
329
329
(a)
(b)
400
500
700
800
900
λ (nm)

APPENDIX IV

Electronic and Vibrational Spectroscopy of the Triply Bonded $Mo_2(HPO_4)_4^{2-}$ Ion. Inferences as to the Energetics of δ-Bonding from Spectroscopic Correlations to $Mo_2(SO_4)_4^{4-/3-}$

Introduction[1]

Spectroscopic studies of the $^1(\delta \rightarrow \delta^*)$ transitions of quadruply bonded metal dimers have been of central importance in elucidating the electronic structural details of the δ-bond present in this class of compounds.[2,3] One of the principal themes that has emerged from consideration of the overall spectral behavior of these systems is that the relatively high energy and low intensity of this transition are a direct consequence of the weak overlap of the d_{xy} orbitals that comprise the δ-interaction.[2] The actual contribution of the energetic splitting of the one-electron δ and δ^* levels to the energy of the $^1(\delta\delta^*)$ state, however, has been difficult to assess experimentally,[4-6] and hence quantitative spectroscopic measurements of the extent to which the δ-interaction is perturbed by such variables as metal-metal distance, metal-ligand interactions, and formal charge of the M_2 unit have, for the most part, remained elusive.

Binuclear complexes that span a wide range of d-electron counts and formal metal-metal bond orders have been prepared and structurally characterized, particularly over the last 25 years.[3] Several years ago, compounds containing the $Mo_2(SO_4)_4^{4-/3-}$ ions, which constitute examples of bond orders of $4(\sigma^2\pi^4\delta^2)$ and $3.5(\sigma^2\pi^4\delta^1)$, respectively, were reported[7] and subsequently thoroughly characterized with respect to their spectroscopic properties.[8-12] This series has recently been extended to include an example with a formal bond order of 3 with the discovery of the structurally related $Mo_2(HPO_4)_4^{2-}$ ion,[13,14] which is proposed to possess a $(\sigma^2\pi^4\delta^0)$ electronic configuration. Comparisons of the molecular structures of these three compounds show that the major perturbation to the Mo_2O_8 core across this series is a small, monotonic increase in the metal-metal distance with decreasing bond order (~0.06 Å/δ electron),[13] as anticipated from qualitative electronic struc-

tural considerations. We report herein the results of our electronic and vibrational spectroscopic investigation of the $Mo_2(HPO_4)_4^{2-}$ ion, as well as the correlation of the relative energies of the π, δ, and δ^* levels with metal oxidation state and metal-metal distance for this class of complexes.

Experimental Section

General Procedures.

All chemicals were of reagent grade or comparable quality and were used as received. Elemental analyses were performed by Mr. Larry Henling at the Caltech Analytical Laboratory. Magnetic susceptibilities were obtained at room temperature with a Faraday balance that was calibrated with $HgCo(SCN)_4$. Raman and electronic spectra were acquired using the instrumentation and procedures detailed in chapters II and III, respectively.

$(pyH)_3[Mo_2(HPO_4)_4]Cl$.[15]

A saturated solution of $K_4Mo_2Cl_8$ in N_2-purged 6 N H_3PO_4 was quickly filtered, in air, into an open beaker containing a 5-fold excess of pyridinium chloride. The solution became turbid shortly after dissolution of the salt, and within minutes a gray precipitate had formed. After being stirred for 10 min, the mixture was diluted by 25% with 6 N H_3PO_4, stirred briefly, and filtered. The filtrate was diluted again by 25% with 6 N H_3PO_4, and the deep yellow solution was allowed to stand undisturbed in an open beaker. After 24 h, several fine purple needles were observed to be growing on the wall of the beaker at the solvent/air interface, in addition to a small amount of gray precipitate on the bottom of the beaker. After 3 days, a small crop (10-20 crystals) of long (1-1.5 cm) red-purple blades was carefully removed from the flask and blotted dry between sheets of filter paper. Additional

material could be obtained as small red-purple needles by allowing the combined gray precipitates to stand in the mother liquor in an open beaker for 1 month. This material was washed with a small amount of ethanol and dried *in vacuo*. Anal. calcd (found) for $C_{15}H_{22}N_3ClO_{16}P_4Mo_2$: C, 21.16 (21.10); H, 2.60 (2.56); N, 4.93 (4.91).

Examination of the blade-like crystals under a polarizing microscope revealed sharp extinctions parallel and perpendicular to the blade axis. Most of these crystals were aggregates that were aligned along the blade axis. Small, thin single crystals could be obtained by breaking up these aggregates; all spectral data in this appendix refer to such crystals. These crystals were strongly dichroic, transmitting yellow and red-purple light for their parallel and perpendicular extinctions, respectively. Examination of a typical crystal by X-ray photographic methods showed it to be consistent with the previously reported[13] orthorhombic space group (*Pbam*) and lattice constants. The crystallographic *c* axis was found to be colinear with the long blade axis (yellow extinction) of the crystal, and the well-developed crystal face was determined to be (100). The yellow and reddish-purple extinction directions therefore correspond to polarization parallel and perpendicular, respectively, to the linear -(Mo-Mo-Cl-)$_\infty$ chains (C_{2h} site symmetry) of the crystal, i.e., respectively parallel and perpendicular to molecular *z*.

$Cs_2[Mo_2(HPO_4)_4]2H_2O$.

A 50% saturated solution of $(pyH)_3[Mo_2(HPO_4)_4]Cl$ in N_2-purged 6 N H_3PO_4 was treated dropwise with a saturated solution of CsCl in the same solvent. The product precipitated immediately, as a fine purple powder, in nearly quantitative yield.

Results and Discussion

Magnetism.

Although the $(\sigma^2\pi^4\delta^0)$ electronic configuration proposed[13,14] for $Mo_2(HPO_4)_4^{2-}$ seemed very likely to be correct, a recent report of paramagnetism for the $Os_2(O_2CR)_4Cl_2$ compounds,[16] which possess two electrons in excess of a quadruple bond, made magnetic confirmation of the singlet ground state desirable. A room temperature (297 K) Faraday measurement on our preparation of $(pyH)_3[Mo_2(HPO_4)_4]Cl$ showed it to be rigorously diamagnetic, in accord with previous predictions, with the observed susceptibility of χ_m = -100(10) x 10^{-6} emu/mol being in fair agreement with that calculated by standard methods[17] (-350 x 10^{-6} emu/mol).

Raman Spectroscopy.

The Raman spectra obtained for $(pyH)_3[Mo_2(HPO_4)_4]Cl$ and $Cs_2[Mo_2(HPO_4)_4]2H_2O$ upon 363.8-nm excitation are reproduced in Figure 1.[18] The strongest feature in each spectrum is a line at ~360 cm^{-1} that is readily assigned to $\nu(Mo_2)$ by analogy to the previously reported metal-metal stretching frequencies of $Mo_2(SO_4)_4^{4-}$ (371 cm^{-1})[8,9] and $Mo_2(SO_4)_4^{3-}$ (373, 386 cm^{-1})[9] (the dual frequencies observed for the latter ion are a consequence of the existence of two crystallographically distinct dimers in the unit cell). Although the trend of $\nu(Mo_2)$ among the Mo_2(II,II) and Mo_2(II,III) sulfates is not an obvious one, the frequency of the Mo_2(III,III) phosphate is clearly lower than both of them, in accord with its lower bond order and longer metal-metal bond. Additional evidence that this is a reasonable assignment for $\nu(Mo_2)$ comes from comparison with the $^2(\delta \rightarrow \delta^*)$ excited state of the Mo_2(II,III) sulfate,[11,12] which has a formal bond order of 2.5$(\sigma^2\pi^4\delta^{*1})$ and a concomitantly lower metal-metal stretching frequency

Figure 1. Raman spectra of (a) $Cs_2[Mo_2(HPO_4)_4]2H_2O$ and (b) $(pyH)_3[Mo_2(HPO_4)_4]Cl$ (λ_{ex} = 363.8 nm) at room temperature.

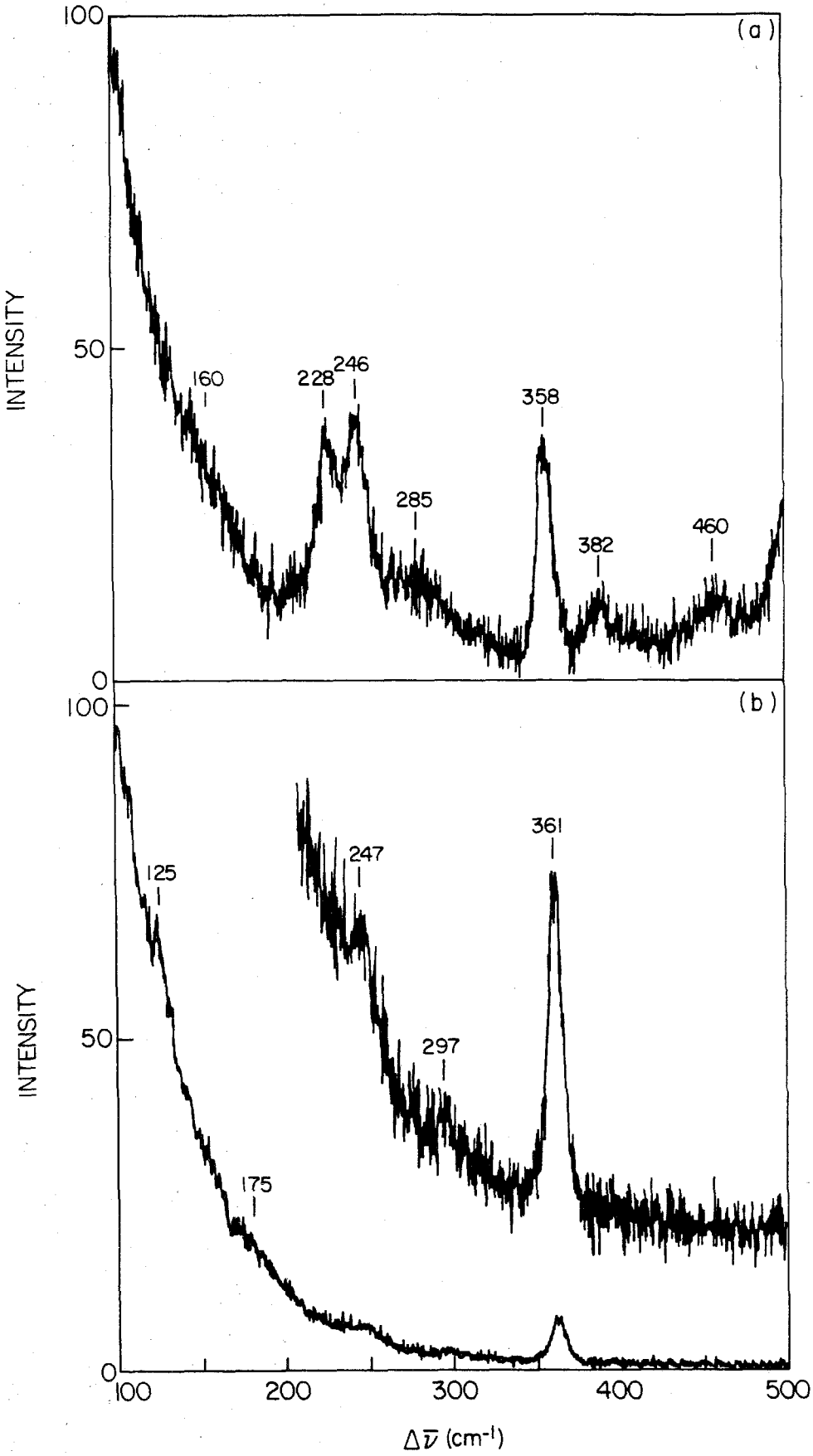
(a)
(b)
INTENSITY
INTENSITY
100
50
0
100
50
0
160
228
246
285
358
382
460
125
175
247
297
361
100
200
300
400
500
Δν̄ (cm⁻¹)

$\nu(Mo_2) = 350\ cm^{-1}$.[19]

With respect to the frequencies of metal-ligand vibrations, each Raman spectrum shows well-defined lines between 200 and 300 cm^{-1}; analogous lines observed for the Mo_2 sulfates have been assigned[9] to ν(Mo-O(sulfate)) modes. These assignments seem reasonable, although deformation modes (δ(Mo-O)) are also candidates for lines in this region.[20] The pyH^+ salt should, in addition, possess a feature attributable to the ν(Mo-Cl) mode, although the extreme length of this bond (2.91 Å)[13] suggests that it must lie at relatively low frequency. The shoulder at 125 cm^{-1}, which has no counterpart in the Cs^+ spectrum, seems reasonable in this regard. Additional weak features observed below 200 cm^{-1} remain unassigned; δ(Mo-O) deformation modes undoubtedly contribute to this region of the spectrum.[9,20]

Finally, lines to higher frequency of $\nu(Mo_2)$ are presumably associated with vibrations of the phosphate moiety; "free" PO_4^{3-} has modes at 420 and 567 cm^{-1},[21] and the sulfate complexes again show analogous lines.[9]

Electronic Spectroscopy.

Electronic absorption spectra have been reported in the visible region for solutions of $Mo_2(HPO_4)_4^{2-}$,[14] as well as for a KBr pellet of the Cs^+ salt,[13] at room temperature. The two spectra are virtually identical, consisting of weak bands at λ_{max} 428 nm (ϵ = 63 $M^{-1}cm^{-1}$) and λ_{max} 548 (ϵ 107).[14] We have examined a dilute CsCl pellet of $Cs_2[Mo_2(HPO_4)_4]2H_2O$ at 5 K and found an additional, relatively intense absorption centered at 250 nm. Neither this feature nor the previously reported visible bands displayed vibronic structure at low temperature, however.

The polarized single-crystal absorption spectra of $(pyH)_3[Mo_2(HPO_4)_4]Cl$ at room and low temperature are displayed in Figures 2 and 3, respectively.[22] These spectra show strongly $\sigma(x,y)$-polarized bands with nearly temperature-independent maxima at 542 and 420 nm, and which are clearly analogous to those observed in

Figure 2. Polarized single-crystal absorption spectrum of $(pyH)_3[Mo_2(HPO_4)_4]Cl$ at room temperature. The σ spectrum is vertically offset from the π spectrum by 0.15 optical density units. The dashed line is the calculated isotropic spectrum, ϵ (isotropic) $= (1/3)(\epsilon_\pi + 2\epsilon_\sigma)$, with the π baseline.

Figure 3. Polarized single-crystal absorption spectrum of $(pyH)_3[Mo_2(HPO_4)_4]Cl$ at 18K. The σ spectrum is vertically offset from the π spectrum by 0.06 optical density units.

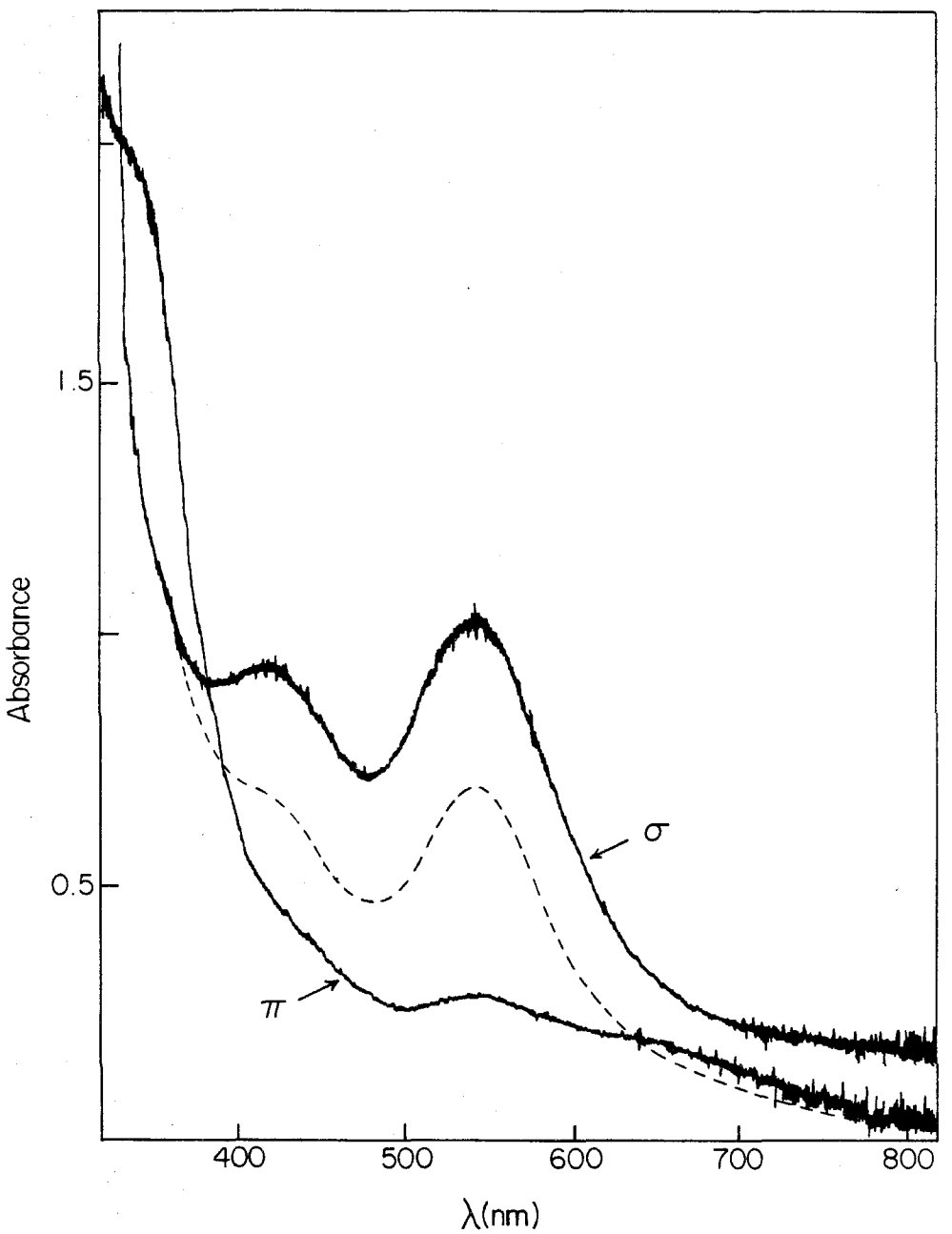
Absorbance
1.5
0.5
400
500
600
700
800
λ(nm)
σ
π

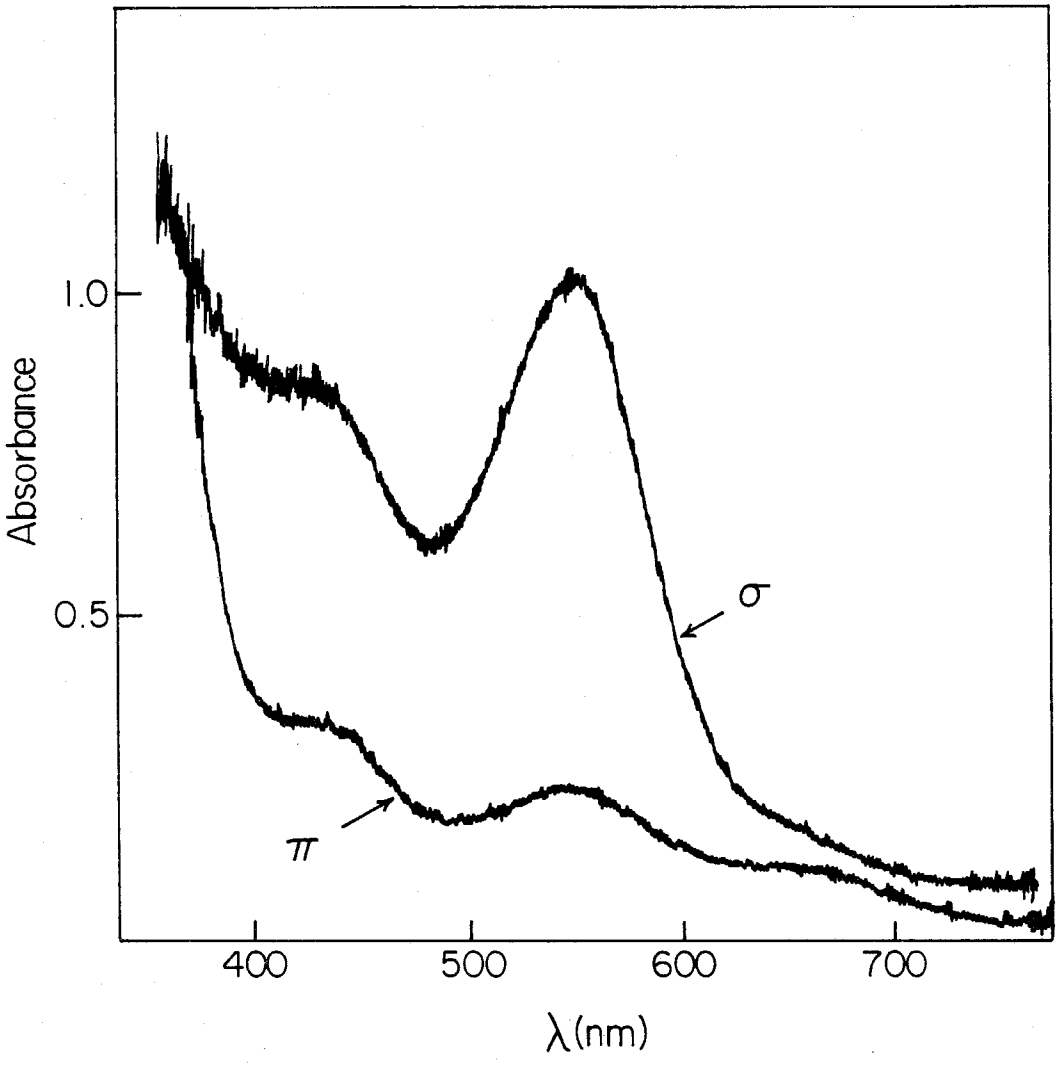
Absorbance
1.0
0.5
400
500
600
700
λ(nm)
σ
π

solution. The integrated intensity of each band in $\pi(z)$-polarization decreases with decreasing temperature, indicating that it is vibronically induced. The oscillator strength of the 542-nm band in x,y-polarization is independent of temperature, suggesting that this transition is dipole-allowed. In contrast, the 420-nm band in this polarization is less well defined at low temperatures, indicating that it is losing intensity and is thus likely to be dipole-forbidden in x,y- as well as z-polarization. The fact that this band is located on the low-energy tail of a much more intense transition makes our conclusions for the 420-nm band less certain than for the 542-nm band, however.

In addition to the two transitions that have analogues in the solution spectrum of $Mo_2(HPO_4)_4^{2-}$, two previously unreported bands were observed in the single-crystal spectra. The first is a broad, weak feature at ~670 nm that is predominantly z-polarized, although a weak shoulder in x,y-polarization at roughly the same wavelength is evident at low temperature. At room temperature, this band contributes only to the long-wavelength tail in the calculated isotropic absorption spectrum (Figure 2). Since a similar tail is seen in both the solution[14] and pellet spectra,[13] we consider the 670-nm band to be an authentic absorption of the $Mo_2(HPO_4)_4^{2-}$ chromophore. The second previously unreported band of $(pyH)_3[Mo_2(HPO_4)_4]Cl$ is a predominantly z-polarized absorption centered at 340 nm that, in contrast, has *no* counterpart in either the pellet spectrum of $Cs_2[Mo_2(HPO_4)_4]2H_2O$ or in solution spectra,[14] and which accounts for the visibly more reddish-purple color of the Cs^+ adduct. We infer from the fact the 340-nm absorption is unique to the pyH^+ compound that this band is not metal-metal-localized, and suggest that it is attributable to an LMCT transition involving the infinite-chain-bridging axial chloride ligands present in this particular salt. The extreme length of the Mo-Cl bonds could conceivably account for the relative weakness of this transition. A calculation

by Norman *et al.* on the $(\sigma^2\pi^4\delta^2\pi^{*2}\delta^{*1})$ ground state of the structurally related $Ru_2(O_2CH)_4Cl_2^-$ ion[23] assigns the highest occupied halide level to be a_{1g} σ(Ru-Cl), located at slightly higher energy than $\delta(Ru_2)$. The most likely assignment of the observed band is therefore σ(Mo-Cl)$\rightarrow\delta(Mo_2)$, which is dipole-forbidden. Unfortunately, we were unable to extend our low-temperature measurements to sufficiently high optical density to test the implied temperature-dependent intensity of this assignment.

Assignment of the Metal-Metal Transitions.

The absorption bands of $(pyH)_3[Mo_2(HPO_4)_4]Cl$ at 542 and 420 nm, and probably also that at 670 nm, are likely to be electronic transitions associated with its metal-metal bonding framework. In deriving assignments for these bands, we draw heavily upon comparisons to the data accumulated by Martin and co-workers for the Mo_2(II,II)[10] and Mo_2(II,III)[12] sulfate complexes. We assume that the bridging HPO_4^{2-} and SO_4^{2-} ligands are very similar from an electronic standpoint, and such comparisons as are available[7,13,14,24] support this contention.

The metal-metal-localized electronic transitions between the π- and δ-based manifold of states of $Mo_2(HPO_4)_4^{2-}$ and $Mo_2(SO_4)_4^{4-/3-}$ are set out in Table I. For the Mo_2(II,II) sulfate complex, which has a $(\sigma^2\pi^4\delta^2)$ ground state, crystal spectra of the K^+ salt show[10] the lowest energy transition to be the strongly z-polarized, moderately intense (ϵ_{max} 170 in solution)[11] $^1(\delta \rightarrow \delta^*)$ absorption at 515 nm. The one-electron-oxidized, $(\sigma^2\pi^4\delta^1)$-configured Mo_2(II,III) sulfate displays[12] as its lowest transition the similarly intense,[11] z-polarized $^2(\delta \rightarrow \delta^*)$ band centered at 1400 nm, the large red shift being understandable in terms of the large contribution of two-electron terms to the energy of the singlet transition.[4,5] The $(\sigma^2\pi^4)$ Mo_2(III,III) phosphate cannot, of course, have a $\delta \rightarrow \delta^*$ transition, and thus its lowest energy allowed transitions are likely to be $\pi \rightarrow \delta$ and $\pi \rightarrow \delta^*$ (Table I). Both of these

Table 1. Spin-Allowed Electronic Transitions Involving the π, δ, δ^*, and π^* Levels of $Mo_2(SO_4)_4^{4-/3-}$ and $Mo_2(HPO_4)_4^{2-}$. [a]

Orbital Transition	Assignment (position/nm)			Electric Dipole Polarization
	Mo_2(II,II) $\leftarrow {}^1A_{1g}$	Mo_2(II,III) $\leftarrow {}^2B_{2g}$	Mo_2(III,III) $\leftarrow {}^1A_{1g}$	
$\pi(e_u)\rightarrow\delta(b_{2g})$	b	^2E_u(595)	^1E_u(542)	x,y
$\pi(e_u)\rightarrow\delta^*(b_{1u})$	^1E_g(400)	^2E_g(417)	^1E_g(420)	dipole-forbidden
$\pi(e_u)\rightarrow\pi^*(e_g)$	c	c	$^1A_{2u}$(250?)	z
$\delta(b_{2g})\rightarrow\delta^*(b_{1u})$	$^1A_{2u}$(515)	$^2B_{1u}$(1400)	b	z
$\delta(b_{2g})\rightarrow\pi^*(e_g)$	c	c	b	dipole-forbidden

[a] $\underline{D_{4h}}$ molecular symmetry. [b] Transition does not occur in this species. [c] Not assigned.

transitions should also be present in the Mo_2(II,III) sulfate, while the Mo_2(II,II) sulfate can possess only the $\pi \rightarrow \delta^*$ transition.

The single-crystal absorption spectrum of $Mo_2(SO_4)_4^{3-}$ showed, in addition to $^2(\delta \rightarrow \delta^*)$, weak bands at 595 nm ($x,y$-polarized, temperature-independent intensity) and 417 nm (indefinite polarization and thermal behavior). These compare quite closely in energy and behavior to the 542- and 420-nm absorptions observed by us for $Mo_2(HPO_4)_4^{2-}$, and we suggest that these bands may be assigned to the $\pi \rightarrow \delta$ and $\pi \rightarrow \delta^*$ transitions, respectively. The spectrum of $Mo_2(SO_4)_4^{4-}$ also contains a weak band of mixed polarization at 400 nm which, by analogy to the 417- and 420-nm bands of Mo_2(II,III) and Mo_2(III,III) systems, could be attributable to the $\pi \rightarrow \delta^*$ transition.

Martin and co-workers considered a $\pi \rightarrow \delta$ ($^2E_u \leftarrow {}^2B_{2g}$) assignment for the visible absorptions of the Mo_2(II,III) sulfate, but they argued that the intensities of these bands were too low for dipole-allowed transitions. In view of the similarly small oscillator strengths of the dipole-allowed $\delta \rightarrow \delta^*$ transitions of the sulfate compounds, however, we suggest that the observed intensities are actually quite reasonable. Moreover, there is one very satisfying aspect of our assignments. The *difference* of the energies of the $\pi \rightarrow \delta$ and $\pi \rightarrow \delta^*$ transitions should equal the one-electron orbital splitting of the δ and δ^* levels; the above assignments of these bands yield a δ/δ^* splitting of 7175 cm^{-1}, in essentially perfect agreement with the directly observed 7175-cm^{-1} energy[11,12] of the $^2(\delta \rightarrow \delta^*)$ transition of this complex.[25]

Application of this analysis to the Mo_2(III,III) phosphate yields a δ/δ^* orbital splitting of 5100 cm^{-1},[26] reduced, as expected, as a result of the longer bond distance and lower bond order of this complex.[27] By assuming that the average energy of the δ and δ^* levels remains constant for the bond order 3 and 3.5 complexes,

then our assignments yield the energy level diagram shown in Figure 4. One consequence of this assumption is that the energy of the π level is nearly independent of the differences between the bond orders and metal-metal distances of these two compounds. Inasmuch as the δ-interaction is significantly weaker than the π-interaction in these complexes, the former's sensitivity to bond order and bond distance should be dramatically more marked than the latter's. By additionally assuming that the constant energy of the π level extends to the bond-order 4 case, then our assignment of the $\pi \rightarrow \delta^*$ transition of Mo_2(II,II) sulfate allows us to infer a one-electron δ/δ^* splitting of $\sim$8500 cm^{-1} for the quadruple bond, which is in reasonable agreement with the results of calculations[28] on other Mo_2(II,II) complexes possessing similar $^1(\delta \rightarrow \delta^*)$ transition energies.[29]

We also wish to consider briefly the assignments of the two other bands observed in the solid-state spectra of $Mo_2(HPO_4)_4^{2-}$. The weak, predominantly z-polarized feature at $\sim$670 nm in the single-crystal spectra of $(pyH)_3[Mo_2(HPO_4)_4]Cl$ is attributable to the $^3(\pi \rightarrow \delta)$ ($^3E_u \rightarrow {}^1A_{1g}$) excitation, which should possess both z- and x,y-allowed components. The intensity of this band relative to its singlet counterpart, as well as the resulting singlet-triplet splitting ($\sim$3500 cm^{-1}), are in reasonable agreement with expectations for a second-row transition metal complex.[30] Finally, our pellet spectrum of $Cs_2[Mo_2(HPO_4)_4]2H_2O$ showed a very intense absorption maximum at 250 nm. We consider it most unlikely that intense charge-transfer transitions involving the bridging phosphate or axial water ligands would occur at this low an energy and thus tentatively suggest that this band be assigned to the $^1(\pi \rightarrow \pi^*)(Mo_2)$ transition. Comparable UV data for the analogous sulfate complexes, however, have not yet been reported.

Figure 4. Energies of the π, δ, and δ^* levels of $Mo_2(HPO_4)_4^{2-}$, $Mo_2(SO_4)_4^{3-}$, and $Mo_2(SO_4)_4^{4-}$. Calculated or estimated energies are given in parentheses; all other values are spectroscopically determined.

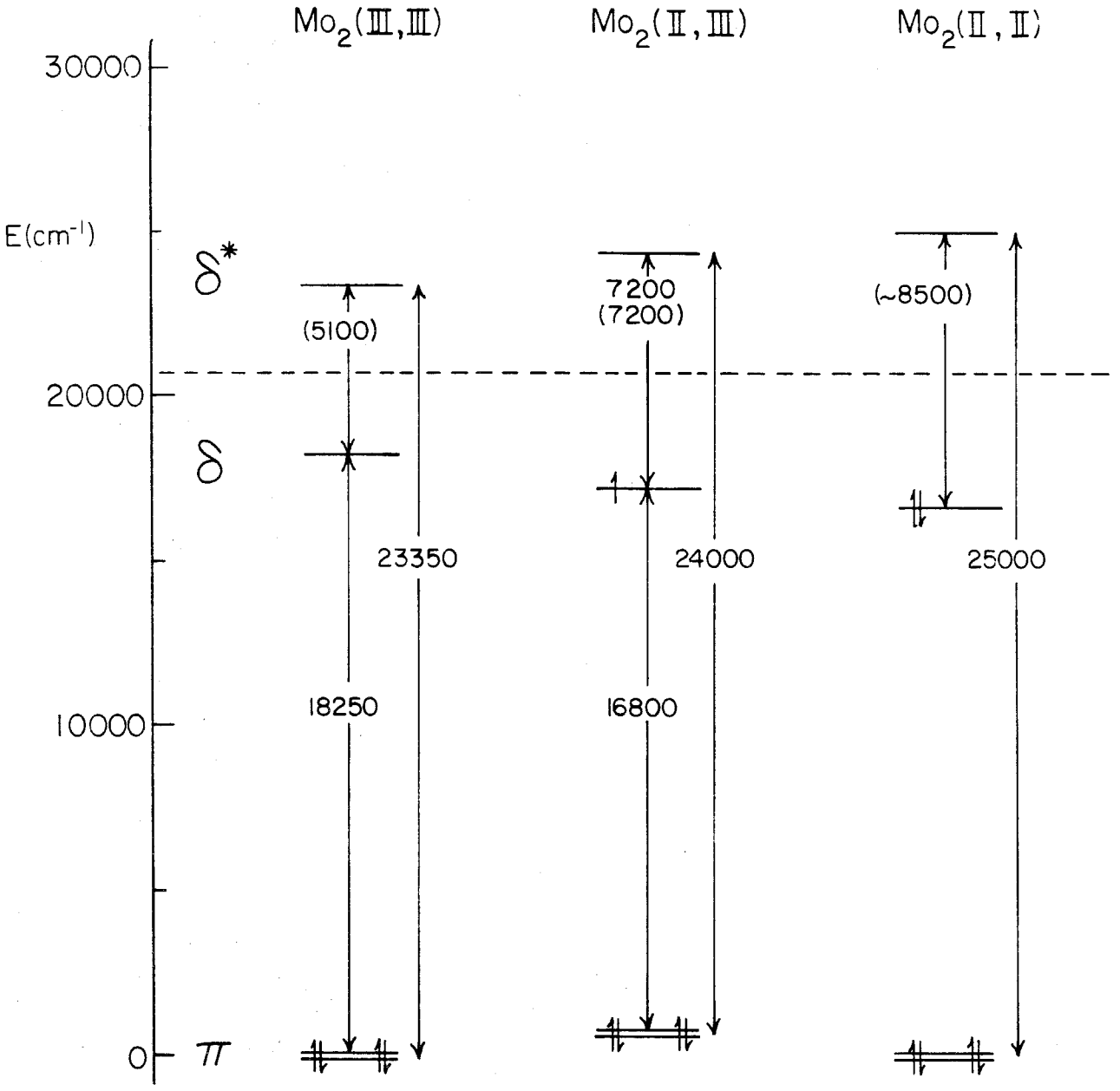
Mo2(III,III)
Mo2(II,III)
Mo2(II,II)
30000
E(cm-1)
δ*
20000
δ
10000
0
π
(5100)
7200
(7200)
(~8500)
23350
24000
25000
18250
16800

References and Notes

1. The contents of this appendix have been published separately: Hopkins, M. D.; Miskowski, V. M.; Gray, H. B. *J. Am. Chem. Soc.* **1986**, *108*, 959-963.
2. Trogler, W. C.; Gray, H. B. *Acc. Chem. Res.* **1978**, *11*, 232-239.
3. Cotton, F. A.; Walton, R. A. "Multiple Bonds Between Metal Atoms"; Wiley: New York, 1982.
4. Chapter IV. Hopkins, M. D.; Zietlow, T. C.; Miskowski, V. M.; Gray, H. B. *J. Am. Chem. Soc.* **1985**, *107*, 510-512.
5. Campbell, F. L., III: Cotton, F. A.; Powell, G. L. *Inorg. Chem.* **1985**, *24*, 177-181.
6. Manning, M. C.; Trogler, W. C. *J. Am. Chem. Soc.* **1983**, *105*, 5311-5320.
7. Bowen, A. R.; Taube, H. *J. Am. Chem. Soc.* **1971**, *93*, 3287-3289. Bowen, A. R.; Taube, H. *Inorg. Chem.* **1974**, *13*, 2245-2249. Cotton, F. A.; Frenz, B. A.; Pedersen, E.; Webb, T. R. *Inorg. Chem.* **1975**, *14*, 391-398.
8. Angell, C. L.; Cotton, F. A.; Frenz, B. A.; Webb, T. R. *J. Chem. Soc., Chem. Commun.* **1973**, 399-400.
9. Loewenschuss, A.; Shamir, J.; Ardon, M. *Inorg. Chem.* **1976**, *15*, 238-241.
10. Cotton, F. A.; Martin, D. S.; Fanwick. P. E.; Peters, T. J.; Webb, T. R. *J. Am. Chem. Soc.* **1976**, *98*, 4681-4682.
11. Erwin, D. K.; Geoffroy, G. L.; Gray, H. B.; Hammond, G. S.; Solomon, E. I.; Trogler, W. C.; Zagars, A. A. *J. Am. Chem. Soc.* **1977**, *99*, 3620-3621.
12. Fanwick, P. E.; Martin, D. S.; Webb, T. R.; Robbins, G. A.; Newman, R. A. *Inorg. Chem.* **1978**, *17*, 2723-2727.
13. Bino, A.; Cotton, F. A. *Angew. Chem., Int. Ed. Engl.* **1979**, *18*, 462-463. Bino, A.; Cotton, F. A. *Inorg. Chem.* **1979**, *18*, 3562-3565.

14. Bino, A. *Inorg. Chem.* **1981**, *20*, 623-626.

15. This revision of the original synthesis was worked out in consultation with Dr. A. Bino with the aim of obtaining material suitable for single-crystal absorption spectroscopy.

16. Behling, T.; Wilkinson, G.; Stephenson, T. A.; Tocher, D. A. *J. Chem. Soc., Dalton Trans.* **1983**, 2109-2116.

17. Earnshaw, A. "Introduction to Magnetochemistry"; Academic Press: New York, 1968.

18. We obtained Raman spectra using UV (363.8 nm) excitation with the aim of achieving preresonance enhancement with UV electronic absorption bands (*e.g.*, $\pi \rightarrow \pi^*$, LMCT: *vide infra*) that are much more intense than those observed in the visible region. Raman scattering by these solids is indeed stronger for UV excitation, and some selective enhancement of $\nu(Mo_2)$ is observed.

19. With regard to the metal-metal stretching frequencies of the Mo_2(II,II) and Mo_2(II,III) sulfates, assuming $r(M_2) \propto [k(M_2)]^{-1/3}$ (*cf.* Badger's rule) using Mo_2(III,III) phosphate as a benchmark ($k = 3.7$ mdyne/Å; M_2 approximation) leads to calculated values of ~390 and 375 cm^{-1} for the bond order 4 and 3.5 cases, respectively. Similar application to the $^2(\delta \rightarrow \delta^*)$ excited state of Mo_2(II,III) sulfate yields a bond lengthening of ~0.04 Å on the change from bond order 3 to 2.5.

20. Bratton, W. K.; Cotton, F. A.; Debeau, M.; Walton, R. A. *J. Coord. Chem.* **1971**, *1*, 121-131.

21. Nakamoto, K. "Infrared and Raman Spectra of Inorganic and Coordination Compounds"; Wiley: New York, 1978; p 142.

22. Neither the crystal spectra of the pyH^+ salt nor the pellet spectrum of the Cs^+ salt displayed electronic absorptions in the near-infrared. In addition

to demonstrating the absence of intrinsic electronic transitions in this region, this result rules out the possibility of contamination of these materials with $Mo_2(HPO_4)_4^{3-}$ ions,[14] which should display a $\delta \rightarrow \delta^*$ absorption below 1000 nm.[11,12]

23. Norman, J. G., Jr.; Renzoni, G. E.; Case, D. A. *J. Am. Chem. Soc.* **1979**, *101*, 5256-5267.

24. Pt_2(III,III) sulfate/phosphate complexes: Orlova, V. S.; Muraveiskaya, G. S.; Evstaf'eva, O. N. *Russ. J. Inorg. Chem.* **1975**, *20*, 753-758. Bancroft, D. P.; Cotton, F. A.; Falvello, L. R.; Han, S.; Schwotzer, W. *Inorg. Chim. Acta* **1984**, *87*, 147-153.

25. The Mo_2(II,II) and Mo_2(II,III) sulfate complexes should also have a $\delta \rightarrow \pi^*$ transition that is absent in the Mo_2(III,III) phosphate. The close coincidence of the visible absorption bands for the latter two complexes, as well as the reproduction of the $^2(\delta \rightarrow \delta^*)$ transition energy by this calculation, makes assignment of either the 417- or 595-nm band of $Mo_2(SO_4)_4^{3-}$ to $\delta \rightarrow \pi^*$ far less satisfactory than those proposed here. The spectra of the sulfate complexes contain[10,12] additional weak bands between 300 and 350 nm for which a $\delta \rightarrow \pi^*$ assignment is possible.

26. Since the actual peak position of the 420-nm band of $Mo_2(HPO_4)_4^{2-}$ is not well determined in our single-crystal spectra, we used the 428- and 548-nm values taken from solution.[14] Vertical transition energies were used in all instances.

27. In extending this analysis to $Mo_2(HPO_4)_4^{2-}$ we are assuming that the contributions to interconfigurational transitions (*e.g.*, $\pi \rightarrow \delta^*$) from two-electron terms will roughly cancel out when the differences between these transition energies are taken, thus yielding one-electron splittings of the type directly measured in the spectrum of $Mo_2(SO_4)_4^{3-}$. Such an approximation cannot, of course, be

applied to transitions between covalent and ionic states (*e.g.*, $^1(\delta \rightarrow \delta^*)$).[4,5]

28. $Mo_2Cl_8^{4-}$: $E(\delta/\delta^*) = 7900\ cm^{-1}$ (Norman, J. G., Jr.; Ryan, P. B. *J. Comput. Chem.* **1980**, *1*, 59-63). $Mo_2Cl_4(PMe_3)_4$: $E(\delta/\delta^*) = 8070\ cm^{-1}$ (Cotton., F. A.; Hubbard, J. L.; Lichtenberger, D. L.; Shim, I. *J. Am. Chem. Soc.* **1982**, *104*, 679-686).

29. Analogous studies have been reported for $Re_2Cl_4(PR_3)_4^{2+/+/0}$ ($\sigma^2\pi^4\delta^2\delta^{*n}$, $n = 0, 1, 2$). (Bursten, B. E.; Cotton, F. A.; Fanwick, P. E.; Stanley, G. G.; Walton, R. A. *J. Am. Chem. Soc.* **1983**, *105*, 2606-2611. Cotton, F. A.; Dunbar, K. R.; Falvello, L. R.; Tomas, M.; Walton, R. A. *ibid.* **1983**, *105*, 4950-4954). Extensive mixing between metal- and ligand-based levels of these systems, and concomitantly lower energy LMCT transitions, precluded a spectroscopic analysis as straightforward as that presented here for the Mo_2 sulfate/phosphate complexes, for which such complications are likely to be minimal.

30. An alternative assignment for the 670-nm band is $^1(\sigma(Mo_2) \rightarrow \delta(Mo_2))$ ($^1B_{2g} \leftarrow {}^1A_{1g}$; dipole-forbidden); recent photoelectron spectroscopic studies of other triply metal-metal bonded complexes indicate that the σ and π molecular orbitals of these species are nearly degenerate (Kober, E. M.; Lichtenberger, D. L. *J. Am. Chem. Soc.* **1985**, *107*, 7199-7201).